Development of a New Cathode for Aqueous Rechargeable Batteries

A thesis presented in partial fulfilment of the
requirements for the degree of
Doctor of Philosophy
in
Chemistry
at Massey University, Palmerston North
New Zealand

MASSEY UNIVERSITY

Kelsey Leigh Mortensen

2015

Abstract

The demand for low-cost energy storage is a current issue. Existing batteries are unable to meet this constraint due to the high raw material prices, in particular the metal content. The risk of fluctuating metal prices and future availability will not meet the market demand and therefore alternative materials need to be considered.

The focus of this project was to develop a non-metal based battery electrode specifically for stationary battery systems. This study presents fundamental concepts required to form a rechargeable electrochemical storage device utilising hydrogen peroxide as the electroactive species. This involved two key aspects: immobilisation of hydrogen peroxide in order to prevent self-discharge and catalytic regeneration of hydrogen peroxide from hydroxide ions. Although the construction of the device was not within the scope of this project, the chemical and electrochemical analysis of potential compounds were evaluated at a molecular level. In particular, the synthesis and molecular behaviour of a urea-based ’binder‘ that will immobilise hydrogen peroxide, and an oxoammonium ’catalyst‘ to reform hydrogen peroxide during recharge of the battery. Additionally, the attachment of these compounds to a surface was also evaluated.

Analysis of the interactions between substituted ureas (‘binder’) and hydrogen peroxide proved challenging. Although these findings suggest that adduct formation is occurring, the methods undertaken were not able to determine the equilibrium constant or strength of binding. They did however give an indication of the quantity of hydrogen peroxide in the synthesised adducts and this methodology can be applied to the range of hydrogen peroxide adducts. Additionally, functionalisation of surfaces with a diazonium-containing substituted urea was achieved and is a viable method for attaching the ‘binder’ to the electrode substrate material.

The second key step is to incorporate a rechargeable aspect to the battery system. An oxoammonium cation was proposed to act as a 'catalyst' to replenish H_2O_2 during charging. Details regarding the synthetic methodology for synthesis of nitroxide-containing compounds, incorporating diazonium functionalities for attachment to a surface, were obtained. Of particular interest was the amido-TEMPO structure that was electrochemically attached to a carbon surface electrode. Evaluation of its ability to form H_2O_2 was achieved using a bi-potentiostat where a current density of 0.21 A m^{-2} was observed. This novel idea shows promise and demonstrates the ability for the catalyst to replenish H_2O_2 in an aqueous battery system.

Acknowledgements

I would like to take the opportunity for thank a number of people of who have assisted to my PhD research and thesis. First off I would like to thank my primary supervisor Professor Simon Hall for the support, encouragement and perseverance over the course of this project. Your insightfulness and ability to see potential in all this work has not only pushed me forward, but also challenged me throughout. Thank you for allowing me to be a part of this great adventure and all the time and effort required for this project. Thank you also to Associate Professor Gareth Rowlands for the continual support, assistance and most importantly, always being there when I needed help or advice. Your outstanding knowledge and logical thinking are appreciated and are to be greatly commended. Also, thank you to Associate Professor Mark Waterland for his assistance in Raman, IR and his contributions to general discussions in this project.

A special mention must go to my colleagues Dr Krishanthi Jayasundera and Veronica Brown for their assistance in the synthesis and evaluation of a number of compounds. Your efforts are appreciated and have greatly contributed towards not only my thesis but towards the overall project. I must also acknowledge Nessha Wise for her assistance with the electrochemistry experiments, Luke Liu for the isotherm data, Ashley Way for performing computational calculations, Haidee Dykstra for assistance with Raman and Jason Hindmarsh for the ssNMR data.

In addition I would like to thank Dr Pat Edwards for his specialised assistance in NMR spectroscopy and Associate Professor Paul Plieger for technical assistance in X-ray analysis. Thank you to all the past and present lab/institute colleagues who despite not knowing what my project entailed were always willing to assist during my research and thesis writing, even if that involved non-chemistry jargon.

I also must acknowledge the MacDiarmid Institute, Synthodics and the Institute of Fundamental Sciences for financial support to allow me to undertake this project.

Lastly, I would like to thank my fiancé James who was my biggest supporter. Your love and support carried me through this journey and for that, I am very grateful. You have a gift of always making me smile and the ability to pick me up in times of need. I am excited to continue the journey with you afterwards. To my family, thank you for the continual encouragement and the “your almost there” pep talks. Mum and dad, I appreciate all that you have done for me and I hope this makes you proud.

Table of Contents

List of Figures

List of Schemes

List of Tables

Abbreviations and Symbols

δ	chemical shift
AAS	atomic absorption spectroscopy
AcOH	acetic acid
Ah	ampere hours
aq	aqueous
Ar	aromatic
ATR	attenuated total reflectance
ax	axial
BDMS	bromodimethylsulfonium bromide
BET	Brunauer-Emmett-Theory
Boc	*tert*-butyloxycarbonyl
CA	chronoamperometry
$CDCl_3$	deuterated chloroform
CDI	*N,N'*-carbonyldiimidazole
CE	counter electrode
CEP	concerted electron transfer process
conc.	concentrated
COSY	correlation spectroscopy
CV	cyclic voltammetry
DCC	*N,N'*-dicyclohexylcarbodiimide
DCE	dichloroethane
dba	dibenzylideneacetone
DFT	density functional theory
DMDQ	2,5-dimethoxy-1,4-benzoquinone
DMF	*N,N*-dimethylformamide
DMSO	dimethyl sulfoxide
DPU	diphenylurea
eq.	equivalent
Eq.	equatorial
ESI	electrospray ionisation
EtOAc	ethyl acetate

EtOH	ethanol
EDG	electron donating group
EDTA	ethylenediaminetetaacetic acid
EPR	electron paramagnetic resonance
eV	electron volts
EWG	electron withdrawing group
Fc	Ferrocene
Fc^+	Ferrocenium
Fmoc	fluorenylmethyloxycarbonate
FT	fourier transform
GC	glassy carbon
HOBt	hydroxybenzotriazole
HOMO	highest occupied molecular orbital
HR-MS	high resolution mass spectrometry
IR	infra-red spectroscopy
ITC	isothermal titration calorimetry
kJ	kilojoules
kW	kilowatts
kWh	kilowatt hour
LUMO	lowest unoccupied molecular orbital
(m)	medium
mAh/g	milliampere hours per gram
*m*CPBA	*meta*-chloroperoxybenzoic acid
MAS	magic angle spin
ME	microelectrode
MeCN	acetonitrile
MeOH	methanol
mV/s	millivolts per second
MW	megawatts
MS	mass spectrometry
mp	melting point
MP2	Møller-Plesset
m/*z*	mass/charge

NEt_3	triethylamine
NMM	N-methylmorpholine
NMR	nuclear magnetic resonance
nOe	nuclear Overhauser effect
NOESY	nuclear Overhauser effect spectroscopy
PAN	polyacrylonitrile
Ph	phenyl
PG	protecting group
ppm	parts per million
PTC	phase transfer catalyst
RE	reference electrode
RDE	rotating disk electrode
RF	radio frequency
RRDE	rotating ring disk electrode
RT/rt	room temperature
s	solid
(s)	strong
sec	seconds
ss	solid-state
SEM	scanning electron microscope
TBAH	tetrabutylammonium hydroxide
TEMPO	2,2,6,6-tetramethylpiperidin-1-yloxyl
TFA	trifluoroacetic acid
TGA	thermogravimetric analysis
THF	tetrahydrofuran
TMIO	1,1,3,3-tetramethyl-2,3-dihydroisoindol-2-yloxyl
TMS	trimethylsilylacetylene
TLC	thin layer chromatography
UHP	urea hydrogen peroxide
UV-Vis	ultraviolet-visible spectroscopy
US	United States
V	volts
(w)	weak

WE	working electrode
Wh/kg	watt hours per kilogram
Wh/L	watt hours per litre
W/kg	watts per kilogram
W/L	watts per litre

CHAPTER ONE

Introduction

1.1 Background to this work

Throughout human history we have relied on the balance between the supply and demand of energy in economic development. Historically, the most convenient means to obtain energy for technological activities is through the chemical energy inherent in combustion processes. Over the last century, electricity generation in particular, has become a major need and unlike other energy sources such as coal and natural gas, it cannot be stored and must be utilised as it is being generated. Harnessing the chemical energy stored in fossil fuels by combustion accounts for around 80% of the global final energy consumption, of which for the purpose of generating electricity, fossil fuels contributes 78%.[1,2] This not only causes a significant accumulation of greenhouse gases[3] in the atmosphere, but also progressively depletes the readily obtained resources (through drilling and mining) making it unsustainable over the longer term. Since the middle of the last century nuclear generation of electricity looked to be promising for larger economies; here nuclear fission rather than chemical combustion processes are harnessed. However, the progressive concerns over storage of hazardous wastes (over tens of thousands of years) and the need for marked investment to replace early power stations has meant that this generation method has become less attractive. A substantial blow was dealt to the nuclear energy sector with the 2011 Fukushima disaster. Following this, a large number of nuclear power stations in Japan were shut down (as they were also in Germany) and the electricity generation shortfall was predominantly made up through combustion of natural gas.[4,5,6]

Against this background, electricity generation from renewable sources is becoming of greater interest. Renewable energy utilises resources such as wind, solar, hydro and geothermal, contributing to a total of 77% of New Zealand's electrical energy being from renewable sources. New Zealand has a high level of

hydroelectric and geothermal electricity generation (58% for hydroelectric and 13% for geothermal compared to 16% and <0.4% respectively worldwide).[1,7] The remaining 6% is provided by wind and bioenergy (4.5% and 1.5% respectively).

Fluctuations of energy demand can vary on a season-to-season, day-to-day and even minute-to-minute basis where stored energy must convert to electricity at peak periods and reduce production in times of lower demand. Hydroelectricity involves the ability to move water from reservoirs through a water turbine, which generates electricity almost instantaneously in periods of high demand. Geothermal response to demand is similar, however is dependent on steam availability and in some cases local depletion of water. Smaller, less assured over shorter-time renewable energy sources such as wind and solar may contribute to the total energy supply but offer little ability to respond to rapid changes in demand. In the NZ setting wind is a developing capability (currently 4.5% of total electricity generation) while solar (either as thermal or photovoltaic) is not implemented to any level of significance on the NZ national grid.

A potential method to store energy generated from intermittent and highly variable primary sources such as wind and solar is with electrochemical cells, otherwise known as batteries (the term 'battery' relates to one or more cells connected to form a unit with a single positive and a single negative terminal). These cells can store energy in a driven (i.e. non-spontaneous) 'charging' process where electrochemical potential energy of the device is raised through an oxidation process at the cathode (the positive terminal) and a reduction process at the anode (the negative terminal). This stored electrochemical potential energy can be released and harnessed externally through the spontaneous 'discharge' process where the reactions at the anode and cathode are reversed and hence these systems are identified as 'rechargeable' or 'secondary'. The charging process of batteries can often tolerate the variable supply of energy from wind and solar sources and the discharge processes are often capable of variable discharge rates to accommodate variations in the electricity demand. This might be either for electricity systems remote from the local electricity grid

(peak power demands of the order of kilowatts, kW) or as part of a national electricity grid (peak demands of the order of megawatts, MW).

Several technical metrics may be used to categorise rechargeable batteries with respect to the ability to store and deliver energy:

i) Volumetric energy density, the energy stored per unit volume of the battery, usually expressed as Wh/L (Watt hours per litre),

ii) Gravimetric energy density, the energy stored per unit mass of the battery, usually expressed as Wh/kg (Watt hours per kilogram),

iii) Power density, the rate this energy can be delivered, expressed either volumetrically (W/L) or gravimetrically (W/kg).

Over and above this is the critical economic metric of the cost of the battery, typically expressed in terms of the amount of energy stored and in US dollars and as US$/kWh.

1.2 Stationary Battery Systems

The energy storage and delivery requirements for battery systems associated with storing renewable energy are orders of magnitude larger than those required for portable devices (e.g. portable telecommunication, computing and entertainment devices) and hence these more substantial batteries are typically termed 'stationary' since ease of movement (e.g. weight and volume) are not over-riding factors for utilisation. A range of battery chemistries have been either utilised or proposed for energy storage to assist with utilisation of renewable energy generation. These include (discharge process from left to right hand side of each equation):

i) Lead-acid

Negative electrode:

$$Pb(s) + HSO_4^-(aq) \rightleftharpoons PbSO_4(s) + H^+(aq) + 2e^- \quad 1.1$$

Positive electrode:

$$PbO_2(s) + HSO_4^-(aq) + 3H^+(aq) + 2e^- \rightleftharpoons PbSO_4(s) + 2H_2O(l) \quad 1.2$$

Overall reaction:

$$Pb(s) + PbO_2(s) + 2HSO_4^-(aq) + 2H^+(aq) \rightleftharpoons 2PbSO_4(s) + 2H_2O(l) \quad 1.3$$

ii) Zinc air

Negative electrode:

$$Zn(s) + 4OH^-(aq) \rightleftharpoons Zn(OH)_4{}^{2-}(aq) + 2e^- \quad 1.4$$

followed by:

$$Zn(OH)_4{}^{2-}(aq) \rightleftharpoons ZnO(s) + H_2O(l) + 2OH^-(aq) \quad 1.5$$

Positive electrode:

$$\frac{1}{2}O_2(g) + H_2O(l) + 2e^- \rightleftharpoons 2OH^-(aq) \quad 1.6$$

Overall reaction:

$$Zn(s) + \frac{1}{2}O_2(g) \rightleftharpoons ZnO(s) \quad 1.7$$

iii) Sodium-sulfur

Negative electrode:

$$2Na(s) \rightleftharpoons 2Na^+(aq) + 2e^- \quad 1.8$$

Positive electrode:

$$2Na^+(aq) + xS(s) + 2e^- \rightleftharpoons Na_2S_x(s) \quad 1.9$$

Overall reaction:

$$2Na(s) + xS(s) \rightleftharpoons Na_2S_x(s) \quad 1.10$$

iv) Fuel cells

Fuel cells differ from batteries due to the requirement for a continuous source of fuel and oxygen/air to sustain the chemical reaction that converts the fuel into electricity. A standard Hydrogen-Oxygen Fuel Cell can be used as a primary source of electrical energy. The reaction of hydrogen gas and oxygen to form water creates an electrical current, which is sustainable until the supply of reactants is exhausted. The system effectively becomes rechargeable through regeneration of hydrogen elsewhere.

Negative electrode:

$$2H_2(g) \rightarrow 4H^+(aq) + 4e^- \quad 1.11$$

Positive electrode:

$$O_2(g) + 4H^+(aq) + 4e^- \rightarrow 2H_2O(l) \quad 1.12$$

Overall reaction:

$$2H_2(g) + O_2(g) \rightarrow 2H_2O(l) \quad 1.13$$

v) Lithium ion systems

Primary lithium systems comprise of a cell design that uses lithium in the zero oxidation state as the charged anode. These include liquid cathode, solid cathode and solid electrolyte lithium cells. Typical examples of secondary, or rechargeable lithium–ion batteries employ an intercalated lithium compound as the cathodic electrode material and a graphitic carbon as the anode.

Negative electrode:

$$xLiC_6(s) \rightleftharpoons xLi^+(aq) + xe^- + xC_6(s) \quad 1.14$$

Positive electrode:

$$Li_{1-x}CoO_2(s) + xLi^+(aq) + xe^- \rightleftharpoons LiCoO_2(s) \quad 1.15$$

Overall:

$$xLiC_6(s) + Li_{1-x}CoO_2(s) \rightleftharpoons xC_6(s) + LiCoO_2(s) \quad 1.16$$

Lead-acid, zinc-air, sodium-sulfur and lithium ion battery systems have a range of performance metrics in terms of energy density, power density and durability. Further performance metrics include those of ‘efficiency’ and ‘cycle life’.

Efficiency can either be coulometric – what percentage of electrical charge used to charge a battery may be recovered during the subsequent discharge; or in energy terms – what percentage of the energy used to charge a battery can be recovered during the subsequent discharge? Coulometric inefficiencies are indicative of competing side reactions and occlusion of electrode materials, while energy efficiencies indicate coulometric inefficiencies and/or loss of

energy due to ohmic heating (due to the internal resistance of the battery system).

Cycle life is a measure of the number of charge-discharge cycles to some specified depth of discharge (the proportion of theoretical storage capacity) above a specified coulometric or energy efficiency. Successful stationary energy storage systems are anticipated to require cycle lives > 1500 cycles.

Although the lead-acid battery has high coulometric and energy efficiencies (70-90%) and power densities of up to 600 W/kg, its downfall is its low energy density (30 – 50 Wh/kg) and limited durability of between 500 – 1000 cycles and at low depths of discharge.[8] In contrast, the zinc-air system is known for its high energy density (350-500 Wh/kg). However the cyclability is poor due to the solubility of the anode discharge product $Zn(OH)_4^{2-}$ in the electrolyte leading to dynamically unstable electrode geometries (known as 'shape change').[9] Additionally, despite having a high energy density, the performance-limiting reaction in the zinc-air system is the electrocatalysis of oxygen. Few catalyst materials meet this rigorous demand, although advances in metal oxide and nanocarbon hybrids are recent attractive developments.[10,11] Typical energy densities of the sodium-sulfur battery are in the range of 150-240 Wh/kg and at specific powers of 200 W/kg. With an efficiency of between 75-95% and a respectable durability of 2500 cycles, the sodium-sulfur battery shows promise. Unfortunately it uses its own energy storage capacity to maintain operating temperatures at 300 °C, consequently reducing its overall performance and effective energy efficiency.[8,12] In addition, the solid alumina ceramic electrode separator is brittle and can develop microfissures.[13,14] As a result liquid sodium and sulfur has the potential to come in contact with each other causing explosive and violent results. However, advances in this area have developed a sodium-sulfur battery that operates at room temperature with the addition of a composite sulfur-carbon electrode.[15] Rechargeable lithium-ion batteries have the advantage of a high energy densities (100-250 Wh/kg) and power densities (300 W/kg) in combination with coulometric efficiencies approaching 100%.[16] Developments into increasing the performance of this system by changing the

composition of the electrode materials have rapidly driven this technology forward.[17-21] The main drawback in the lithium systems is the limited mineable sources of lithium. Table 1.1 outlines the performance metrics of the outlined batteries.

Table 1.1 Summary of performance metrics for a selection of the types of rechargeable batteries.

Battery Type	Energy density (Wh/kg)	Power density (W/kg)	Durability (cycles)	Operating Temperature (°C)
Lead-Acid	30 - 50	75 - 600	500 - 1000	-15 - 50[22]
Zn-air	300 - 500	100	20 - 100	-10 - 55[23]
Sodium-sulfur	150 - 240	150 - 230	2500	300 - 350[8]
Lithium ion	150 - 250	150 - 300	400 - 10,000	-20 - 60[24,25]

Lithium is the least dense of all metals (0.534 g cm^3) and exists in nature as either Li_2CO_3 or LiCl. The Earth's crust contains approximately 20 mg of lithium per kg of material (20-70 ppm) with a small contribution to the total amount of Li being the 0.25 ppm from seawater.[26] In terms of accessible and economically viable reserves of lithium, 13% was reported to be in hard rock and mineral deposits while the remaining 87% was present in brine deposits.[27] The most recent data from the US Geological Survey in 2013 revealed that a total of 35,000 tonnes of lithium is produced each year from brine and mineral sources.[28] If one were to assume that in the next 20 years, the proportion of vehicles produced

would predominantly be plug-in hybrids, the lithium demand would exceed supply with each battery requiring 1.4 kg of purified lithium carbonate per kWh of available capacity.[29] If all the mined lithium (given as lithium carbonate 185,000 tonnes) was manufactured into 16 kWh batteries for hybrid vehicles, a total of 8.25 million cars could be produced per year. However, of the 13 $x10^6$ tonnes of the world's lithium reserves available based on current economic considerations, the price of the produced material would be expected to dramatically increase (currently at US$4,600 per tonne of lithium carbonate) increasing the already high US$600-1200/kWh hurdle of the lithium-ion batteries.[8,27,30]

The leading battery in terms of cost is the lead acid battery at 100-150 US$/kWh.[30,31] This is considerably lower than that for Li-ion batteries and Na-S batteries (US$300-500/kWh).

1.3 The case for new stationary battery systems

As the demand for low-cost energy storage is a current issue, existing batteries are unable to meet this constraint due to the high raw material prices. Key to this is metal content; the risk of fluctuating metal prices and future availability will not meet the intended market therefore alternative materials need to be considered.

The fluctuating price of nickel provides a prime example of risk of using such a material in batteries. In 2007 the price of nickel reached US$52/kg prior to the global recession, and even during 2014 the price fluctuated between US$15-20/kg.[32] With such an unreliable price for a key component of a battery system, the use of nickel in large stationary battery systems (for example in nickel-zinc or nickel cadmium batteries) is unlikely.

Alternatives to consider are the lower risk metals, such as zinc. At approximately US$1.90/kg it is considerably less expensive and has 300 times greater mining availability than lithium.[33] Based on componentry costs it is anticipated that zinc-air batteries can be produced at less than US$100/kWh, but the desired

2000-10,000 cycle life has been found to be challenging.[30] Other zinc containing batteries are not as promising as the zinc-air battery. A rechargeable nickel-zinc battery only attains 55-85 Wh/kg although has a high power density of 140-200 W/kg.[34] Overall, fluctuating nickel prices and the poor performance of the zinc electrode make product development in this area risky and potentially non-rewarding.

This then poses the question as to whether a large stationary electrochemical storage device, or at least one of the electrodes for the battery, can be produced without requiring a metal-centered redox couple.[35] One of the key considerations for development of any electrode system is the 'capacity' of the materials based on Faraday's Law (the amount of electric charge that is passed per mass of the material) and usually quoted in mAh g^{-1}. The utilisation of non-metal electrodes has been explored and can be characterised into several categories:

i) Classical conductive polymers. These include cation exchange polymers such as polyaniline,[36] polyacetylene and polypyrrole.[37] The conductivity of the polymer is crucial to performance with this being dependent on the doping level (redox state) of the polymer.[38] Conductive polymers have been demonstrated with a practical capacity of *ca.* 150 mAh g^{-1} due to the upper limit posed by the doping level (the mass of the dopant constituents contributing to the effective 'molecular mass' of all species involved in the redox process).[39]

ii) Organosulfur compounds. These contain disulfide bonds and have a high discharge capacity of 500 mAh g^{-1}. However, the cycle-life (10-100) is inadequate due to the progressive dissolution of the active material into the electrolyte.[39, 40]

iii) Pendant-type polymers. A stable nitroxyl polyradical, poly(2,2,6,6-tetramethylpiperidinyloxy methacrylate) (PTMA) has been fabricated into a cathode active material to produce a rechargeable battery with a low discharge capacity of 77 mAh g^{-1}.[41,42] Recently, a combination of a polypyrrole derivative with a nitroxyl radical produced a polymer with a discharge capacity of 115 mAh g^{-1}. This increase in capacity has

been ascribed to the flexible linking side-chain on the conductive polypyrrole backbone that assists with the transport of charge in the bulk of the aggregated polymer.[43]

iv) Quinone-based derivatives. Quinones are commonly found in biological molecules such as in vitamin K, co-enzyme Q_{10} and also are important in electron-transport systems of biological structures.[39] The use of 1,4-benzoquinone in a two-electron battery electrode process has various issues regarding the dissolution of the organic compound into the electrolytes. A modified quinone, 2,5-dimethoxy-1,4-benzoquinone (DMBQ), shows a reduced solubility in the solvent system (THF/MeCN) and thus reduced dissolution. An electrode was fabricated from a mixture of acetylene black, DMBQ and a conductive additive to give an initial discharge capacity of 312 mAh g^{-1}.

This suggests that non-metal based battery electrodes have not developed sufficiently. Indeed, the recognition of the need for battery electrodes not dependent on metal-based redox processes has not been widely been considered. The work presented in this thesis, in part, builds on the recognition of the potential utility of oxygen-based redox chemistry, but without requiring metal-based electrocatalysts. Consequently, it is useful to provide a brief overview of oxygen-based systems.

The reduction of oxygen, O_2, either from the atmosphere or from a gas storage system, is a common feature between metal-air batteries and fuel cells. Both systems suffer from the slow kinetics of oxygen reduction at the cathode which is limiting advances in practical electrochemical performance.[10] Catalytic reduction of O_2 from the air is complex in any air-breathing battery or fuel cell system. The oxygen reduction reaction is generally performed at platinum (or platinum group metal) catalysts and can proceed through two possible pathways

i) a two-electron reduction to give H_2O_2 as an intermediate

$$2H^+(aq) + O_2(g) + 2e^- \rightarrow H_2O_2(aq) \qquad 1.17$$

ii) a more efficient four-electron pathway to produce H_2O.

$$4H^+(aq) + O_2(g) + 4e^- \rightarrow 2H_2O(l) \quad 1.18$$

Of great concern, and causing limitations in the large-scale commercialisation of fuel cells, is the price and availability of the platinum group metals. Although platinum has the highest efficiency amongst the metals for catalysing the reduction of oxygen, it is plagued by catalyst poisoning, in particular by sulfur containing compounds.[44] A pioneering paper in 2011 by Wang *et al.* developed a metal-free alternative for the oxygen reducing catalyst with the introduction of vertically-aligned carbon nanotubes doped with nitrogen (VA-NCNTs).[44] This displayed increased electro-activity and durability compared to platinum materials and hence is a possible replacement of the metal-containing electrode.

Oxygen electrodes are complex compared to most other battery cathodes given the requirement for a gas-permeable membrane. This membrane selectively permits diffusion of oxygen to the electrode with the exclusion of CO_2, without permitting the evaporation or loss of the aqueous electrolyte. The exclusion of CO_2 is desirable since in aqueous alkaline systems insoluble carbonate salts will form that tend to interfere with the electrolyte conductivity and the operation of the membrane system.

With respect to the chemistry of oxygen in an alkaline electrolyte, the cathode reactions can be given as:

$$O_2(g) + 2H_2O(l) + 4e^- \rightarrow 4OH^-(aq) \quad 1.19$$

or

$$O_2(g) + H_2O(l) + 2e^- \rightarrow HO_2^-(aq) + OH^-(aq) \quad 1.20$$

followed by

$$HO_2^-(aq) + H_2O(l) + 2e^- \rightarrow 3OH^-(aq) \quad 1.21$$

and with a side reaction

$$2HO_2^-(aq) \rightarrow 2OH^-(aq) + O_2(g) \qquad 1.22$$

The slow kinetics of the reduction of oxygen stems from the strong dioxygen bond (498 kJ mol^{-1}) and the difficulty of breaking this bond electrochemically. This combined with the technical challenges of developing a robust air-breathing membrane electrode have led to consideration of an alternative cathode based on the oxygen system in the present study.

1.4 The use of hydrogen peroxide as a cathode system

Here, the use of hydrogen peroxide, H_2O_2, as the oxidised species in a cathode is considered. This species is capable of a two-electron reduction process, does not rely on exchange with the gas phase and is not based on metals. This might be considered as involving one half of the electrochemistry pathway of an air electrode.

The utilisation of hydrogen peroxide as an electroactive species is not a new concept. H_2O_2 has been successfully used as an oxidant in liquid fuel cells where the main disadvantage was the limited H_2O_2 concentration.[45] In an aqueous electrolyte H_2O_2 is readily soluble and is reduced to soluble hydroxide ions in a two-electron process. It was found that using H_2O_2 as an oxidant improved the cell potential in terms of reaction activity and mass transport when compared to an O_2 electrode.[45] Unfortunately H_2O_2 is inherently unstable and has a propensity to decompose by the disproportionation reaction

$$2H_2O_2(aq) \rightarrow 2H_2O(l) + O_2(g) \qquad 1.23$$

Although this is a slow process in pure aqueous solutions it can be accelerated by the presence of a plethora of other solutes, or in contact with many solid materials. Such disproportionation would act to 'self-discharge' the battery system by consuming the electroactive species. Furthermore, the freely soluble hydrogen peroxide and its decomposition product, oxygen gas, are able to

migrate through the electrolyte and discharge the anode species leading to a second mode of battery self-discharge. These self-discharge processes are uncontrolled and do not lead to flow of electrons in an external circuit and so design considerations must be made to avoid these events.

1.5 The New Cathode concept

Prior to the present study an underlying premise was made that if H_2O_2 could be immobilised to form an insoluble species in an aqueous electrolyte that the self-discharge with the anode species would not take place.[35,47] It is known that urea-based compounds will form stable adducts with H_2O_2. In chemical terms an adduct occurs by the addition of two distinct species forming a new compound without the addition or loss of any of their components of the two species. The urea-H_2O_2 adduct in the solid state is known to produce a stable source of H_2O_2 and hence may act to:

- locate the redox system at the electrode and
- prevent disproportionation when in contact with a battery electrode system (including physical support structure and electrolyte).

The charge and discharge processes of a battery electrode are heterogeneous with the critical redox processes taking place at the electrode-solution interface (in most aqueous batteries this is a solid-liquid interface). Batteries are usually designed to maximise the total area of this interface at each electrode. Consequently, any cathode involving immobilised H_2O_2 should aim to load this insoluble material onto a high surface area and conductive substrate. Here, this concept has been combined with that of the proposition of avoiding metals in the development of new batteries.

Carbon was selected as the substrate material in this early study and is considered a viable candidate for development of a final electrode system. It is an electrically conductive material (but not in the diamond form) and has already been employed in number of electrochemical systems including lithium-ion batteries and metal-air systems. There are many types of carbon available from ill-defined ‘soots’ to pristine carbon nanotubes and fullerenes; each having

different physical and chemical properties. Carbon is available in high surface areas (>1000 m^2 g^{-1}) and can be chemically-functionalised to change its properties.

This combination of carbon substrate and immobilised H_2O_2 has been referred to as a 'New Cathode' in successful funding applications and proposals for the overall project that this study forms part of. Preliminary tests show that the New Cathode in alkaline conditions, paired with a zinc anode will have a cell potential of 1.25 V. This is in the region of 'low voltage' battery systems, which are not inappropriate for use in large stationary systems. It is noted that other workers are also exploring this low voltage region for stationary battery systems.[46]

The proposed New Cathode is planned to operate in a manner distinct from most aqueous battery electrode systems. Other systems are dominated by metal anodes and metal oxide cathodes (in the charged state). These materials form both the high-surface area electrically conductive substrate and the electroactive material. As discharge takes place there is a progressive physical and chemical transformation of the materials and effectively an ever-advancing electrode-electrolyte interface. For example in the case for the lead anode in the lead-acid battery, the location of the lead-electrolyte interface shifts towards the bulk of the lead phase (and then becomes progressively covered by insulating a solid lead sulfate phase). In the case of the New Cathode the electrode-electrolyte substrate (the high-surface area carbon substrate) is static and the electroactive material is a molecular layer thick coating on this substrate. In some respects this concept is similar to the operation of supercapacitor electrode materials.

Immobilisation of the H_2O_2 was proposed in the preceding work to this study to be through the formation of adducts with derivatives of urea. In turn these urea moieties require attachment to the surface of the carbon substrate. In the design of the overall project it was proposed that chemical functionalisation of high surface area carbon materials provided opportunities to immobilise H_2O_2; to form what is termed here a 'binder' for H_2O_2. An adequate binder must have the

ability to attach to the carbon structure in addition to non-covalently bonding to H_2O_2 in a reversible manner (Fig. 1.1).

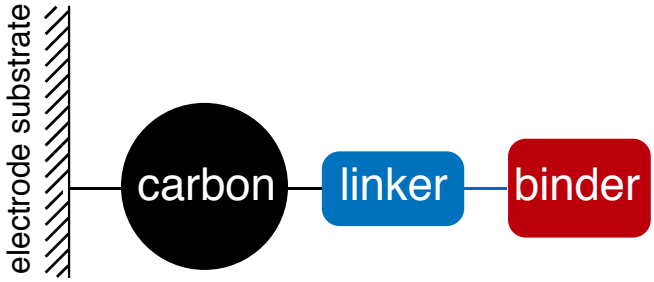

Fig. 1.1. Schematic representation for the New Cathode concept: an H_2O_2 adduct-forming binder, a linker species to attach the binder to a high surface area carbon particle (black circle above) which in turn is in electrical contact with the electrode substrate

As introduced earlier, H_2O_2 is known to form adducts with urea to give a stable urea-hydrogen peroxide solid. The theoretical specific capacity of the system presented in Fig. 1.1 is dependent on the mass contributions of the binder, linker and high surface area carbon particulates (as with other battery electrode systems the theoretical specific capacity does not include consideration of the inert electrode substrate). For example, a theoretical specific capacity of 275 mAh g^{-1} was predicted for the two-electron reduction of H_2O_2 together with a 1000 m^2 g^{-1} carbon substrate and a binder in combination with a linker having a molecular mass of 185 g mol^{-1}.[35,47] This compares well with the theoretical specific capacity for the rechargeable alkaline nickel cathode of 298 mAh g^{-1}. This suggests that the New Cathode is based on a potentially viable premise; carbon particulates are available at 1000 m^2 g^{-1} and the molecular mass employed above is sufficient to account for a urea entity together with other chemical constituents to achieve the goal. Further, either decreasing the mass contributions from the binder and linker or increasing the specific surface area of the high surface area carbon particulates will lead to higher theoretical specific capacities for the New Cathode.

The novelty of this work was extended to incorporate a rechargeable aspect to the battery system. As far as can be determined there are no reports in the literature, in patent documentation or in battery industry reports that relates to development of rechargeable hydrogen peroxides-based cathodes.

The general commercial process of H_2O_2 production by anthraquinones (described in Section 4.1.1) cannot be readily adapted for the mass constraints of the New Cathode. A review of the literature (preceding the present study) in the development of the New Cathode concept fortuitously identified that oxoammonium species (+N=O) are capable of oxidising hydroxide ions to hydrogen peroxide.

$$2\ {+N{=}O} + 2OH^- \rightarrow 2\ N\text{-}O\bullet + H_2O_2 \qquad 1.24$$

This offers a potential route for replenishing H_2O_2 during charging, provided in turn there is a mechanism for reforming the oxoammonium species so that it would act overall as an electrocatalytic species. Further, given the nitroxide species undergoes redox processes, there is a need to fix this species at the New Cathode; a soluble form would likely promote self-discharge at the battery anode.

Consequently, in addition to designing and attaching a H_2O_2 binder to the carbon substrate, development of a New Cathode will require the parallel design and attachment of a nitroxide catalyst.

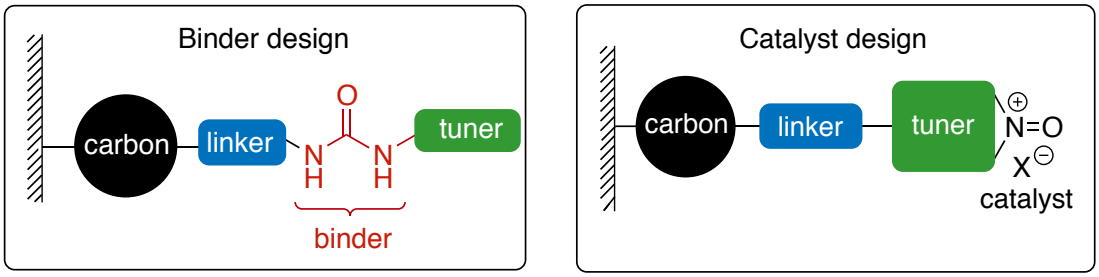

Fig. 1.2. Extension of the New Cathode binder concepts shown in Fig. 1.1 to include a tethered catalyst based on the assumption of use of urea binding

centre and a nitroxide catalyst, each of which will be tuned by substituent species and attached to a carbon particle surface by a linker species.

This study commenced with the premise that a urea moiety would provide the H_2O_2 binding capability through formation of an adduct and that a nitroxide moiety would provide the catalytic regeneration capability (Fig. 1.2). Both urea and nitroxide moieties have the potential to be 'tuned' with respect to performance on binding and regeneration performance. Attachment of an electron-donating or electron-withdrawing tuner and/or tuners of varying size or hydrophobicity will likely offer advantageous electrode performance.

Initially Pinson's method of diazonium attachment was considered for grafting these compounds to a carbon surface (Eq. 1.25).[48] This involves the electrochemical reduction of a diazonium species forming a new chemical bond to the surface (provided in detail in Section 5.1).

$$R\text{-}N_2^+ + e^- + \text{surface} \rightarrow R\text{-surface} + N_2 \qquad 1.25$$

To become viable on a large scale, the efficiency of the preparation of these materials must lead to a lower intrinsic cost for the New Cathode compared to the existing metal-based electrode systems. This costing would ultimately have to include consideration of the number and type of synthetic steps, cost of raw materials, purification and the appropriate treatment of the associated waste produced. Beyond this the synthesis of the binder and catalyst would need to be considered on an industrial scale and potential pathways analysed by provisional costs. This is beyond the scope of the present study. However, initial consideration of these factors was made.

Since the New Cathode is reliant on surface reactions rather than those for bulk phase, it is imperative that high surface area supports are used to increase the specific capacity of the new electrode material. This requires an appropriate mass proportion of the binder and catalyst in the electrode to be determined. In addition, an evaluation must be made of any other inert materials (for example

compounding materials for adhesion and cohesion of carbon particulates) with respect to transfer of electrical charge from a conductive high surface area carbon particle to adjacent carbon particles as well as through to the conductive electrode substrate.

In the present study the binder and catalyst were assembled on separate carbon surfaces; formation of the New Cathode would require incorporation of mixtures of two separately-derivatised carbon materials onto a single electrode substrate. Ultimately this might prove unsatisfactory since such an approach introduces the risk that H_2O_2 formed by the catalyst on one particle has sufficient time to diffuse into the bulk of the electrolyte (or disproportionate) before it can be bound to the binder on an adjacent particle. If this were to be found the case, then future work by others would require loading of binders and catalysts on the same carbon particle. The association constant of the binder towards H_2O_2 and the kinetics of forming H_2O_2 by the catalyst will determine the binder to catalyst content in the coated carbon mixtures.

1.6 Scope of this work

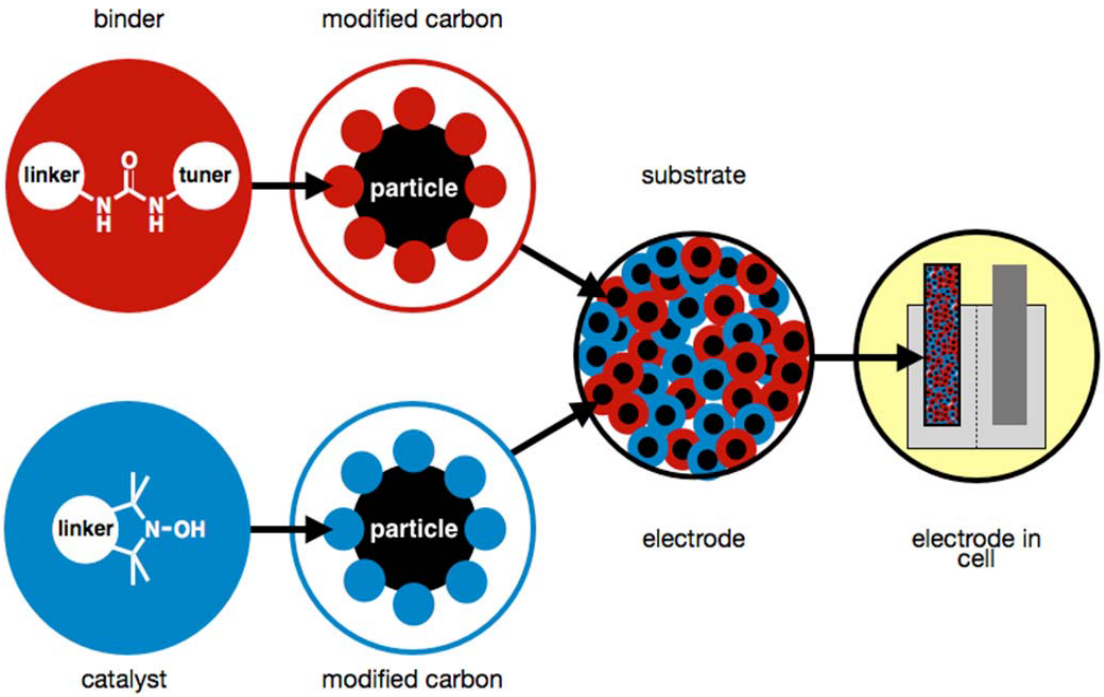

Fig. 1.3. Schematic representation of the key stages for the overall project in the development of a New Cathode. Copy (with permission) of a figure used in the

successful grant application to the Ministry of Business, Innovation and Employment (MBIE), Smart Ideas Fund, Application PROP-38127-SIP2-MAU. This figure in turn was based on a diagram contained in a confidential Patent Landscape Report prepared by Dr Stephen Parker, Patent Attorney with IPPC, Auckland, NZ in July 2012.

Once assembled the New Cathode must then be capable of performing against the following criteria:

- It must be capable of undergoing discharge and charge processes on an appropriate timescale.
- It must be energy efficient.
- It must be physically robust and remain dimensionally stable.

The metrics will depend on the situation prevailing in the stationary battery market at the time. A first estimate is that 5 hour discharge and charge rates, >85% energy efficiency and a cycle-life of 5000 cycles would likely be minimum criteria.

Over and above this, the economic performance will ultimately determine the success or not of the New Cathode. It is not unlikely that the stationary market will demand capital costing for energy storage in the range US$100-200/kWh.

Completion of the research and development stages for the overall project embodied in Fig. 1.3 are well beyond the scope of a single PhD thesis. Indeed, a minimum of 16 person years has been allocated (in terms of time and funding) to achieve the goal of developing a proof of concept battery electrode. The present project represents the starting point for the overall project and deals predominantly with the design and synthesis of the candidate binder and catalyst species. Some preliminary evaluation measurements are then provided to test the underlying premises of the New Cathode. Subsequent work by others will move the early research findings presented here through to the technical development necessary to incorporate the new chemistry into an electrode structure.

Alongside the progression of the work presented in this thesis, other project members undertook additional work to assist in the characteristic interaction of urea with H_2O_2. This work was performed and showed from a theoretical point of view the complexity of the urea-hydrogen peroxide interaction. Calculations were achieved using Amsterdam Density Functional (ADF) with a combination of functional and basis sets.[49] Preliminary studies by another project member were also performed on the simple model urea-hydrogen peroxide compound using spectroscopic analysis. The key points are described in Chapter 4 to assist in establishing a connection with the present work.[50]

1.7. Structure of this thesis

This introduction has outlined the general design and criteria of the proposed New Cathode. Given this project is a combination of organic synthesis and physical chemistry; the structure of each chapter is constructed in the style anticipated by those sub-disciplines of Chemistry.

Chapter 2, '*Synthetic methodology of structural binder*', involves the critical analysis and utility of a range of synthetic strategies to form substituted ureas. A library of compounds was synthesised for a range of binders with different tuner species. In addition a method for forming the linker containing the diazonium functionality for attachment to a carbon substrate was identified.

Chapter 3, '*Synthetic methodology of catalyst*', details the synthetic methodology for synthesis of 5 nitroxide-containing compounds. Diazonium functionalities were incorporated into the design for attachment to carbon substrates.

Chapter 4, '*Molecular Behaviour*', reports attempts to evaluate interactions between synthesised binders and H_2O_2 through use of a range of physical and analytical techniques. Also an initial investigation was made into the production of H_2O_2 with a nitroxide catalyst.

Chapter 5, '*Modification of Carbon Materials*', reports preliminary investigations into surface modification by diazonium coupling of low and high surface area

carbon substrates together with the subsequent electrochemical response of these materials.

Chapter 6, '*Conclusions and Future Directions*', provides an overview of the main findings of the present work and the recommendations for the subsequent work on the overall project to develop a New Cathode.

While fundamental research was required for this project, there was a clear commercial outcome intended for the overall project from the outset. The approach throughout this work, and the work by other researchers in this project was for the development of new intellectual property (IP) and the protection of this either through filing patents or maintaining trade secrets (or a combination of the two). Consequently, publications were not a primary aim and have not arisen yet from this work since IP protection has not yet been sought.

CHAPTER TWO

Structural Binder

2.1 Introduction

In the 1870s, Fenton reported one of the first syntheses of urea. This involved the reaction of anhydrous phosgene with ammonia (Reaction 1 in Scheme 2.1).[51] Using phosgene gas on an industrial scale is unattractive due to its toxicity. A more efficient and safer method based on the Bosch-Meiser process was developed in 1922.[52] Ammonia and carbon dioxide are directly combined in a two-step exothermic process that first forms an ammonium carbonate intermediate before giving urea (Reaction 2 in Scheme 2.1).[53] As high temperatures and pressures are required, this method is not used outside industrial settings.[54]

(1) $$COCl_2 + 4NH_3 \rightarrow (NH_2)_2CO + 2NH_4Cl$$

(2) $$2NH_3 + CO_2 \rightleftharpoons H_2N\text{-}COONH_4 \rightleftharpoons (NH_2)_2CO + H_2O$$

Scheme 2.1. (1) Fenton reaction. (2) Bosch-Meiser process.

Urea itself does not have the characteristics that are required for this project. Its poor stability in base and lack of functionality for attachment to a surface render this molecule inappropriate. However, a substituted urea might overcome these limitations. A bulky substituent could prevent nucleophilic attack at the carbonyl group while a second substituent could act as a linker to the surface.

Substituted ureas are an important class of organic molecule, and can be prepared by a variety of different synthetic routes. They occur in many natural products[55] and are widely used in the pharmaceutical,[56] agrochemical and biological industries[57] due to their herbicidal,[58] antidiabetic[59] and peptidomimetic[60,61] properties (Fig. 2.1).

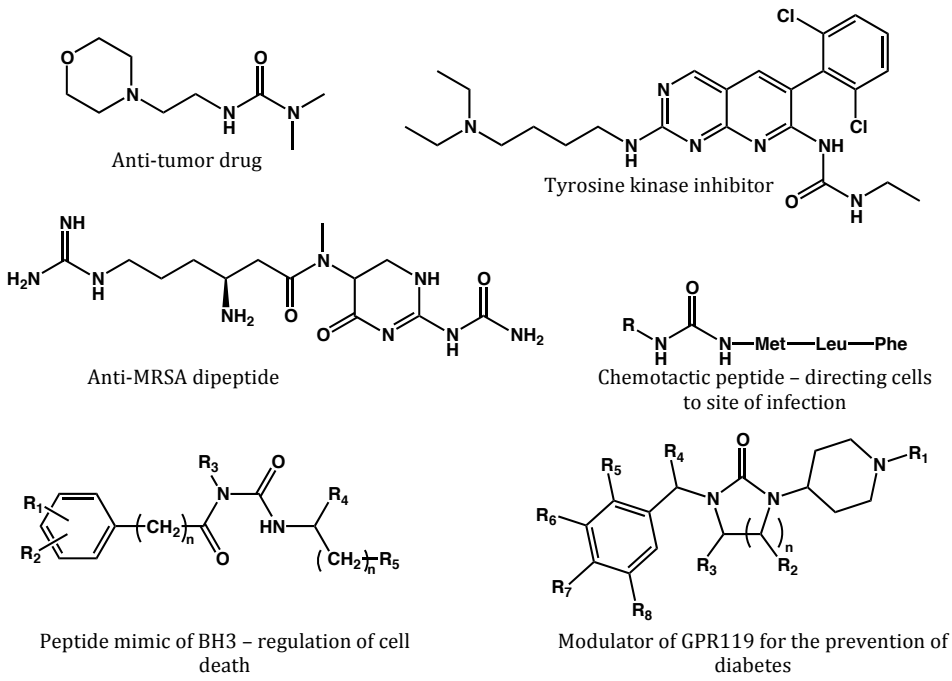

Fig. 2.1. Examples of urea-containing compounds used in industrial applications.[56-61]

2.1.1 Binder design

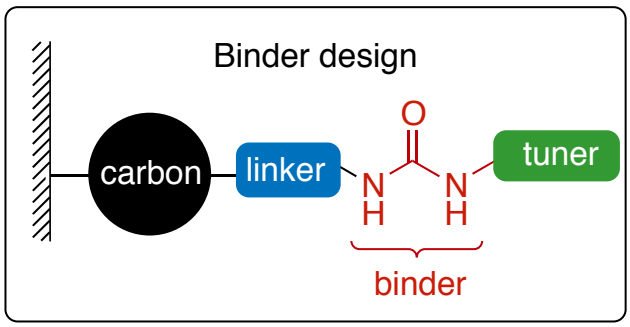

Fig. 2.2. Design of the H_2O_2 binder for attachment to carbon surfaces.

The design of the binder requires the nitrogen atoms of the urea to be connected to a linker and tuner (Fig. 2.2). The tuner is to adjust the strength of binding of the H_2O_2 to the urea, while the linker joins the urea functionality to a surface. One, or both, groups must also protect the urea from hydrolysis. This requires the synthesis of a non-symmetrical urea.

Symmetrical ureas are readily prepared using the classical phosgene method. Non-symmetric ureas are a more difficult proposition. Most methods suffer from competing homo-coupling as well as the desired cross-coupling. It is difficult to activate one half of the molecule and smoothly react it with the desired coupling partner. Most methods involve highly reactive intermediates and are plagued by side products and reactions. Industrial processes still rely on highly toxic phosgene in their synthetic processes due to its high efficiency and the high cost associated with the substitution of chemicals and equipment for alternative, safer reagents.

Two strategies will be considered for the attachment of a substituent (Fig 2.3); Addition of R' to a pre-existing urea functionality (blue), or the formation of a C–N bond (red) to form the urea moiety. Forming the bond in blue requires either a strong Lewis acid (eg. $AlCl_3$),[62] $NaNO_2$ with an acid catalyst,[62] or in the case of forming a new N-N bond, addition of N_2H_4 to form a semicarbazide.[63]

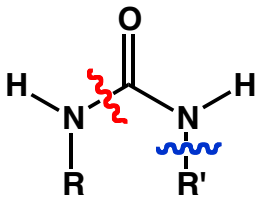

Fig. 2.3. Modified urea showing the two disconnections that form a di-substituted urea. Reaction with a pre-existing urea (blue) or formation of a C–N bond to form the urea moiety (red).

Synthetically it is more convenient to form the N–C bond to the carbonyl moiety (red) as this allows more variety and versatility of adjoining R groups. A variety of ureas can be made rapidly, permitting formation of a library of molecules that is required for further investigation in this project.

2.2 Synthesis of Unsymmetrical Ureas

Below is a critical discussion of the main synthetic routes to unsymmetrical ureas and a rationale for our choice of methodology. The decision was based on a

number of criteria including: safety of reagents, ease of synthesis, ability for variability, potential for up scaling, and time. A recent review by I. Gallou discusses alternative reagents used for forming these unsymmetrical ureas.[64]

2.2.1 Isocyanate Formation

The key to the majority of syntheses of unsymmetrical ureas is the formation of an isocyanate intermediate and its reaction with a suitable amine (Scheme 2.2). Medicinal chemists frequently use the combination of an isocyanate with a variety of amines to prepare libraries in search of a lead compound.[65,66] The electrophilicity and linear arrangement of the isocyanate group allows for nucleophilic attack at the carbon. This precedes a rearrangement to form the urea (Scheme 2.2). Care needs to be taken as moisture can cause decomposition of the isocyanate to CO_2 and an amine that can participate in the formation of symmetrical ureas.

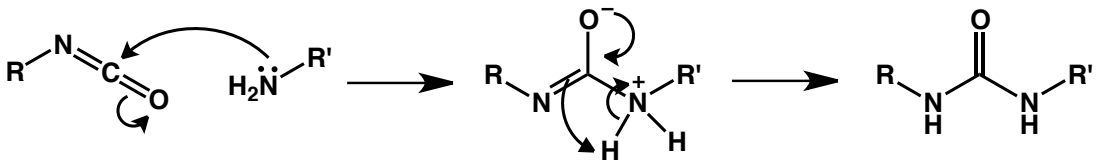

Scheme 2.2. General scheme for nucleophilic addition of an amine to an isocyanate followed by a rearrangement to form a substituted urea.

What differentiates the various syntheses is how the isocyanate is formed. Classically, phosgene (**I**) has been used to convert amines into isocyanates (Scheme 2.3). The electrophilic character of phosgene results in the formation of intermediate **II**, which collapses to give the isocyanate **III**. The isocyanate can be attacked by a second equivalent of the initial amine to give a symmetric urea or a different amine to give the unsymmetrical product. This requires a base such as pyridine or NEt_3 to neutralise the resulting HCl. There are many disadvantages associated with phosgene including its high toxicity and the inconvenience of handling a gas.[67,68] As a result newer routes have been established which use safer and less reactive reagents.

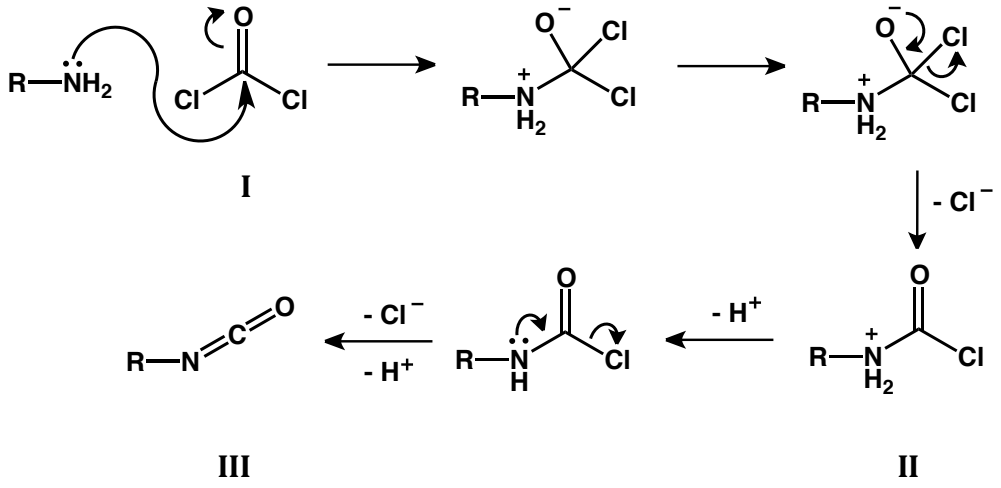

Scheme 2.3. Isocyanate formation from phosgene and an amine through intermediate **II**.

Triphosgene (**IV**), which is a solid at room temperature, is a safer alternative for phosgene (**I**) (Fig. 2.4).[67] Although, it can react with moisture and other nucleophiles to produce phosgene, therefore, similar operating procedures and safety precautions should be followed.[69]

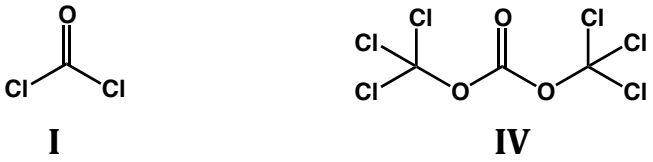

Fig. 2.4. Phosgene (**I**) and triphosgene (**IV**).

Another phosgene replacement is *N,N'*-carbonyldiimidazole (CDI) which has been reported as a mild, safe and versatile reagent for the synthesis of unsymmetrical ureas.[70-72] Unfortunately, carbamoyl imidazoles are less reactive than the analogous acyl chloride and need to be activated before substitution with a second amine will occur (Scheme 2.4). Activation is by N-alkylation with MeI, or analogous electrophile, giving a resonance-stabilised imidazole salt (**V**). This salt is now reactive towards nucleophilic substitution of a second amine compound to form the desired urea. As this method requires activation, nucleophilic substitution is controlled through a step-wise mechanism enabling

the use of two different amine reactants. These compounds readily react with primary and secondary amines at room temperature forming the desired unsymmetrical ureas in high yields (72-99%).[71]

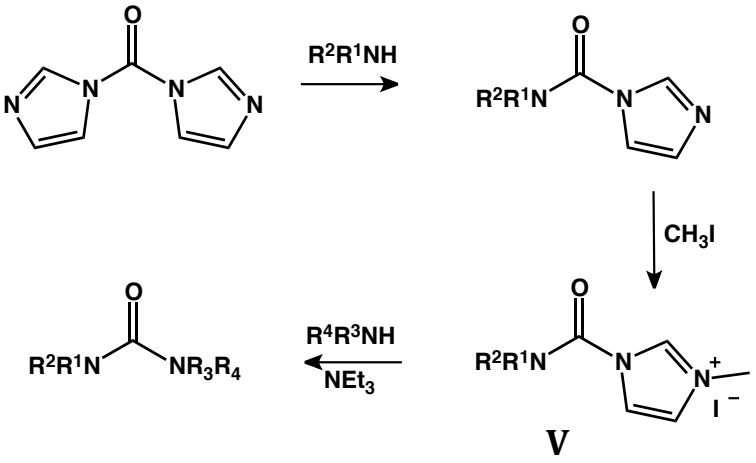

Scheme 2.4. Step-wise formation of a tetra-substituted urea using CDI.

Alternatively, there are a number of reactions that transform carboxylic acid derivatives into isocyanates. These all share a common rearrangement mechanism and involve a nitrogen group that possesses a suitable leaving group. The most common of these is the Curtius rearrangement, which expels nitrogen gas from an acyl azide (Scheme 2.5).[73] This rearrangement requires heating, especially for aromatic acyl azides,[74] which are known to be more stable than their aliphatic counterparts. Temperatures over 75 °C are required to promote the rearrangement for an aromatic acyl azide, otherwise amide formation competes as the external amine simply displaces the azide.

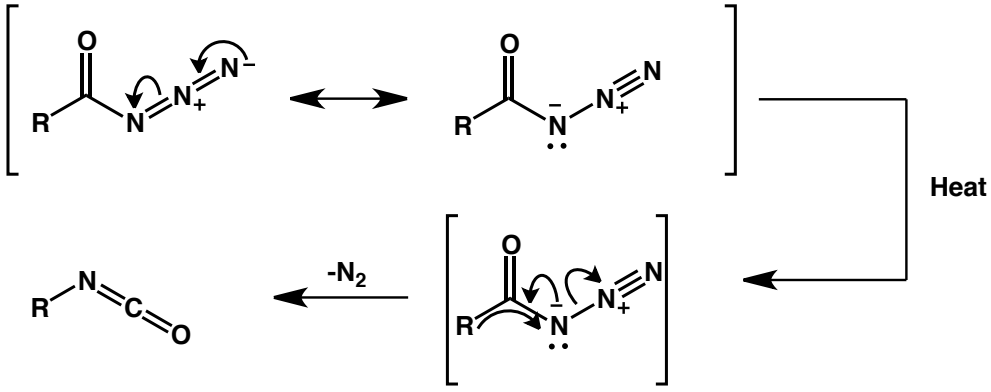

Scheme 2.5. Curtius Rearrangement mechanism.

The Lossen rearrangement converts hydroxamic acid derivatives into the corresponding isocyanate. This is based on the activation of hydroxamic acid by converting the OH group to a good leaving group and deprotonating the N-H functionality. Chemically this is normally achieved by O-acylation or phosphorylation, but milder reagents such as bromodimethylsulfonium bromide (BDMS) and N-methylmorpholine (NMM) are also possible (Scheme 2.6).[75] As the hydroxamic acid is normally formed from a carboxylic acid or acyl chloride, it seems impractical to add extra steps to the synthetic route if this method was used.

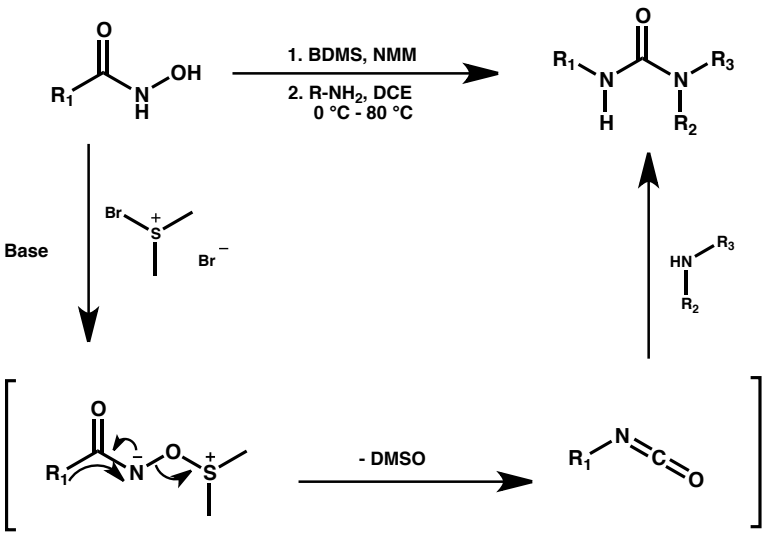

Scheme 2.6. Lossen rearrangement with BDMS, NMM and an amine to form a substituted urea.

In an alternative method, the Hoffman-like rearrangement of amides is initiated by powerful oxidising agents, such as hypervalent iodine, to synthesise ureas and carbamates.[76] Formation of the isocyanate from an amide is through elimination of the iodosylbenzene followed by rearrangement and deprotonation to form the desired intermediate (Scheme 2.7). This supposedly simple method is favourable due to its low toxicity, short reaction times and favourable yields. An advantage of this method in the formation of a library of molecules is its ability to prepare symmetric, asymmetric and heterocyclic ureas. However, the explosive properties and use of the uncommon iodosobenzene reagent makes the feasibility of industrial application low.

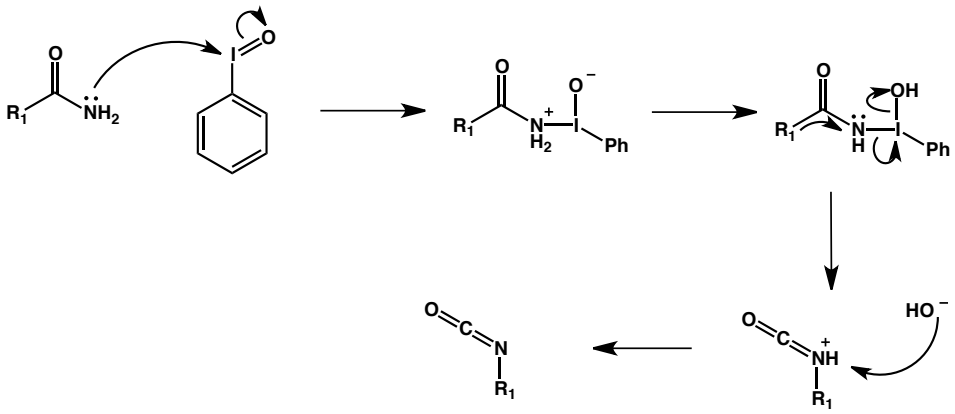

Scheme 2.7. Proposed mechanism of isocyanate formation by reductive elimination and rearrangement of the iodosobenzene derivative.

Glebowska *et al.* describes a nitrosation of 1,3-dimethylurea with $NaNO_2$, H_2SO_4 and substitution with an N-alkylamine (Scheme 2.8).[62] This falls under the category of both substitution of a pre-existing urea and formation of an isocyanate. Activation of 1,3-dimethylurea by nitrosation forms a N-nitrosoalkylurea intermediate.[77] This intermediate readily decomposes to an isocyanate, retaining one original substituted group. Although this method is advantageous if a change of substituted alkyl group is required, it is heavily plagued by steric and conformational restraints.

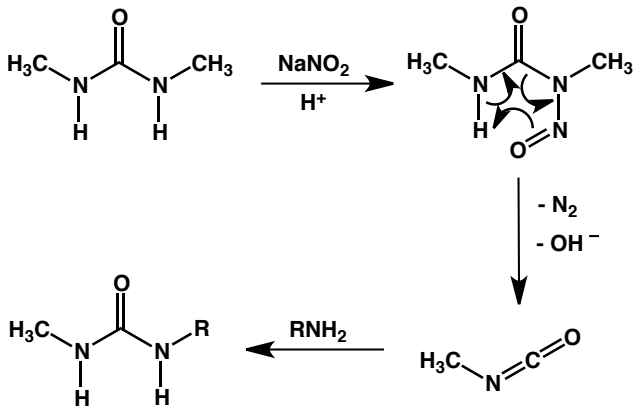

Scheme 2.8. Activation of 1,3-dimethylurea by nitrosation and subsequent substitution.

2.2.2 Alternatives to Isocyanates

An alternative route to ureas that avoids the synthesis of an isocyanate involves the substitution of a carbamate or a pre-existing form of urea. This method favours the addition of secondary amines in which making the isocyanate is impossible. Activated carbamates such as *p*-nitrophenylcarbamate (R-NHCOO(*p*-$NO_2C_6H_4$) form a urea on reaction with a second amine component; however, reactivity decreases on the addition of more substituents on the amine. Lee *et al*. have described a methodology that allows the conversion of carbamates to ureas by reaction with aluminium amides.[78] Normally such a transformation requires much harsher conditions, such as the formation of carbamoyl chloride. The Lewis acid-mediated reaction showed promise in the formation of di-, tri- and tetra-substituted ureas from a range of widely used carbamate protecting groups (>90% yields). Unfortunately, efficiency is dependent on nucleophilicity and steric properties of the amine, although extending the reaction time and increasing the temperature produces the product in similar conversion rates to simpler amines.

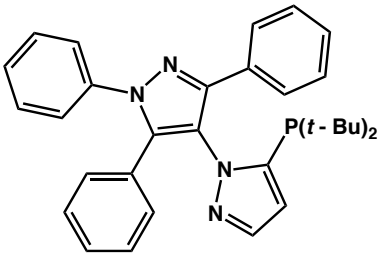

Fig. 2.5. Bippyphos ligand.

Kotecki *et al*. developed a general method for the preparation of substituted aryl ureas by Buchwald-Hartwig palladium-catalysed amidation (Scheme 2.9).[79] They reported the N-arylation of ureas using aryl and heteroaryl chlorides (or bromides) with the bippyphos ligand (Fig. 2.5) and $Pd_2(dba)_3$ to give desired ureas in high yields (>99%).

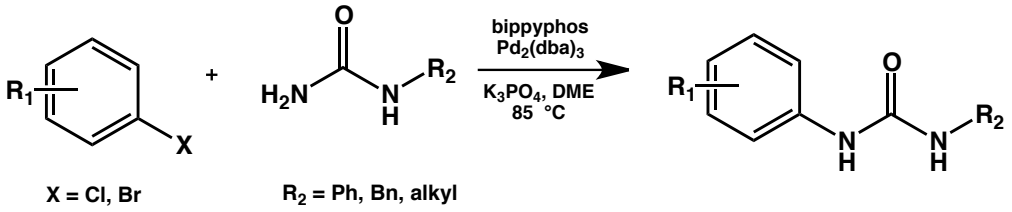

Scheme 2.9. N-arylation of urea using a heteroaryl chloride or bromide.

Although this method is high yielding and relatively inexpensive, the specificity of the ligand for a limited number of aryl compounds is evident as isolatable yields are greatly affected by steric hindrance in addition to the functionality at R_1 and R_2. Activation of the aryl halide is not necessary and the coupling with either electron donating or electron withdrawing groups on the aryl halide is possible. Notable limitations include sterically-hindered aryl halides that reduce conversion rates significantly (<29% for 1-chloro-2,6,-dimethylbenzene) and due to slow reaction rates resulted in disproportionation of the product into *N,N'*-diphenylurea and *N,N'*-diarylurea.

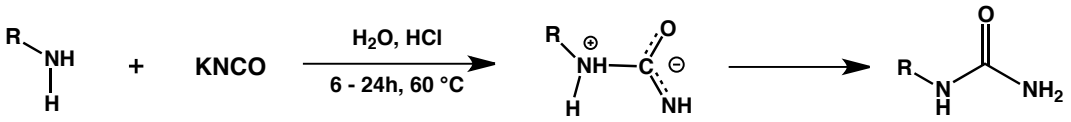

Scheme 2.10. Substituted urea formation by reaction of a primary amine and potassium cyanate through a zwitterion intermediate.

In 2010, De Luca reported the conversion of amines to mono substituted ureas by treatment with sodium or potassium cyanate in an aqueous acidic solvent (Scheme 2.10).[58] This relatively straightforward reaction proceeds quickly with aliphatic amines, but requires much longer reaction times for aromatic amines. This was explained by the rate determining step involving the proton transfer of the zwitterionic intermediate, which for weakly basic aromatic amines does not occur at low pH levels.[80] When using aromatic amines, acetic acid was substituted for HCl to improve results as the reaction of weakly basic nucleophiles with cyanic acid is pH dependent. Unfortunately, this reaction is slow and microwave irradiation is needed to reduce reaction times.

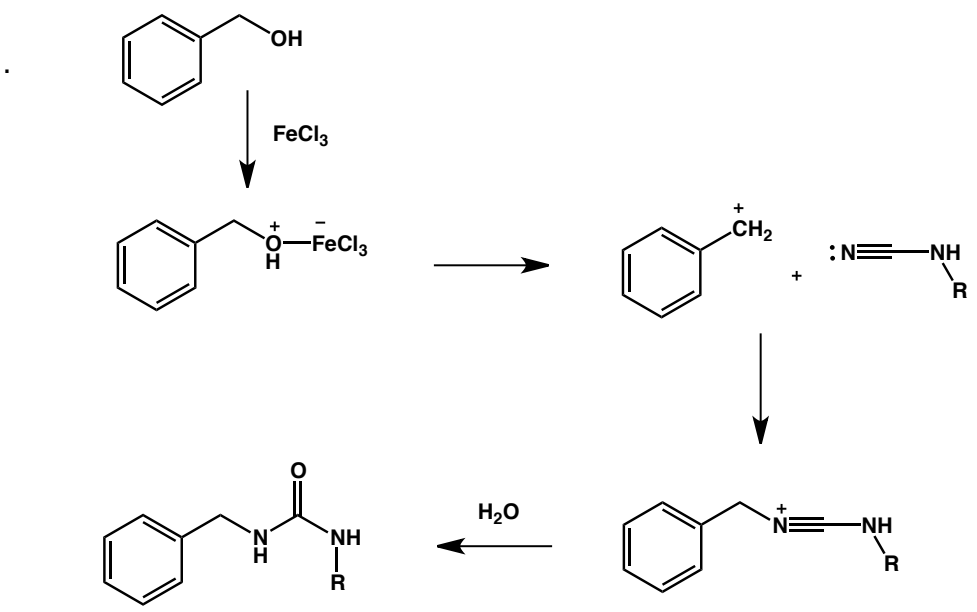

Scheme 2.11. Ritter-like reaction with iron(III) to form unsymmetrical ureas.

Basavaprabhu *et al*. have explored the use of iron(III) in the synthesis of unsymmetrical di- and trisubstituted ureas in a variation of the Ritter reaction.[81] The Ritter reaction is a classical C-N bond formation that transforms a nitrile into an N-alkyl amide, under strongly acidic conditions. The strong Lewis acid, $FeCl_3$, creates a carbocation, which is attacked by the cyanamide resulting in the formation of a nitrilium ion. Hydrolysis of this intermediate forms the desired substituted urea in variable yields. The authors assume that this method will work for all alcohols, yet it is clearly dependent on the stability of the carbocation. Benzyl alcohol (Scheme 2.11) is utilised to form the benzyl cation which is stabilised by delocalisation of the charge due to the overlap of the empty p-orbital in the π bond. An alternative example uses *t*-butyl alcohol that has a stabile tertiary carbocation due to hyperconjugation or inductive effects, although this requires 0.5 eq. of acetic acid to form an ester, promoting this carbocation formation. The introduction of an electron-withdrawing group (EWG) onto the cyanamide decreases its reactivity, however high yields are still obtained for a small variety of coupling reactants. The limitations that the alcohol requires the appropriate carbocation stability and the lengthy reaction times restrict the capability to form a large library of compounds.

2.3 Physical Properties

2.3.1 Urea

Urea has been identified as an effective binder for hydrogen peroxide, as demonstrated by the commercially available compound urea-hydrogen peroxide (UHP), an organic solid used for the addition of peroxide in non-aqueous systems. To understand how our proposed molecules are going to bind to H_2O_2, we first must look at the properties of urea and the interaction between urea and H_2O_2. This may provide guidelines when designing new substituted ureas. The ability for urea to form an adduct is due to its ability to form hydrogen bonds. Urea has four hydrogen bond donors; the two hydrogens on each nitrogen, and 4 potential hydrogen bond acceptors, the two lone pairs of the nitrogen atoms and two of the electronegative oxygen (Fig. 2.6). The lone pairs of electrons on the nitrogens are delocalised, which give some physical properties mentioned below.[82]

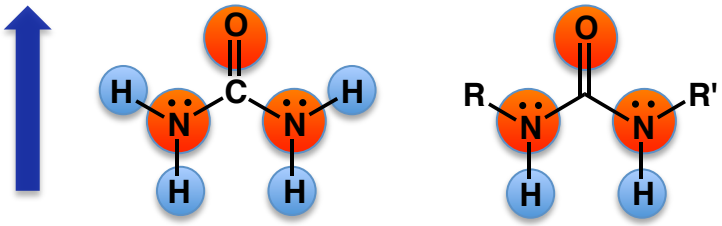

Fig. 2.6. Urea (left) and di-substituted urea (right). Orange atoms are hydrogen bond acceptors; blue atoms are hydrogen bond donors. Blue arrow indicates direction of dipole moment.

2.3.1.1 Conformations of Urea

The ability for the C–N bond to rotate allows for 4 conformations of urea (Fig. 2.7). In a simple urea the energy of all conformations are the same. In a substituted urea the energy difference between s-*cis* and s-*trans* conformations will determine which conformation is preferred.

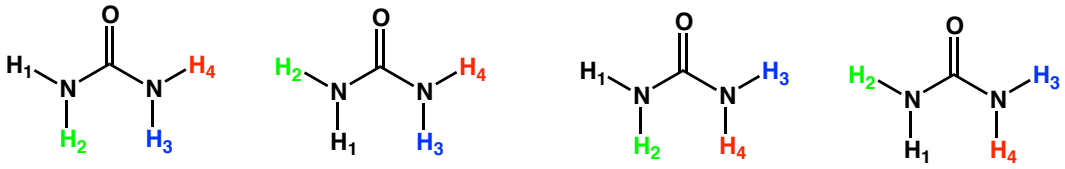

Fig. 2.7. Four conformations of urea rotating around the C – N bond.

Urea is known to have a non-planar C_2 symmetry in the gas-phase, but is planar in the crystal structure. The interaction with the nearest neighbours of urea is alone insufficient to induce the molecule to become completely planar. It requires long-range crystal packing forces.[83] The conformation in a di-substituted urea is directed by the substituents. Diphenylurea (DPU) exists in a *trans-trans* conformation promoting a more planar structure (Fig. 2.8).[84,85]

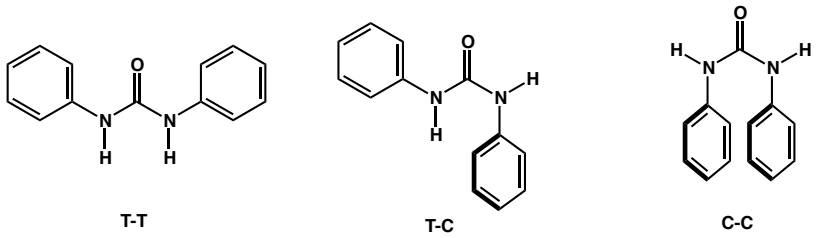

Fig. 2.8. Conformations of diphenylurea in *trans-trans* (T-T), *trans-cis* (T-C) and *cis-cis* (C-C) orientations.

2.3.1.2 Resonance forms and diamagnetic susceptibility of urea

The measurement of a dipole moment (μ) indicates the net polarity of a molecule. This is determined by the charge separation within the molecule and how far apart they are. The higher the dipole moment the more polarised the compound, e.g. NaCl has a large charge separation (9.0 debyes) characteristic of a strong ionic bond. Urea has a dipole moment of 4.65 debyes, which is more than 1 unit higher than a simple amide.[86] This can be interpreted by considering the contribution of a number of resonance forms. In particular the charge separation between the positive nitrogen and negative oxygen atoms at each extreme of the resonance form (Fig. 2.9). The net dipole moment of urea is in the direction of the carbonyl oxygen (Fig. 2.6).

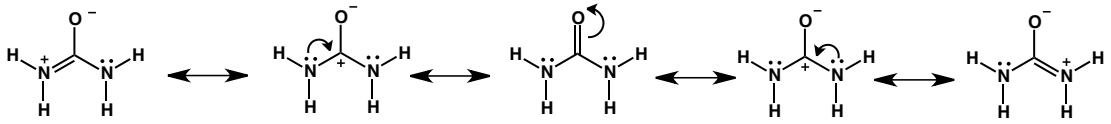

Fig. 2.9. Resonance structures of urea.

Symmetrical di-substituted ureas, such as DPU, have symmetrical charge separation forms giving an overall moment of 4.6 debyes, comparable to urea.

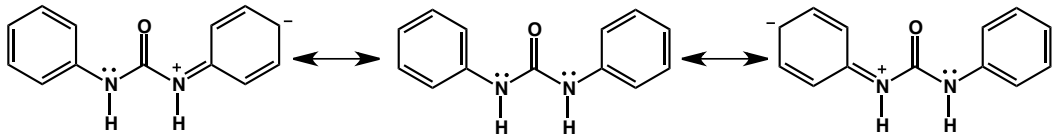

Fig. 2.10. Resonance structures of DPU showing extended conjugation.

DPU is stabilised by additional conjugation with each phenyl ring (Fig. 2.10). Conjugation permits the distribution of the negative charge through one phenyl ring to the other, while both the nitrogens can remain positively charged and the oxygen negatively charged (Fig. 2.11).[86] The contribution from both resonance forms assists to balance out the resultant moment to give a higher than expected dipole moment.

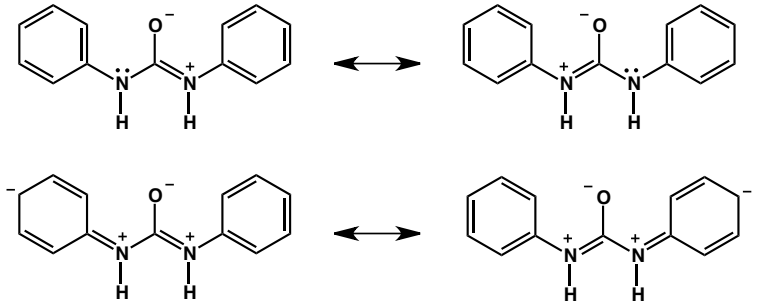

Fig. 2.11. Resonance structures of DPU showing additional delocalisation.

The addition of substituents, in particular those with different electronic properties, produces an unsymmetrical urea where the moment decreases due

to opposing forces. As this is likely to decrease dramatically, it may affect the intermolecular dipole-dipole interactions with hydrogen peroxide.

2.3.2 Structure of Urea complexes

2.3.2.1 UHP complexes

As urea is both a good hydrogen bond donor and acceptor, it readily forms adducts as demonstrated by co-crystal formation. Ureas have been incorporated into anion sensors,[87,88] photochemistry[89] and macro cyclic host molecules,[85,90] because of their ability to form strong intermolecular bonds with a variety of guests. Urea phosphate ($CO(NH_2)_2.H_3PO_4$) is a mass-produced fertilizer for the simultaneous injection of phosphorus and nitrogen into soil. This is a 1:1 adduct based on hydrogen bonding, that when dissolved in water dissociates.

Urea hydrogen peroxide (UHP) is an adduct formed from urea and aqueous hydrogen peroxide, without the loss of atoms. Tenetar first produced the stable adduct of UHP in the early 1900s however, the crystal structure was not described until 1941 by Chia Si Lu.[91] Hydrogen peroxide has two hydrogen bond donors and two acceptors that are able to form multiple interactions with urea. The crystal structure of the UHP complex identifies the four hydrogens in urea to be hydrogen bonded with each oxygen atom of the hydrogen peroxide (Fig. 2.12). Theoretical MP2 (Møller-Plesset) and DFT (density functional theory) calculations by Dobado predicted five additional structures of UHP in a 1:1 urea:H_2O_2 complex (Fig. 2.12, **A**-**F**). Two of these complexes have a lower binding energy than that found in the crystal structure (**E** and **F**). Both these structures showed an O-H---$O_{(Urea)}$ carboxyl hydrogen bond plus an additional H-O---$NH_{(Urea)}$ bond. As the crystal structure correlates to complex (**A**), additional hydrogen bonding, packing forces and a larger dipole moment must account for the stability in the solid state. As the calculations are performed in the gas phase, the interpretation is limited. Our target binder will be in an aqueous phase and the similarity between H_2O_2 and H_2O binding has not been taken into consideration for these calculations.

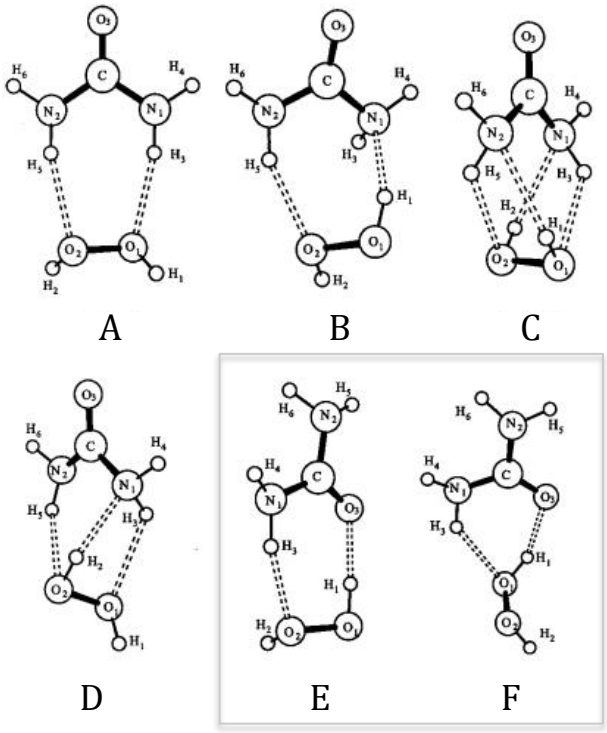

Fig. 2.12. Structures of UHP shown from calculations to be possible complexes. **A** is the crystal structure, **E** and **F** have the lowest binding energies. Reprinted with permission from Dobado *et al*.[92] Copyright 1998 American Chemical Society.

2.3.2.2 Structure of Substituted Urea Complexes

The di-substitution of urea reduces its number of hydrogen bond donors by half. This decreases the available interaction sites when binding to hydrogen peroxide, suggesting that the conformation of the donors and strength of the interaction will become more important.

Etter has described the adducts of various diarylureas and guest molecules.[93] As in the crystal structure of UHP, diarylureas also prefer the NH protons to adopt an *anti* relationship to the carbonyl. The co-crystal of 1,3-bis(*m*-nitrophenyl)urea (**VI**) and THF demonstrates the typical bonding arrangement (Fig. 2.13). This orientation permits the acceptor of the guest molecule to form two hydrogen bonds with each N-H proton. Etter's findings show it is essential to have at least one electron-withdrawing group on the aryl ring in order for complex formation. This induces intra-molecular stabilisation. The strength of the proton acceptor in

the urea is dramatically reduced due to the weak CH_{Ortho}---O occurring in response to binding the guest molecule.

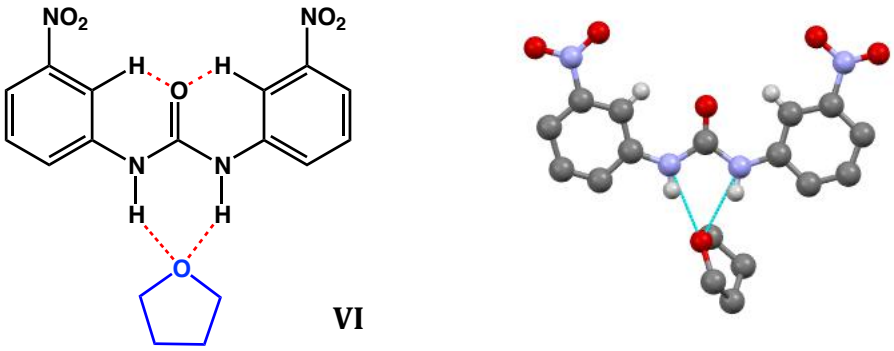

VI

Fig. 2.13. Left: 1,3-Bis(*m*-nitrophenyl)urea complex with THF. Hydrogen bonding shown in red. Right: Crystal structure of complex. (Details of synthesis and X-ray data in experimental).

Trends in formation of diarylurea adducts are not explainable simply from size constraints or pK_a. For example, N-H protons should be more acidic with *para*-NO_2 groups but these derivatives are less effective than *meta*-NO_2. Weak proton acceptors such as water, ethyl acetate and alcohols do not form co-crystals with diarylureas as they are unable to overcome the strength of the internally hydrogen-bonded urea carbonyl oxygen. In this instance homo coupling of the diarylurea is preferred.

Based on the results presented by Etter, binding of a guest compound to a diarylurea involves several factors. As hydrogen peroxide has both hydrogen bond acceptors and donors it is uncertain how it will interact with the urea.

2.3.3 Equilibrium between urea + H_2O_2 and UHP

The equilibrium constant for the simple urea and hydrogen peroxide complex has not been investigated experimentally. This is possibly due to the challenges characterising UHP. The equilibrium of the formation of UHP is:

$$\text{Urea} + H_2O_2 \rightleftharpoons \text{UHP} \qquad 2.1$$

$$K = \frac{[\mathrm{UHP}]}{[\mathrm{Urea}]\,[\mathrm{H_2O_2}]} \qquad 2.2$$

The aim of the initial stages of the project was to distinguish which substituted ureas would give the highest equilibrium constant, *K*. A high *K* value favours the right hand side of the equilibrium, suggesting there are more products than reactants. In the proposed battery system a high formation of product is needed, as residual H_2O_2 is able to short circuit the system.

2.4 Project Constraints

As this project is for a commercial purpose, it requires strict guidelines on materials, molecular constraints and functionalities.
Limitations include the following:

- Size of binder must be < 185 $gmol^{-1}$ in order to give a storage capacity on a 1000 m^2 g^{-1} surface, of 0.217 Ah g^{-1}. The current benchmark cathode in rechargeable alkaline batteries is the nickel cathode at 0.289 Ah g^{-1}.
- It must have the capability to attach to a surface.
- The binder must be stable to the basic conditions found in the proposed battery system. It must survive in 7M KOH for an extended period of time.
- The synthesised ureas must be tuneable to allow for modifications to permit stronger binding to H_2O_2.
- The binder must not irreversibly react with, or be destroyed by H_2O_2.
- The binding to H_2O_2 must be a reversible system in order for the battery to discharge.

2.5 Results and Discussion

As outlined earlier, the design of our ureas had to meet a number of requirements. As a result our initial targets were 1,3-disubstituted ureas (R,R' – Fig. 2.14). This target retains the two N-H atoms and the adjacent carbonyl oxygen permitting hydrogen bonding to the H_2O_2, as described by Dobado.[92] It was believed that this would maximise the chances of binding.

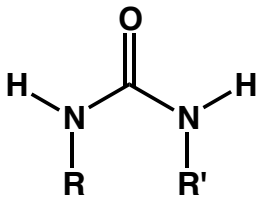

Fig. 2.14. Di-substituted urea.

A phenyl ring was to be used for one substituent, as it possessed a number of attractive properties including rigidity and ease of further functionalisation. A benzene ring is planar in nature, therefore allows side-by-side stacking when attached to a surface (Fig. 2.15). Stacking of the phenyl ring allows vertical stacking through covalent attachment to the surface, maximising π-π interactions. It may also stack face-on using non-covalent adsorption through van der Waals interactions. Until further investigative studies are performed (discussed in Chapter 5) the mode of stacking on the surface is unknown.

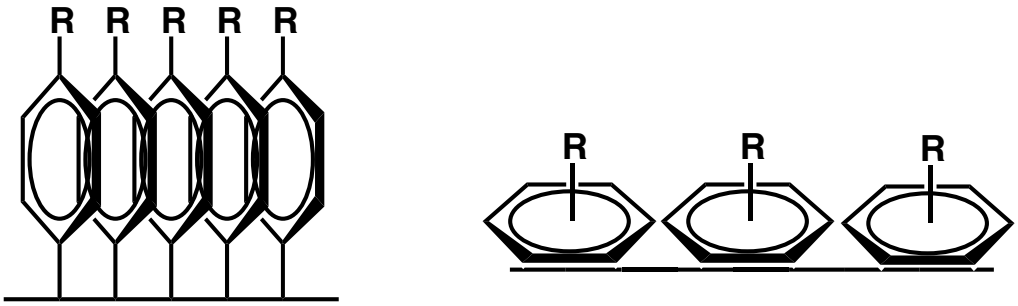

Fig. 2.15. Types of side-by-side stacking. Vertical covalent attachment and face-on adsorption of phenyl compounds on a surface.

One of the simplest and most convenient routes to the phenyl-substituted ureas utilises the Curtius rearrangement. Starting from either a carboxylic acid or acyl chloride, the rearrangement gives an isocyanate that can react with a primary amine to give the di-substituted urea. We have used this method to synthesise the library of compounds.

The reactivity of the isocyanate significantly decreases in the order 1° > 2° aliphatic amines > 1° aromatic amines. The reactivity can be tuned by incorporating substituents that alter the electrophilic character of the carbon in the isocyanate functionality. Electron withdrawing substituents increase the electrophilicity on this carbon. In the present study R will predominantly be an aromatic ring, correlating to the linker in the binder design (Fig. 2.14). Therefore, phenylisocyanate has been used as the electrophile. Its stability is largely due to the additional delocalisation of the negative charge on the aromatic ring (Fig 2.16). This allows urea formation to be a more readily achieved and efficient reaction.

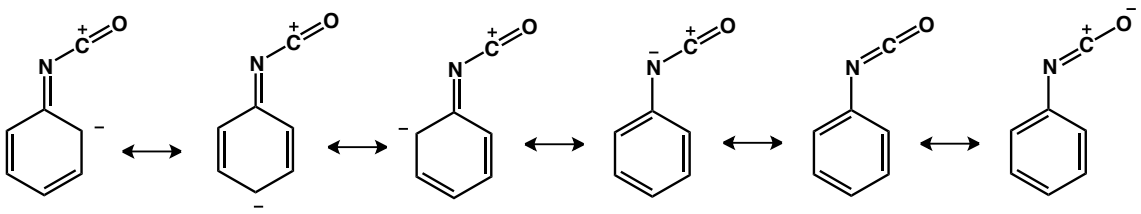

Fig. 2.16. Resonance forms of phenylisocyanate.

Steric hindrance also plays an important role in the rate of reaction and its efficiency. The proximity of bulky groups to the isocyanate will slow addition. A compromise between the ease of synthesis, ability for binding and its survival in basic conditions will determine the effectiveness of the substituted urea.

Incorporation of groups that have a possibility of binding H_2O_2 directly, although is not ideal for comparison studies, must also be taken into consideration. Incorporation of one or multiple electron-withdrawing or electron-donating groups may assist in tuning the hydrogen bonding ability of the urea moiety to better meet the requirements of adduct formation. This will be achieved by combining phenylisocyanate with a variety of amines to make up the tuner proportion of the binder design.

2.5.1 Synthesis of Substituted Ureas

Initial objectives were to synthesise a variety of di-substituted ureas from phenyl isocyanate and the corresponding amines. It is unclear how each urea will bind hydrogen peroxide, as there are no studies of this phenomenon to the best of our knowledge. Therefore, it is desireable to synthesise a wide range of ureas that would permit us to define general binding guidelines, distinguishing a good binder from a poor one.

The synthesis of phenylisocyanate (**S1**) from benzoic acid (**S2**) utilised oxalyl chloride and catalytic DMF (N,N'-dimethylformamide) to form benzoyl chloride. The acyl chloride was immediately reacted with sodium azide in dry toluene to give the acyl azide (Scheme 2.12). Curtius rearrangement of the acyl azide at an elevated temperature (90 °C) formed phenyl isocyanate which, due to the questionable stability, was not isolated before addition of the corresponding amine. Purification of the subsequent urea was achieved either by recrystallisation, or separation by column chromatography.

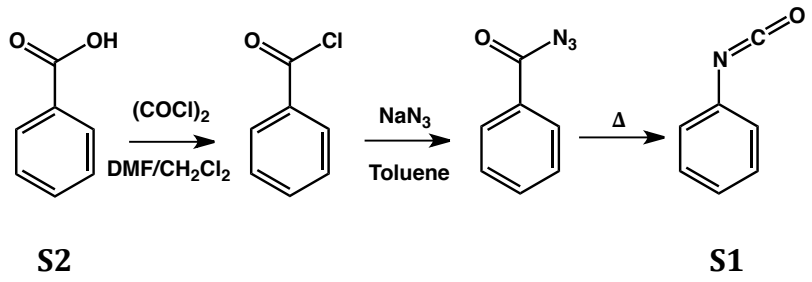

S2 **S1**

Scheme 2.12. Scheme of the reaction from benzoic acid to phenylisocyanate.

While it was possible to make phenylisocyanate, and in initial experiments this was done, it was more convenient to use commercially available **S1**. Broad ranges of amines were reacted with phenylisocyanate that ranged from small alkyl chains to large bulky substituents with differing electronic properties (Scheme 2.13). Urea formation was a relatively high yielding reaction in most circumstances. Amines with an electron-withdrawing group (EWG), such as 3,5-bis(trifluoromethyl)aniline, required increased reaction times in comparison to amines with an electron-donating group (EDG). This reactivity is directly due to

the nucleophilicity of the amine, although in cases such as the o-nitroaniline, the steric bulk of the nitro group also contributes to the lower reactivity. As the objective was to synthesise a library of compounds, the requirement for optimised reactions in each case was minimal.

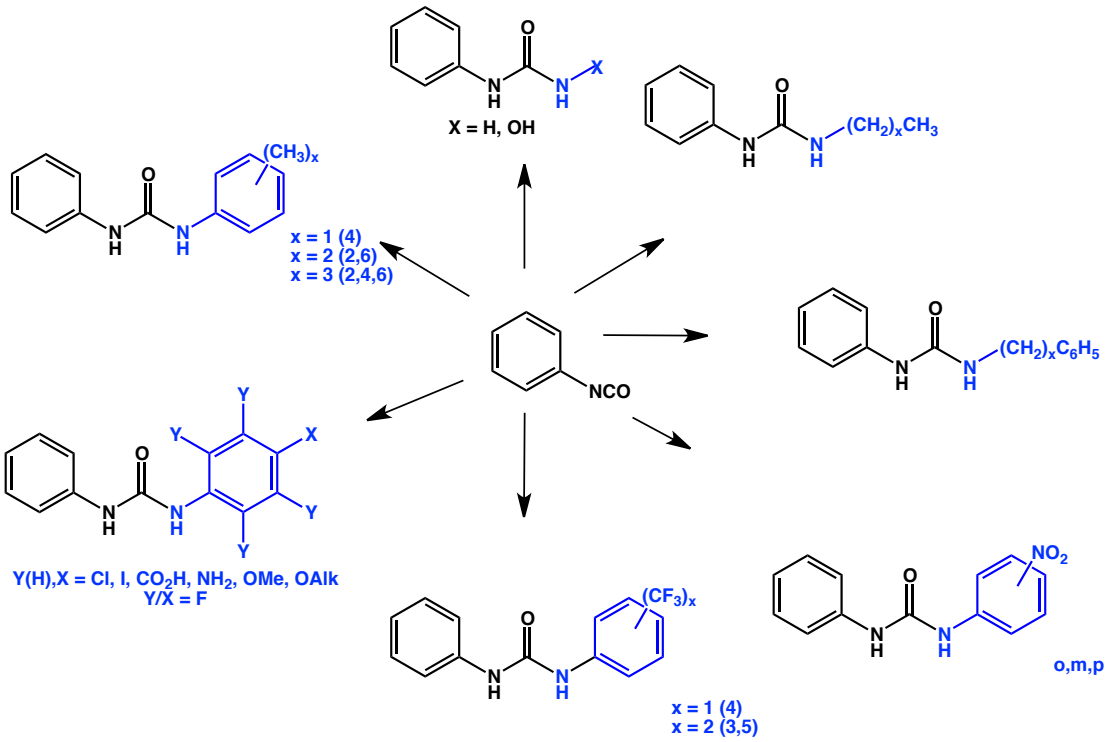

Scheme 2.13. Reaction scheme of phenylisocyanate with a variety of amines.

There was little guidance to the exact hydrogen bonding arrangement of the ureas with hydrogen peroxide, but one of the goals of this part of the project was to try and identify a pattern. It was anticipated that there would be a correlation between the N-H shift in the ^{1}H NMR to the ability of the binders to interact with H_2O_2. Working under the assumption that H-bonding between the H_2O_2 oxygen and urea N-H was important; it was assumed that EDG would reduce the acidity of the N-H and thus its H-bonding ability. If this were correct, only a negligible change in chemical shift of the N-H would be seen. The ^{1}H NMR of the ureas was not satisfactory in $CDCl_3$ as fast exchange of the N-H protons meant that N-H peaks were not consistently observed. Furthermore, not all ureas were soluble in this solvent. Use of the more polar solvent d_6-DMSO meant that there was strong hydrogen bonding between solvent and urea resulting in more defined N-H peaks. Analysis of DPU (**2**) by 2D NOESY showed chemical exchange of the N-H

with residual water in the sample, although none with the DMSO. As the di-substituted ureas can exist in multiple conformations, NOESY shows the correlation between the N-H and CH_{Ortho} on the aryl ring (Fig. 2.17).

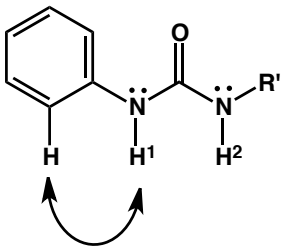

Fig. 2.17. Substituted phenyl urea. Arrow indicates NOE between aryl proton and N-H proton seen by 2D NMR.

Table 2.1. Compounds **1** – **24** were synthesised and subjected to ^{1}H NMR in *d*$_6$-DMSO with focus on the urea N-H protons (R is phenyl ring). Labelling as shown in Fig. 2.17.

Compound	R'	H^1	H^2	ΔH
1	$(CH_2)_3CH_3$	8.88	6.42	2.46
2	C_6H_5	8.65	8.65	-
3	$CH_2C_6H_5$	8.56	6.61	1.94
4	$(CH_2)_7CH_3$	8.35	6.09	2.26
5	$(CH_2)_{15}CH_3$	8.35	6.05	2.30
6	$C(CH_3)_3$	8.25	5.98	2.27
7	H	8.52	5.84	2.68
8	OH	8.81	8.73	0.08
9	C_6H_3 - 3,5-CF_3	8.96	9.38	0.42
10	C_6H_4 - *p*-CF_3	8.80	9.09	0.29
11	C_6F_5	8.48	9.06	0.58
12	C_6H_4 - *p*-NO_2	8.91	9.42	0.51
13	C_6H_4 - *m*-NO_2	8.83	9.21	0.38
14	C_6H_4 - *o*-NO_2	9.59	9.83	0.24
15	C_6H_4 - *p*-N=N-Ph	8.82	9.14	0.32
16	C_6H_4 - *p*-I	8.69	8.80	0.11
17	C_6H_4 - *p*-Cl	8.69	8.80	0.11
18	C_6H_4 - *p*-CO_2H	8.78	9.05	0.27
19	C_6H_4 - *p*-CH_3	8.60	8.54	0.06
20	C_6H_3 - 2,6-CH_3	8.72	7.70	1.02
21	C_6H_2 – 2,4,6-CH_3	8.67	7.61	1.06
22	C_6H_4 - *p*-NH_2	8.53	8.47	0.06
23	C_6H_4 - *p*-OCH_3	8.51	8.49	0.02
24	C_6H_4 - *p*-OAlk	8.56	8.44	0.12

Electron donating alkyl groups results in a more shielded N-H[2] and hence a higher field shift is observed eg. compounds **1**, **3 - 6**. This is in comparison to compound **2**, which was considered the "baseline". A similar argument has been used for strongly electron donating substituents on aryl rings such as NH_2 and OCH_3, except to a lesser extent (**22-24**) (Fig. 2.18). An alternative argument involves conjugation. Ortho substituents will reduce conjugation, as the aromatic ring will find it harder to align with the lone pair. The number of methyl groups in compounds **19-21** greatly affects its donating ability, the more methyl groups the greater the push of electrons onto the nitrogen.

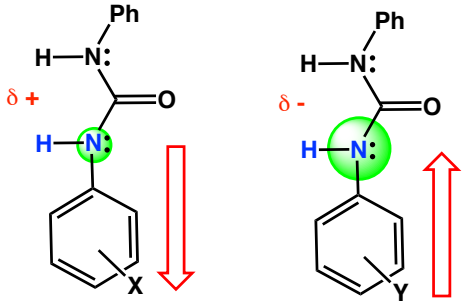

Fig. 2.18. Representation of a substituted phenylurea where X is an electron-withdrawing group increasing the acidity of the N-H, Y is electron-donating group increasing basicity of C=O. Both might assist H-bonding. Relative negativeness of the nitrogen shown by the green area. Arrow indicates direction of electron density movement.

The molecules with an electron-withdrawing group, CF_3, NO_2 or CO_2H, remove electron density from the π system making it more electronegative (**12-18**) (Fig. 2.18). This is communicated to the N-H attached directly to the ring and results in the proton being deshielded, shifting the chemical shift downfield. The number of electron-withdrawing groups also influences chemical shift with more groups pulling greater electron density from the aromatic ring and therefore the nitrogen (**9-10**). In addition, this nitrogen atom's lone pair is less likely to form an amide-like resonance form with the carbonyl. The other N-H is therefore more likely to form this amide-like resonance form. This could account for the increase in deshielding of H[1] by magnetic anisotropy of the π bond. The halide substituted phenyl ring (**16-17**) has the ability to donate non-

bonding electrons into the ring through the π-framework (resonance donation). However, due to its electronegativity, inductive withdrawal effects are predominant, deshielding NH^2. The five fluorines in compound **11** produce similar chemical shifts to the trifluoride (**10**), also deshielding the neighbouring N-H. Mono-substituted urea, **7,** has the lowest chemical shift for NH^2 as it is dominated by shielding effects of the nitrogen. Whereas, the electronegative oxygen in hydroxyurea **8** pulls electron density away from the nitrogen, deshielding the N-H.

Unfortunately, the location of N-H frequencies is not a reliable method for the identification of amine and amine-like structures. The chemical shifts are highly variable due to temperature, acidity, solvent and amount of hydrogen bonding availability.[94] The pattern shown by these results demonstrate how an EWG or EDG influence the N-H bond by increasing or decreasing the acidity respectively. Further discussion of substituted ureas and the interaction with H_2O_2 is developed in Chapter 4.

2.5.2 Alternatives to Urea

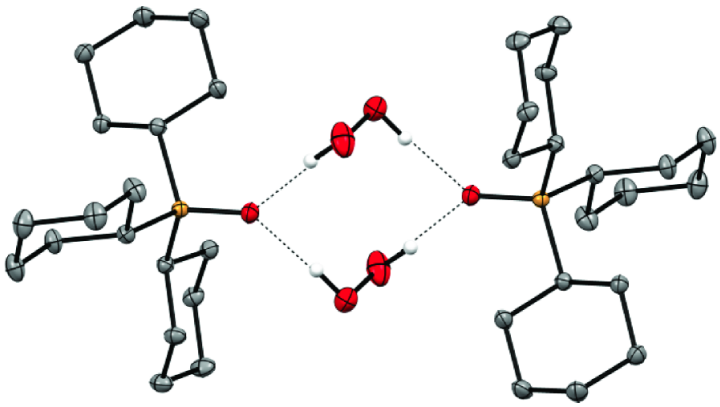

Fig. 2.19. A crystal structure of two tricyclohexylphosphine oxide compounds bridged by two H_2O_2 molecules. Reproduced from Hilliard[95] with permission from The Royal Society of Chemistry.

The urea functionality was proposed for this system due to its known ability to bind H_2O_2 and form a stable complex, UHP. On further investigation, a stable tricyclohexylphosphine oxide adduct with H_2O_2 has been made which only

binds through the oxygen in P=O. This 1:1 complex forms a cyclic dimeric structure with two hydrogen bonds to the phosphine oxide oxygen atom in the typical range for hydrogen bonds of 1.876 Å. However, substituted phosphine oxides are inferior for the New Cathode system because:

i) The molecular weight of the compound would be too heavy to allow a large enough energy density output.
ii) Phosphine oxides are a strong non-specific binder to metal and metal salts, therefore competitive binding with hydrogen peroxide would be an issue.
iii) As the phosphine oxide is required to be attached to the surface through one of the ligands, it places the P–O bond at a tetrahedral angle diminishing the access for multiple H_2O_2 molecules to interact.

The crystal structure reveals that the unit cell contains two phosphine compounds bridged by two hydrogen bonded H_2O_2 molecules (Fig. 2.19). Adduct formation can be seen by ^{31}P solid-state NMR as there are two isotropic lines attributed to the phosphorus nuclei in the unit cell being magnetically independent. The P–O bond in this adduct is lengthened compared to the corresponding phosphine oxide which can be accredited to hydrogen bonding with hydrogen peroxide. This unique bonding arrangement with H_2O_2 raises further question into what is the best mode of binding is. This indicates that the N-H atoms are not essential; therefore alternative compounds could possibly bind H_2O_2 just as well, if not better than urea.

In order to focus on the binding ability of the oxygen atom and mimic these phosphine oxides, it was decided to investigate carbamate, amide and sulfonamides. This idea is supported by DFT calculations by Dobado of the hydrogen bonding electronic properties identifying that only the C(O) and one N-H atom is needed for complex formation.[92]

Adapting Scheme 2.2, butanol and methanol was reacted with phenylisocyanate, to furnish carbamates **25** and **26**. Benzoic acid was activated with thionyl

chloride before it was dissolved in THF and cooled. Addition of butylamine produced amide **27** as a yellow oil. Toluenesulfonyl chloride reacted with butylamine to form **28** as a white/cream solid while methanesulfonyl chloride reacted with aniline in a similar reaction to give sulfonamide **29**.

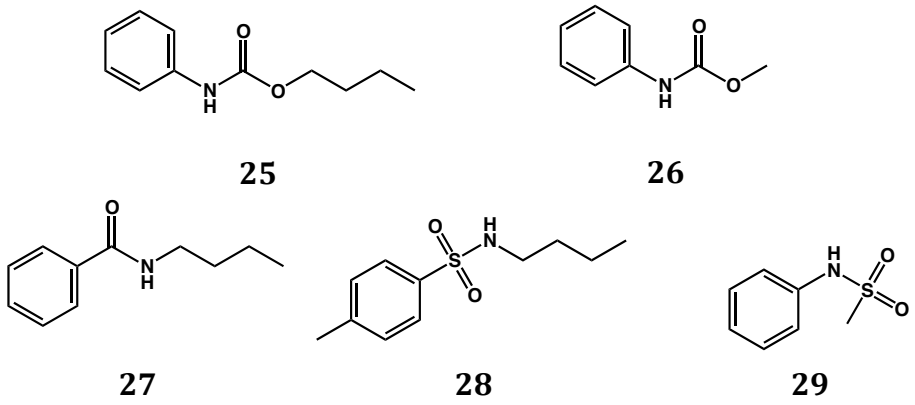

Fig. 2.20. Potential non-urea binders.

To establish the binding efficiency of these alternative compounds in comparison to the ureas, they were not synthesised to potentially attach to a surface. If after further experimentation they were found to be efficient binders, the appropriate steps will be undertaken to synthesise a diazonium-containing compound.

2.5.3 H_2O_2 Adduct Formation

The preparation of the urea and hydrogen peroxide adduct has changed negligibly since the first report in the early 1900s, with the most recent publications following the original method. This method formed UHP by mixing urea with a slight excess of 30% H_2O_2 (2:3), heating between 57 – 60 °C for a few minutes then cooling allowing the formation of colourless, elongated needles (Eq. 2.3).[91] Formation of the adduct was extremely low yielding or unsuccessful in the absence of heat.

$$\text{Urea} + H_2O_2 \rightleftharpoons \text{Urea} \bullet H_2O_2 \qquad 2.3$$

The requirement for heating is not fully understood. The assumption has been made that a sphere of water encapsulates the urea in solution; therefore thermal energy is necessary to weaken the hydrogen bonding to reduce solvation. This displacement of water allows the opportunity for hydrogen peroxide to replace these interactions. Additional hydrogen bonding sites are available in H_2O_2 favouring the UHP complex formation. This method was tested on simple water-soluble compounds such as urea, N-methylurea and 1,3-dimethylurea. Unfortunately, the formation of an adduct was not always guaranteed with the majority of the product being self-associated urea. According to patents granted in 1997[96] and 2010,[97] the H_2O_2 adducts of N-methylurea and 1,3-dimethylurea are liquids, rendering this method useless.

Inconveniently, the targeted synthetic binders, **1** – **29**, are not water-soluble complicating the formation of a complex. At first, compound **1** was stirred in a 1:1 ratio of 30% H_2O_2 in methanol, the urea was slightly soluble in methanol so this system permits monophasic mixing of the urea and H_2O_2. After slight heating this did not show any evidence of adduct formation, by IR (infra-red spectroscopy), mp (melting point) or NMR. Water remained in the product, possibly interacting strongly with **1** itself, and as water does not form an azeotrope with MeOH, it could not be removed under vacuum.

While it would have been possible to form water soluble urea derivatives (eg. PEG, NH_3^+), it was believed this may be counter productive as it would introduce a second group that could interact with the H_2O_2. Furthermore it was quicker to make anhydrous H_2O_2. There are two possible routes to prepare anhydrous H_2O_2: the removal of water, or extraction of H_2O_2 from an aqueous solution. Due to the difference in vapour pressure between H_2O and H_2O_2 (17.5 mmHg and 1.36 mmHg at 20 °C respectively)[98], if the pressure was sufficiently reduced an increase in H_2O_2 concentration may be achieved through distillation of water. Other methods such as fractional crystallisation may also increase aqueous H_2O_2 concentration by reducing the amount of H_2O.[99] Supercooling of the mixture crystallises the mixed H_2O_2-water crystals with a higher H_2O_2 content. This method requires over 90% hydrogen peroxide solution to start

with, therefore is unfeasible as it is not easily sourced and is highly dangerous.[98] None of the methods that increase H_2O_2 concentration were attractive as the danger involved also increased.

A 2009 paper reveals that serine can act as an organic extractor to remove H_2O_2 from an aqueous solution.[100] After the formation of a serine-H_2O_2 adduct (Fig. 2.21) at -20 °C (5 hours), they decanted off the mother liquor and the solid was dried in a desiccator for 2 days after which it was added to EtOAc. This organic peroxide solution is based on the decomposition of the serine-H_2O_2 crystals into insoluble serine and soluble hydrogen peroxide. Following the filtration of serine the solution may be concentrated by removal of EtOAc. This method is effective yet highly dangerous as it first requires a hydrogen peroxide solution greater than 60% to form the amino acid-H_2O_2 crystals. This concentration is considered dangerous due to its explosive tendencies. Consequently this route was highly discouraged as it poses multiple safety risks that the laboratory facilities were not equipped for.

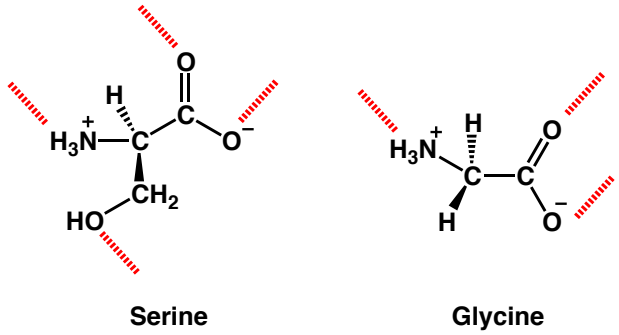

Fig. 2.21. Hydrogen bonding interactions with H_2O_2 indicated in red (from crystal structure).[100]

A glycine perhydrate adduct has also been prepared (Fig. 2.21).[100] This had an increased H_2O_2 percentage in comparison to UHP (40.5% and 36% respectively). The analysis of this complex was by permanganatometry and elemental analysis with supplementary contribution from FTIR. The symmetric and asymmetric stretching of O–O–H exhibited a peak at 2780 cm^{-1} and a broad shoulder above 3000 cm^{-1}.

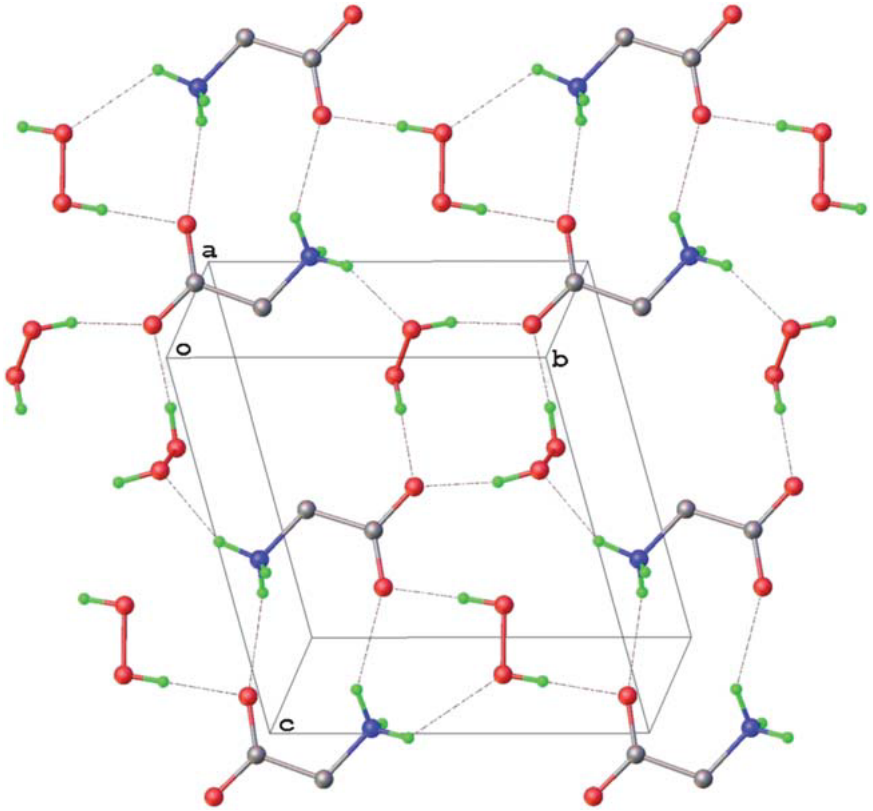

Fig. 2.22. Crystal lattice structure of per-glycine. Hydrogen bonds shown as dashed lines. Reproduced from Prikhodchenko, Petr V, Ref.[101] with permission from The Royal Society of Chemistry.

The ability of these adducts to form is partly due to the zwitterionic nature of amino acids. Ammonium groups serve as donors of H-bonds and hydroxyl (serine) and carboxylate moieties, serve as acceptors (Fig. 2.22). These small and flexible amino acids assist in forming a tight network with H_2O_2 through multiple hydrogen bonding interactions from several molecules, not just one.[101] The direct use of an amino acid in the New Cathode system is consequently unfeasible due to pH restrictions.

It was simpler to make an anhydrous organic solution of hydrogen peroxide by exploiting the low solubility of urea in most organic solvents. A THF solution of H_2O_2 could be prepared by stirring UHP (3.5 g) in THF (30 ml) under argon at room temperature for 1 hour. The urea was filtered off and the resulting solution was between 0.9 - 1.1 M (2.5%) according to permanganometry. (An alternative H_2O_2 analysis method is explained in Chapter 4). Within the

literature, this anhydrous peroxide solution is useful in epoxidation[102] and other water sensitive oxidations.[103]

Preliminary testing for adduct formation with compound **1** produced mixed results. On addition of the THF:H_2O_2 solution (1:1 ratio with respect to urea) a possibility of 4 options could occur.

a) Solid crystals of **1**: H_2O_2 would form or precipitate out of solution.
b) Adduct forms but remains soluble in THF. Removal of THF is required to obtain the product.
c) No interaction occurs.
d) Self-association of **1**.

The correct ratio of THF:H_2O_2 to **1** must be utilised to achieve option a). Unfortunately, the limited solubility of **1** in THF greatly increases the amount of solvent slowing the rate of interaction and decreasing the chance of crystallisation. Consequently the removal of the solvent was performed and the resulting solids assayed to determine if option b) or c) occurred.

Following option a), the initial tests by H_2O_2 dip stick and the presence of H_2O_2 in ^{1}H NMR (see Section 4.2) suggest peroxide is present in the solid product. These observations would also be explained by residual H_2O_2 unbound to the urea in the product. The peroxide test strips and proton NMR of H_2O_2 cannot differentiate between the bound and unbound state. However, this is sufficient evidence to continue on to find a quantitative method of analysis of the H_2O_2 adducts. Adduct formation of compounds **1-29** was made following this procedure. Investigation of the quantitative approach of the H_2O_2 adducts is explained in further detail in Chapter 4.

2.5.4 Synthesis for Attachment to a Surface

The selected method for attachment of the binder to the carbon surface is by diazonium coupling. This coupling technique is explained in detail in Chapter 5. It requires the preparation of binders that contain the diazonium functionality.

The optimum position for the diazonium is *para* to the urea, to allow for greater surface loading. This vertical attachment of the urea to the surface is described in Section 2.5. The stability of diazonium salts depends on both the structure of the substrate and the counter ion. While most diazonium salts are very reactive it has been shown that the tetrafluoroborate (BF_4^-) salts tend to form the most stable compounds. These are often stable at room temperature, although are stored at 0 °C for safety and longevity. Nitrates, perchlorates and iodides must be handled with care, as they are particularly explosive, and therefore have been avoided.

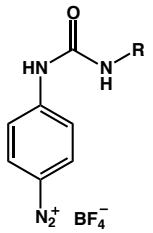

As a diazonium salt would not survive the synthetic sequences for urea preparation, we targeted the synthesis of an amine and then proposed to transform this into the diazonium species at the end. Amines are also reactive and need to be protected. This can be achieved with the appropriate protecting group (A), such as Boc (*tert*-butyloxycarbonyl), or by masking them as a nitro group (B) (Scheme 2.14). The amino protecting group must be sufficiently labile to not damage the urea in either the protection or deprotection stages. The reduction of the nitro group also poses potential problems with the possibility of reducing other substituents in the substituted urea. Fortunately, there are a variety of orthogonal reducing conditions such as H_2, Pd/C, $SnCl_2$ and $TiCl_3$ that should avoid side reactions.

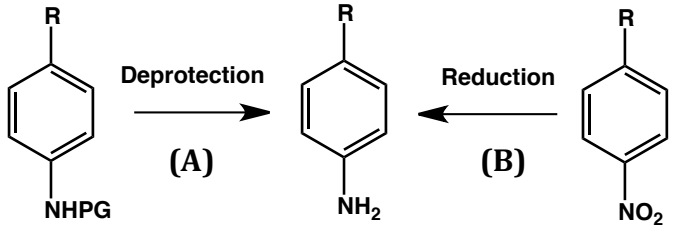

Scheme 2.14. Two strategies to form an arylamine where R is the urea functionality: (A) Deprotection of a protecting group (PG) and (B) reduction of a nitro moiety.

In order to reduce dimerisation of the primary amine with the isocyanate, initial focus was on the protection of the aniline nitrogen as a Boc carbamate. The Boc group is an acid labile protecting group that is stable to most bases and nucleophiles. The reaction of 4-aminobenzoic acid with Boc anhydride and NaOH gave the protected amine (**30**) in a 76% yield. Once the amine was protected, the acid was converted into the isocyanate (Scheme 2.15). Regular thionyl chloride-mediated conversion of an acid to an acyl chloride was not employed as it was thought the excess HCl formed would cleave the Boc group. Instead a milder reaction was attempted using addition of oxalyl chloride and DMF performed at 0 °C. The addition of t-Boc decreases solubility of the reactant therefore THF was added to aid solubility of the acyl chloride before nucleophilic acyl substitution with NaN_3.

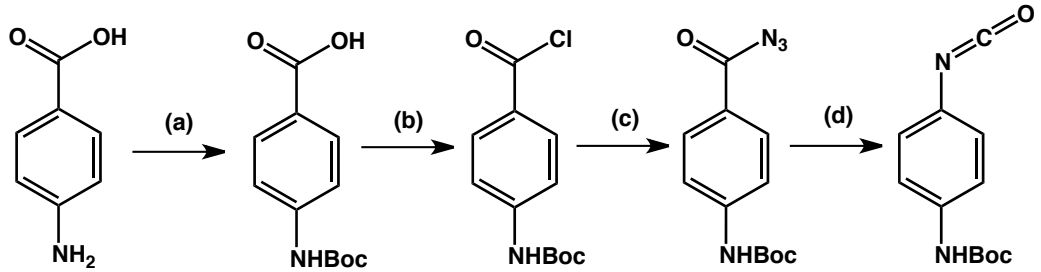

30 **31**

Scheme 2.15. (a) Boc_2O, NaOH, 76%, (b) Oxalyl chloride, DMF – not isolated (c) NaN_3, 74% (d) Heated in toluene at 110 °C for 90 mins, 73%.

The acyl azide precipitates out of the aqueous solution to give a white powder with a strong IR stretch at 2137 cm^{-1} corresponding to the N_3 stretch. The Curtius rearrangement is performed in toluene to enable the higher temperatures and energy required for rearrangement. Toluene is also suitable for addition of the amine without separation of the potentially unstable isocyanate. This forms compound **32** when using butylamine, which can be deprotected by stirring in HBF_4 for 30 minutes. Deprotection of the protecting group is very efficient with a near quantitative conversion by thin layer chromatography (TLC) of the aryl amine produced (**33**) (Scheme 2.16).

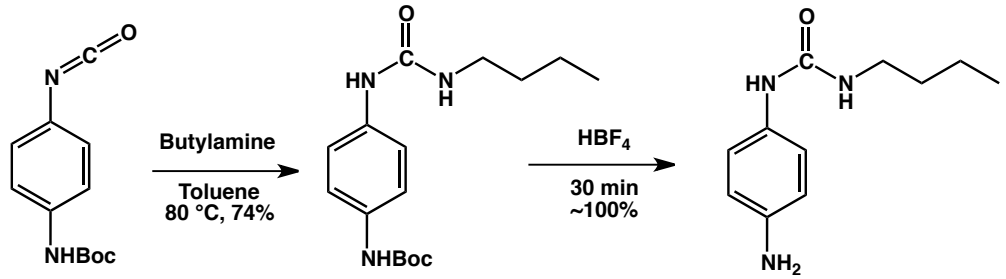

Scheme 2.16. Deprotection of Boc protected aminophenylurea.

The attempt to prepare the aryl amine from the nitro substituted urea required formation of compound **12**. This was achieved by either reacting phenylisocyanate with 4-nitroaniline, or reacting 4-nitrophenylisocyanate with aniline (Scheme 2.17). Both methods gave **12** with good yields (69% and 73% respectively). The resulting aryl nitro urea was readily reduced by $SnCl_2$ in EtOH at 70 °C. This is one less step than the protection method, and produces a clean final product. The phenyl amino urea (**22**) degrades over time turning lilac in colour at room temperature, therefore must be kept under a nitrogen atmosphere in the freezer at 4 – 6 °C and used as required. Purification of **22** proved difficult due to its limited solubility in organic solvents and inability to fully dissolve in acid.

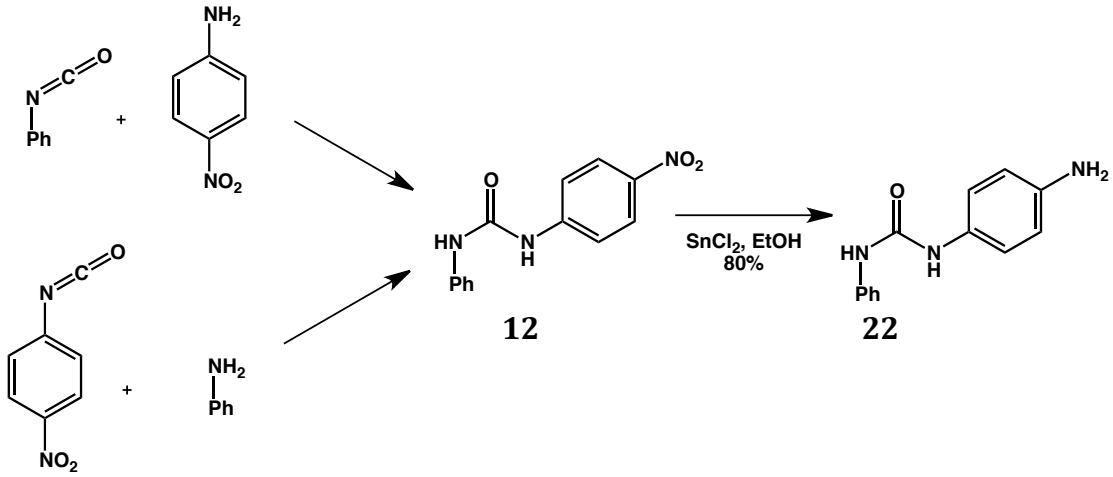

Scheme 2.17. Two pathways to form **22** by nucleophilic addition of an isocyanate with an arylamine followed by reduction of the nitro moiety with $SnCl_2$ in EtOH.

2.5.4.1 Diazonium Attachment

Diazonium compounds are generally formed by reacting a primary amine with dilute HCl and $NaNO_2$ at low temperature (0 °C). Fortunately, when using the Boc protecting group, presented above, the deprotection and diazotisation steps could be achieved in a one-pot sequence. The addition of HBF_4 not only cleaves the Boc group but also is utilised as the counter ion in the arenediazonium salt formation. However as successful as this reaction was, it was easier and involved less synthetic steps to form urea **22** from the nitro derivative by the above method (Scheme 2.17).

In the present study, initial experiments for attachment of a urea to a surface were based on phenyl substituted urea where R was substituted for a phenyl ring (Scheme 2.18). To isolate the diazonium salt, addition of $NaNO_2$ to **22** produced a yellow precipitate that was filtered off. The stability of diazonium salts are questionable so were made immediately before use. If stored at 0-5 °C under inert conditions, the compound will survive for a few weeks, although each sample was evaluated by ^1H NMR before use.

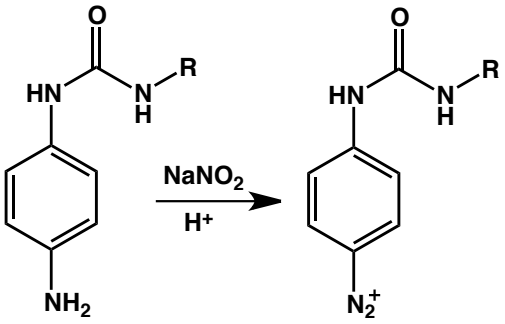

33 **34**

Scheme 2.18. General scheme for diazotisation of urea aryl amine.

Before attempting attachment to a surface, with all the associated limitations of structural analysis, two methods were used to confirm the formation of the diazonium salt: ^1H NMR and a solution phase reaction. Standard ^1H NMR showed a down field shift in the two aryl doublets indicating the presence of the electron-withdrawing group, N_2^+. The Heck-Matsuda reaction was chosen for testing by derivatisation, as it is a reliable reaction involving the addition of a

diazonium salt to sp^2 hybridised carbon centres. It is advantageous over previous established Heck-like reactions that use halides and triflates, as phosphine ligands are not required, thus removing the need for anaerobic conditions. The Heck-Matsuda reaction has high reactivity at room temperature and is a suitable test reaction for our synthesised diazonium compounds.[104] The diazonium salt was successfully reacted with methyl acrylate to give a stable product, which could readily be identified by ^{1}H NMR. Two clear doublets with J-couplings of 16 Hz are prominent, characteristic of di-substituted alkene protons. Further analysis by ^{13}C NMR, IR and HR-MS (Na^+ 319.1036 m/z , calc. 319.1053 m/z) confirmed evidence of the product.

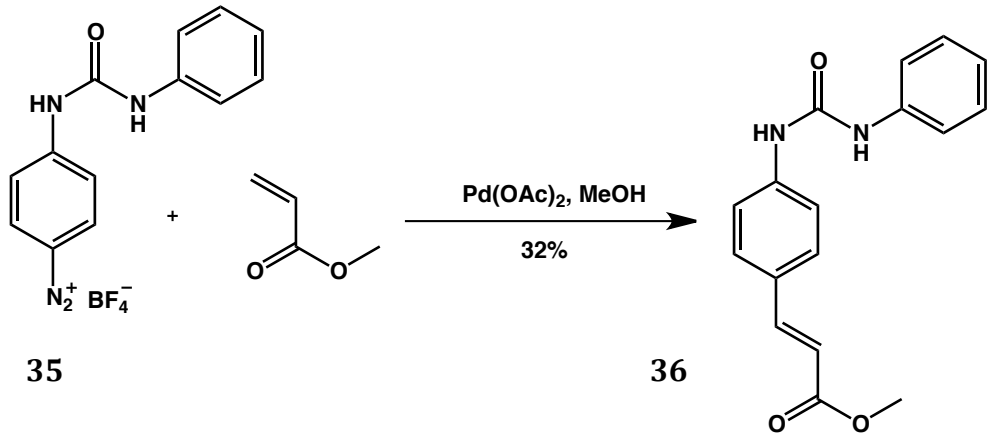

35 **36**

Scheme 2.19. Heck-Matsuda reaction with diphenyldiazonium salt **35** and methyl acrylate catalysed by palladium acetate.

The Heck-Matsuda is an effective reaction to show the presence of the aryl diazonium, however the mechanism involves the assistance of palladium to couple the reactants. Azo coupling is an alternative method that takes advantage of the electrophilicity of the diazonium species by coupling with an activated arene (Scheme 2.20). The use of azo dyes is predominant in industrial applications where the reaction is used for formation of dyes and pigments in textiles, food and colour applications.

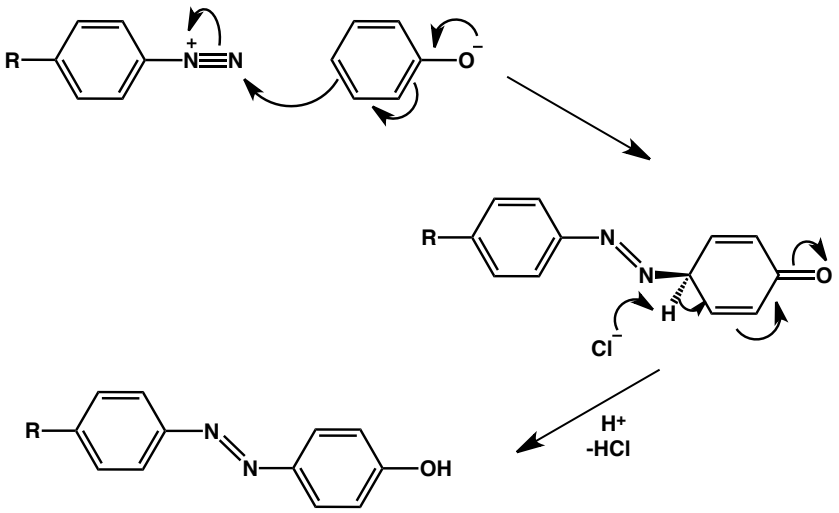

Scheme 2.20. General mechanism for the coupling of an aryl diazonium with phenoxide to form an azo dye.

Combining an electrophilic aryldiazonium, with a strongly *p*-directing nucleophile such as phenol under basic conditions forms a brightly coloured product. As these compounds absorb light at a longer wavelength due to the extensive conjugated system, a brown/orange solid precipitated out of solution following neutralisation. Analysis by ^{1}H NMR in d_6-DMSO revealed two N-H protons at 9.08 and 8.81 ppm in accordance with aromatic peaks associated with three aryl rings. Additional analysis by ^{13}C NMR and HR-MS (Na^+ found 355.1145 m/z, calc. 355.1165 m/z) showed good evidence that coupling has occurred. Decomposition to a dark brown/black material occurred at 245 °C.

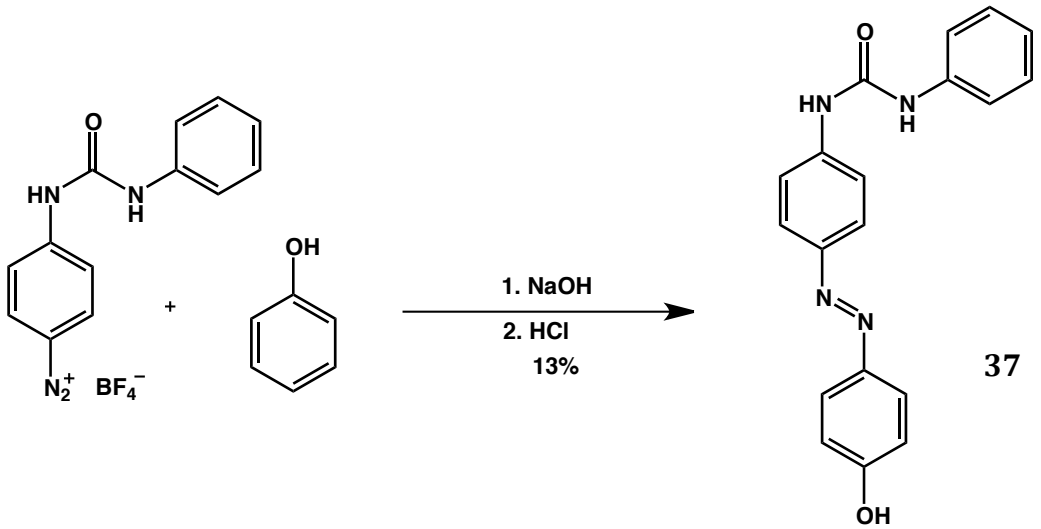

Scheme 2.21. Azo coupling of diphenyldiazonium salt with phenol under basic conditions to form compound **37**.

The formation of product **36** and azo dye **37**, show the ability of the diazonium salt **35** to undergo further reactions. The low yield of these reactions does not necessarily reflect the reactivity or efficiency of the diazonium species to couple to a carbon substrate. It does indicate that the diazonium salt formation is inefficient leading to these small yields. It clearly highlights that the diazonium salt is a versatile compound and confirms our ability to make a substituted urea capable of undergoing further coupling, such as to a surface. An alternative methodology by avoiding the unnecessary isolation of the diazonium salt assisted to increase the yield. This can be taken into consideration when coupling to a carbon substrate to increasing attachment efficiency.

This project was only concerned with the methodology of attaching a substituted urea to a carbon substrate. Compound **2** was used as the model for further investigation when attaching to the carbon substrate (Chapter 5). The ability to produce a diazonium salt of this molecule for covalent attachment has been demonstrated and it is a procedure that can be applied for many of the alternate ureas.

2.6 Experimental

General Procedure 1 - Isocyanate Formation

A solution of benzoic acid (4.5 g, 36.8 mmol, 1.0 eq.) in CH_2Cl_2 (35 ml) was cooled in an ice bath to 0 °C and placed under an atmosphere of argon. Oxalyl chloride (10.5 ml, 112 mmol, 3.0 eq.) was added and the resulting mixture stirred at this temperature for a further 10 mins. Catalytic DMF (0.4 ml, 5.2 mmol) was added dropwise over 15 mins and allowed to warm to rt then stirred for a further 60 minutes. The solvent was removed *in vacuo* affording a reactive colourless liquid to which anhydrous toluene (40 ml) was immediately added. NaN_3 (9.5 g, 146 mmol, 4 eq.) was added to the reaction mixture and stirred vigorously overnight under an atmosphere of argon. The reaction was heated to 80 °C and maintained at this temperature for 5 hours to allow isocyanate formation.

General Procedure 2 – Nucleophilic Attack of Phenylisocyanate

To a solution of the amine derivative, **R'** (2 mmol, 2 eq.) in anhydrous toluene (10 ml) was added phenylisocyanate (1 mmol, 1 equiv). The reaction was stirred at 80 °C overnight and the solvent removed *in vacuo* to give the crude urea. Subsequent purification was achieved by column chromatography or recrystallization (see below for specific conditions).

Synthesis of 1 1-butyl-3-phenylurea

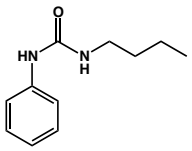

The title compound **1** was prepared according to general procedure 2 with the addition of phenyl isocyanate (5 ml, 46 mmol, 1.0 eq.) to butylamine (9.0 ml, 93.5 mmol, 2 eq.) in toluene (100 ml). The crude material was recrystallised from MeOH to afford **1** as a white crystalline solid (8.05 g, 91 %). ^{1}H NMR (400 MHz, DMSO-d_6): δ (ppm) = 8.88 (s, 1H, NH), 7.37 (d, J = 7.6 Hz, 2H, H_{Arom}), 7.18 (t, J = 7.6 Hz, 2H, H_{Arom}), 6.84 (t, J = 7.6 Hz, 1H, H_{Arom}), 6.42 (t, J = 5.6 Hz, 1H, NH), 3.05 (q, 2H, CH_2), 1.40 – 1.28 (m, 4H, CH_2CH_2), 0.87 (t, J = 6.8 Hz, 3H, CH_3). ESI-MS: *m/z* 193.19 $([M+H])^+$. MP (°C): 132 – 133. Data comparable to previous publications.[79,105-107]

Synthesis of 2 1, 3 - diphenylurea

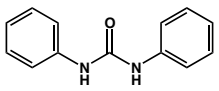

Compound **2** was prepared in accordance to general procedure 2 with the addition of phenyl isocyanate (0.1 ml, 0.92 mmol, 1.0 eq.) to aniline (0.17 ml, 1.86 mmol, 2.0 eq.) in toluene (5 ml). Recrystallization in MeOH afforded long white crystals of the title compound (0.185 g, 95 %) ^{1}H NMR (125 MHz, DMSO-d_6): δ (ppm) = 8.65 (s, 2H, NHs), 7.46 (d, J = 7.5 Hz, 4H, H_{Ortho}), 7.28 (t, J = 7.5 Hz, 4H, H_{Meta}), 6.97 (t, J = 7.5 Hz, 2H, H_{Para}). Data similar to previous publications.[73,79,108]

Synthesis of 3 1-benzyl-3-phenylurea

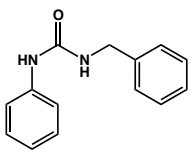

The title compound **3** was prepared according to general procedure 2 with the addition of phenylisocyanate (0.55 ml, 5 mmol, 1 eq.) to benzylamine (0.55 ml, 5 mmol, 1 eq.) in toluene. Further purification was not required (1.0 g, 89 %). ^{1}H NMR (500 MHz, DMSO-

d$_6$): δ (ppm) = 8.53 (s, 1H, NH), 7.38 – 7.40 (m, 2H, H_{Arom}), 7.28 – 7.35 (m, 4H, H_{Arom}), 7.20 – 7.26 (m, 3H, H_{Arom}), 6.89 (dt, J = 1.1, 8.3 Hz, 1H, H_{Arom}), 6.59 (t, J = 6.0 Hz, 1H, NH), 4.30 (d, J = 6.0 Hz, 2H, C*H*$_2$) ^{13}C NMR (125 MHz, DMSO-*d*$_6$): δ (ppm) = 155.7, 140.9, 140.8, 129.1, 128.8, 127.6, 127.2, 121.6, 118.2, 43.2. Data similar to previous publications.[79,109]

Synthesis of 4 1-octyl-3-phenylurea

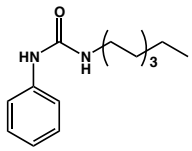

Primarily following general procedure 2, a solution of n-octylamine (1.5 ml, 9.05 mmol, 1 eq.) in anhydrous CH_2Cl_2 (20 ml) was added phenylisocyanate (1 ml, 9.09 mmol, 1 eq.) slowly over 30 mins. The reaction stirred at room temperature overnight after which the solvent was removed *in vacuo* to give a white solid (2.05 g, 91 %). ^{1}H NMR (500 MHz, $CDCl_3$): δ (ppm) = 7.29-7.26 (m, 4H, H_{Arom}), 7.17 (bs, 1H, NH), 7.07-7.03 (m, 1H, H_{Arom}), 5.40 (bs, 1H, NH), 3.21 (t, J = 7.5 Hz, 2H, NHC*H*$_2$), 1.47 (m, 2H, C*H*$_2$CH$_3$), 1.31 – 1.26 (m, 10H, CH_2CH_2), 0.90 (t, J = 7.0 Hz, 3H, CH_3). Similar to literature.[110] ^{1}H NMR (500 MHz, DMSO-*d*$_6$): δ (ppm) = 8.36 (s, 1H, NH), 7.38 (dd, J = 8.6, 1.0 Hz, 2H, H_{Arom}), 7.21 (t, J = 7.5 Hz, 2H, H_{Arom}), 6.87 (tt, J = 7.4, 1.0 Hz, 1H, H_{Arom}), 6.09 (t, J = 5.6 Hz, 1H, NH), 3.07 (q, 2H, CH_2), 1.42 (m, 2H, CH_2), 1.29 – 1.27 (m, 10H, CH_2CH_2), 0.87 (t, J = 6.5 Hz, 3H, CH_3).

Synthesis of 5 1-hexadecyl-3-phenylurea

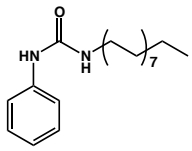

Compound **5** was prepared similarly to compound **4** (above) where n-hexadecylamine (0.5 g, 2.07 mmol, 1 eq.) in anhydrous CH_2Cl_2 (20 ml) was added phenylisocyanate (0.22 ml, 2.01 mmol, 1 eq.) slowly over 30 mins. Precipitate immediately formed. Continued to stir at rt overnight. Solvent was removed *in vacuo* to give a white solid. Precipitated from hot hexane (0.62 g, 86 %). ^{1}H NMR (500 MHz, DMSO-*d*$_6$): δ (ppm) = 8.35 (s, 1H, NH), 7.37 (dd, J = 8.5, 1.0 Hz, 2H, H_{Arom}), 7.20 (dt, J = 7.4, 1.0 Hz, 2H, H_{Arom}), 6.87 (tt, J = 7.3, 1.0 Hz, 1H, H_{Arom}), 6.08 (t, J = 5.6 Hz, 1H, NH), 3.06 (q, 2H, CH_2), 1.41 (m, 2H, CH_2), 1.28 – 1.24 (m, 28H, CH_2CH_2), 0.86 (t, J = 7.5 Hz, 3H, CH_3). Data similar to literature.[111]

Synthesis of 6 1-(*tert*-butyl)-3-phenylurea

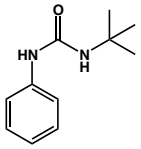

Compound **6** was prepared according to procedure 2 with the addition of phenylisocyanate (0.1 ml, 0.92 mmol, 1 eq.) to a solution of *tert*-butylamine (0.106 ml, 1.0 mmol, 1.1 eq) in dry toluene (5 ml). Crude material was recrystallised from MeOH to give **6** as a white solid (45 mg, 25 %) ^{1}H NMR (400 MHz, DMSO-d_6): δ (ppm) = 8.25 (s, 1H, NH), 7.35 (d, J = 8.4 Hz, 2H, Ar_{Ortho}), 7.20 (t, J = 8 Hz, 2H, Ar_{Meta}), 6.87 (t, J = 7.6 Hz, 1H, Ar_{Para}), 5.98 (s, 1H, NH), 1.29 (s, 9H, CH_3). ^{13}C NMR (100 MHz, DMSO-d_6): δ (ppm) = 154.9, 141.1, 129.1, 121.2, 117.8, 49.5, 29.5. Data similar to literature.[81] (except for N-Hs as they have >100 fold excess water).

Synthesis of 7 1-phenylurea

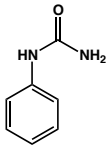

To a stirred suspension of compound **3** (0.226 g, 1 mmol, 1 eq.) was added 10 % (w/w) Pd/C in EtOH (10 ml). Following a drop of HCl, the reaction was stirred overnight under an atmosphere of H_2. The solution was filtered over celite and the solvent removed *in vacuo* to give a colourless solid (130 mg, 96 %). ^{1}H NMR (500 MHz, DMSO-d_6): δ (ppm) = 8.48 (s, 1H, NH), 7.38 (dd, J = 8.6, 1.0 Hz, 2H, Ar_{Ortho}), 7.20 (t, J = 7.3 Hz, 2H, Ar_{Meta}), 6.88 (dt, J = 7.3, 1.1 Hz, 1H, Ar_{Para}), 5.80 (s, 2H, NH_2). ^{13}C NMR (125 MHz, DMSO-d_6): δ (ppm) = 156.0, 140.6, 128.6, 121.0, 117.7. Data similar to published material.[112]

Synthesis of 8 1-hydroxy-3-phenylurea

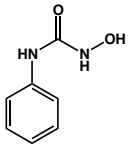

Hydroxylammonium chloride (1.55 g, 22.9 mmol, 2.1 eq.) was stirred with CH_2Cl_2 followed by the parallel slow addition of phenylisocyanate (1.2 ml, 11 mmol, 1 eq.) and NEt_3 (1.45 ml, 10.4 mmol, 0.95 eq.) separately. Once all reactants were added and bubbling ceased, the solution was stirred at 55 °C for 16 hours. The solvent was removed under reduced pressure (mixture of NEt_3.HCl and product) and purified by column chromatography (50:50 Hexane/EtOAc with 1% AcOH). Rf = 0.3. Fractions were combined and recrystallised in MeOH to give title compound **8** as a white solid (44 mg, 2.6 %). ^{1}H NMR (400 MHz, DMSO-d_6): δ (ppm) = 8.96 (s, 1H, NH), 8.83

(s, 1H, NH), 8.76 (s, 1H, O*H*), 7.62 (dd, J = 8.5, 1.1 Hz, 2H, Ar_{Ortho}), 7.25 (t, J = 7.6 Hz, 2H, Ar_{Meta}), 6.97 (tt, J = 7.4, 1.0 Hz, 1H, Ar_{Para}). Data similar to literature.[113]

Synthesis of 9 1-(3,5-bis(trifluoromethyl)phenyl)-3-phenylurea

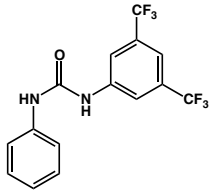

Compound **9** was synthesised following procedure 2 with the addition of phenylisocyanate (0.33 ml, 3 mmol, 1 eq.) to a solution of 3,5-bis(trifluoromethyl)-aniline (0.470 ml, 3 mmol, 1 eq.) in toluene (15 ml). The reaction was diluted with n-hexane and the white precipitate filtered (0.65 g, 66 %). ^{1}H NMR (500 MHz, DMSO-d_6): δ (ppm) = 9.38 (s, 1H, NH), 8.97 (s, 1H, NH), 8.13 (s, 2H, H_{Ortho}), 7.63 (s, 1H, H_{Para}), 7.47 (dd, J = 8.5, 1.1 Hz, 2H, Ar_{Ortho}), 7.30 (t, J = 7.5, 2H, Ar_{Meta}), 7.02 (dt, J = 7.3, 1.1, 1H, Ar_{Para}). Data similar to literature.[114]

Synthesis of 10 1-phenyl-3-(4-(trifluoromethyl)phenyl)urea

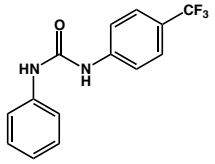

Compound **10** was prepared according to procedure 2 with the addition of phenylisocyanate (0.1 ml, 0.92 mmol, 1 eq.) to a solution of 4-(trifluoromethyl)aniline (0.127 ml, 1.01 mmol, 1.1 eq.) in dry toluene (5 ml). Crude material was recrystallised from MeOH to give **10** (183 mg, 71 %). ^{1}H NMR (400 MHz, DMSO-d_6): δ (ppm) = 9.09 (s, 1H, NH), 8.80 (s, 1H, NH), 7.68-7.63 (m, 4H, $H_{Ortho,Meta}$), 7.47 (d, J = 7.6 Hz, 2H, Ar_{Ortho}), 7.31 (t, J = 7.6 Hz, 2H, Ar_{Meta}), 7.01 (t, J = 7.6 Hz, 1H, Ar_{Para}). Data similar to literature.[115]

Synthesis of 11 1-(perfluorophenyl)-3-phenylurea

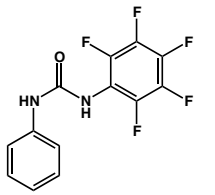

Compound **11** was prepared with slight alteration to procedure 2 with the portion wise addition of perfluoroaniline (366 mg, 2 mmol, 1 eq.) to a solution of phenylisocyanate (0.22 ml, 2 mmol, 1 eq.) in dry toluene (8 ml). Allowed to reflux at 80 °C for 2 days. Solution was diluted with n-hexane and the precipitate filtered and dried (536 mg, 90 %). ^{1}H NMR (500 MHz, DMSO-d_6): δ (ppm) = 9.06 (s, 1H, NH), 8.48 (s, 1H, NH), 7.44 (d, J = 7.8 Hz, 2H, Ar_{Ortho}), 7.28 (t, J = 7.2 Hz, 2H, Ar_{Meta}), 7.00 (t, J = 7.2 Hz, 1H, Ar_{Para}) ^{13}C NMR (125 MHz, DMSO-d_6): δ (ppm) = 152.4, 143.3 (dd, J =

245, 6 Hz), 139.7, 138.8 (dt, J = 248, 14 Hz), 137.6 (dt, J = 246, 15 Hz), 129.2, 122.7, 118.8, 114.5 (t, J = 14 Hz).

Synthesis of 12 1-(4-nitrophenyl)-3-phenylurea

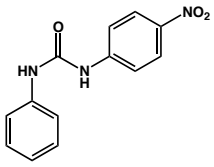

Compound **12** was synthesised following procedure 2 with the addition of phenylisocyanate (0.1 ml, 0.92 mmol, 1 eq.) to a solution of *p*-nitroaniline (140 mg, 1.01 mmol, 1.1 eq.). Recrystallisation from MeOH was attempted but due to its limited solubility precipitated out immediately to give a light cream solid (1.56 g, 69 %). ^{1}H NMR (500 MHz, DMSO-d_6): δ (ppm) = 9.42 (s, 1H, NH), 8.91 (s, 1H, NH), 8.20 (d, J = 7.5 Hz, 2H, H_{Meta}), 7.70 (d, J = 9.5 Hz, 2H, H_{Ortho}), 7.48 (d, J = 7.5 Hz, 2H, Ar_{Ortho}), 7.32 (t, J = 8.5 Hz, 2H, Ar_{Meta}), 7.03 (t, J = 7.5 Hz, 1H, Ar_{Para}). Data similar to literature references.[73,79]

Synthesis of 13 1-(3-nitrophenyl)-3-phenylurea

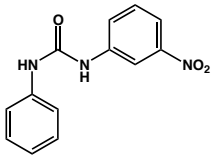

Compound **13** was synthesised following procedure 2 with the addition of phenylisocyanate (0.15 ml, 1.38 mmol, 1 eq.) to a solution of *m*-nitroaniline (0.193 g, 1.39 mmol, 1.01 eq.). Crude material was recrystallised from MeOH (0.219 g, 62 %). ^{1}H NMR (400 MHz, DMSO-d_6): δ (ppm) = 9.22 (s, 1H, NH), 8.84 (s, 1H, NH), 8.57 (t, J = 2.0 Hz, 1H, H_{Ortho}), 7.83 (dt, J = 8.0, 0.8 Hz, 1H, H_{Para}), 7.72 (dt, J = 7.2, 0.8 Hz, 1H, H_{Ortho}), 7.57 (t, J = 8.0 Hz, 1H, H_{Meta}), 7.58 (d, J = 7.6 Hz, 2H, Ar_{Ortho}), 7.31 (t, J = 8.4 Hz, 2H, Ar_{Meta}), 7.01 (t, J = 7.2 Hz, 1H, Ar_{Para}) ^{13}C NMR (125 MHz, DMSO-d_6): δ (ppm) = 152.9, 148.6, 141.5, 139.7, 130.5, 129.3, 124.7, 122.8, 119.1, 116.7, 112.6.

Synthesis of 14 1-(2-nitrophenyl)-3-phenylurea

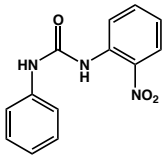

Compound **14** was synthesised following procedure 2 with the addition of phenylisocyanate (0.15 ml, 1.38 mmol, 1 eq.) to a solution of *o*-nitroaniline (0.196 g, 1.42 mmol, 1.03 eq.). Purification was by silica column (1:1 Hexane/EtOAc). (0.230 g, 66 %). ^{1}H NMR (400 MHz, DMSO-d_6): δ (ppm) = 9.82 (s, 1H, NH), 9.58 (s, 1H, NH), 8.29 (dd, J = 8.4, 0.8 Hz, 1H, H_{Ortho}), 8.09 (dd, J = 8.4, 1.6 Hz, 1H, H_{Meta}), 7.70 (t, J = 7.2 Hz, 1H, H_{Meta}), 7.48 (d, J = 8.0 Hz, 2H, Ar_{Ortho}), 7.31 (t, J = 7.6 Hz, 2H, Ar_{Meta}), 7.21 (dt, J =

6.0, 2.0 Hz, 1H, H_{Para}), 7.01 (t, J = 7.2 Hz, 1H, Ar_{Para}). ^{13}C NMR (100 MHz, DMSO-d_6): δ (ppm) = 160.1, 152.3, 139.7, 138.2, 135.4, 135.3, 129.3, 125.9, 123.1, 122.7, 119.1.

Synthesis of 15 1-phenyl-3-(4-(phenyldiazenyl)phenyl)urea

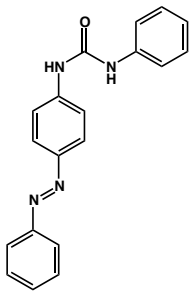

Phenylisocyanate (0.03 ml, 0.27 mmol, 1.04 eq.) was added to a solution of aniline yellow (51.7 mg, 0.26 mmol, 1 eq.) in anhydrous CH_2Cl_2 (5 ml). The reaction mixture was stirred at room temperature overnight, where a coloured precipitate formed. The solvent was removed *in vacuo* to give an orange solid which was purified by silica gel chromatography (10% EtOAc/ Hexane) to give a golden yellow solid (52.3 mg, 63 %). ^1H NMR (500 MHz, DMSO-d_6): δ (ppm) = 9.14 (s, 1H, NH), 8.82 (s, 1H, NH), 7.90-7.85 (2 x d, 4H, 2 x H_{Arom}), 7.69 (d, J = 7.0, 2.0 Hz, 2H, H_{Arom}), 7.59 (t, J = 7.0 Hz, 2H, H_{Arom}), 7.53 (d, J = 7.5 Hz, 1H, H_{Arom}), 7.49 (dd, J = 8.5, 1.0 Hz, 2H, H_{Arom}), 7.31 (t, J = 8.0 Hz, 2H, H_{Arom}), 7.02 (t, J = 7.5 Hz, 1H, H_{Arom}). Data similar to literature.[116]

Synthesis of 16 1-(4-iodophenyl)-3-phenylurea

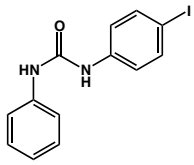

Compound **16** was synthesised following procedure 2 with the addition of phenylisocyanate (0.15 ml, 1.38 mmol, 1 eq.) to a solution of *p*-iodoaniline (0.304 g, 1.39 mmol, 1 eq.). Crude material was recrystallised from MeOH to give faint purple crystals (0.306 g, 66 %). ^1H NMR (400 MHz, DMSO-d_6): δ (ppm) = 8.76 (s, 1H, NH), 8.67 (s, 1H, NH), 7.58 (d, J = 8.6 Hz, 2H, H_{Ortho}), 7.43 (d, J = 7.9 Hz, 2H, Ar_{Ortho}), 7.31-7.24 (m, 4H, H_{Meta}/Ar_{Meta}), 6.96 (t, J = 7.2 Hz, 1H, Ar_{Para}). ^{13}C NMR (125 MHz, d_6-DMSO): δ (ppm) = 152.8, 140.1, 139.9, 137.8, 129.3, 122.5, 120.9, 118.8, 85.1. Data similar to literature.[117]

Synthesis of 17 1-(4-chlorophenyl)-3-phenylurea

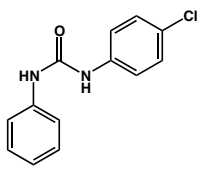

Compound **17** was synthesised following procedure 2 with the addition of phenylisocyanate (0.1 ml, 0.92 mmol, 1 eq.) to a solution of *p*-chloroaniline (129 mg, 1.01 mmol, 1.1 eq.). Purification was not required (0.17 g, 76 %). ^1H NMR (500 MHz, DMSO-d_6): δ

(ppm) = 8.80 (s, 1H, NH), 8.69 (s, 1H, NH), 7.49 (dd, J = 6.5, 2.0 Hz, 2H, H_{Ortho}), 7.45 (dd, J = 8.5, 1.0 Hz, 2H, Ar_{Ortho}), 7.33 (dd, J = 7.0, 2.0 Hz, 2H, H_{Meta}), 7.29 (t, J = 7.5 Hz, 2H, Ar_{Meta}), 6.98 (t, J = 7.5 Hz, 1H, Ar_{Para}). Data similar to previous publications.[118]

Synthesis of 18 4-(3-phenylureido)benzoic acid

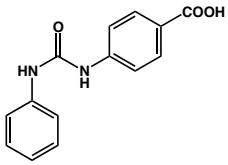

Compound **18** was synthesised following procedure 2 with the addition of phenylisocyanate (0.15 ml, 1.38 mmol, 1.02 eq.) to a solution of 4-aminobenzoic acid (0.185 g, 1.35 mmol, 1 eq.). Crude material was recrystallised in MeOH to give a white solid (0.184 g, 52 %). ^{1}H NMR (400 MHz, DMSO-d_6): δ (ppm) = 12.57 (bs, 1H, OH), 9.02 (s, 1H, NH), 8.76 (s, 1H, NH), 7.86 (d, J = 8.4 Hz, 2H, H_{Ortho}), 7.55 (d, J = 8.4, 2H H_{Meta}), 7.45 (d, J = 7.6 Hz, 2H, Ar_{Ortho}), 7.28 (t, J = 7.6 Hz, 2H, Ar_{Meta}), 6.98 (t, J = 7.2 1H, Ar_{Para}) ^{13}C NMR (125 MHz, DMSO-d_6): δ (ppm) = 167.5, 152.7, 144.5, 139.8, 131.0, 129.3, 124.1, 122.6, 118.9, 117.7.

Synthesis of 19 1-phenyl-3-(*p*-tolyl)urea

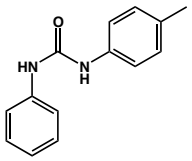

Compound **19** was prepared according to procedure 2 with the addition of phenylisocyanate (0.1 ml, 0.92 mmol, 1 eq.) to a solution of *p*-tolylaniline (108 mg, 1.01 mmol, 1.1 eq) in dry toluene (5 ml). Crude material was recrystallised from MeOH to give **19** as long white needles (173 mg, 84 %). ^{1}H NMR (400 MHz, DMSO-d_6): δ (ppm) = 8.60 (s, 1H, NH), 8.54 (s, 1H, NH), 7.44 (d, J = 8.4 Hz, 2H, Ar_{Ortho}), 7.34 (d, J = 8.4 Hz, 2H, H_{Meta}), 7.28 (t, J = 8.4 Hz, 2H, Ar_{Meta}), 7.09 (d, J = 8.4 Hz, 2H, H_{Ortho}), 6.96 (t, J = 8.4 Hz, 1H, Ar_{Para}), 2.25 (s, 3H, CH_3). ^{13}C NMR (100 MHz, DMSO-d_6): δ (ppm) = 153.1, 140.3, 137.6, 131.1 129.6, 129.2, 122.2, 118.8, 118.6, 20.8. Data analogous to literature.[79]

Synthesis of 20 1-(2,6-dimethylphenyl)-3-phenylurea

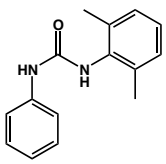

Compound **20** was prepared according to procedure 2 with the addition of phenylisocyanate (0.1 ml, 0.92 mmol, 1 eq.) to a solution of 2,6-dimethylaniline (0.23 ml, 1.88 mmol, 2.04 eq) in dry toluene (5 ml). Crude material was recrystallised from MeOH to give **20**

(0.198 mg, 90 %). ^{1}H NMR (400 MHz, DMSO-d_6): δ (ppm) = 8.73 (s, 1H, NH), 7.71 (s, 1H, NH), 7.46 (d, J = 8.0 Hz, 2H, Ar_{Ortho}), 7.25 (t, J = 7.2 Hz, 2H, Ar_{Meta}), 7.06 (d, J = 4.4 Hz, 1H, Ar_{Para}), 7.07 (s, 2H, H_{Meta}), 6.93 (t, J = 7.6 Hz, 1H, H_{Para}), 2.22 (s, 6H, Me). ^{13}C NMR (400 MHz, DMSO-d_6): δ (ppm) =153.6, 140.8, 136.0, 135.8, 129.1, 128.6, 128.1, 126.4, 121.8, 18.7. Data similar to previous publication.[119]

Synthesis of 21 1-(mesityl)-3-phenylurea

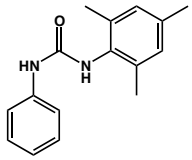

Compound **21** was prepared according to procedure 2 with the addition of phenylisocyanate (1 ml, 10 mmol, 1 eq.) to a solution of mesitylamine (1.68 ml, 12 mmol, 1.2 eq) in dry toluene (30 ml). The solution was diluted with hexane and the precipitate filtered to give the title compound (1.7g, 66 %). ^{1}H NMR (500 MHz, DMSO-d_6): δ (ppm) = 8.66 (s, 1H, NH), 7.60 (s, 1H, NH), 7.43 (d, J = 7.8 Hz, 2H, Ar_{Ortho}), 7.24 (t, J = 7.8 Hz, 2H, Ar_{Meta}), 6.91 (t, J = 7.2 Hz, 1H, Ar_{Para}), 6.87 (s, 2H, H_{Meta}), 2.22 (s, 3H, *p*-CH_3), 2.16 (s, 6H, *m*-CH_3). ^{13}C NMR (125 MHz, DMSO-d_6): δ (ppm) = 153.3, 140.4, 135.3, 134.9, 132.7, 128.7, 128.3, 121.3, 117.8, 20.5, 18.2. Data similar to literature.[73]

Synthesis of 22 1-(4-aminophenyl)-3-phenylurea

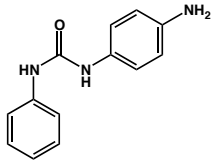

Compound **22** was synthesised from the reduction of **12** (1.52 g, 5.91 mmol, 1 eq.) by $SnCl_2.2H_2O$ (6.7 g, 29.7 mmol, 5 eq.), refluxing at 80 °C overnight in EtOH (50 ml). Reaction was followed by TLC (10% MeOH/CH_2Cl_2) then poured into ice and basified (pH = 8) with 2M NaOH. The product was extracted into EtOAc (3x) and combined organic layers were dried over $MgSO_4$ and removed *in vacuo* to give a white/cream powder (1.07g, 80 %). ^{1}H NMR (400 MHz, DMSO-d_6): δ (ppm) = 8.48 (s, 1H, NH), 8.13 (s, 1H, NH), 7.42 (dd, J = 8.6, 1.0 Hz, 2H, Ar_{Ortho}), 7.25 (t, J = 8.4 Hz, 2H, Ar_{Meta}), 7.07 (d, J = 8.7 Hz, 2H, H_{Ortho}), 6.93 (t, J = 7.3 Hz, 1H, Ar_{Para}), 6.51 (d, J = 8.7 Hz, 2H, H_{Meta}), 4.77 (s, 2H, NH_2). Similar to published data.[120]

Synthesis 23 1-(p-anisidine)-3-phenylurea

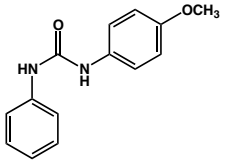

Compound **23** was prepared according to procedure 2 with the addition of phenylisocyanate (0.55 ml, 5 mmol, 1 eq.) to a solution of p-anisidine (738 mg, 6 mmol, 1.2 eq) in dry toluene (20 ml). Solution was diluted with hexane and the precipitate filtered (1.0 g, 82 %). ^{1}H NMR (500 MHz, DMSO-d_6): δ (ppm) = 8.51 (bs, 1H, NH), 8.49 (bs, 1H, NH), 7.36 (d, J = 8.5, 2H, Ar_{Ortho}), 7.34 (d, J = 8.0 Hz, 2H, H_{Ortho}), 7.26 (t, J = 7.0 Hz, 2H, Ar_{Meta}), 6.95 (td, J = 8.0, 1.0 Hz, 1 H, Ar_{Para}), 6.87 (d, J = 8.0 Hz, 2H, H_{Meta}), 3.72 (s, 3H, OCH_3). Comparable to published data.[79]

Synthesis of 24 1-(4-(decyloxy)phenyl)-3-phenylurea

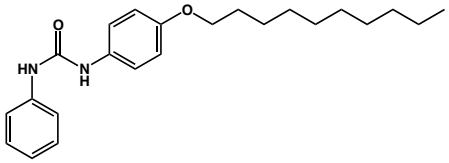

Step 1: Synthesis of **4-decyloxyaniline** (**24A**).[121] 4-Aminophenol (2.00 g, 18.4 mmol, 1 eq.) was dissolved in dry DMF and heated to 100 °C whilst NaH (60%, 0.85 g, 1.15 eq.) added portion-wise. 1-Bromodecane (3.8 ml, 18.3 mmol, 1 eq.) and a few crystals of NaI were added and stirred at 150 °C for 16 hours. The solution was cooled and extracted several times into $CHCl_3$ which was combined and washed with H_2O and Brine (x3), dried over $MgSO_4$ and solvent was removed *in vacuo*. Purified by silica column with a gradient column of MeOH/CH_2Cl_2 (Increasing MeOH 0-10%) with **24A** solidifying on standing. (Rf: 0.3) (1.63 g, 36 %). ^{1}H NMR (500 MHz, $CDCl_3$): δ (ppm) = 6.74 (d, J = 6.5 Hz, 2H, H_{Ortho}), 6.67 (d, J = 6.5 Hz, 2H, H_{Meta}), 3.87 (t, J = 6.5 Hz, 2H, OCH_2), 1.73 (m, 2H, OCH_2CH_2), 1.43 (m, 2H, $OCH_2CH_2CH_2$), 1.34-1.26 (m, 12H, CH_2 x 6), 0.89 (t, J = 6.5, 3H, CH_3).

Step 2: Title compound **24** was synthesised as in procedure 2 with the addition of phenylisocyanate (0.85 ml, 7.8 mmol, 1 eq.) to a solution of **24A** (1.6 g, 6.42 mmol, 0.82 eq.) in dry toluene (40 ml). Following removal of solvent *in vacuo* the solid was washed with hexane and filtered to give **24** as a crème solid (1.78 g, 75 %). ^{1}H NMR (400 MHz, DMSO-d_6): δ (ppm) = 8.55 (s, 1H, NH), 8.43 (s, 1H, NH), 7.43 (dd, J = 8.8, 1.6 Hz, 2H, Ar_{Ortho}), 7.33 (d, J = 9.2 Hz, 2H, H_{Ortho}), 7.26 (t, J = 7.6 Hz, 2H, Ar_{Meta}), 6.94 (t, J = 7.6 Hz, 1H, Ar_{Para}), 6.84 (d, J = 9.2 Hz, 2H, H_{Meta}), 3.89 (t, J = 6.4 Hz, 2H, OCH_2CH_3), 1.68 (m, 2H, OCH_2CH_3), 1.41-1.18 (m, 14H, $(CH_2)_7CH_3$), 0.852 (t, J = 6.8 Hz, 3H, CH_3). ^{13}C NMR (125 MHz, DMSO-d_6): δ (ppm)

= 154.3, 153.2, 140.4, 133.1, 129.2, 122.0, 120.4, 118.5, 115.1, 68.0, 31.8, 29.5, 29.4, 29.3, 29.2, 29.2, 26.0, 22.6, 14.4.

Synthesis of 25 butyl phenylcarbamate

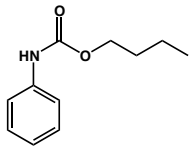

Compound **25** was formed using general procedure 1 using benzoic acid (1.0 g, 8.2 mmol, 1 eq.). Following general procedure 2, addition of butanol (0.75 mL, 8.2 mmol, 1 eq.) was substituted for the amine derivative. Purification was achieved by silica column chromatography (15% EtOAc/Hexane) to give a white solid (0.314 g, 20 %). ^{1}H NMR (500 MHz, DMSO-d_6): δ (ppm) = 9.58 (s, 1H, NH), 7.46 (d, J = 7.5 Hz, 2H, Ar_{Ortho}), 7.27 (t, J = 7.5 Hz, 2H, Ar_{Meta}), 6.98 (t, J = 7.5 Hz, 1H, Ar_{Para}), 4.08 (t, J = 6.5 Hz, 2H, OCH_2), 1.60 (q, J = 7.0 Hz, 2H, OCH_2CH_2), 1.39 (m, 2H, CH_2CH_3), 0.93 (t, J = 7.5 Hz, 3H, CH_2CH_3) ^{13}C NMR (125 MHz, DMSO-d_6): δ (ppm) = 154.1, 139.7, 129.2, 122.7, 118.6, 64.3, 31.1, 19.1, 14.1.

Synthesis of 26 methyl phenylcarbamate

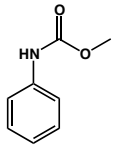

Compound **26** was formed by the addition of phenylisocyanate (0.5 ml, 4.6 mmol, 1 eq.) to a cooled solution of pyridine (1 ml, 12.4 mmol, 2.7 eq.) and anhydrous methanol (0.5 ml, 12.3 mmol, 2.7 eq.). The reaction mixture was stirred at rt overnight, added to water and extracted into EtOAc (x 2). The combined organic layer was dried over $MgSO_4$ and removed under reduced pressure to afford a white solid (0.57 g, 83 %). ^{1}H NMR (400 MHz, $CDCl_3$): δ (ppm) = 7.49 (d, J = 8.0 Hz, 2H, H_{Ortho}), 7.32 (t, J = 7.6 Hz, 2H, H_{Meta}), 7.08 (t, J = 7.2 Hz, 1H, H_{Para}), 6.68 (bs, 1H, NH), 3.79 (s, 3H, CH_3). Data similar to literature.[122]

Synthesis of 27 N-butyl-Benzamide

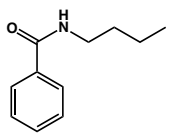

The title compound **27** was prepared in partial accordance with general procedure 1 with the addition of oxalyl chloride (3.4 ml, 36 mmol, 3 eq.) to benzoic acid (1.5 g, 12 mmol, 1 eq.) in CH_2Cl_2. Following removal of the solvent under reduced pressure, the product was dissolved in THF and cooled to 0 °C. K_3PO_4 (3.4 g, 15 mmol) was added in one portion followed by butylamine (1.2 ml, 12 mmol, 1 eq.) and stirred at rt for 1

hour. Solvent was removed (*in vacuo*) and the material extracted into EtOAc and washed with H_2O and brine. Organic phase dried over $MgSO_4$ and solvent removed under reduced pressure. Crude material was purified by column chromatography (9:1 hexane/EtOAc) to give a pale yellow solid (1.0 g, 47 % yield). ^{1}H NMR (500 MHz, DMSO-d_6): δ (ppm) = 8.42 (s, 1H, NH), 7.83 - 7.86 (m, 2H, H_{Arom}), 7.48 - 7.52 (m, 1H, H_{Arom}), 7.42 – 7.45 (m, 2H, H_{Arom}), 3.26 (q, J = 5.8 Hz, 2H, CH_2), 1.51 (m, 2H, CH_2), 1.32 (m, 2H, CH_2), 0.89 (t, J = 7.4 Hz, 3H, CH_3) ^{13}C NMR (125 MHz, DMSO-d_6): δ (ppm) = 166.1, 134.8, 130.9, 128.2, 127.1, 38.9, 31.3, 19.7, 13.7.

Synthesis of 28 N-butyl-4-methylbenzenesulfonamide 120

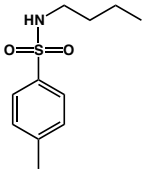

4-Toluenesulfonyl chloride (1.5 g, 7.9 mmol, 1 eq.) was dissolved in CH_2Cl_2 (20 mL) and butylamine (1.5 mL, 15.7 mmol, 2.0 eq.) and triethylamine (1.1 mL, 7.9 mmol, 2.0 eq.) was added under Ar. The solution was stirred over night at rt and before it was washed with H_2O (2 x 25 mL), dried over $MgSO_4$ and the solvent removed under reduced pressure to give a colourless sold (0.89 g, 50 %). ^{1}H NMR (500 MHz, $CDCl_3$): δ (ppm) = 7.77 (dd, J = 8.3, 1.8 Hz, 2H, H_{Ar}), 7.30 (d, J = 8.0 Hz, 2H, H_{Ar}), 5.04 (bs, NH, 1H), 2.91 (t, J = 7.1 Hz, 2H, NHCH_2), 2.42 (s, 3H, ArCH_3) 1.42 (m, 2H, CH_2CH_2CH_3), 1.28 (m, 2H, CH_2CH_3), 0.83 (t, J = 7.3 Hz, 3H, CH_3). Data similar to literature.[123]

Synthesis of 29 N-phenylmethanesulfonamide

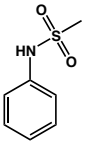

Methanesulfonyl chloride (0.23 ml, 3 mmol, 1 eq.) was added to a cooled solution of aniline (0.54 ml, 5.9 mmol, 2.0 eq.) and pyridine (1.5 ml, 18 mmol, 6.0 eq.) in anhydrous CH_2Cl_2 (10 ml) under argon. The solution was slowly warmed to rt and stirred at this temperature overnight. The red solution was washed with 2M HCl, water (x2) and brine (x2) and the organic layer was dried over $MgSO_4$ and concentrated under reduced pressure to give a white solid. (0.27 g, 53 %). ^{1}H NMR (400 MHz, $CDCl_3$): δ (ppm) = 7.48 (bs, 1H, NH), 7.34 (t, J = 7.2 Hz, 2H, H_{Ortho}), 7.28 (d, J = 7.6 Hz, 2H, H_{Meta}), 7.18 (t, J = 7.2 Hz, 1H, H_{Para}), 3.01 (s, 3H, CH_3). Data similar to literature.[124]

Synthesis of 30 4-((*tert*-butoxycarbonyl)amino)benzoic acid

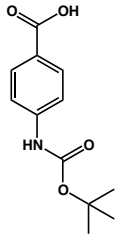

Title compound **30** was prepared by the addition of Boc_2O (2.90 g, 13.3 mmol, 1.25 eq.) and crushed NaOH (0.68 g, 17.0 mmol, 1.6 eq.) to a solution of 4-aminobenzoic acid (1.45g, 10.6 mmol, 1 eq.) in 30 ml t-BuOH/H_2O (1:1). The solution was stirred at rt overnight and monitored by TLC (3:1 CH_2Cl_2/EtOH). The organic solvent was removed by reduced pressure before cooled in ice. 1 M HCl (~ 15 ml) was added to produce a white precipitate that was filtered, washed with H_2O and dried under vacuum to give a white powder that did not require further purification (1.90 g, 76 %). ^{1}H NMR (500 MHz, DMSO-d_6): δ (ppm) = 9.72 (s, 1H, NH), 7.84 (dd, J = 7.0, 2.0 Hz, 2H, H_{Ar}), 7.56 (d, J = 8.5 Hz, 2H, H_{Ar}), 1.49 (s, 9H, 3xCH_3). ^{13}C NMR (125 MHz, DMSO-d_6): δ (ppm) = 167.5, 153.0, 144.2, 130.8, 124.6, 117.7, 80.1, 28.5.

Synthesis of 31 and 32

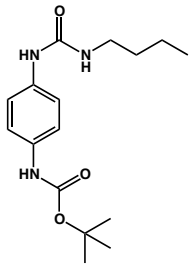

*Step 1- Synthesis of **31 (tert-butyl-(4-isocyanatophenyl)carbamate)**:* Compound **30** (1.0 g, 4.2 mmol, 1 eq.) was suspended in anhydrous CH_2Cl_2 (60 ml) and cooled in ice under argon. Oxalyl chloride (1.9 ml, 11.5 mmol, 2.7 eq.) was added dropwise over 30 mins followed by 0.1 ml DMF. Reaction mixture was stirred at room temperature for 2 hours. The solvent was removed under reduced pressure and redissolved in H_2O/THF (3:2). The mixture was cooled in ice to 0 °C after which a solution of NaN_3 (1.21 g, 18.6 mmol, 4.4 eq.) in H_2O (10 ml) was added dropwise over 20 minutes. Following stirring overnight at rt for 2 days, the mixture was extracted with CH_2Cl_2 (3 x 30 ml), dried over $MgSO_4$ and solvent removed under reduced pressure to give a light yellow/crème solid (0.812 g, 74 %). Solid was immediately dissolved in toluene (50 ml) and refluxed at 110 °C for 90 mins before removing solvent under reduced pressure (0.533 g, 74 %). *Step 2 – Synthesis of **32 (tert-butyl-(4-(3-butylureido)phenyl)carbamate)**:* **31** (0.263 g, 1.1 mmol, 1 eq.) was immediately dissolved in dry toluene (35 ml) and butylamine (0.21 ml, 2.2 mmol, 2.0 eq.) added drop wise. Reaction was stirred at 80 °C overnight before removing the solvent under reduced pressure to give a tan yellow solid (0.255 g,

74 %). ^{1}H NMR (500 MHz, MeOD-*d*$_4$): δ (ppm) = 7.90 (d, J = 8.5 Hz, 2H, H_{Ar}), 7.45 (d, J = 8.5 Hz, 2H, H_{Ar}), 2.91 (t, J = 7.5 Hz, 2H, NHC*H*$_2$), 1.63 (m, 2H, C*H*$_2$), 1.53 (s, 9H, C(C*H*$_3$)$_3$), 1.40 (m, 2H, C*H*$_2$CH$_3$), 0.95 (t, J = 7.5 Hz, 3H, C*H*$_3$). ^{13}C NMR (125 MHz, DMSO-*d*$_6$): δ (ppm) = 173.7, 153.6, 131.1, 128.6, 127.8, 117.1, 79.6, 39.1, 29.3, 27.3, 19.3, 12.5.

Synthesis of 33 1-(4-aminophenyl)-3-butylurea

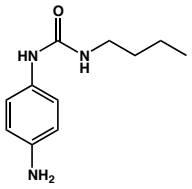

Deprotection of compound **32** (0.34 g, 1.10 mmol, 1 eq.) was achieved by addition of 50% HBF_4 (10 ml) at 0 °C. The solution was stirred at this temperature for 5 minutes then at rt for 30 mins before being freeze-dried overnight. ^{1}H NMR (500 MHz, MeOD-*d*$_4$): δ (ppm) = 8.17 (d, J = 8.5 Hz, 2H, H_{Ar}), 7.55 (d, J = 8.5 Hz, 2H, H_{Ar}), 2.95 (t, J = 7.5 Hz, 2H, NHC*H*$_2$), 1.64 (m, 2H, C*H*$_2$), 1.41 (m, 2H, C*H*$_2$CH$_3$), 0.95 (t, J = 7.5 Hz, 3H, C*H*$_3$).

Synthesis of 34 4-(3-butylureido)benzenediazonium tetrafluoroborate

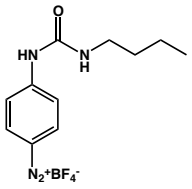

Deprotection and diazotisation of compound **32** (0.106 g, 0.34 mmol, 1 eq.) was achieved by addition of 50% HBF_4 (3 ml) at 0 °C. The solution was stirred at this temperature for 5 minutes then at rt for 30 mins. The solution was cooled again before the drop wise addition of $NaNO_2$ (53 mg, 0.77 mmol, 2.3 eq.) in H_2O (0.5 mL) over 5 minutes. Solution was stirred for a further 15 minutes and freeze-dried overnight to give a brown solid (59.3 mg, 56 %). ^{1}H NMR (500 MHz, MeOD-*d*$_4$): δ (ppm) = 8.73 (d, J = 8.5 Hz, 2H, H_{Ar}), 7.48 (d, J = 8.0 Hz, 2H, H_{Ar}), 2.95 (t, J = 7.6 Hz, 2H, NHC*H*$_2$), 1.65 (quint, J = 15.4, 15.3, 2H, C*H*$_2$), 1.47-1.40 (m, 2H, C*H*$_2$CH$_3$), 0.99 (t, J = 7.4 Hz, 3H, C*H*$_3$). ^{13}C NMR (125 MHz, MeOD-d$_4$): δ (ppm) = 141.6, 134.6, 132.6, 131.6, 119.8, 39.2, 29.1, 19.2, 12.4.

Synthesis of 35 4-(3-phenylureido)benzenediazonium tetrafluoroborate

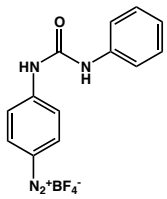

The title compound **35** was prepared by cooling a solution of **22** (0.25 g, 1.1 mmol, 1 eq.) in H_2O (5 ml) with 50% HBF_4 (0.2 ml) before addition of a cooled solution of $NaNO_2$ (82.2 mg, 1.2 mmol, 1.1 eq.) in H_2O (0.5 ml). The reaction was stirred in ice for 15 minutes followed by 45 minutes at rt. The solid precipitate was collected by filtration to give a light yellow solid (0.28 g, 80 %). ^{1}H NMR (400 MHz, DMSO-d_6): δ (ppm) = 10.14 (s, 1H, NH), 9.25 (s, 1H, NH), 8.51 (d, J = 9.2 Hz, 2H, H_{Meta}), 7.90 (d, J = 9.2 Hz, 2H, H_{Ortho}), 7.49 (d, J = 7.6 Hz, 2H, Ar_{Ortho}), 7.35 (t, J = 7.2, 2H, Ar_{Meta}), 7.08 (t, J = 7.2 Hz, 1H, Ar_{Para}) ^{13}C NMR (125 MHz, DMSO-d_6): δ (ppm) = 151.7, 138.6, 135.5, 129.5, 129.3, 123.9, 119.2, 118.9, 101.9. ESI-MS: *m/z* 239.41 [M^+]. IR / cm^{-1}: 2234.6 (s), 1730 (s), 1526 (s), 1094 (s).

Synthesis of 36 methyl-3-(4-(3-phenylureido)phenyl)acrylate

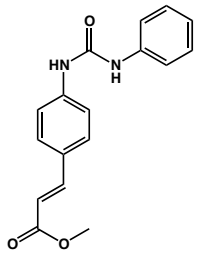

A solution of **35** (0.1963 g, 0.6 mmol, 1 eq.) was dissolved in MeOH (10 ml) and placed in a sealed flask that was evacuated and replaced with Ar. $Pd(OAc)_2$ (10%) was added quickly and resealed, followed by methylacrylate (0.3 ml, 3.3 mmol, 5.5 eq.). The reaction was heated to 50 °C for 30 minutes then stirred at rt overnight. Approximately 30 ml of EtOAc was added to the reaction before filtering over celite. The solvent was removed under reduced pressure and redissolved in CH_2Cl_2. Following washing with water and brine, the organic layer was dried over $MgSO_4$ and solvent removed under reduced pressure to give a pale yellow/brown solid (57.2 mg, 32 %). ^{1}H NMR (500 MHz, DMSO-d_6): δ (ppm) = 8.94 (s, 1H, NH), 8.75 (s, 1H, NH), 7.65 (d, J = 8.5 Hz, 2H, H_{Meta}), 7.61 (d, J = 16.0 Hz, 1H, C*H*), 7.52 (d, J = 8.5 Hz, 2H, H_{Ortho}), 7.46 (dd, J = 8.5, 1.0 Hz, 2H, Ar_{Ortho}), 7.30 (t, J = 7.5 Hz, 2H, Ar_{Meta}), 7.00 (t, J = 7.4 Hz, 1H, Ar_{Para}), 6.51 (d, J = 16.0 Hz, 1H, C*H*), 3.72 (s, 3H, OCH_3). ^{13}C NMR (125 MHz, DMSO-d_6): δ (ppm) = 167.4, 152.7, 144.9, 142.5, 139.9, 129.9, 129.3, 127.9, 122.6, 118.8, 118.4, 115.6, 51.8. IR / cm^{-1}: 2963, 1722, 1639, 1594, 1553, 1443, 1262 (s), 1094 (bs), 1022 (bs). HR/ESI-MS: *m/z* 297.1226 (expected 297.1234) [M+H]$^+$, 319.1036 (expected 319.1053) [M+Na]$^+$.

Synthesis of 37 1-(4-((4-hydroxyphenyl)diazenyl)phenyl)-3-phenylurea

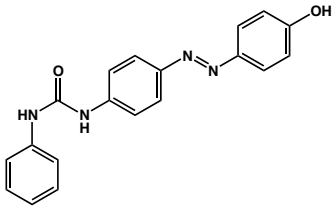

Compound **35** (0.298 g, 1.25 mmol, 1 eq.) was dissolved in H_2O (5 ml) where a separate solution of phenol (0.123 g, 1.31 mmol, 1.05 eq.) in 2 ml NaOH was added slowly giving an immediate colour change to dark orange. Following stirring for 30 minutes at rt, the solution was neutralised to pH 7 and the precipitate collected by filtration. The solid was thoroughly dried in a vacuum pump to give a dark brown/red powder (55 mg, 13 %). MP (°C): 218.9 – 219.1 (Decomposed at 245 °C). ^{1}H NMR (400 MHz, DMSO-d_6): δ (ppm) = 10.19 (s, 1H, OH), 9.08 (s, 1H, NH), 8.79 (s, 1H, NH), 7.79 (d, J = 8.6 Hz, 2H, H_{Ortho}), 7.75 (d, J = 9.1 Hz, 2H, H_{Meta}), 7.64 (d, J = 8.6 Hz, 2H, H_{Ortho}), 7.48 (d, J = 7.8 Hz, 2H, Ar_{Ortho}), 7.30 (t, J = 7.4 Hz, 2H, Ar_{Meta}), 6.99 (t, J = 6.9 Hz, 1H, Ar_{Para}), 6.92 (d, J = 9.1 Hz, 2H, H_{Ortho}). ^{13}C NMR (125 MHz, DMSO-d_6): δ (ppm) = 160.8, 152.8, 147.3, 145.8, 142.6, 139.9, 129.3, 124.8, 123.7, 122.6, 118.8, 118.5, 116.3. HR/ESI-MS: *m/z* 333.1363 (expected 333.1346) $[M+H]^+$, 355.1145 (expected 355.1165) $[M+Na]^+$.

Synthesis of 38 4-nitrobenzenediazonium

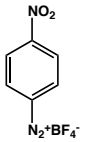

4-nitroaniline (1.0 g, 7.26 mmol, 1 eq.) was dissolved in H_2O (5 ml) and a solution of 50% HBF_4 (3.5 ml) was added before cooling to 0 °C in ice. $NaNO_2$ (0.55 g, 8.04 mmol, 1.1 eq.) was dissolved in H_2O (1.5 ml) in a separate flask before it was cooled in ice. This solution was added drop wise to the aniline solution, stirred for a further hour in ice and the precipitate was filtered. The crude material was dissolved in minimal acetone and diethyl ether was added until no more precipitate formed where it was filtered and washed with more ether to give a pale yellow solid (1.17 g, 68 %). ^{1}H NMR (500 MHz, DMSO-d_6): δ (ppm) = 8.94 (d, J = 9.3 Hz, 2H, H_{Meta}), 8.73 (d, J = 9.3 Hz, 2H, 2H, H_{Ortho}). IR / cm^{-1}: 2207 (s), 1541 (s), 1299 (s), 1112 (s), 1042 (s). Data similar to literature.[302]

Synthesis of VI 1,3-bis(3-nitrophenyl) urea

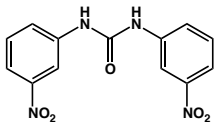

Triphosgene (105 mg, 0.35 mmol, 0.4 eq.) was weighed into a closed 2-neck flask; anhydrous toluene (15 ml) was added and sealed under Ar. A solution of 3-nitroaniline (130 mg, 0.94 mmol, 1.0 eq.) and NEt_3 (280 µl, 2 mmol, 2.1 eq.) in toluene (10 ml) was slightly heated until dissolved and added slowly via syringe over 15 mins to the 2-neck flask. White gas was produced and the resulting solution was stirred at rt overnight. The white precipitate NEt_3.HCl was filtered off and more 3-nitroaniline (141 mg, 1.02 mmol, 1.1 eq.) in anhydrous toluene (10 ml) was added to the solution. The combined solution was refluxed at 110 °C overnight. The solvent was removed *in vacuo* to give a tan solid (156.6 mg, 55 %). ^{1}H NMR (500 MHz, DMSO-d_6): δ (ppm) = 9.43 (s, 2H, NH's), 8.56 (s, 2H, H_{Ortho}), 7.86 (dd, J = 8.0, 1.0 Hz, 2H, $H_{Para,}$), 7.77 (d, J = 8.0 Hz, 2H, H_{Ortho}), 7.59 (t, J = 8.2 Hz, 2H, H_{Meta}). Data similar to literature.[93,125]

Complexation of VI with THF 1,3-bis(3-nitrophenyl) urea: THF complex

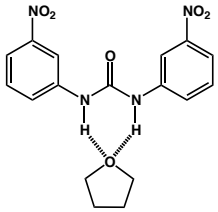

Single crystals of $C_{17}H_{18}N_4O_6$ [1,3-bis(3-nitrophenyl) urea:THF] were co-crystallised in a solution of THF to produce yellow prisms upon slow evaporation. A suitable crystal was selected and analysed on a Rigaku RAXIS conversion diffractometer. The crystal was kept at 140 K during data collection. Using Olex2,[126] the structure was solved with the Superflip[127-129] structure solution program using Charge Flipping and refined with the ShelXL[130] refinement package using Least Squares minimisation.

Crystal structure determination of [1,3-bis(3-nitrophenyl)urea:THF]. **Crystal Data** for $C_{17}H_{18}N_4O_6$ (M =374.35): triclinic, space group P-1 (no. 2),a = 8.21760(10) Å, b = 9.5145(2) Å, c = 11.5146(8) Å, α = 85.493(6)°, β = 71.205(5)°, γ = 87.001(6)°, V = 849.29(7) Å^3, Z = 2, T = 140 K, μ(CuKα) = 0.955 mm^{-1}, $Dcalc$ = 1.464 g/mm^3, 11628 reflections measured (14.424 ≤ 2Θ ≤ 143.974), 3098 unique (R_{int} = 0.0495, R_{sigma} = 0.0473) which were used in all calculations. The final R_1 was 0.0450 (I > 2σ(I)) and wR_2 was 0.1264 (all data).

Protons were found using the riding model except the urea protons, which were found by the difference map.

Synthesis of 77

2-ethyl-6-[(phenylcarbamoyl)hydrazino]benzoiso-quinoline-1,3-dione

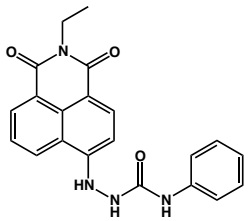

Procedure was followed in accordance with Ali *et al.*[131]

Step 1: 4-Bromo-1,8-napthalic anhydride (515 mg, 1.8 mmol, 1 eq.) and ethylamine (70% solution in water) (0.15 ml, 1.9 mmol, 1.05 eq.) were refluxed in 1,4-dioxane (35 ml) overnight. The solution was poured in H_2O and the precipitate filtered. Crude material immediately used in next step. *Step 2:* Crude napthalamide (565 mg, 0.66 mmol) was added hydrazine monohydrate (excess) and heated to 130 °C for 1 hour. The mixture was poured into water and the yellow precipitate filtered and dried to yield **2-ethyl-6-hydrazino-benzoisoquinoline-1,3-dione** (313 mg, 66%). Used immediately in next step. *Step 3:* Phenylisocyanate (0.15 ml, 1.4 mmol, 1.2 eq.) was added to the above amine (313 mg, 1.2 mmol, 1 eq.) in dry MeCN (25 ml) and refluxed at 85 °C overnight. The resulting precipitate was collected and purified by hot filtration with CH_2Cl_2:MeOH (1:4) to give the title compound as dark yellow solid (83 mg, 18 %). ^{1}H NMR (500 MHz, DMSO-d_6): δ (ppm) = 10.70 (bs, 2H, urea-NH), 10.09 (s, 1H, Napth-NH), 8.85 (d, J = 8.0 Hz, 1H, Naph-H_{Ar}), 8.56 (d, J = 7.0 Hz, 1H, Napth-H_{Ar}), 8.39 (d, J = 8.0 Hz, 1H, Napth-H_{Ar}), 7.89 (t, J = 7.5 Hz, 1H, Napth-H_{Ar}), 7.46 (d, J = 7.0 Hz, 2H, Ar_{Ortho}), 7.28 (t, J = 7.5 Hz, 2H, Ar_{Meta}), 7.05 (d, J = 8.5 Hz, 1H, Napth-H_{Ar}), 6.97 (t, J = 7.0 Hz, 1H, Ar_{Para}), 4.08 (d, J = 6.5 Hz, 2H, CH_2), 1.21 (t, J = 6.5 Hz, 3H, CH_3). Data similar to literature.[131]

CHAPTER THREE

Synthesis of catalysts for regeneration of H_2O_2

3.1 Introduction

The oxidation of a hydroxide ion to a hydroxyl radical is a one-electron process; therefore it requires a one-electron oxidant. Metal oxidants such as manganese, iron, cobalt and nickel complexes can achieve this transformation[132] but are inappropriate for the New Cathode. The goal of this project is to avoid metals. Also, the oxidant must be able to attach to the electrode surface to prevent self-discharge of the system. Therefore, an organic oxidant that can survive in basic conditions is required. Bipyridinium and benzoquinone are organic oxidants that allow one or two electron oxidation but decompose in highly alkali solutions.[133,134] Benzoquinone appears to undergo hydroxylation to form hydroxy-benzosemiquinone through a nucleophilic conjugate addition of the hydroxide ion instead.[135]

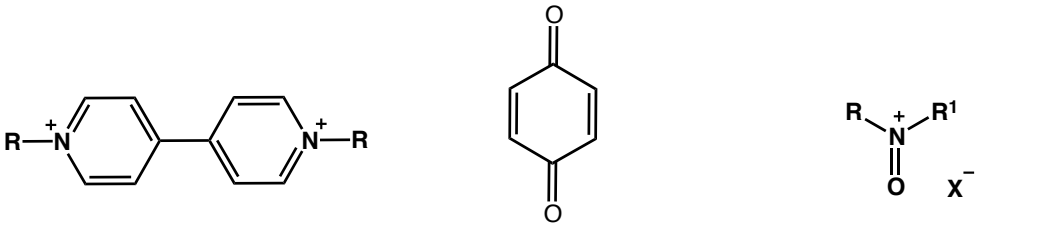

Bipyridinium Benzoquinone *N*-oxoammonium salt

Fig. 3.1. Organic oxidants.

More promising candidates are the *N*-oxoammonium salts (Fig. 3.1). This class of molecule has seen considerable use in organic chemistry. They have been catalysts for the oxidation of alcohols to aldehydes[136,137] since the late 1970s and have evolved to allow the selective reactions with amines,[138] phosphines, phenols and ketones.[139] While the use of an oxoammonium salt in a battery system is not novel there is considerable untapped potential in this area. The electrochemical conditions, the attachment and even the function of the catalyst

are all new. Many research groups have been attracted to the reversible electrochemical reaction of the oxoammonium cation for the development of polymers[140] as a charge-storage material in rechargeable batteries.[42,141] Polymer electrodes are advantageous due to the metal-free, and in some instances organic solvent-free,[141] conditions.

Many types of nitroxides have been used in oxidations (Fig. 3.2) and some of these could be modified to meet our strict guidelines, including stability under highly basic conditions.

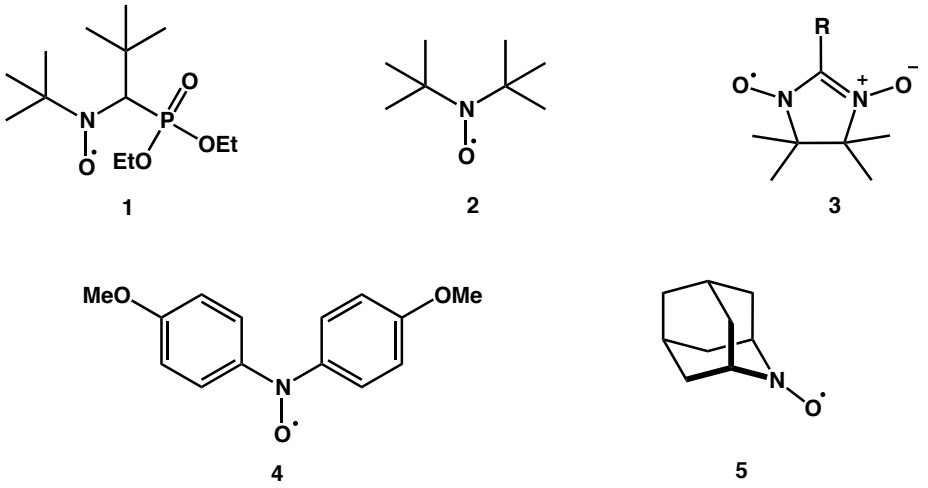

Fig. 3.2. Examples of nitroxides. 1,[142] 2-4,[143] 5.[144]

3.2 Background of Nitroxides

3.2.1 Structural characteristics of Nitroxides

Nitroxides are persistent, stable radicals that contain an unpaired electron delocalised over the nitrogen and oxygen atoms (Scheme 3.1). Delocalisation is responsible for the high stability of the radical centre (~420 kJ/mol)[145] as it is more thermodynamically favourable than the O-O product of dimerisation.

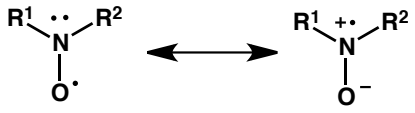

Scheme 3.1. Delocalisation of nitroxide.

The non-bonding pair of electrons on the nitrogen $2p_z$ orbital overlaps with the unpaired electron in the oxygen $2p_z$ orbital. This gives a doubly occupied π-orbital and the singly occupied π*-orbital (Fig. 3.3) generating a three-electron bond.[146]

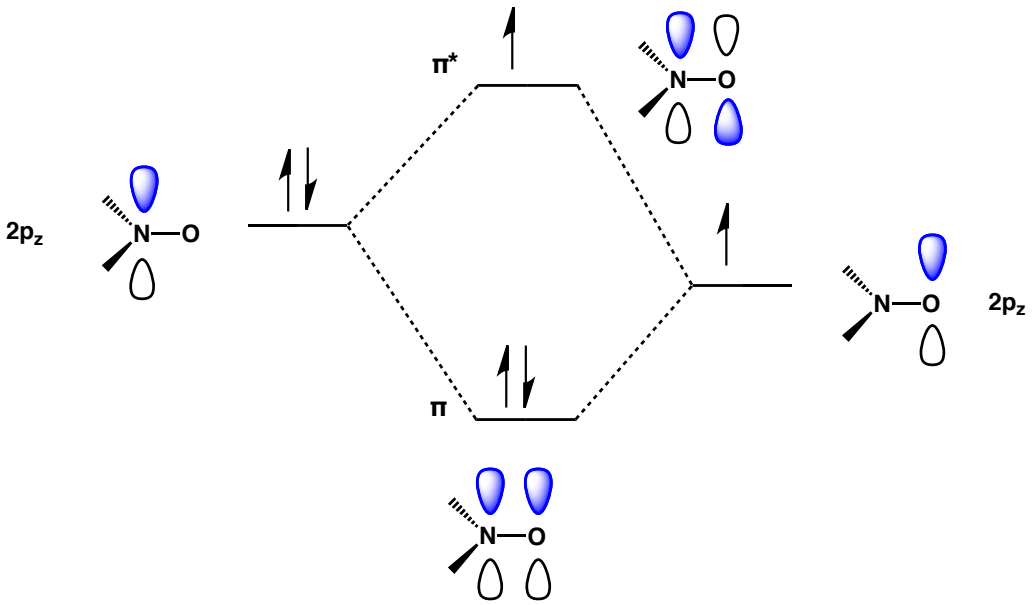

Fig. 3.3. Orbital diagram representative of a nitroxide.

While the stability of the nitroxide moiety has an electronic basis, the adjacent substituents are essential to preventing its decomposition. When α-hydrogens are present, it has been shown that the nitroxide moiety can disproportionate to give a nitrone and hydroxylamine species (Scheme 3.2).

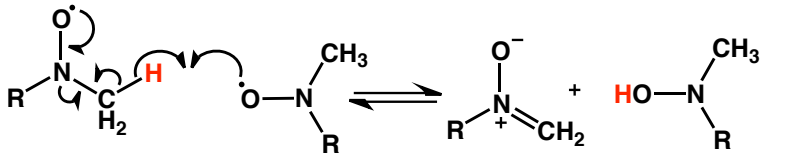

Scheme 3.2. Disproportionation of an unprotected nitroxide to give a nitrone and hydroxylamine species.

Aromatic substituents are unsuitable for the formation of persistent radicals as delocalisation of the spin density of the unpaired electron onto the ring increases the reactivity of the nitroxide.[147,148] This carbon-centered radical

enables the dimerisation with another nitroxide radical to give an amine and nitrone fragmentation products.

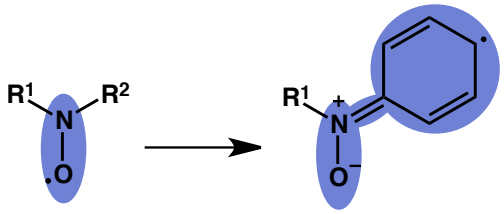

Scheme 3.3. Delocalisation of nitroxide depicted by shaded area.

The most widely studied nitroxides, due to their stability and the absence of the degradation pathways presented above, include PROXYL, TEMPO and TMIO (Fig. 3.4). The adjacent methyl groups protect the nitroxide centre and thus permit the radicals to be handled under common laboratory conditions. The 5-membered ring 2,2,5,5-tetramethylpyrrolidin-1-yloxyl (PROXYL) and 6-membered ring 2,2,6,6-tetramethylpiperidin-1-yloxyl (TEMPO) are the most widely reported nitroxides in the literature possibly due to their commercial availability. 1,1,3,3-Tetramethylisoindolin-2-yloxyl (TMIO) fuses PROXYL with an aromatic ring to give a molecule that is more readily functionalised expanding the array of stable radical compounds.

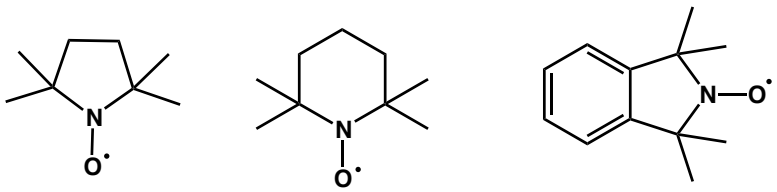

Fig. 3.4. Promising nitroxides.

3.2.2 Redox properties of Nitroxides and Oxoammonium cations

3.2.2.1 Oxidation

Nitroxides may behave as a weak oxidant or a weak reductant depending on the reactant present in the solution. The oxidation of a nitroxide normally requires a strong oxidant to form the oxoammonium salt (Scheme 3.4). These species are more reactive due to their electron deficiency and higher reduction potentials. In

alkali conditions many oxidants have been used, eg. Cl_2, Br_2, $NaBrO_2$, $NaClO_2$/NaOCl, $K_3Fe(CN)_6$,[149] $RuCl_2(PPh)_3/O_2$.[145]

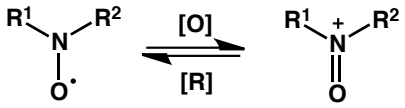

Scheme 3.4. Redox of nitroxide with oxoammonium cation.

Formation of a nitroxide from a secondary amine also requires a strong oxidant. The most common is *meta*-chloroperoxybenzoic acid (*m*CPBA), although others such as a tungstate catalyst with H_2O_2 will also furnish the product with respectable yields. Initially this forms the hydroxylamine species. The oxidation from the hydroxylamine to the radical species is relatively simple using mild oxidants such as PbO_2. Auto-oxidation in atmospheric O_2, although slow, is also a viable way to obtain the nitroxide (Scheme 3.5).

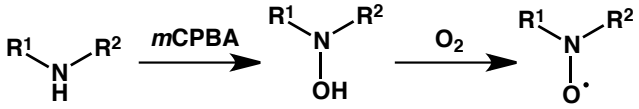

Scheme 3.5. Oxidation of an amine with *m*CPBA and O_2 to form a nitroxide.

3.2.2.2 Reduction

Many reactions are based on the reactivity of the oxoammonium salt, however some are based on the reduction of nitroxides as used in photochemistry and thermolysis.[150]

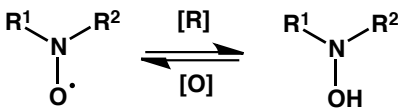

Scheme 3.6. Redox of nitroxides to hydroxylamines

Nitroxides may be reduced in solution to give hydroxylamines by ascorbic acid,[151] hydrazine derivatives and *p*-phenylenediamine (Scheme 3.6). It may also

be reduced by metal ions such as Cu^{+} and Fe^{2+}. For example, ascorbic acid is a mild reductant that can release one electron owing to the resonance-stabilisation of the radical ion, to form semidehydroascorbate (Scheme 3.7). More powerful reducing agents, such as Na_2S, $NaBH_4$ and $SnCl_2$, may reduce the hydroxylamine further to generate secondary amines.

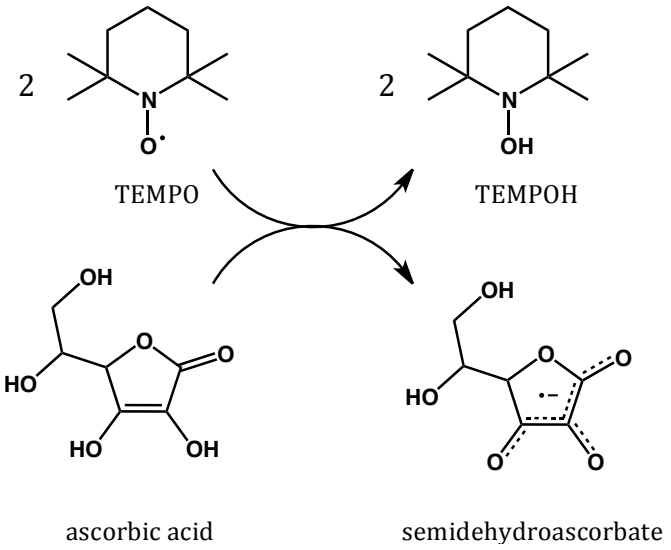

Scheme 3.7. Reduction of TEMPO to the corresponding hydroxylamine with ascorbic acid.

Combining all the redox reactions generates a relationship that connects all species by electron transfer between compounds (Scheme 3.8). This clearly shows the two-electron coupling between the secondary amine and hydroxylamine species and the one-electron coupling of the nitroxide with the oxoammonium cation and hydroxylamine species.

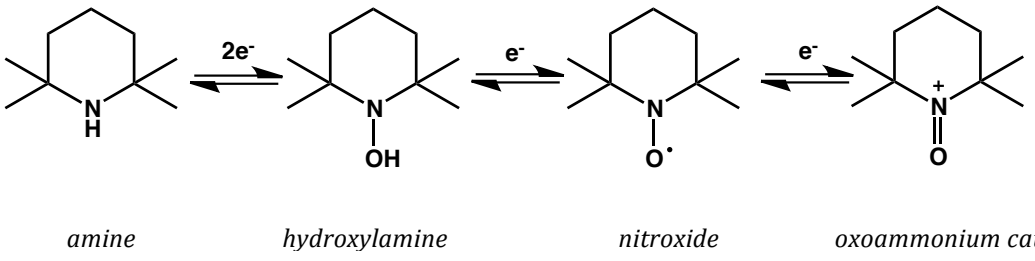

Scheme 3.8. Combination of all the redox processes that connect these species.

3.2.2.3 Redox of oxoammonium catalysts in the oxidation of alcohols

In the oxidation of alcohols in a weakly alkali solution, the oxoammonium cation abstracts a proton from the substrate and is reduced to the hydroxylamine. For regeneration of the catalyst, the nitrosonium ion (+N=O) can react with one molecule of the hydroxylamine to generate the TEMPO radical (Scheme 3.9).[145] A primary oxidant is required that continuously oxidises the radical species regenerating the nitrosonium ion, permitting the use of a catalytic amount.

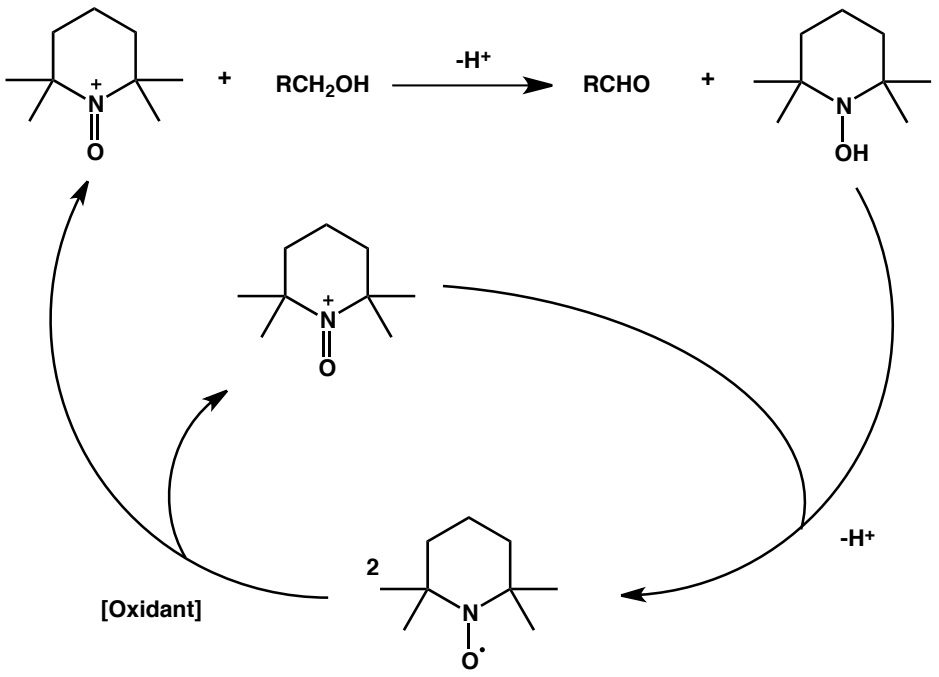

Scheme 3.9. Oxidation of a primary alcohol with an oxoammonium catalyst to give an aldehyde and hydroxylamine.

In our proposed system the oxidation of hydroxide ion is a one-electron process; therefore our product is the nitroxide radical, not the hydroxylamine. This reduces the need for oxidation of the N-OH species. The one-electron oxidation of the nitroxide regenerates the oxoammonium cation. This will be performed electrochemically when attached to the surface, although a primary oxidant must be added when performing the reaction in solution.

3.3 Objectives of this work

The aim of this part of the project was to attach a nitroxide onto a surface. Once attached it will then undergo electrochemical oxidation (Fig. 3.5) to the oxoammonium cation. The oxoammonium cation can potentially oxidise a hydroxide ion by abstraction of a single electron. This reduces the cation to a radical, which can be re-oxidised through electrochemical oxidation completing the catalytic cycle.

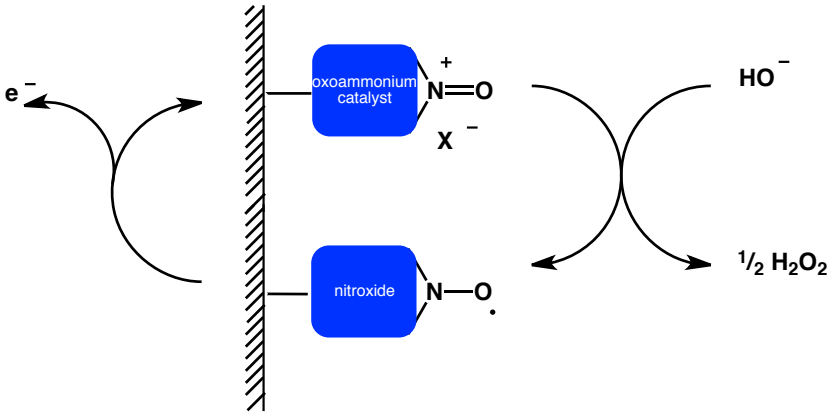

Fig. 3.5. Illustration of the objective of the catalyst.

3.4 Nitroxide templates

Endo first reported that 4-methoxy-TEMPO underwent a one-electron oxidation to give an oxoammonium cation that could be used to oxidise 2 hydroxide ions to give hydrogen peroxide (Scheme 3.10).[152] A primary assumption here is that two hydroxy radicals combine to form one hydrogen peroxide molecule. The influence of pH on the reaction was prominent as higher yields of H_2O_2 were observed for pH 9-11 in both aqueous phosphate and carbonate buffer solutions.

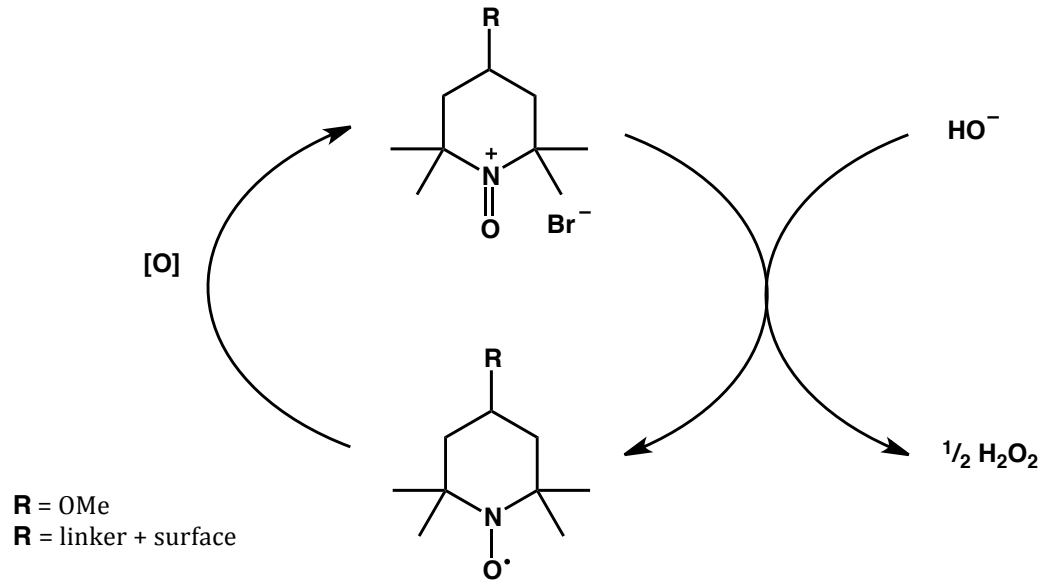

Scheme 3.10. Proposed scheme of the oxidation of hydroxide. First reported for R = OMe.[152]

Due to its extensive use in chemistry, TEMPO and its oxoammonium salt were chosen as the initial model. Analogous forms of TEMPO, that differ in substituents and oxidation potentials were to be investigated and attached to a surface. The outcome is not to design an exact template that is to be used in the battery system, but to identify what characteristics are needed for the best result under typical battery conditions. The free radical, TEMPO (2,2,6,6-tetramethylpiperidin-1-yloxyl), is a precursor for the oxoammonium catalyst (TEMPO+). TEMPO is a 6-membered heterocycle that posses a nitroxide moiety flanked by vicinal methyl groups. It is the most prominent stable radical used in chemistry and biochemistry for applications in pro-fluorescent probes, spin labelling, spin trapping and in antioxidants.[153] The radical nature of TEMPO causes practical problems for the synthesis. Radical side reactions such as alkylation are an issue.[154] ^{1}H NMR is of little value as TEMPO is paramagnetic.

3.4.1. Spectroscopy of Nitroxides

Generally, radical species have short lifetimes and therefore are difficult to detect spectroscopically. In comparison to other free radicals, nitroxides are a stable and kinetically persistent radical. This allows characterisation by methods such as electron paramagnetic resonance (EPR) spectroscopy. EPR is similar to NMR except that it measures the energy differences found between electrons of different spin states instead of protons.

Unfortunately, the physical features that make radicals ideal for study by EPR result in the same compounds being unsuitable for ^{1}H NMR. The nitroxide is paramagnetic causing interference with NMR experiments by interacting with nuclear spins thereby causing rapid intramolecular and intermolecular relaxation of nearby protons.[147] This causes broadening of peaks decreasing the ability to determine the accurate chemical shifts of the structure. It is crucial for a synthetic chemist to gain structural information on their target compounds; therefore NMR spectroscopy is often the key for initial product analysis. There are several possibilities that can be utilised to prevent the broadening of peaks. An increase in the concentration of up to 3 M may shorten the electron spin relaxation time.[147] Alternatively the use of a paramagnetic solvent such as di-*tert*-butyl nitroxide can be used as a spin relaxer. Lee *et al*. described the use of phenylhydrazine to reduce the nitroxide *in situ.*[155] This leads to the corresponding *N*-hydroxylamine giving rise to well resolved proton spectrums (Scheme 3.11).

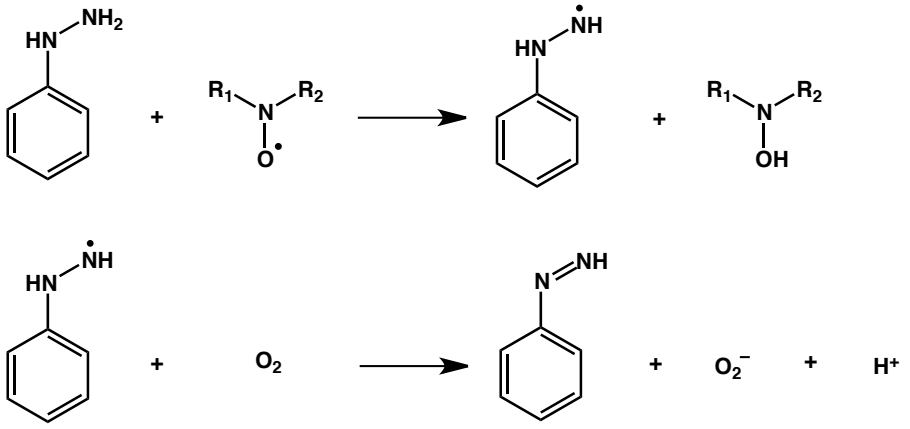

Scheme 3.11. Possible scheme for nitroxide reduction using phenylhydrazine for NMR.[156]

Mass spectrometry of nitroxides produces interesting results. Smith demonstrates that the ESI-MS of several nitroxides is dominated by oxidation rather than protonation.[157] In some instances, fragmentation of TMIO-derived nitroxides is more significant whereas piperidinyl nitroxides are less so. In each case the predominant peaks are the $M^{+\bullet}$, $MH^{+\bullet}$ and $MH_2^{+\bullet}$ ion species.

3.5 Catalyst Design

The proposed TEMPO-derived catalysts must be tethered to the carbon electrode. We plan to achieve this through an amine functionality capable of diazotisation as discussed in Chapter 2. The distance between the nitroxide moiety and the surface (x) may affect the ability of the electrochemical system to deliver an electron to the electrode, re-oxidising the catalyst (Fig. 3.7).

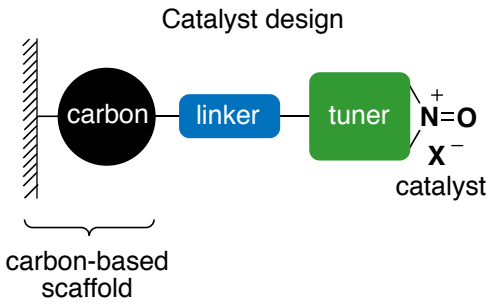

Fig. 3.6. Illustration of the proposed catalyst design.

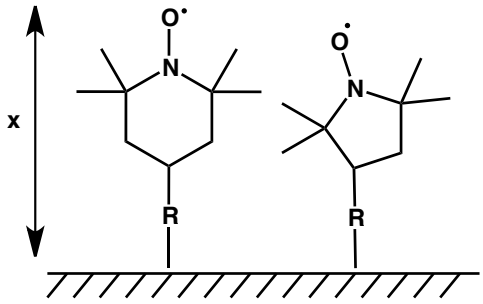

Fig. 3.7. Proposed catalysts that has varying distance (x) from the nitroxide moiety to the surface.

The tuner, which contains the catalytic moiety, is either a 5 or 6 membered ring. It was proposed that the internal angle of the ring may be of significance to its catalytic ability. The 5 membered ring has increased ring strain that potentially allows the nitroso functionality to be less hindered by the adjacent methyl groups thus effecting the oxidation potential. A linker to the carbon surface connects a TEMPO-like template, including the catalytic functional group (Fig. 3.6). The linker may possess different electronic properties, structural

flexibilities and base stability. The backbone of the linker will generally include a phenyl ring as it can be easily functionalised, permitting stacking onto a surface in analogous fashion to the substituted ureas (Section 2.5).

3.6 Results and Discussion

A key step was the proof that an oxoammonium salt, such as TEMPO or a close derivative, could generate H_2O_2 from hydroxide anions. This would confirm the validity of the 1984 paper (see Chapter 4 for details). This first required the oxidation of TEMPO from the nitroxide to the oxoammonium salt, which is the active species in the oxidation of hydroxide.

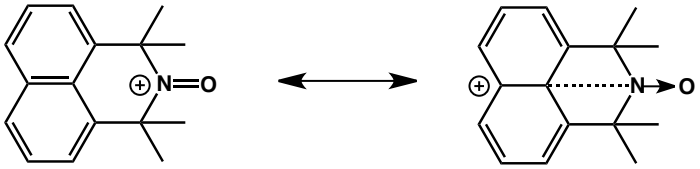

39

Fig. 3.8. Delocalisation of positive charge in the cation azaphenalene species by hyperconjugation (dotted line).

Oxidation potentials of the nitroxides are directly related to the size and flexibility of the heterocycle, and the electronics of the substituents. The ease of nitroxide oxidation is influenced by the flexibility of the ring and how readily the nitrogen can adopt a planar conformation.[158] Piperidine and pyrrolidine derivatives are both relatively easy to oxidise, but the presence of the aromatic ring in isoindoline restricts flexibility leading to higher redox potentials. Azaphenalenes (**39**), despite having two fused aromatic rings, are more readily oxidised. It is thought that this is due to delocalisation of the cationic species by hyperconjugation with the napthyl moiety (Fig 3.8).[158,159]

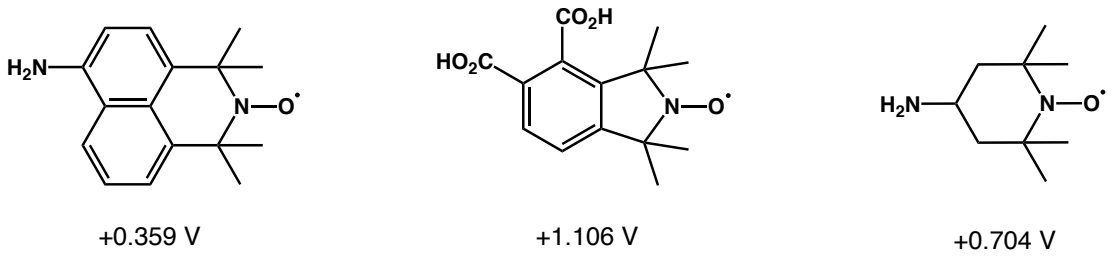

Fig. 3.9. Oxidation potentials of three nitroxide compounds.

Electron donating substituents on the aromatic ring can also help stabilise the charge on the oxidised species hence tend to have a smaller oxidation potential (Fig. 3.9). Potentials can range from +0.3 to +1.2 V for nitroxides.[158] As this can be relatively high, the formation of the oxoammonium ion requires stronger oxidants such as an acid, bromine, chlorine, or a Lewis acid such as an aluminium halide. The ability for the oxoammonium salt to be isolated depends on its stability and practical considerations such as solubility. Physical and chemical properties of the oxoammonium are also dependent on the associated anion. This is largely due to their hygroscopic character and light sensitivity.

All of the desired products were initially synthesised in the stable radical form, with the intention of undergoing a one-electron oxidation once attached to a carbon surface. However, to verify the formation of the oxoammonium salt and study their properties the reactions were performed in solution first.

3.6.1 Oxidation of TEMPO

Following the procedure described by Endo,[152] a solution of Br_2 in CCl_4 was added to TEMPO forming a brick red solid, which was isolated by filtration. Hunter *et al.* also described a similar method, employing chlorine gas as the oxidant, which produced an insoluble orange solid.[139] In order to avoid CCl_4, due to its toxicity and limited availability in New Zealand, an alternative method using dichloroethane (DCE) and hexane was tested (Scheme 3.12). Due to its success this method was used in subsequent oxidation experiments (see experimental). Unfortunately, the use of bromine as the oxidant results in

formation of a salt with uncertain stoichiometry; it is unclear whether it exists as bromide, tribromide or a combination of both.[160] The assumption has been made that it exists as a monobromide and can be controlled by the amount of Br_2 added in the reaction. Mass spectrometry supports our assumption by the presence of both the single bromide isotopes at 79 and 81 m/z, and the absence of the other bromide anions. TEMPO was oxidised with bromine to give compound **40** as a bright red salt in less than 30 minutes. The product shows a distinct nitroso stretch (N=O) in the IR at 1602 cm^{-1} and promising ^1H NMR in d_8-THF showing sharpening of peaks indicating the compound is no longer paramagnetic.[161] The oxidation could also be achieved under aqueous conditions. This involved BF_4^- as the counter anion and NaOCl as the oxidant. This method required cooling to 0 °C and stirring for 1 hour to produce a bright yellow solid (**41**). The melting point (160-161 °C) was similar to the literature[162] and also showed a strong nitroso stretch (N=O) at 1627 cm^{-1} previously seen in oxoammonium salts.

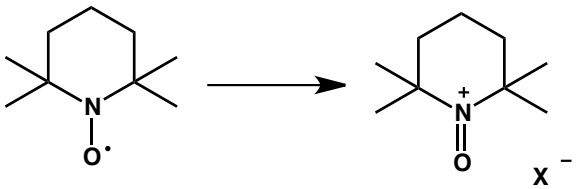

40/41

Scheme 3.12. Oxidation of TEMPO to TEMPO+ under new conditions.

Table 3.1. Oxidation of TEMPO conditions.

	X	Conditions	Yield (%)
40	Br^-	Br_2, DCE/Hexane	48
41	BF_4^-	HBF_4, NaOCl, H_2O	75

The oxoammonium salt (**40**) was then employed in the oxidation of hydroxide ions to hydrogen peroxide. Initial experiments with TEMPO+ (1 mmol) and a 0.1 M potassium hydroxide solution gave promising results. A decrease in pH

from 14 to 7 indicates the consumption of hydroxide ions. Also a positive reading of peroxide with the test strips/dip sticks was observed. These Quantofix® test strips measure a semi-quantitative amount of O_2^{2-} in mg/L after neutralisation to pH 5-7 with citric acid. Unfortunately, after further investigation it was discovered that the nitrosonium ion gives a false positive reading with these test strips. Other structures with similar features were also tested with the peroxide test strips to determine whether a certain functional group was causing the false positive. These compounds include TEMPO, KOH, TBAB and 4-methoxypyridine N-oxide, which all gave readings of 0 mg/L (Fig. 3.10). It appears that strong oxidising agents interfere with the H_2O_2 determination in the test strips.

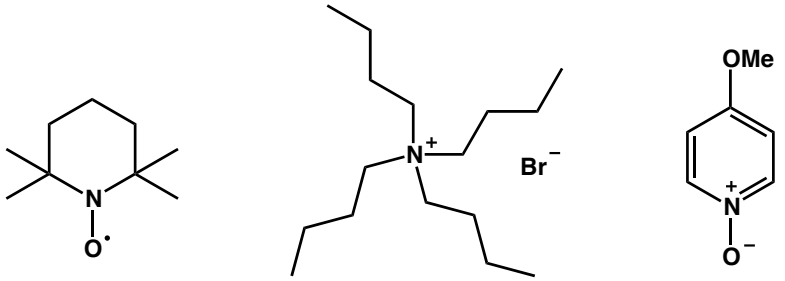

Fig. 3.10. a) TEMPO b) tetrabutylammonium bromide (TBAB) c) 4-methoxypyridine N-oxide

The Endo publication reported extraction of the nitroxyl radical by-product from the aqueous solution with ether. The concentration of the remaining aqueous H_2O_2 solution was determined by iodometric titration. As residual oxoammonium salt remains in aqueous solution, its potential interference causes suspicion into Endo's results. According to their results, an almost stoichiometric amount of H_2O_2 was formed. However, ether is also good at forming a mixture with H_2O_2, so loss of H_2O_2 into the ether layer is a potential problem. Although they claim to see H_2O_2 by mass spectrometry, there are doubts about the validity of this method and the means by which the controls were confirmed. Therefore, in order to test the formation of H_2O_2 from hydroxide ions, the catalyst needs to be effectively separated from the aqueous layer. This could be achieved by either 1) attaching the catalyst to a solid

support or 2) making the catalyst hydrophobic. The attachment to a solid support permits the removal of the catalyst by filtration. As we wanted to characterise each step in the catalytic process, it was unfeasible to directly attach the nitroxide to a carbon surface in these initial stages. Most solid supports are polymer-based and their stability is questionable in H_2O_2. As the catalyst is attached in the stable radical form, it requires the oxidation to the active oxoammonium. This oxidation, as explained earlier, involves strong oxidants and acids that could potentially cleave the catalyst from the support. An alternative strategy was to alkylate 4-hydroxy-TEMPO with a hydrophobic alkane allowing us to effectively form a biphasic system but retaining the ability to perform solution phase chemistry and characterisation without having to cleave it from the support. This was favoured due to the ability for it to exist in a biphasic system (explained further in Chapter 4), which acts like a surface, analogous to an electrode.

*3.6.2 Alkylation of 4-hydroxy-TEMPO to give 4-(decyloxy)-2,2,6,6-tetramethyl-piperidin-1-oxyl (**42**)*

Alkylation of 4-hydroxy-TEMPO with bromodecane required a strong base, NaH, to make an activated nucleophile for S_N2 substitution (Scheme 3.13). Addition of NaI increases the rate of the reaction through the Finklestein substitution. After purification by column chromatography the bright orange oil was subjected to mass spectrometry. An intensity of 100% was seen for the MH^+ at 313.61 m/z (M^+ 32% and MH_2^+ 33%) characteristic of protonated **42**. There is a potential for alkylation to occur at the nitroxide, but it should not be favoured under these conditions.[163]

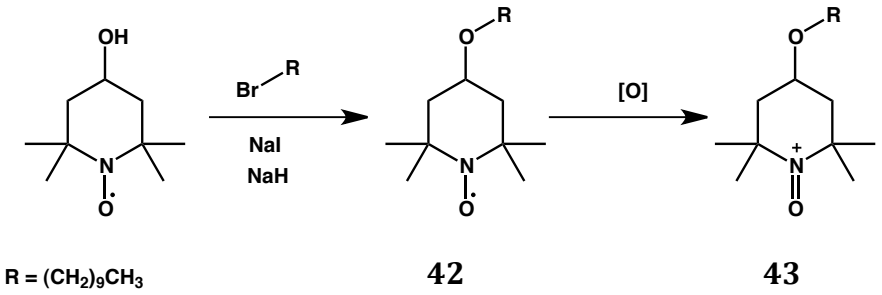

Scheme 3.13. Alkylation of 4-hydroxy-TEMPO followed by the proposed oxidising conditions that are required to form the resulting oxoammonium cation.

The clean oxidation of alkylated TEMPO (**42**) to the oxoammonium cation (**43**) has proven to be a challenge and it is explained in more detail in Section 4.41.

3.7 Synthetic Targets

The catalyst design involves three sections; linker, tuner and catalytic moiety. The tuner investigated in this project is described as a 5 or 6-membered ring that incorporates the catalytic moiety. As it may be directly attached to an aromatic ring, substituents on this ring also change the redox potential of the catalyst. The linker is similar to that of the substituted ureas and a phenyl ring will allow diazonium chemistry to bind the catalyst to the surface. There are a number of different methods to join the phenyl ring to the catalyst. Functionalisation of TEMPO derivatives frequently involves an ester linkage[164] due to the ease of coupling with the commercially available 4-hydroxy-TEMPO. Unfortunately, an ester is susceptible to hydrolysis in strong basic conditions and therefore is not suitable for this project. Excluding the prevalent ester-linkage, 5 analogues of nitroxides were proposed which varied in composition of the tuner and linker, and distance to the surface (Fig 3.11).

Three targets involved the incorporation of an aniline moiety that could later be converted to a diazonium species (**44**-**46**). In one target the aromatic ring was removed completely (**47**). While in the last the aromatic ring was fused to a pyrrolidine ring (**48**). Of these five targets, four follow a conventional linear

synthetic route (**44**, **45**, **47**, **48**). While compound **46** was to be made by the cycloaddition of an alkyne and azide in the so-called 'click' chemistry reaction. In this route the alkyne is already attached to the surface and the nitroxide containing azide is coupled *in situ*.

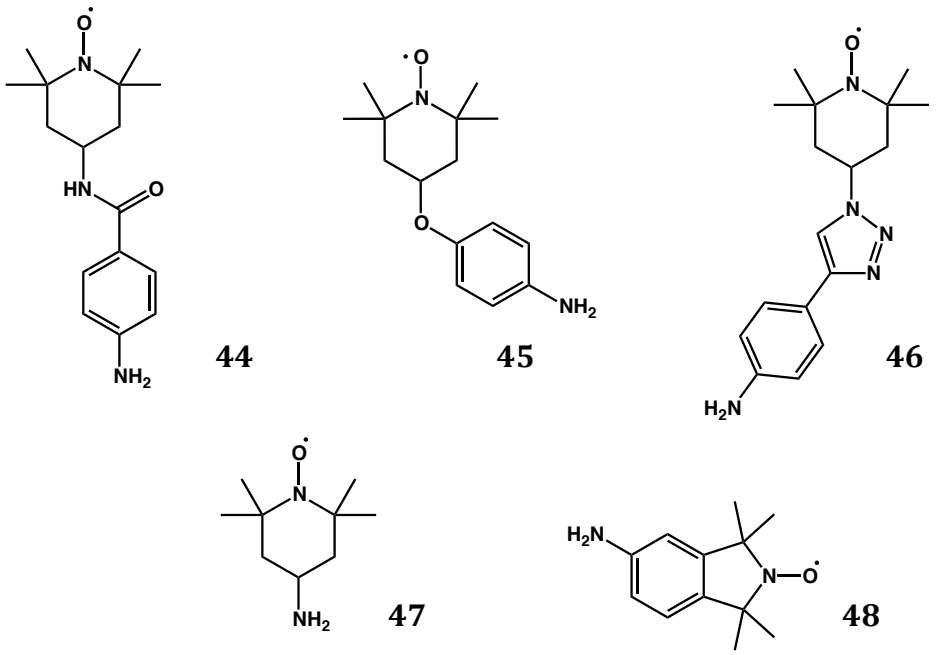

Fig. 3.11. Synthetic targets.

3.7.1 Synthesis of amine-containing nitroxides

*3.7.1.1 Synthesis of 4-amino-N-(1-oxyl-2,2,6,6-tetramethylpiperidin-4yl) benzamide (**44**)*

Functionalised 4-amino-TEMPO derivatives have been prepared by using peptide-coupling reactions with reagents such as DCC and HOBt.[165] 4-Amino-2,2,6,6-tetramethylpiperidine (**49**) was used as a substitute for 4-amino TEMPO (**47**) to avoid the nitroxide radical and additional synthetic steps in its formation. In an analogous fashion, coupling of **49** with fluorenylmethyloxycarbamate (Fmoc) - protected 4-aminobenzoic acid was attempted. This reaction failed due to the presence of two amine nucleophiles in **49** capable of nucleophilic attack, giving multiple products. However, this suggests that the presence of the nitroxide is required for the success of the

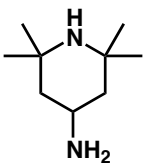

49

coupling reaction by this method. An attempt was also made to couple Fmoc-protected 4-aminobenzoylchloride with **49**. Both of these reactions failed due to the ability of **49** to act as a weak base and cleave the Fmoc protecting group. Consequently this allows further side reactions and polymerisation to occur.

The unsuccessful attempt to shorten the peptide-coupling method, in conjunction with the lengthy procedure to make 4-amino-TEMPO (see below), made this method undesirable. Alternative amine protecting groups were considered, such as boc, benzyl, silyl, and sulfonyl groups, but were discarded due to their instability to subsequent reactions or a lack of suitable deprotection conditions (eg. hydrolysis). The most successful route to form the amide bond was by coupling of 4-nitrobenzoylchloride with **49** to give compound **50** (Scheme 3.14). This method does not require a protecting group and is reliant on the lower basicity of the primary amine in **49** over the sterically hindered secondary amine and reactivity of the acyl chloride due to the electron-withdrawing group.

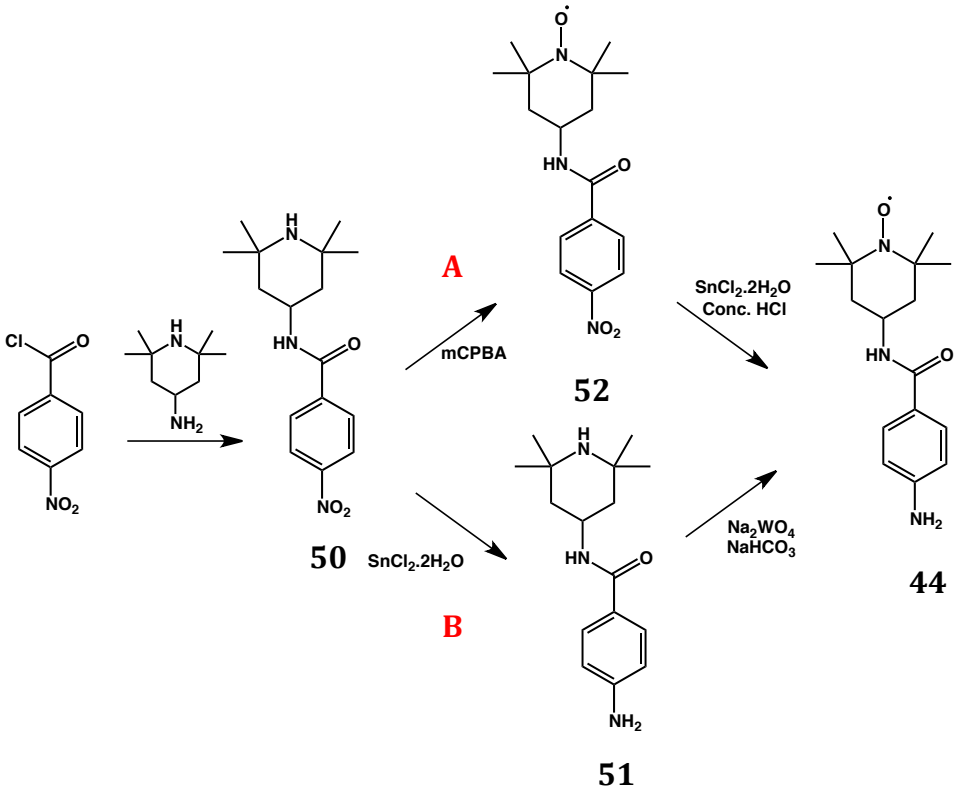

Scheme 3.14. Multiple proposed pathways to synthesise nitroxide **44**.

This route was not without its challenges; it requires either a selective oxidation (Path B) or a selective reduction of an amine (Path A) to form **44**. The oxidation of a secondary amine to a nitroxide with Na_2WO_4 and H_2O_2 has been shown to occur with moderate yields[166-169] but there have, to the best of our knowledge, been no reports of a selective oxidation of an amine in the presence of an aniline. However, an analogous oxidation has been achieved in the presence of an amide (Scheme 3.15).[170] Following the reduction with tin chloride to give compound **51**, unfortunately, in our hands a clean oxidation with Na_2WO_4 and H_2O_2 was not possible. It gave multiple products and little conversion after 48 hours.

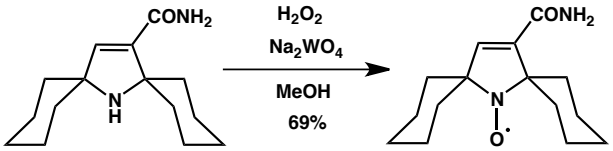

Scheme 3.15. Alternative nitroxide oxidising conditions.

Presumably, the aniline interferes with the oxidation process possibly by forming a nitroso group that initiates its decomposition. Reversing the steps and performing an oxidation followed by a selective reduction (Path A) was more successful. Oxidation was simply achieved by the addition of *m*CPBA in CH_2Cl_2. The mechanism of this reaction is still debated[171] but is believed to proceed through the cleavage of the weak *m*CPBA peracid bond to form the hydroxylamine species. A second oxidation possibly with molecular oxygen can convert the hydroxylamine to the desired radical species. Complex **52** displayed many of the characteristics common to these radical species; it was bright orange and its ^1H NMR displayed typical line broadening.

On addition of phenylhydrazine, the nitroxide radical was reduced to the hydroxylamine, which can be characterised by NMR. When comparing this with compound **50**, an anisotropic contribution from the oxygen must be considered. This through-space anisotropy shields the adjacent methyl groups, exhibiting an up field chemical shift. This shift correlates to the presence of the lone pairs in the oxygen and is absent in the secondary amine.

It is possible to selectively reduce the nitro group in the presence of the nitroxide by treatment with $SnCl_2.2H_2O$ in highly acidic conditions.[166] Following the nitroxide formation, selective reduction of the nitro group (**52**) was performed, which gave compound **44** as a yellow solid. The brightly coloured compound is characteristic of a free radical suggesting the nitroxide was not reduced under these conditions. The distinctive high field shift of the aryl protons in the ^1H NMR with phenyl hydrazine indicates conversion of the electron withdrawing nitro group into an electron donating amine. For further confirmation of the presence of the aryl amine and nitroxide functionality, a methyl trap was employed.

The radical can be trapped by nitroxide alkylation where the resulting species is no longer paramagnetic. The reactivity of the methoxyamine group makes it suitable for a nitroxide protecting group. One possible method for alkylation is by the addition of CH_3Li, at -78 °C.[172] Two more practical methods that generate the methoxyamine include: Fenton chemistry in DMSO[173] or the CuCl-catalysed decomposition of an aldehyde peroxide intermediate.[174] In the former, the methoxyamine is formed from the oxidation of $FeSO_4.7H_2O$ with H_2O_2 (Scheme 3.16 - Reaction 1) and the subsequent addition of a hydroxyl radical to DMSO (Reaction 2).[173] The methyl radical is the leaving group of the intermediate, which further interacts with the radical of the nitroxide forming a new C-O bond.[175] The methylated compound is no longer a radical and exhibits a standard proton NMR without rapid relaxation of proton spins, showing no unpaired electron is present.

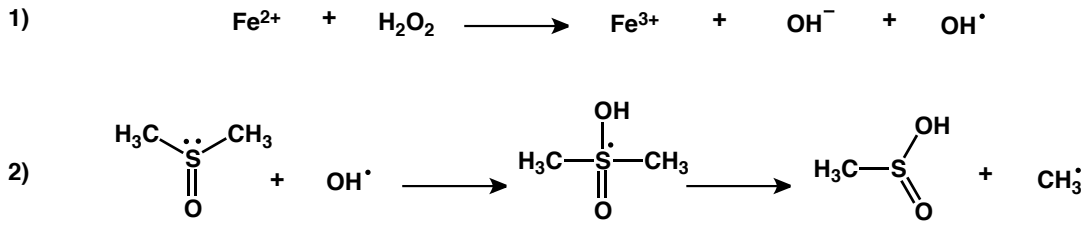

Scheme 3.16. Formation of methyl radical by Fenton's reagent, H_2O_2 and DMSO.

Deprotection of the methyl group has been reported by the oxidation with *m*CPBA in a Cope-type elimination reaction to produce the desired nitroxide in high yields (Scheme 3.17).[173] Unfortunately this route does not produce significant yields in the presence of an arylamine, due to competitive oxidation. Other side-products are possible but can be limited by reducing the amount of *m*CPBA.

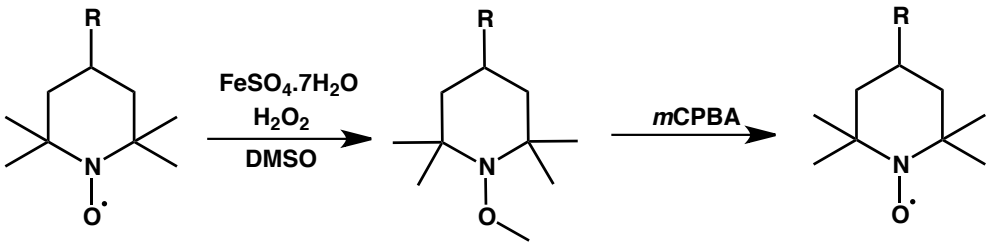

Scheme 3.17. Reversible alkylation of a nitroxide radical.

Nitroxide alkylation using Fenton chemistry was performed on compound **44**. Analysis of the ^{1}H NMR shows a distinct 3 proton signal for the methoxy group at 3.46 ppm, without addition of phenyl hydrazine. The geminal methyl peaks are still less than 0.1 ppm apart suggestive of the anisotropy of the oxygen. Investigation by NOESY also indicates that the methyl has attached at the radical position and not the arylamine, as a cross peak is observed correlating to the close proximity of the adjacent methyl substituents. This indicates we can perform a selective reduction of the nitro group and form the desired **44**.

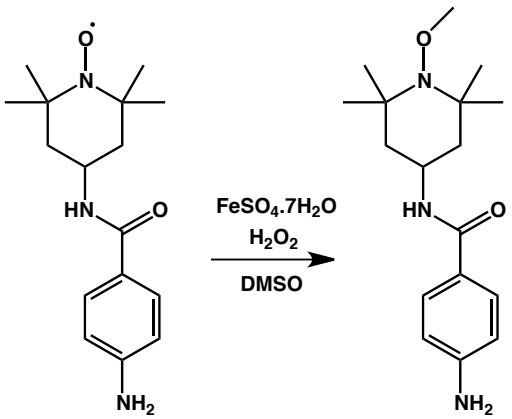

44 **53**

Scheme 3.18. Methyl trap of 4-amido-TEMPO with Fenton's reagent in DMSO.

*3.7.1.2 Synthesis of 4-(4-aminophenoxy)-2,2,6,6-tetramethyl–piperidine-1-oxyl (**45**)*

The ether linkage could be made by nucleophilic aromatic substitution. Deprotonation of 4-hydroxy-TEMPO gave a nucleophile that could add to an electron-deficient aryl chloride. The aromatic substrate is not particularly activated with only a single electron-withdrawing group. As a result it required quite forcing conditions such as the addition of NaH. This is a slow reaction due to the formation of a higher energy Meisenheimer complex and takes stirring overnight at 90 °C with several extra additions of NaH to go to completion. On the addition of water, a bright yellow precipitate forms which was filtered to give compound **54** (Scheme 3.19). The radical has still been preserved through this reaction, as the IR shows a distinguishable N-O• stretch[176] at 1338 cm^{-1}.

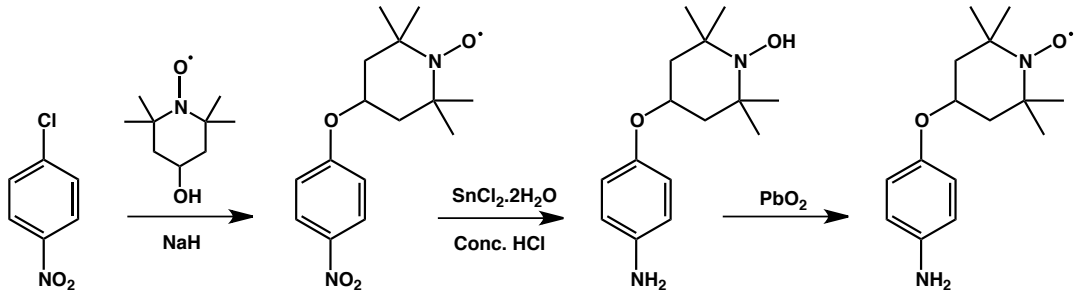

Scheme 3.19. Proposed scheme to synthesise a nitroxide-based catalyst with an ether linkage.

Similar to compound **52**, reduction of the nitro group in **54** is favoured over the full reduction of the nitroxide moiety in strongly acidic conditions. Stirring of **54** with $SnCl_2$•$2H_2O$ required conc. HCl to produce the aryl amine and the hydroxylamine species **55** (80%). The reduction was confirmed by mass spectrometry (ESI) at 265.53 *m*/*z*, TLC (ninhydrin stained) and acylation of the product. Although the restoration of the radical (**45**) from the hydroxylamine is not critical, it may be achieved by adding PbO_2 or bubbling O_2 through the solution. Reduction was also possible by hydrogenation over palladium (1 atmosphere).[167] However, these conditions are strong enough to completely reduce the nitroxide to the corresponding amine. This corresponds to the loss of

single oxygen, seen in the MS at 249 *m*/*z*. Therefore a mixture of reduction products is formed consisting of both the hydroxylamine and fully reduced amine species. The desired hydroxylamine was purified by a gradient silica column (0-10% MeOH/CH_2Cl_2) and re-oxidised to the nitroxide with PbO_2. This obtained the appropriate product in a lower yield (30%) due to this competitive reduction. ^{1}H NMR with phenyl hydrazine clearly showed the up field shift of the two aryl doublets and the methyl peaks, showing the presence of an electron donating amine and the hydroxylamine oxygen respectively.

To clarify the presence of the oxygen in the hydroxylamine and nitroxide species of compounds **54** and **55**, analogous molecules were synthesised where the catalytic moiety is a fully reduced amine. (See experimental for full details). NMR was able to distinguish between each species and therefore confirm the presence of the catalytically active nitroxide or hydroxylamine.

*3.7.1.3 Synthesis of 4-amino-2,2,6,6-tetramethyl-piperidin-1-oxyl (**47**)*

Removal of the aromatic linker in the proposed catalyst enables a smaller molecule and more direct attachment to the surface. Following the procedure of Tansakul *et al.*,[177] 4-azido-TEMPO (**56**) (described in *3.7.3.1*) was dissolved in anhydrous THF and triphenylphosphine (PPh_3) was added in portions over 5 hours (Scheme 3.20). The flask was put under argon and covered in foil and then concentrated ammonium solution was then added. The crude product was dissolved in chloroform and extracted into 10% acetic acid by protonation of the amine. Neutralisation and extraction back into chloroform assists purification producing an orange oil (41%). Mass spectrometry is consistent with the formation of the amino species (172 *m*/*z*), although separation of the product from triphenylphosphine oxide proved very problematic.

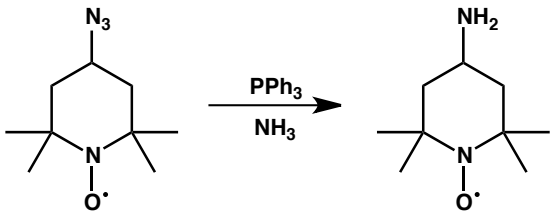

56 **47**

Scheme 3.20. Reduction of 4-azido-TEMPO with triphenylphosphine and ammonia.

*3.7.1.4 Synthesis of 5-amino-1,1,3,3-tetramethylisoindolin-2-oxyl (**48**)*

In 1982 Griffiths[178] reported the first isoindoline-based persistent radical, TMIO. Isoindoline derivatives have many advantages over non-aromatic systems such as TEMPO. Busfield[179] demonstrated that TMIO displays enhanced thermal and chemical stability under various conditions compared to TEMPO. The Bottle group has identified how the fused planar system of TMIO forms a much more rigid bicyclic system useful in profluorescent probes.[167]

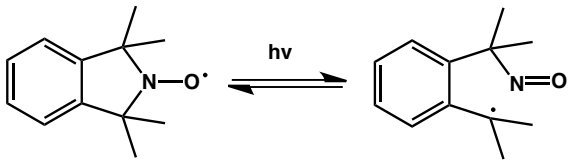

Scheme 3.21. Photoexcitation induced α-cleavage and recombination of TMIO.

When irradiated under light TMIO favours recombination of the cleaved product (Scheme 3.21), unlike TEMPO which undergoes α-cleavage photodegradation resulting in ring opening degradation products (Scheme 3.22).

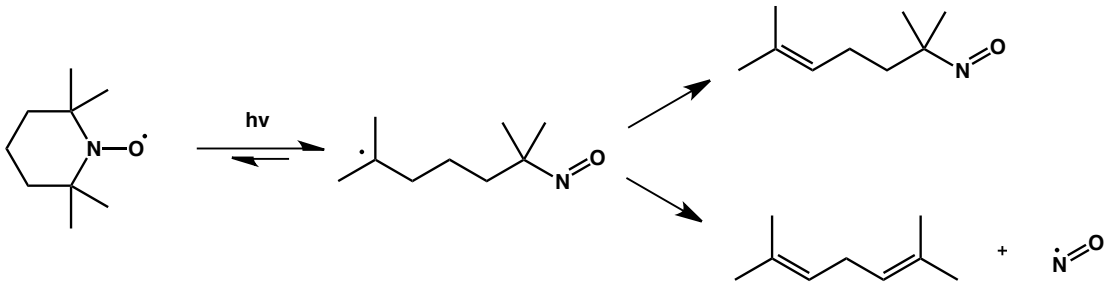

Scheme 3.22. Photodegradation of TEMPO.

Isoindoline derivatives tend to have higher oxidation potentials than other nitroxide radicals. However, its rigidity and chemical stability provides a structurally distinct molecule to the alternative proposed catalysts.

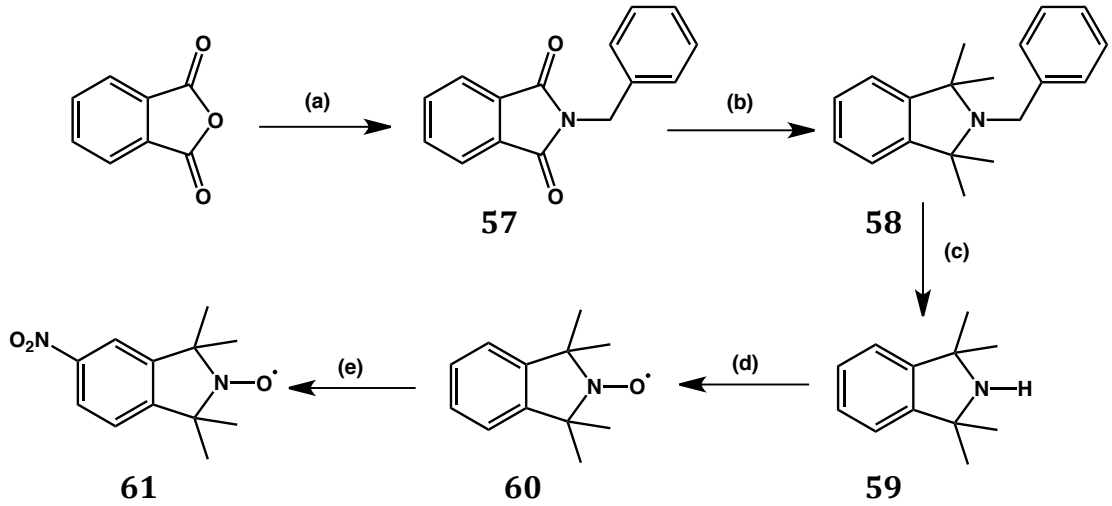

Scheme 3.23. Synthetic route of 5-NO_2-TMIO (**61**). (a) benzylamine, heat, 61% (b) 1. MeMgI, Et_2O; 2. Toluene, reflux, 17% (c) H_2, Pd/C, glacial acetic acid, 97% (d) *m*CPBA, CH_2Cl_2, 89% (e) H_2SO_4, HNO_3, 52%.

Synthesis of 5-amino-TMIO (**48**) (Scheme 3.23/3.24) begins from the phthalic anhydride. First, the condensation reaction with benzylamine generates the desired *N*-benzylphthalimide **57** (Scheme 3.23 (a)). A solvent-free approach was also successfully undertaken with excessive heat. This is followed by exhaustive methylation by a methyl Grignard reagent (Scheme 3.22 (b)), forming the tetra-methylated product **58**. This compound was challenging to make and proved to be temperamental at times. The Grignard reagent was formed by the dropwise addition of iodomethane to a suspension of magnesium in ether under an inert atmosphere. The absence of moisture and oxygen is critical for the success of the reaction. After formation of the Grignard reagent (MeMgI), the solution was concentrated as to minimize the amount of ether present as this can stabilise Grignard reagents and hinder the reaction. Subsequent drop-wise addition of *N*-benzylphthalimide (**57**) in toluene forms the tetramethyl product **58**. When the reaction had reached completion, the remaining reagents were quenched with isopropyl alcohol. Purification of the desired product was achieved by passing a

solution of a concentrated reaction mixture though a basic alumina column with *n*-hexanes. Following removal of the organic solvent, white crystals were obtained in poor yields (17%). This reaction is known for low yields possibly due to the formation of a purple material believed to be polymerisation products.[180] Subsequent deprotection by hydrogenation over Pd/C formed the secondary amine **59** (Scheme 3.22 (c)), which was subjected to oxidation by *m*CPBA to generate the nitroxide species (**60**) (Scheme 3.22 (d)).[166,167,181]

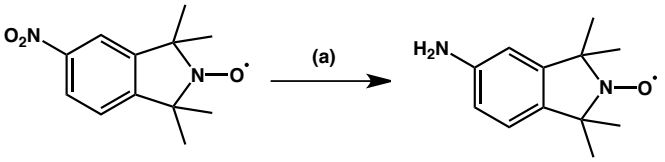

61 **48**

Scheme 3.24. Reduction of **61** with10% Pd/C (w/w), H_2, MeOH.

Classical nitration of **60** with concentrated nitric and sulfuric acid gave nitroxide **61** as an orange solid in good yield (52%). Characterisation by ^{1}H NMR could be achieved after reduction of the radical with phenylhydrazine. Characteristic methyl peaks and the downfield shift of the remaining aromatic protons were consistent with nitro-TMIO analogue. Without phenyl hydrazine, the spectrum displays large broad peaks distinctive of a paramagnetic compound.

Reduction to 4-amino TMIO was first attempted by treatment with $SnCl_2 \bullet 2H_2O$ under acidic conditions in an analogous fashion to **52** and **54**. Unfortunately, these conditions reduced both the NO_2 and nitroxide to amines. The milder reducing conditions utilising H_2, Pd/C were preferred (99%)(Scheme 3.24). This results in formation of the hydroxylamine that could be reoxidised to the bright yellow radical **48** by treatment with PbO_2. This arylamine was susceptible to oxidation under ambient conditions, just as aniline is; therefore the product was produced when required.

3.7.2 Diazotisation of Amines

As the aim was to use diazonium chemistry to attach the nitroxides to the surface, the nitroxide derivatives were specifically designed with a free amine ready for diazotisation. To date there have many reports on the synthesis of TEMPO derivatives but only a few on the diazotisation of these compounds. Two important exceptions are found in the research of Cougnon[165] and Blinco[181]. In order to avoid the potential coupling of the nitroxide and the aryl radical, Cougnon investigated the preparation of the diazonium with contaminant disproportionation of the nitroxide radical to hydroxylamine and oxoammonium (Scheme 3.25). This approach successfully coupled the compound onto a surface where a redox couple characteristic of nitroxide is observed.

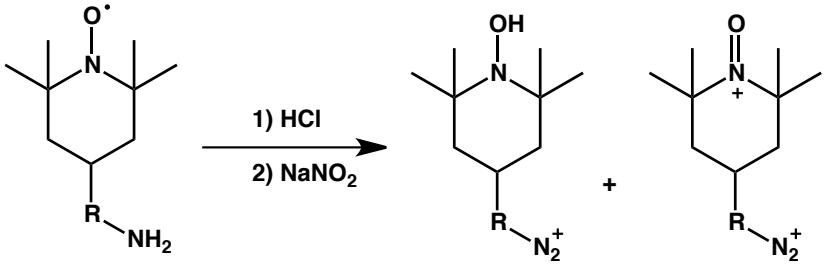

Scheme 3.25. Disproportionation and diazotisation of a nitroxide derivative.

Blinco was the first to isolate a nitroxide diazonium salt (Scheme 3.26).[181] To avoid the acidic disproportionation reaction shown in Scheme 3.25, neutral diazotisation conditions were employed with nitrosyl tetrafluoroborate acting as the source of the nitrosyl cation. This methodology allowed the successful grafting of the diazonium nitroxide radical to glassy carbon, graphene and carbon fibres. Although they produce cyclic voltammograms of the nitroxide before and after grafting, the present work raises concerns about the initial state of the nitroxide upon attachment. There was little evidence to suggest that the radical was present in the diazonium compound initially and immediately after grafting. It is more likely that the hydroxylamine species was bound to the surface and that this underwent electrochemical oxidation in a 2 electron process that gave the oxoammonium cation during the first few scans. This would restore the redox of the oxoammonium and nitroxide showing a one-electron process CV, as they have presented. As multiple scans were not shown,

it may cause some ambiguity in the system in the initial stages of grafting. Furthermore, as the grafting process is performed in solution, the potential for oxidation by molecular oxygen is increased. This could have restored the nitroxide moiety contributing to the EPR and Raman spectra presented in this research.

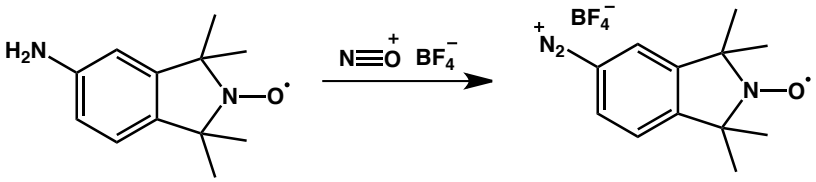

Scheme 3.26. Formation of a TMIO nitroxide diazonium salt from nitrosyl tetrafluoroborate.

3.7.2.1 4-((1-Oxyl-2,2,6,6-tetramethylpiperidin-4-yl)carbamoyl)benzenediazonium

Changing the counter ion from a chloride to the tetrafluoroborate often furnishes more stable diazonium salts.[182] Therefore **44** was dissolved in acetonitrile and cooled to 0 °C. Treatment with HBF_4 and $NaNO_2$ was followed by precipitation with diethyl ether (43%)(Scheme 3.27). The resulting solid showed a peak in FTIR at 2295 cm^{-1} characteristic of the N-N stretching frequency of a diazonium species.[183] To monitor the reaction, samples of the solution were tested by FTIR; a second peak in this region (2256 cm^{-1}) was also visible which was attributed to the solvent, acetonitrile. Care must be taken if using this solvent as to distinguish between the two different stretching frequencies present in the sample. ESI-MS is of limited use in diazonium formation as the N_2^+ group is readily cleaved making it difficult to observe the molecular ion. Assignment of the fragment at 275 *m/z* corresponds to the aryl cation formed from the loss of molecular nitrogen and this was considered indicative of diazonium formation. This was supported by observation of a peak at 293 *m/z* formed from the aromatic substitution with fluorine. This would be impossible if the aniline was still present.

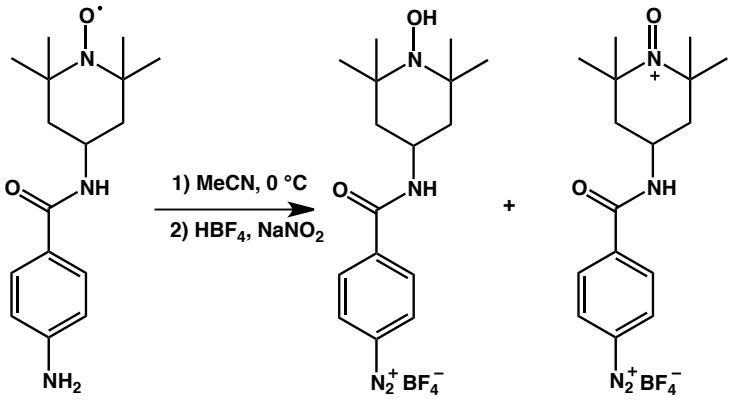

44 **62**

Scheme 3.27 Diazotisation of **44**.

Once again formation of the diazonium species was confirmed by derivatisation. It was decided to avoid the Heck reaction used previously (Section 2.5.4.1) as there was uncertainty as to the effect of the persistent radical on the catalytic cycle. Therefore, coupling the diazonium with phenol produced an azo compound. As acid was used in this diazonium formation, the product exists as the hydroxylamine and oxoammonium species due to its disproportionation. Therefore a combination of these species was used in the azo dye reaction (Scheme 3.28). To a cooled solution of phenol in 2 M NaOH, was added an aqueous solution of **62** dropwise. This immediately generated a brightly coloured solution characteristic of an azo dye. Following stirring overnight, the orange solution was adjusted to pH 7 to protonate the phenoxide, and extracted into EtOAc. Purification was achieved by column chromatography to give a bright orange solid. It can be assumed that the product is the hydroxylamine species, as a bright orange band was unable to move down the column, presumably because it was the oxoammonium azo dye.

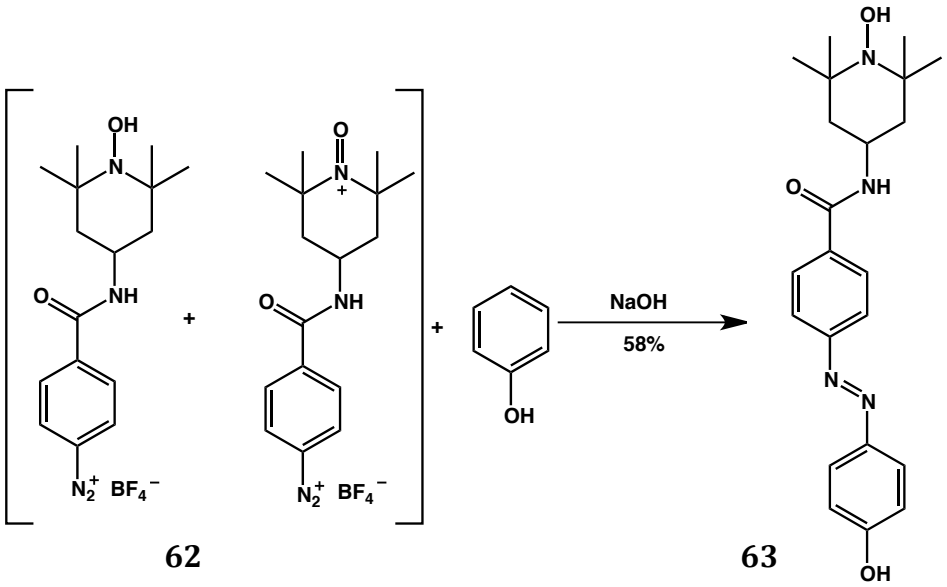

Scheme 3.28. Azo-coupling of diazonium **62** with phenol.

^{1}H NMR showed conclusive evidence that the coupling was at the *para* position of the phenol instead of the *ortho* position, which had been a possibility. As the hydroxylamine can be oxidised to the radical species with oxygen in solution, phenyl hydrazine was added to minimise the broadening effect of the radical species. The presence of the hydroxylamine is evident as the methyl peaks were 0.02 ppm apart, consistent with anisotropic shielding from the oxygen. Furthermore, the ESI-MS shows the three forms of the products: oxoammonium, nitroxide and hydroxylamine peaks at 395, 396 and 397 m/z respectively.

A new method for the diazotisation of **44** was been developed in the present work (Scheme 3.27), which isolates the diazonium BF_4 salt as a solid. Although the composition of the nitroxide is ambiguous, whether it exists as a hydroxylamine or an oxoammonium salt is unimportant when attempting to attach it to a surface. Once bound to an electrochemical surface, a potential can be applied which oxidises or reduces the attached species to a uniform compound. Further surface characterisation of compound **44** is explored in Section 5.3.5.

*3.7.2.2 Attempted diazotisation of **45***

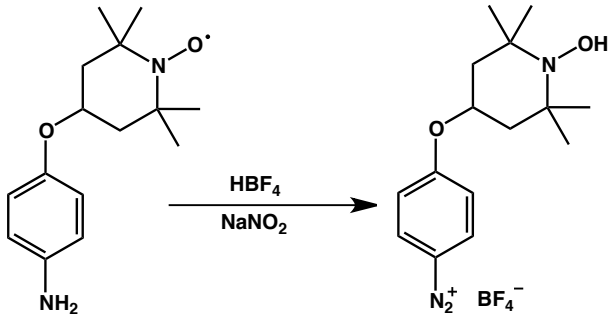

45 **64**

Scheme 3.29. Proposed diazonium formation of nitroxide **45**.

Diazotisation of compound **45** was first attempted under standard aqueous conditions with HBF_4 and $NaNO_2$ (Scheme 3.29). It produced a black material that did not appear to contain either starting material or the diazonium product by ^1H NMR. As this reaction did not produce the diazonium product, alternative conditions were investigated. The use of $NOBF_4$ eliminates the need for the acid mediated formation of the important nitrosyl cation intermediate. Unfortunately these non-acidic conditions did not produce the desired product. Instead the starting material decomposed. ^1H NMR suggests degradation through TEMPO ring-opening as indicated in Fig. 3.12. The reaction immediately turns a deep purple colour, possibly indicating polymerisation of the degradation products. As this molecule fails to form the diazonium species it could not be taken any further in this project.

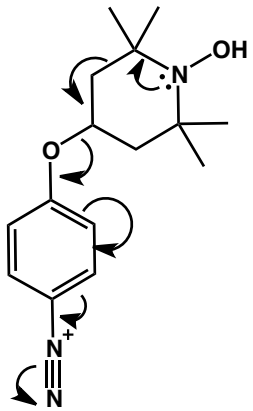

Fig. 3.12. Possible degradation pathway of 4-((1-oxyl-2,2,6,6-tetramethylpiperidin-4-yl)oxy)benzenediazonium.

*3.7.2.3 1,1,3,3 –tetramethyl-2,3-dihydroisoindol-2-yloxyl-5-diazonium tetrafluoroborate (**65**)*

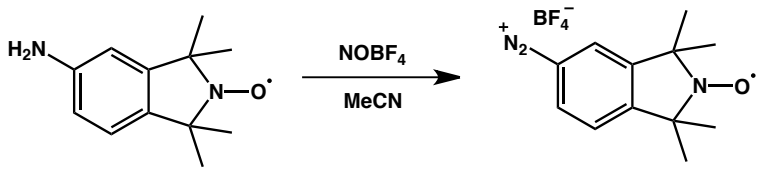

48 **65**

Scheme 3.30. Diazotisation of nitroxide **48** under anhydrous conditions.

With slight modifications to the procedure of Blinco,[181] $NOBF_4$ was placed into a sealed vessel which underwent 3 vacuum cycles to ensure oxygen-free conditions (Scheme 3.30). Distilled acetonitrile was added to the flask and the reaction was cooled to -15 °C. The lowered temperature ensures the exothermic reaction is controlled which helps to decrease degradation and over-oxidation. Following precipitation with ether the solid was filtered to give a tan coloured product. FTIR shows the N-N stretching visible at 2303 cm^{-1}. Further confirmation was achieved by azo coupling with phenol, using the same conditions as in Scheme 3.28. The bright red solution was subjected to purification by column chromatography (1% MeOH/CH_2Cl_2) to afford an orange solid. ^1H NMR shows some broad aromatic peaks suggesting that the dye is in the nitroxide radical oxidation state, and well-defined peaks of EtOAc and CH_2Cl_2, distinctive of intramolecular paramagnetism. Following addition of phenyl hydrazine many more well-defined peaks could be seen and assigned to **66** (Fig. 3.13).

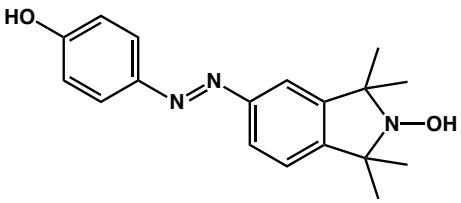

66

Fig. 3.13. Azo dye coupling of diazonium species **65** with phenol

3.7.2.4 Attempted diazotisation of ***47***

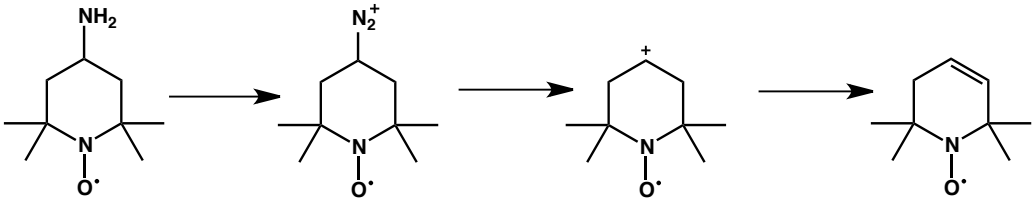

Scheme 3.31. Proposed diazotisation of nitroxide **47**.

Diazotisation of non-aromatic amines generally does not yield a stable or isolatable product. This is due to the absence of resonance stabilisation (Fig. 3.14). It is possible that diazotisation is instantly followed by loss of molecular nitrogen to give a carbocation (Scheme 3.31), likely by E1 elimination. Dinitrogen is a very good leaving group and is also very thermodynamically stable. Hence this is why the carbocation is favoured over the diazonium species. How long the carbocation is present is debatable as it can be subjected to nucleophilic attack, elimination and fragmentation. Alternatively, E2 elimination can form the alkene directly and removes the intermediate carbocation formation.

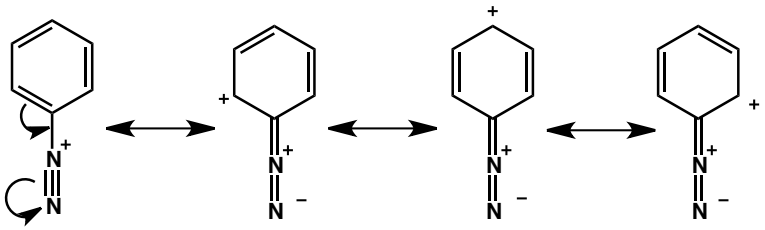

Fig. 3.14. Resonance forms of an aryl diazonium.

4-Amino-TEMPO was subjected to diazotisation with $NaNO_2$ and HCl. The diazonium compound was not isolated due to its increased reactivity. Mass spectrometry of the potential diazonium solution shows a possible carbocation peak at 155 *m/z*. This is not conclusive as two alternative compounds have the same *m/z* that also have the potential to form under these conditions. This includes a) the nucleophilic attack of a hydroxide followed by the elimination of H_2O and b) deprotonation of the α-hydrogen to form the alkene product

(Scheme 3.32). An attempt was made to couple with the diazonium **67** with phenol in solution to avoid isolation of the diazonium. This reaction was not successful and is likely due to the competing degradation reaction, forming the secondary carbocation and other by-products.

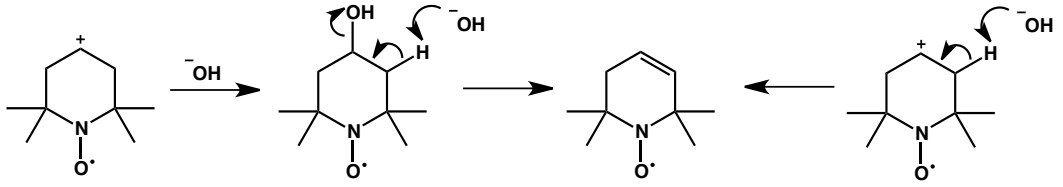

Scheme 3.32. Possible elimination exhibited by diazotisation products of **67**.

3.7.3 Cycloaddition Approach

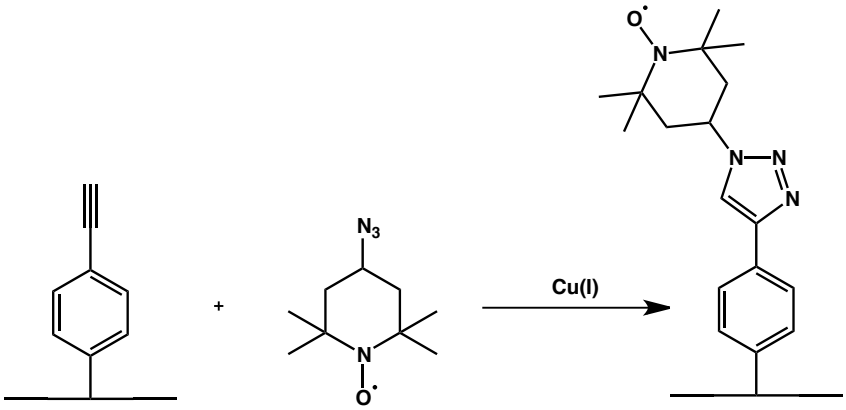

Scheme 3.33. Proposed "click" reaction on a surface.

The use of a triazole group as part of a linker in the catalyst design is tentative, as its base susceptibility at 7 M KOH (proposed electrolyte) is unknown. Our initial synthetic approach for the convergent synthesis of **46** focused on the preparation of two main components of the molecule. Each component would then be combined using copper catalysed azide-alkyne 'click' reaction (Scheme 3.33), analogous to post-modification of an oligonucleotide with a nitroxide radical.[184,185] This attractive method of Cu^{I}-catalysed cycloaddition proceeds under mild conditions and allows azides carrying electron-deficient or electron-rich groups to react efficiently with variously substituted terminal alkynes.[186]

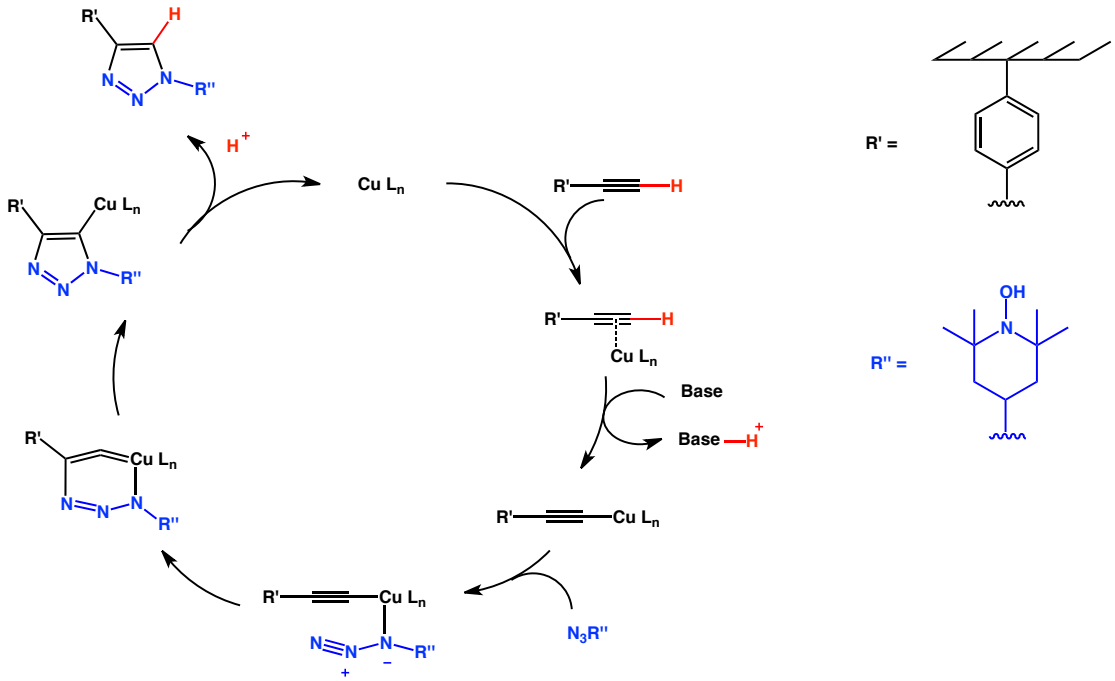

Scheme 3.34. Possible catalytic cycle of the cycloaddition with a terminal alkyne (R') and azido-TEMPO (R'').

This route first involves the functionalisation of a surface with a phenyl ring bearing a terminal alkyne, achieved by diazonium coupling of a protected alkyne (Section 3.7.3.3). This well-known approach allows the formation of a monolayer on the surface without interference from a nitroxide radical.[187] Once deprotected, the alkyne is able to undergo cycloaddition chemistry with 4-azido-TEMPO to form the desired triazole (Scheme 3.34). This convergent synthesis requires reactants: 4-azido-TEMPO (**56**) and the diazonium containing protected alkyne, trimethylsilylethynyl benzenediazonium tetrafluoroborate (**72**).

*3.7.3.1 Synthesis of 4-azido-2,2,6,6-tetramethyl-piperidin-1-oxyl (**56**)*

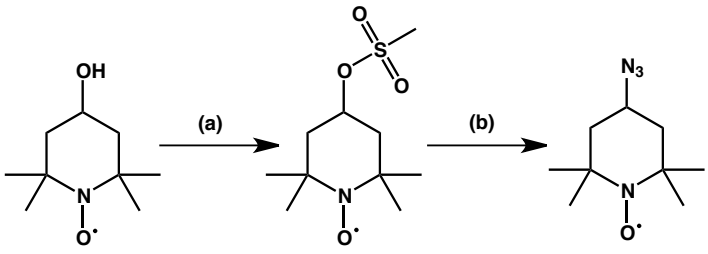

68 **56**

Scheme 3.35. a) $MeSO_2Cl$, pyridine, 0 °C b) NaN_3.

The synthetic approach involves the initial formation of 4-mesyl TEMPO from the commercially available 4–hydroxy TEMPO.[188,189] Following the procedure of Tansakul *et al.*, 4-hydroxy-TEMPO was cooled in an ice/acetone bath. Subsequent dropwise addition of methanesulfonyl chloride resulted in the formation of **68** (Scheme 3.35).[177] The reaction was slow taking over 12 hours to complete with additional amounts of $MeSO_2Cl$ being added periodically. Once the reaction was complete, the product was isolated by extraction with $CHCl_3$ followed by the removal of the solvent to give a deep orange solid (89%). The mesylation was followed by nucleophilic substitution by NaN_3 to form the required product, 4–azido-TEMPO (**56**). This showed a peak in the IR at 2094 cm^{-1} characteristic of an azide (N_3) stretch and the mass spectrum was dominated by a nitroxide peak at 198 *m/z*. ^1H NMR with phenyl hydrazine showed clear chemical shift changes when altering the electronics of the substituted TEMPO. The radical has been preserved through these reactions, as the IR of **56** shows a distinguishable N-O• stretch at 1361 cm^{-1}, similar to the nitroxyl stretch in the commercially available 4-hydroxy-TEMPO and the ^1H NMR is broad.

*3.7.3.2 Synthesis of 2,2,6,6-tetramethyl-4-(4-phenyl-1H-1,2,3-triazol-1-yl)piperidin-1-oxyl via 'click' chemistry (**71**)*

To investigate the conditions for 'click' chemistry of 4-azido-TEMPO with an alkyne, it was decided to optimise the reaction using phenylacetylene (**69**). This

allows characterisation of the products in solution without having to apply surface characterisation techniques. To find the most efficient conditions, coupling partners **69** and **56** were tested in multiple solvents such as CH_2Cl_2, THF and $EtOH/H_2O$ with the CuI catalyst. However, after thorough degassing with oxygen-free argon and addition of a base such as NEt_3, the reaction did not proceed efficiently (<5% yield). A further attempt was made using Cu(II) as the source of catalytic Cu(I). This required a reducing agent to reduce Cu(II) to Cu(I). Sodium ascorbate was used, although it not only reduced the copper, it also reduced the nitroxide. It was found that optimal conditions for this system first required the reduction of the nitroxide to the hydroxylamine in a 1:1 $EtOH/H_2O$ mixture (Scheme 3.36). This was followed by the addition of $CuSO_4$, phenylacetylene and more sodium ascorbate to produce a **70** as a bright yellow solid (69%).

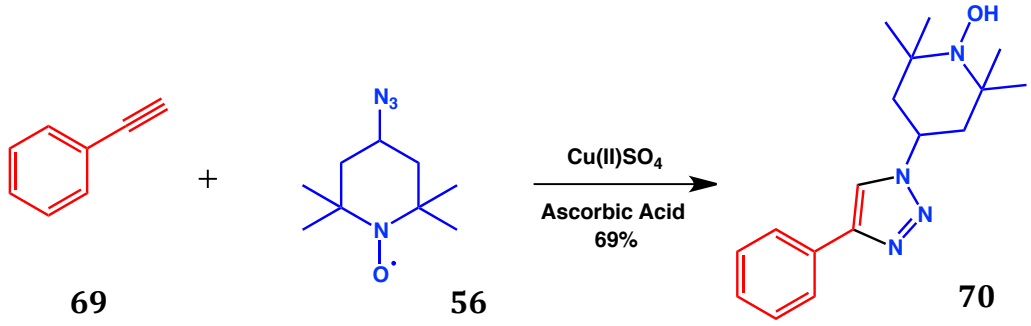

69 **56** **70**

Scheme 3.36. Copper-catalysed azide-alkyne coupling of phenylacetylene with 4-azido-TEMPO.

^1H NMR spectroscopy was possible due to the absence of the nitroxide. The triazole proton was observed at 8.72 ppm (Fig 3.15 below) as a one proton singlet confirming the success of coupling. When oxygen was bubbled through a CH_2Cl_2 solution of **70**, the NMR then exhibited broadening of the proton signals. This oxidised the hydroxylamine back to the nitroxide causing paramagnetic broadening of intra-molecular and inter-molecular protons (Fig 3.15).

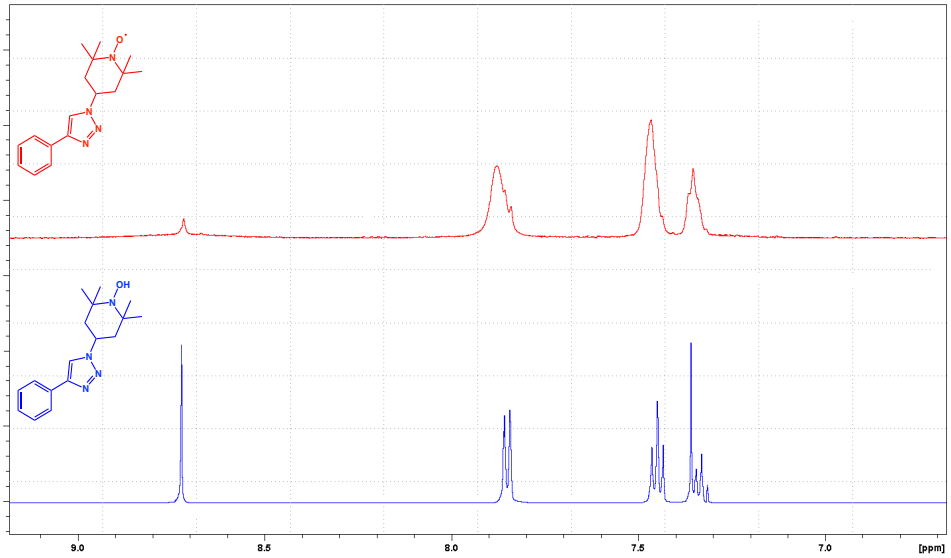

Fig. 3.15. Representative ^{1}H NMR spectrum of **70** in the hydroxylamine (blue) and radical forms (red).

This method could then be applied to the *in situ* formation of the triazole on a carbon surface. This presumably will change the rates and possibly the mechanism by which the 'click' reaction may occur as steric, orientation and porosity factors must be taken into account.

*3.7.3.3 Synthesis of 4-((trimethylsilyl)ethynyl)aniline (**71**)*

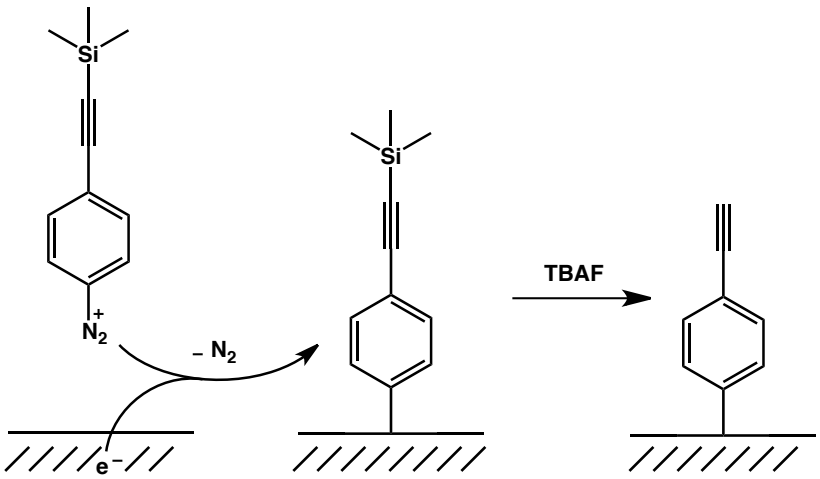

Scheme 3.37. Proposed attachment and cleavage of a trimethylsilyl protected aryl alkyne.

Attaching a phenyl alkyne to a surface first involves the protection of the reactive alkyne functionality. A silyl-protected ethynyl aryldiazonium salt can be electrochemically grafted onto the surface (Scheme 3.37). Deprotection unveils a dense ethynyl aryl monolayer capable of further coupling reactions with molecules in solution.[190,191] This allows further functionalisation possibilities on the surface such as 'click' chemistry of 4-azido-TEMPO. In similar fashion to above, a diazonium coupling method could be used to attach this coupling partner to the surface. This first requires the formation of compound **71**, which contains the protected alkyne and aniline moiety ready for diazotisation. The synthesis of **71** entails the Sonogashira coupling of 4-iodoaniline with trimethylsilylacetylene (TMS) under strict oxygen-free conditions[192] to prevent homocoupling of the alkyne (Scheme 3.38). This reaction uses between 2-5% $Pd(OAc)_2$ catalyst although full conversion is directly correlated to the quantity of oxygen in the reaction vessel.

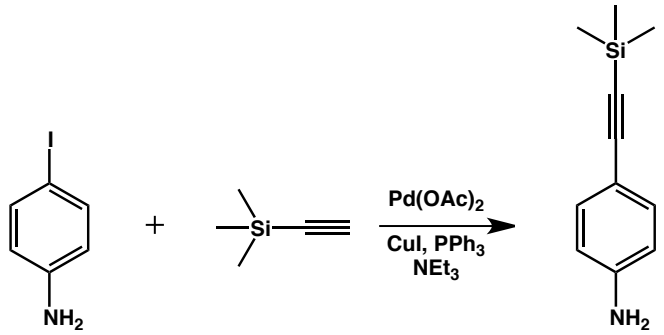

71

Scheme 3.38. Sonogashira coupling of 4-iodoaniline with TMS.

*3.7.3.4 Synthesis of 4-((Trimethylsilyl)ethynyl)benzenediazonium tetrafluoroborate (**72**)*

Diazotisation followed the procedure of Leroux[191] with the addition of $NaNO_2$ to a cooled solution of **71** in H_2O and HBF_4 (Scheme 3.39). After stirring overnight, the diazonium salt was isolated by filtration and the ^1H NMR agreed with the literature data for this compound.[192] It was then coupled to a surface and this chemistry is described in section 5.3.5.

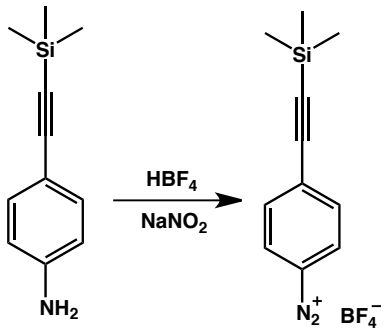

71 **72**

Scheme 3.39. Diazotisation of TMS-protected ethynylaniline.

3.8 Experimental

Synthesis of 40 2,2,6,6-tetramethyl-1-oxopiperidinium bromide

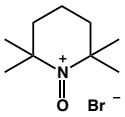

TEMPO (1.58 g, 10.3 mmol, 1 eq.) was dissolved in hexane (30 ml) to which a solution of bromine (0.26 ml, 10.1 mmol, 0.98 eq.) in DCE (5 ml) was added. The reaction was stirred at rt for 15 mins after which the precipitate was collected giving a brick red solid (1.14 g, 48%). ^{1}H NMR (500 MHz, THF-d_8): 3.62 (m, 1H, CH_{eq}), 2.22 (td, J = 18,4.0 Hz, 2H, 2 x H_{eq}), 1.95-1.88 (m, 3H, 2 x H_{ax} , CH_{ax}), 1.57 (s, 6H, 2 x $(CH_3)_{eq}$), 1.43 (s, 6H, 2 x $(CH_3)_{ax}$).ESI-MS: *m/z* 156.28 ([M^+], 100%). IR (cm^{-1}): 1603 (N=O).

Synthesis of 41
2,2,6,6-tetramethyl-1-oxopiperidinium tetrafluoroborate

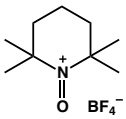

To a slurry of TEMPO (0.5 g, 3.2 mmol, 1 eq.) in 1.6 ml H_2O, 50% HBF_4 (0.67 ml, 5.4 mmol, 1.7 eq.) was slowly added over 15 mins at rt. The solution was cooled to 0 °C before 1.5 ml NaOCl was added. After the reaction was stirred for a further hour the crude material was filtered and washed with $NaHCO_3$ (5 ml), ice cold water (5 ml) and cold ether (20 ml) to give a bright yellow solid. The solid was dried in an oven at 65 °C overnight to give **41** (0.58 g, 75%). mp: Expected (162 – 163 °C)[162] Found (160 – 161 °C). ESI-MS: *m/z* 156.28 ([M^+], 88%), 158.32 ([MH_2^+], 100%). IR (cm^{-1}): 725 (w), 766 (w), 943 (m), 1036 (s), 1049 (s), 1098 (s), 1382 (w), 1472 (w), 1627 (m).

Synthesis of 42 4-(decyloxy)-2,2,6,6-tetramethylpiperidin-1-oxyl

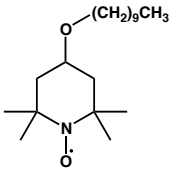

A solution of 4-hydroxy-TEMPO (2.0 g, 11.6 mmol, 1.0 equiv.) in dry DMF (40 ml) was heated to 50 °C and NaH (60%; 1.5 g, 37.5 mmol) was added portion wise over 30 min. while stirring. An immediate colour change from orange to brown was observed. Bromodecane (3.75 ml, 18.1 mmol, 1.6 eq.) and NaI (~ 50 mg) was then added and placed on a condenser at 90°C overnight. The reaction mixture was monitored by TLC and further addition of NaH was added if required. Once the mixture had cooled, $CHCl_3$ (100 ml) was added and washed with H_2O (100 ml) and brine (100ml) repeated 3 times to remove DMF. The organic phase was dried ($MgSO_4$) and the solvent removed under reduced pressure. The crude product was purified by column chromatography (10% EtOAc, 90% Hexane) to give an orange oil (1.64 g, 45%). ^{1}H NMR (400 MHz, d_6-DMSO, $PhNHNH_2$): δ (ppm) = 3.49 (m, 1H, CH), 3.35 (t, J = 6.4 Hz, 2H, OCH_2), 1.83 (dd, J = 12.4, 3.6, 2H, 2 x H_{eq}), 1.45 (t, J = 6.4 Hz, 2H, 2 x H_{ax}), 1.25-1.21 (bs, 16H, $(CH_2)_8$), 1.07 (s, 6H, 2 x $(CH_3)_{eq}$), 1.04 (s, 6H, 2 x $(CH_3)_{ax}$), 0.86 (t, J = 6.4 Hz, 3H, CH_2CH_3). ESI-MS: *m/z* 312.69 ([$M^{+\bullet}$], 32%), 313.69 ([$MH^{+\bullet}$], 100%), 314.70 ([MH_2^+], 33%). IR (cm^{-1}): 1362 (N-O•).[168,172]

Synthesis of 43

4-(decyloxy)-2,2,6,6-tetramethyl-1-oxopiperidinium bromide

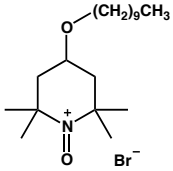

A solution of **42** (0.96 g, 3.1 mmol, 1 eq.) in hexane (10 ml) was covered in tinfoil and a solution of Br_2 (85 µL, 1.7 mmol, 1.1 eq.) in DCE (5 ml) was added slowly. The mixture was stirred at rt for 2 days then the solvent was removed under reduced pressure to give a sticky brown/orange oil. ^{1}H NMR (500 MHz, $CDCl_3$): δ (ppm) =* 3.72 (m, 1H, CH), 3.44-3.41 (2 x t, J_1 = 6.6 Hz, J_2 = 6.5 Hz, 2H, OCH_2), 2.40-2.19 (m, 4H, $CH_{ax/eq}$), 1.73 (s, 3H, CH_3), 1.69 (s, 2H, CH_3), 1.62 (s, 2H, CH_3), 1.57 (m, 2H, OCH_2CH_2), 1.46 (s, 3H, CH_3), 1.38-1.28 (bm, 14H, $(CH_2)_7$), 0.90 (t, J = 7.0 Hz, 3H, CH_2CH_3). ^{1}H NMR (125 MHz, $CDCl_3$): δ (ppm) = 71.2(CH), 69.5(Q), (69.1/68.7), 68.4(Q), 67.8(CH), 42.5, 39.5, 31.8, (30.0/29.9), 29.5, 29.4, 29.3, 29.2, 29.0(CH_3), 28.8(CH_3), (26.2/26.1), 22.6, 22.1(CH_3), 21.7(CH_3), 14.0. * - compound quoted as

both species. See Section 4.41. Assignment of ^{13}C from DEPT135. (Identified as same atom on both structures). ESI-MS: *m/z* 312.74 [M^+], 314.76 [MH_2^+].

Synthesis of 44

4-amino-*N*-(1-oxyl-2,2,6,6-tetramethylpiperidin-4-yl)benzamide

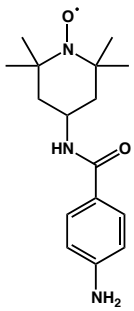

52 (1.06 g, 3.5 mmol, 1 eq.) was placed in a sealed flask and cooled in ice to 0 °C. In a separate vessel, a solution of $SnCl_2.2H_2O$ (2.36 g, 10.5 mmol, 3 eq.) was dissolved in conc. HCl and cooled in ice. The acid solution was added to the sealed flask and stirred at this temperature for 10 mins. Following stirring at rt for 1 hour, the reaction was again cooled in ice before 2M NaOH was added until pH 10. Product **44** was extracted and combined CH_2Cl_2 fractions washed with brine and dried over $MgSO_4$. Removal of volatiles afforded a yellow solid (0.75 g, 75%). ^1H NMR (400 MHz, $CDCl_3$, $PhNHNH_2$): δ (ppm) = 7.58 (d, J = 8.6 Hz, 2H, H_{Ortho}), 6.65 (d, J = 8.6 Hz, 2H, H_{Meta}), 5.78 (d, J = 7.7 Hz, 1H, NH), 4.36 (m, 1H, CH), 3.63 (bs, 2H, NH_2), 1.97 (dt, J = 12.7, 1.6 Hz, 2H, 2 x H_{eq}), 1.44 (t, J = 12.4 Hz, 2H, 2 x H_{ax}), 1.25 (s, 6H, 2 x $(CH_3)_{eq}$), 1.22 (s, 6H, 2 x $(CH_3)_{ax}$).

Synthesis of 45/55

4-(4-aminophenoxy)-2,2,6,6-tetramethylpiperidin-1-oxyl

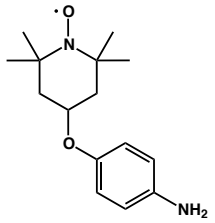

Compound **54** (0.265 g, 0.9 mmol, 1 eq.) was cooled in ice and a cooled solution of $SnCl_2.2H_2O$ (0.72 g, 3.2 mmol, 3.6 eq.) in conc. HCl (36%, 8 ml) was added slowly. The reaction mixture was stirred at this temperature for 30 minutes, then at rt for a further 30 minutes. The solution was cooled and basified to pH = 11 with 2M NaOH, extracted into CH_2Cl_2 (x2) and washed with H_2O and brine. The organic layer was dried over $MgSO_4$ and the solvent removed under reduced pressure (190.1 mg, 80%). ^1H NMR (500 MHz, $CDCl_3$, $PhNHNH_2$): δ (ppm) = 6.79 (d, J = 9.0 Hz, 2H, H_{Arom}), 6.66 (d, J = 9.0 Hz, 2H, H_{Arom}), 4.41 (m, 1H, CH), 2.06 (dd, J = 11.5, 4 Hz, 2H, 2 x H_{eq}), 1.64 (t, J = 12 Hz, 2H, 2 x H_{ax}), 1.25 (s, 6H, 2 x $(CH_3)_{eq}$), 1.24 (s, 6H, 2 x $(CH_3)_{ax}$). ^{13}C NMR (125 MHz, $CDCl_3$): $PhNHNH_2$ δ (ppm) = 150.6, 140.4, 117.9, 116.9, 70.3, 59.1, 44.7, 32.3, 20.7. ^1H NMR (500 MHz, DMSO-d_6, $PhNHNH_2$): δ (ppm) = 6.65 (d, J = 8.7 Hz, 2H, H_{Arom}), 6.50 (d, J = 8.8 Hz, 2H,

H_{Arom}), 4.32 (m, 1H, C*H*), 1.91 (dd, J = 12.2, 3.7 Hz, 2H, 2 x H_{eq}), 1.38 (t, J = 11.7 Hz, 2H, CH_2), 1.09 (s, 12H, 4 x CH_3). ^{13}C NMR (100 MHz, DMSO-d_6): δ (ppm) = 148.5, 143.2, 118.0, 115.4, 70.1, 58.5, 44.9, 32.8, 20.9. ESI-MS: *m/z*: 265.6 ([MH_2^+]), 249.6 ([MH_2^+-O]).

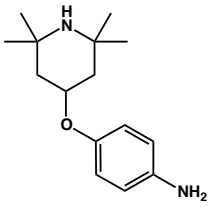

For comparison a full reduction of compound **54** (2.8 g, 9.5 mmol, 1 eq.) was achieved with $SnCl_2.2H_2O$ (11.3, 50 mmol, 5.3 eq,) in EtOH (50 ml) at 75 °C stirring overnight to give 4-((2,2,6,6-tetramethylpiperidin-4-yl)oxy)aniline. 2M NaOH was added to pH = 9 and extracted into EtOAc (x3), washed with water and dried over $MgSO_4$. The solvent was removed under reduced pressure and the crude material was recrystallised from hot EtOAc (1.12 g, 47%). ^{1}H NMR (400 MHz, $CDCl_3$): δ (ppm) = 6.76 (d, J = 8.8 Hz, 2H, H_{Arom}), 6.65 (d, J = 8.8 Hz, 2H, H_{Arom}), 4.50 (m, 1H, CH), 2.07 (dd, J = 13.2, 4.4 Hz, 2H, 2 x H_{eq}), 1.28 (s, 6H, 2 x $(CH_3)_{eq}$), 1.26 (m, 2H, 2 x H_{ax}), 1.23 (s, 6H, 2 x $(CH_3)_{ax}$). ^{13}C NMR (125 MHz $CDCl_3$): δ (ppm) =150.3, 140.4, 117.8, 116.4, 71.9, 52.3, 44.2, 34.3, 28.8. ESI-MS: *m/z*: 249.31 [MH^+], 125.22 [MH_2]$^{2+}$.

Synthesis of 47 4-amino-2,2,6,6-tetramethyl-piperidin-1-oxyl

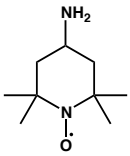

Following a procedure by Tansakul[177], to a solution of **69** (0.4 g, 2.04 mmol) in anhydrous THF (5.5 ml) was added triphenylphosphine (2.01 g, 7.66 mmol) in portions over 5 hours. Concentrated ammonia solution (5.0 ml) was added before covered in foil and stirred for 2 days under Ar. Solvent was removed *in vacuo* (<40 °C) before redissolved in $CHCl_3$ (50 ml) and extracted into 10% acetic acid (2 x 25 ml). The combined aqueous layer was neutralised with saturated $NaHCO_3$ using 1 ml 2M NaOH to slightly basify, extracted into $CHCl_3$ (3 x 30 ml), dried over $MgSO_4$ and concentrated *in vacuo* to give an orange oil (141.6 mg, 41%). ESI-MS: *m/z* 172.39 [$MH^{+\bullet}$], 173.40 [MH_2^+].

Synthesis of 48 5-amino-1,1,3,3-tetramethylisoindoline-2-oxyl

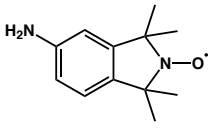

A solution of **61** (0.30 g, 1.28 mmol) in MeOH (10 ml) was added Pd/C (10% w/w, 31 mg) and stirred overnight at rt with H_2 (1 atmosphere). A small spatula of PbO_2 was added and stirred for another 30 mins. The reaction mixture was filtered over celite and

washed with MeOH. The organic solvent was removed under reduced pressure to give the desired product (0.26 g, 99%). ^{1}H NMR (500 MHz, $CDCl_3$, $PhNHNH_2$): δ (ppm) = 7.00 (d, J = 6.8 Hz, 1H, H_{Ar}), 6.68 (d, J = 6.8 Hz, 1H, H_{Ar}), 6.55 (s, 1H, H_{Ar}), 3.70 (bs, 2H, NH_2), 1.50 (s, 6H, 2 x $(CH_3)_{eq}$), 1.49 (s, 6H, 2 x $(CH_3)_{ax}$). ESI-MS: *m/z*: 207.74 ([MH_2^+]).

Synthesis of 50

4-nitro-*N*-(2,2,6,6-tetramethylpiperidin-4-yl)benzamide

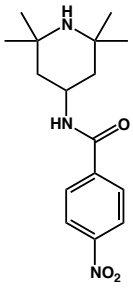

A solution of 4-nitrobenzoyl chloride (2.0 g, 11mmol, 1 eq.) in dry CH_2Cl_2 (40 ml) was cooled to 0 °C in ice. 4-Aminopiperidine (2.1 ml, 12 mmol, 1.1 eq.) was slowly added and the reaction mixture warmed to rt then refluxed for 3 hours. Once cooled, H_2O (50 ml) was added in addition to 2 M NaOH to neutralise the solution. The organic layer was separated and concentrated under vacuum. Addition of 2 ml NaOH formed a precipitate and was collected by filtration (1.28 g, 38.2%). ^{1}H NMR (400 MHz, DMSO-d_6): δ (ppm) = 8.54 (d, J = 7.6 Hz, 1H, N*H*), 8.30 (d, J = 8.8 Hz, 2H, H_{Arom}), 8.06 (d, J = 8.8 Hz, 2H, H_{Arom}), 4.28 (q, J = 4 Hz, 1H, C*H*), 1.71 (dd, J =12.4, 3.6 Hz, 2H, CH_2), 1.18 (s, 6H, 2 x CH_3), 1.16 (m, 2H, CH_2), 1.05 (s, 6H, 2 x CH_3), 0.98 (s, 1H, N*H*).

Synthesis of 51

4-amino-*N*-(2,2,6,6-tetramethylpiperidin-4-yl)benzamide

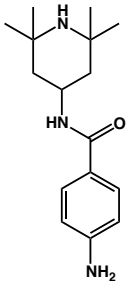

$SnCl_2.2H_2O$ (0.94 g, 4.16 mmol, 5.1 eq.) was added to a solution of **50** (0.25 g, 0.82 mmol, 1 eq.) in 96% EtOH (15 ml). The reaction mixture was stirred at 70 °C overnight then cooled in ice and 2 M NaOH added until pH = 8. The product was extracted in EtOAc (3 x 40 ml) and washed with H_2O and brine, dried over $MgSO_4$ and the solvent removed *in vacuo* to give a pale yellow solid (0.152 g, 67.6%). ^{1}H NMR (400 MHz, $CDCl_3$): δ (ppm) = 7.58 (dd, J = 2, 6.4 Hz, 2H, H_{Ar}), 6.65 (dd, J = 2.0, 6.8 Hz, 2H, H_{Ar}), 5.76 (d, J = 7.6 Hz, 1H, NH), 4.42 (m, 1H, CH), 3.99 (bs, 2H, NH_2), 1.99 (dd, J = 4.0, 12.8, 2H, C$H_{2(ax)}$), 1.28 (s, 6H, 2 x $CH_{3\,(ax)}$), 1.26 (m, 2H, C$H_{2\,(eq)}$), 1.16 (s, 1H, NH), 1.13 (s, 6H, 2 x $CH_{3\,(eq)}$).

Synthesis of 52

4-nitro-*N*-(1-oxyl-2,2,6,6-tetramethylpiperidin-4-yl)benzamide

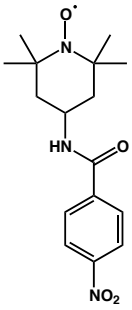

50 (0.38 g, 1.24 mmol, 1 eq.) was dissolved in CH_2Cl_2 (16 ml) and *meta*-chloroperoxybenzoic acid (0.65 g, 3.76 mmol, 3 eq.) was added in portions. The solution was stirred at rt for 1 hour then was washed with 2 M NaOH (2 x 20 ml), 2 M H_2SO_4 (10 ml), H_2O (20 ml) and brine (20 ml). The organic phase was dried with $MgSO_4$ and the solvent removed *in vacuo* to give a bright orange solid (0.31 g, 77.4%). ^{1}H NMR (500 MHz, $CDCl_3$, $PhNHNH_2$): δ (ppm) = 8.27 (d, J = 8.7 Hz, 2H, H_{Meta}), 7.94 (d, J = 8.7 Hz, 2H, H_{Ortho}), 4.50(m, 1H, CH), 2.07 (dd, J = 13.0, 3.3 Hz, 2H, 2 x H_{eq}), 1.89 (t, J = 11.8 Hz, 2H, 2 x H_{ax}), 1.40 (s, 6H, 2 x $(CH_3)_{eq}$), 1.38 (s, 6H, 2 x $(CH_3)_{ax}$).

Synthesis of 53

4-amino-*N*-(1-methoxy-2,2,6,6-tetramethylpiperidin-4-yl)benzamide

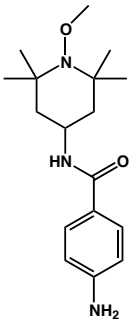

$FeSO_4.7H_2O$ (0.04 g, 0.14 mmol) and **44** (0.011 g, 0.036 mmol) was dissolved in DMSO (1 ml) and placed under argon. H_2O_2 (30%, 0.02 ml, 0.18 mmol) was added and continued to stir for 2 hours at rt. 1M NaOH was added to quench the reaction and the dark orange solution was extracted into $CHCl_3$ (2 x 10 ml), washed with H_2O (3 x 10 ml). The organic phase was removed under reduced pressure (9.6 mg, 86.1%). ^{1}H NMR (400 MHz, $CDCl_3$): δ (ppm) = 7.56 (d, J = 8.4 Hz, 2H, H_{Arom}), 6.64 (d, J = 8.4 Hz, 2H, H_{Arom}), 5.75 (d, J = 7.2 Hz, 1H, N*H*), 4.29 (m, 1H, C*H*), 3.61 (s, 3H, OCH_3), 1.87 (d, J = 8.8 Hz, 2H, CH_2), 1.41 (m, 2H, CH_2), 1.21 (s, 12H, 4 x CH_3).

Synthesis of 54

4-(4-nitrophenoxy)-2,2,6,6-tetramethylpiperidin-1-oxyl

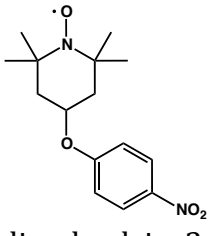

A solution of dry DMF (35 ml) and 4-hydroxy-TEMPO (2.02 g, 11.7 mmol, 1 eq.) was heated to 90 °C while adding NaH (60%, 1.01 g, 25 mmol, 2.1 eq.) in small increments. After placing on a condenser, 4-chloronitrobenzene (1.85 g, 11.6 mmol, 1 eq.) was dissolved in 3 ml DMF (dry) and added dropwise down the condenser. The

reaction vessel was covered in foil and kept at this temperature overnight. After the reaction had cooled, H_2O (10 ml) was added instantly producing a precipitate, which was filtered to give a bright yellow solid (3.14 g, 92%). ^{1}H NMR (500 MHz, $CDCl_3$): $PhNHNH_2$ δ (ppm) = 8.23 (d, J = 9.5 Hz, 2H, H_{Arom}), 6.95 (d, J = 9.5 Hz, 2H, H_{Arom}), 4.70 (m, 1H, CH), 2.11 (dd, J = 12, 4.5 Hz, 2H, 2 x H_{eq}), 1.77 (t, J = 12 Hz, 2H, 2 x H_{ax}), 1.44 (s, 1H, N-OH), 1.32 (s, 6H, 2 x $(CH_3)_{eq}$), 1.30 (s, 6H, 2 x $(CH_3)_{ax}$). ^{13}C NMR (125 MHz, $CDCl_3$, $PhNHNH_2$): δ (ppm) = 162.9, 141.3, 126.1, 115.1, 70.1, 60.7, 43.7, 31.5, 20.9. ^{1}H NMR (500 MHz, DMSO-*d*$_6$, $PhNHNH_2$): δ (ppm) = 8.22 (d, J = 9.2 Hz, 2H, H_{Ortho}), 7.15 (d, J = 9.2 Hz, 2H, H_{Meta}), 4.86 (m, 1H, CH), 2.03 (dd, J = 12.5, 4.0 Hz, 2H, 2 x H_{eq}), 1.55 (t, J = 11.6 Hz, 2H, 2 x H_{ax}), 1.19 (s, 6H, 2 x $(CH_3)_{eq}$), 1.14 (s, 6H, 2 x $(CH_3)_{ax}$). ^{13}C NMR (100 MHz, DMSO-*d*$_6$): δ (ppm) = 163.2, 141.1, 126.4, 116.3, 70.6, 58.5, 44.1, 36.2, 32.6. IR (cm^{-1}): 1338 (s) NO_2 and N-O stretch, 1511 (s) NO_2. Mp: Found (163 – 169 °C).

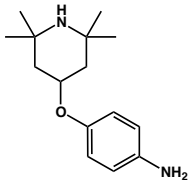

To compare against **2,2,6,6-tetramethyl-4-(4-nitrophenoxy)piperidine**, the same procedure was followed except following stirring overnight the reaction mixture was extracted into EtOAc and purified by column chromatography (10% MeOH/Acetone). Minor product (~14%). ^{1}H NMR (400 MHz, $CDCl_3$): δ (ppm) = 8.21 (d, J = 7.2 Hz, 2H, H_{Arom}), 6.94 (d, J = 7.2 Hz, 2H, H_{Arom}), 4.80 (m, 1H, CH), 2.11 (dd, J = 12.8, 4 Hz, 2H, 2 x H_{eq}), 1.37 (s, 6H, 2 x $(CH_3)_{eq}$), 1.27 (m, 2H, 2 x H_{ax}), 1.26 (s, 6H, 2 x $(CH_3)_{ax}$). ESI-MS: *m/z* 279.38 [MH^+].

Synthesis of 56 4-azido-2,2,6,6-tetramethyl-piperidin-1-oxyl

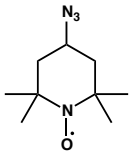

To a solution of **68** (2.62 g, 10.5 mmol, 1 eq.) in dry DMF (25 ml) was added NaN_3 (1.48 g, 22.8 mmol, 2.2 eq.) in portions over 15 minutes. The solution was refluxed at 110 °C under Ar overnight. Upon cooling, Et_2O (100 ml) was added and the organic mixture before being washed with $NaHCO_3$ (75 ml) and H_2O (75 ml) repeated 3 times to remove DMF. The organic layer was dried over $MgSO_4$ and concentrated *in vacuo* to give an orange oil which solidified to give long red/orange crystals. If purification required a gradient silica column from 2 – 10% MeOH/CH_2Cl_2 gave the title compound (1.26 g, 61.0%). ^{1}H NMR (500 MHz, $CDCl_3$, $PhNHNH_2$): δ (ppm) = 3.65 (m, 1H, CH), 1.91 (dt, J = 1.5, 11 Hz, 2H, CH_2), 1.61 (t, J = 12 Hz, 2H, CH_2), 1.31 (s, 1H,

NOH), 1.27 (s, 6H, 2 x CH_3), 1.21 (s, 6H, 2 x CH_3) Similar to literature.[177] ^{13}C NMR (100 MHz, $CDCl_3$):$PhNHNH_2$ δ (ppm) = 58.3, 52.8, 44.2, 32.9, 20.1. IR (cm^{-1}): 2094 (s) N_3 stretch, 1361 (m) N-O• stretch. Mp: 59 – 61 °C. ESI-MS: *m/z* 197.25 ([M^+], 35%), 198.27 ([$MH^{+\bullet}$], 100%), 199.26 ([$MH_2^{+\bullet}$], 45%).

Synthesis of 57 2-benzylisoindoline-1,3-dione

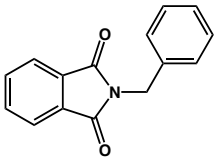

Phthalic anhydride (10.1 g, 68 mmol, 1 eq.) and benzylamine (7.5 ml, 68 mmol, 1 eq.) was heated until all dissolved (melted). Following cooling at rt for 5 mins, CH_2Cl_2 (120 ml) was slowly added. Organic solution was washed with 2M H_2SO_4, 2M NaOH, Brine and H_2O (100 ml), dried over $MgSO_4$ and solvent removed on a rotary evaporator to give a white solid (10.0g, 61.2%). ^{1}H NMR (500 MHz, DMSO-d_6): δ (ppm) = 7.90 (dd, J = 5.5, 3.5 Hz, 2H, H_{Ar}), 7.86 (dd, 5.0, 3.5 Hz, 2H, H_{Ar}), 7.34-7.31 (m, 5H, Ar), 4.78 (s, 2H, CH_2).

Synthesis of 58 2-benzyl-1,1,3,3-tetramethylisoindoline

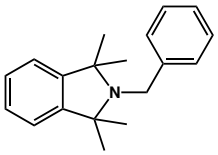

Following a similar procedure by Griffiths[193] and Jayawardena[180], pre-dried magnesium (50 g) was added to a flame-dried 3-necked flask with a crystal of iodine. This flask was equipped with a dropper, Dean-Stark and a double jacket condenser connected to a pump delivering chilled water. Anhydrous ether (250 ml) was combined with MeI (110 ml, 251 g, 1.76 mol, 7 equiv.) and after an initial addition (50 ml) to initiate the reaction, was added drop wise at a rate that maintained constant rate of reaction. After the activity has ceased the internal temperature was increased to 80 °C to allow the concentration of the Grignard reagent. The reaction mixture was allowed to cool to 68 °C, then a solution of N-benzylphthalimide (60 g, 0.253 mmol) in toluene (500 ml) was added. The reaction mixture was refluxed for 3 hours and then concentrated by distillation. Once cooled, mixture was diluted with n-hexanes (500 ml) and cooled further in ice whereby a controlled addition of iso-propylalcohol (200 ml) was used to quench the reaction. In a large separating funnel, the mixture was mixed with H_2O and extracted several times with hexane. Air was bubbled through the combined organic layer and ¾ of solvent was removed on a rotary evaporator.

The resulting purple slurry was passed through a column of basic alumina and solvent removed under reduced pressure to give a golden oil that crystallised under vacuum. Crude material was recrystallised from MeOH to give white crystals (11.3 g, 16.9%). ^{1}H NMR (500 MHz, $CDCl_3$): δ (ppm) = 7.52 (d, J = 7.5 Hz, 2H, H_{Ar}), 7.34 (t, J = 7.5 Hz, 2H, H_{Ar}), 7.30-7.28 (m, 3H, Ar), 7.18 (dd, J = 3.5, 5.5 Hz, 2H, Ar), 4.05 (s, 2H, C*H*$_2$), 1.36 (s, 12H, 4xC*H*$_3$). MS(ESI): *m/z* = 266.45 [MH$^+$]. This data agrees with those previously reported by Griffiths.[193]

Synthesis of 59 1,1,3,3-tetramethylisoindoline

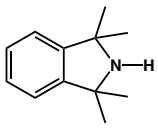

58 (10 g, 37.7 mmol) was dissolved in glacial acetic acid (150 ml) and placed in hydrogenation chamber with Pd/C (10% w/w, 1g). Following a reaction time of 4 hours, the mixture was filtered over celite. The solvent was removed under reduced pressure to give an oily substance. On addition of water, extraction by ether removed left over starting material. Following addition of 10M NaOH to basify solution, several CH_2Cl_2 extractions removed the desired product. Combined organic solutions were dried over $MgSO_4$, filtered and the solvent removed on a rotary evaporator under reduced pressure to give an oil that solidified on standing (6.4 g, 97.0%). MS(ESI): *m/z* = 176.29 [MH$^+$]. NMR not obtained of intermediate species.

Synthesis of 60 1,1,3,3-tetramethylisoindoline-2-oxyl

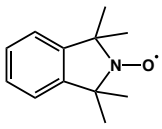

59 (6.4 g, 36.6 mmol, 1 eq.) was dissolved in CH_2Cl_2 (200 ml) and *m*CPBA (10 g, 57.9 mmol, 1.6 eq.) was added portionwise over ½ hour. An immediate colour change was seen to yellow/orange. Solution continued to stir at rt for a remaining ½ hour and monitored by TLC (40:60 EtOAC/Hexane). Once complete the solution was washed with 5M NaOH, 5M HCl, H_2O and brine, dried over $MgSO_4$ and the solvent was removed on the rotary evaporator. Crude material was dissolved in hexane and hot filtered to remove remaining starting reagents. Recrystallisation from hexane produced orange crystals (6.2 g, 89.2%). ^{1}H NMR (500 MHz, $CDCl_3$, $PhNHNH_2$): δ (ppm) = 7.21 (d, J = 7.5 Hz, 2H, H_{Ar}), 6.89 (dd, J = 1.5, 6.5 Hz, 2H, H_{Ar}), 1.52 (s, 12H, 4xC*H*$_3$)

Synthesis of 61 5-nitro-1,1,3,3-tetramethylisoindoline-2-oxyl

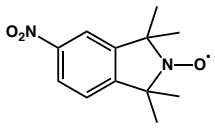

TMIO (**60**) (4.5 g, 23.7 mmol) was slowly dissolved in conc. H_2SO_4 (40 ml) in a cooled ice bath at 0 °C before heating to 50 °C for 1 hour. The mixture was cooled again to 0-5 °C where HNO_3 (10 ml) was added drop wise maintaining this temperature before warming to rt followed by heating to 80 °C overnight. Once cooled the mixture was poured into ice (100 ml) and basified to pH = 9 with NaOH. The desired material was extracted into diethylether, dried over $MgSO_4$ and removed the solvent under reduced pressure. Crude material was recrystallised from hot EtOH to give orange block crystals (2.8 g, 52.4%). ^{1}H NMR (500 MHz, $CDCl_3$ $PhNHNH_2$): δ (ppm) = 8.03 (dd, J = 7.5, 2.5 Hz, 1H, H_{Ar}), 7.90 (d, J = 2.5 Hz, 1H, H_{Ar}), 7.16 (dd, J = 7.5, 2.5 Hz, 1H, H_{Ar}), 1.51 (s, 6H, 2xCH_3), 1.49 (s, 6H, 2xCH_3).

Synthesis of 62

4-((1-hydroxy-2,2,6,6-tetramethylpiperidin-4-yl)carbamoyl) benzenediazonium tetrafluoroborate

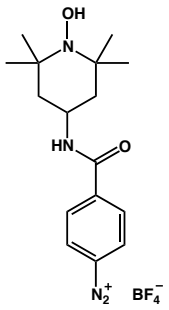

A solution of **44** (0.418 g, 1.44 mmol, 1 eq.) was dissolved in anhydrous MeCN (10 ml) and cooled in an ice/salt bath to -10 °C. 50% HBF_4 (1 ml, 15.7 mmol) was added followed by a drop wise addition of a cooled solution of $NaNO_2$ (0.132 g, 1.91 mmol, 1.3 eq.) in H_2O (1 ml). The reaction mixture was stirred in ice for 30 minutes, followed by 1 hour at room temperature. Diethyl ether was added until a precipitate formed which was filtered to give a light yellow solid (0.286 g, 50.8%). IR (cm^{-1}): 2298 (m) N_2 stretch. ESI-MS: *m/z* 275([M-N_2^+]). Unable to obtain NMR due to reactivity of diazonium species (effervescence seen when dissolved in available deuterated solvents).

Synthesis of 63

***N*-(1-hydroxy-2,2,6,6-tetramethylpiperidin-4-yl)-4-((4-hydroxyphenyl) diazenyl)benzamide**

A solution of phenol (28.5 mg, 0.303 mmol, 1.1 eq.) was dissolved in 2 M NaOH (2.5 ml) and cooled in ice. A cooled solution of **62** (0.105 g, 0.27 mmol, 1 eq.) in H_2O (2.5 ml) was slowly added to the basic solution where an instant orange

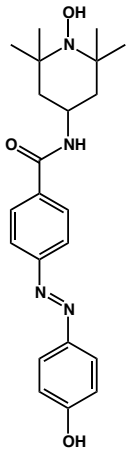

colour change was observed. The solution continued to stir in ice for 30 minutes then overnight at room temperature. 2 M HCl was used to neutralise the pH before extracted into EtOAc (3 x 10 ml). The combined organic layers were dried over $MgSO_4$ and solvent removed *in vacuo*. Solid was purified on silica column (15 cm, 1:1 EtOAc/Hexane) to afford **63** as a orange solid (62.4 mg, 58.3%). ^{1}H NMR (500 MHz, DMSO-d_6, $PhNHNH_2$): δ (ppm) = 8.31 (d, J = 7.5 Hz, 1H, NH), 8.01 (d, J = 8.5 Hz, 2H, H_{Ar}), 7.86 (d, J = 9.0 Hz, 2H, H_{Ar}), 7.84 (d, J = 9.0 Hz, 2H, H_{Ph}), 7.16 (s, 1H, NO*H*), 6.97 (d, J = 8.5 Hz, 2H, H_{Ph}), 4.23 (m, 1H, CH), 1.76 (d, J = 11.3 Hz, 2H, $CH_{2\,(ax)}$), 1.54 (t, J = 12.5, 2H, $CH_{2(eq)}$), 1.18 (s, 6H, 2 x $CH_{3\,(ax)}$), 1.16 (s, 6H, 2 x $CH_{3\,(eq)}$). ^{13}C NMR (125 MHz, DMSO-d_6): δ (ppm) = 165.4, 161.9, 153.9, 145.8, 128.9, 125.6, 122.2, 117.1, 116.5, 58.4, 45.2, 41.4, 33.2, 20.1. ESI-MS: *m/z* 395.82 [M^+], 396.82 [$MH^{\bullet+}$], 397.83 [MH_2^+], 197.24 [$M\text{-}H_2]^{2-}$.

Synthesis of 65

1,1,3,3-tetramethyl-2,3-dihydroisoindol-2-yloxyl-5-diazonium

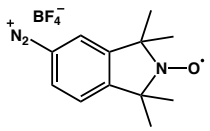

Adapting the method from Blinco,[181] nitrosonium tetrafluoroborate (0.253 g, 2.16 mmol, 1.4 eq.) was placed in a sealed flask and replaced the air with Ar. MeCN (2 ml) distilled over CaH_2 was added to the flask and the solution cooled to -15°C in an ice/salt bath. A solution of **48** (0.314 g, 1.53 mmol, 1 eq.) dissolved in MeCN (2.5 ml) was added drop wise to the nitrosonium solution ensuring the solution remains chilled. The reaction mixture was stirred at this temperature for 45 minutes followed by 1 hour at rt. Diethyl ether (~5 ml) was added until a precipitate formed which was collected by filtration and thoroughly washed with ether to give tan solid (0.103 g, 22.0%). IR (cm^{-1}): 2303 (m) N_2+ stretch.[183] Unable to obtain NMR due to reactivity of the diazonium species.

Synthesis of 66

5-((4-hydroxyphenyl)diazenyl)-1,1,3,3-tetramethylisoindolin-2-ol

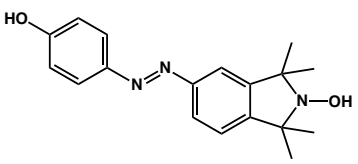

Phenol (22.7 mg, 0.24 mmol, 1.2 eq.) was dissolved in 2 M NaOH (1 ml) and cooled in ice to 0 °C. Compound **65** (62.6 mg, 0.21 mmol, 1 eq.) was dissolved in H_2O (3 ml) and cooled in ice before added to the basic solution dropwise maintaining the temperature between 0-5 °C. The reaction was stirred at this temperature for 30 minutes then at rt overnight. The mixture was neutralised with H_2SO_4 and extracted twice into EtOAc, dried over $MgSO_4$ and the solvent removed under reduced pressure. Purification was by silica column chromatography (1% MeOH/CH_2Cl_2) to give an orange solid (48.8 mg, 76%). ^{1}H NMR (500 MHz, DMSO-*d*$_6$, $PhNHNH_2$): δ (ppm) = 10.3 (bs, 1H, OH), 7.80 (d, J = 8.9 Hz, 2H, Ar), 7.73 (dd, J = 8.0, 1.5 Hz, 1H, H_{Ar}), 7.67 (s, 1H, N-OH), 7.63 (d, J = 1.1 Hz, 1H, H_{Ar}), 7.39 (d, J = 8.1 Hz, 1H, H_{Ar}), 6.96 (d, J = 8.8 Hz, 2H, Ar), 1.37 (s, 6H, 2 x CH_3), 1.35 (s, 6H, 2 x CH_3). ^{13}C NMR (125 MHz, DMSO-*d*$_6$, $PhNHNH_2$): δ (ppm) = 161.2, 152.4, 148.6, 147.2, 145.7, 128.8, 125.2, 123.0, 122.9, 116.4, 115.1, 66.4, 26.8, 26.8.

Synthesis of 68

4-methansulfonyloxy-2,2,6,6-tetramethylpiperidin-1-oxyl

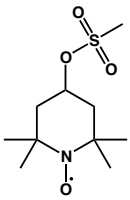

4-Hydroxy-TEMPO (2.0 g, 11.6 mmol, 1 eq.) was dissolved in dry pyridine (10 ml) and cooled in an ice/acetone bath under argon. Methanesulfonylchloride (1.8 ml, 23.2 mmol, 2 eq.) was added drop wise over 15 minutes. The reaction was stirred in the ice bath overnight allowing a gradual increase in temperature as the ice melted. Reaction was monitored by TLC, and further addition of $MeSO_2Cl$ is added if required. Mixture was cooled in ice and sat. $NaHCO_3$ was added slowly then extracted 3 x into $CHCl_3$. Organic layers were combined and washed with $NaHCO_3$ and H_2O then dried over $MgSO_4$ and solvent removed *in vacuo*. Gave red/orange crystals (2.6 g, 89.2%). ^{1}H NMR (400 MHz, DMSO-*d*$_6$, $PhNHNH_2$): δ (ppm) = 4.82 (m, 1H, C*H*), 3.18 (s, 3H, CH_3), 2.01 (dd, J = 13.6, 4.0 Hz, 2H, CH_2), 1.58 (t, J = 11.6 Hz, 2H, CH_2), 1.11 (s, 6H, CH_3), 1.10 (s, 6H, CH_3), 1.01 (s, 1H, O*H*). ESI-MS: *m/z* 251.25 [$MH^{+\bullet}$], 252.26 [$MH_2^{+\bullet}$].

Synthesis of 70

2,2,6,6-tetramethyl-4-(4-phenyl-1*H*-1,2,3-triazol-1-yl)piperidine-1-ol

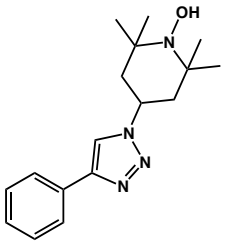

Azido-TEMPO (**56**) (0.114 g, 0.578 mmmol, 1 eq.) and sodium ascorbate (0.118 g, 0.596 mmol, 1.05 eq.) was stirred in a thoroughly degassed solution of 1:1 EtOH/H_2O mixture (10 ml) for 10 minutes. $CuSO_4.5H_2O$ (35.6 mg, 0.143 mmol), sodium ascorbate (23.4 mg, 0.118 mmol) and phenylacetylene (65 µl, 0.592 mmol, 1 eq.) was added to this solution where it stirred at 60°C for 48 hours in the absence of light. The reaction mixture was extracted into EtOAc (50 ml) and washed with H_2O (50 ml). The organic solution was dried over $MgSO_4$ and removed under reduced pressure to give a bright yellow solid (0.12 g, 69.2%). ^{1}H NMR (500 MHz, DMSO-d_6): δ (ppm) = 8.72 (s, 1H, $CH_{(triazole)}$), 7.85 (dd, J = 8.4, 1.2 Hz, 2H, H_{Ortho}), 7.45 (t, J = 7.5 Hz, 2H, H_{Meta}), 7.35 (s, 1H, OH), 7.30 (t, J = 7.4 Hz, 1H, H_{Para}), 4.92 (m, 1H, CH), 2.07 (dd, J = 12.4, 3.8 Hz, 2H, 2 x H_{eq}), 1.98 (t, J = 12.6 Hz, 2H, H_{ax}), 1.19 (s, 6H, 2 x CH_3), 1.16 (s, 6H, 2 x CH_3).

Synthesis of 71 4-((trimethylsilyl)ethynyl)aniline

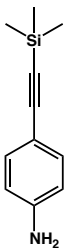

4-Iodoaniline (1.14 g, 5.21 mmol, 1 eq.), palladium(II) acetate (52.9 mg, 0.235 mmol), copper(I) iodide (101.7 mg, 0.534 mmol) and triphenylphosphine (64.9 mg, 0.247 mmol) were dissolved in triethylamine (10 ml) and the mixture degassed using three freeze-thaw-saturate-with-nitrogen cycles. Trimethylsilylacetylene (0.75 ml, 5.27 mmol, 1 eq.) was added by syringe and the mixture carefully degassed by boiling briefly under reduced pressure. After stirring at rt overnight, hexane was added and triethylaminehydrogen iodide removed by filtration over celite. The filtrate was removed under vacuum and recrystallised from hot hexane to give a light brown solid (0.77g, 78%). ^{1}H NMR (500 MHz, DMSO-d_6): δ (ppm) = 7.27 (d, J = 8.8 Hz, 2H, H_{Ar}), 6.57 (d, J = 8.5 Hz, 2H, H_{Ar}), 3.79 (bs, 2H, NH_2), 0.23 (s, 9H, $Si(CH_3)_3$). ESI-MS: *m/z* 190.00 [MH^+].

Synthesis of 72

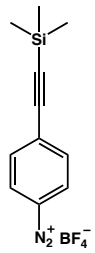

4-((trimethylsilyl)ethynyl)benzenediazonium tetrafluoroborate

71 (52 mg, 0.273 mmol, 1 eq.) was dissolved in H_2O (5 ml) and 50 % HBF_4 (5 ml) and cooled 0 - 5 °C. $NaNO_2$ (30 mg, 0.435 mmol, 1.6 eq.) was dissolved in 0.5 ml H_2O and added to the reaction mixture drop wise. It was continued to stir at this temperature for 10 minutes then at rt overnight. The precipitate was filtered and washed with ice-cold Et_2O to give a brown solid (17.9 mg, 22.7%). ^1H NMR (500 MHz, $CDCl_3$): δ (ppm) = 8.53 (d, J = 9.1 Hz, 2H, H_{Ortho}), 7.74 (d, J = 9.1 Hz, 2H, H_{Meta}), 0.28 (s, 9H, $Si(CH_3)_3$).

Synthesis of 76 N-(1-oxyl-2,2,6,6-tetramethylpiperidin-4-yl)benzamide

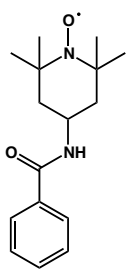

Step 1: **N-(2,2,6,6-tetramethylpiperidin-4-yl)benzamide (76a) -** 4-Aminopiperidine (4 ml, 23.2 mmol, 1 eq.) was slowly added to a solution of 4-benzoyl chloride (3 ml, 26 mmol, 1.1 eq.) in THF:pyridine (20 ml, 10:1) and stirred at rt for 2 hours then refluxed for a further hour. The organic solvent was removed under reduced pressure and the remaining material was neutralised with 2 M NaOH before it was extracted into CH_2Cl_2, washed with water, 0.1 M NaOH and brine, dried over $MgSO_4$ and the solvent was removed under reduced pressure (2.42 g, 42%). No further purification was required. ^1H NMR (400 MHz, $CDCl_3$): δ (ppm) = 7.76 (d, J = 8.0 Hz, 2H, H_{Ortho}), 7.51 (t, J = 7.4 Hz, 1H, H_{Para}), 7.45 (t, J = 7.4 Hz, 2H, H_{Meta}), 5.91 (d, J = 7.0 Hz, 1H, C(O)NH), 4.47 (m, 1H, CH), 2.02 (dd, J = 12.4, 3.7 Hz, 2H, 2 x H_{eq}), 1.32 (s, 6H, 2 x $(CH_3)_{eq}$), 1.17 (s, 6H, 2 x $(CH_3)_{ax}$), 1.02 (t, J = 12.2 Hz, 2H, 2 x H_{ax}). ESI-MS: *m/z* 261.63 [MH^+]. *Step 2:* The title compound was prepared by portion wise addition of *m*CPBA (1.87 g, 10.8 mmol, 2.6 eq.) to a solution of **76a** (1.04 g, 4.2 mmol, 1 eq.) in CH_2Cl_2 (30 ml) and stirred for 1 hour at rt. The organic solution was washed with 2 M NaOH (x2), HCl, brine and water and dried over $MgSO_4$ before the solvent was removed under reduced pressure. Recrystallisation from toluene gave bright orange crystals (0.71 g, 62%). ^1H NMR (500 MHz, $CDCl_3$, $PhNHNH_2$): δ (ppm) = 7.77 (d, J = 7.0 Hz, 2H, H_{Ortho}), 7.53 (t, J = 7.0 Hz, 1H, H_{Para}), 7.46 (t, J = 7.0 Hz, 2H, H_{Meta}), 6.11 (d, J = 7.0 Hz, 1H, C(O)NH), 4.48 (m, 1H, CH), 2.06 (dd, J = 13.0, 2.0 Hz, 2H, 2 x H_{eq}), 1.67 (t, J = 12.5

Hz, 2H, 2 x H_{ax}), 1.34 (s, 6H, 2 x $(CH_3)_{eq}$), 1.33 (s, 6H, 2 x $(CH_3)_{ax}$). ESI-MS: *m/z* 277.53 [MH_2^+]. IR (cm^{-1}): 1631 (C=O), 1337 (N-O•).

Synthesis of 78 1-oxyl-2,2,6,6-tetramethylpiperidin-4-yl pivalate

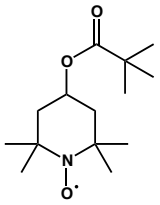

To a solution of 4-hydroxy-TEMPO (172 mg, 1 mmol, 1 eq.) in dry THF (5 ml), NaH (60%; 80 mg, 2 mmol, 2 eq.) was added portionwise. The mixture was refluxed under Ar for 30 min before pivaloyl chloride (128 µL, 1.5 mmol, 1.5 eq.) was slowly added. The reaction continued to reflux for a further 3 hours. The solvent was removed under reduced pressure and the material redissolved in $CHCl_3$, washed with H_2O, dried over $MgSO_4$ and solvent removed under reduced pressure. Purification was by silica chromatography (10:1, Hexane/EtOAc) to afford the title compound as an orange solid (110 mg, 42%). ^{1}H NMR (500 MHz, DMSO-*d*$_6$, $PhNHNH_2$): δ (ppm) = 4.90 (m, 1H, C*H*), 1.80 (dd, J = 11.8, 3.5 Hz, 2H, 2 x H_{eq}), 1.43 (t, J = 11.5 Hz, 2H, 2 x H_{ax}), 1.11 (s, 9H, $C(CH_3)_3$), 1.09 (s, 6H, 2 x $(CH_3)_{eq}$), 1.07 (s, 6H, 2 x $(CH_3)_{ax}$). ^{13}C NMR (125 MHz, DMSO-*d*$_6$, $PhNHNH_2$): δ (ppm) = 176.9, 66.1, 57.9, 43.5, 38.1, 31.8, 26.7, 21.3. ESI-MS: *m/z* 258.34 [MH_2^+].

Synthesis of 79 2,2,6,6-tetramethyl-1-oxo-4-(pivaloyloxy)piperidinium

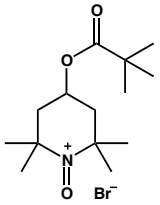

To a stirred solution of **78** (92 mg, 0.36 mmol, 1 eq.) in CCl_4 (0.3 ml) a solution of Br_2 (7 µL, 0.13, 0.75 eq.) in CCl_4 (1.5 ml) was added dropwise at rt. A dark precipitate formed and filtered to give a dark orange solid (63 mg, 51%). ^{1}H NMR (500 MHz, DMSO-*d*$_6$): δ (ppm) = 5.30 (m, 2H, 2 x C*H*,C1/2*), 4.45 (d, J = 13.6 Hz, 2H, 2 x H_{eq},C1), 4.12 (d, J = 15.3 Hz, 2H, 2 x H_{ax}, C1), 2.64 (s, 6H, 2 x $(CH_3)_{eq}$,C1), 2.46 (m, 2H, 2 x H_{eq}, C2), 2.44 (s, 6H, 2 x $(CH_3)_{ax}$, C1), 2.29 (d, J = 14.5 Hz, 2H, 2 x H_{ax},C2), 1.66 (s, 6H, 2 x $(CH_3)_{eq}$, C2), 1.63 (s, 6H, 2 x $(CH_3)_{ax}$, C2), 1.17 (s, 18H, 2 x $C(CH_3)_3$, C1/2). * - Two compounds C1 and C2 in a 1:1 mixture. ESI-MS: *m/z* 256.30 [M^+]. IR (cm^{-1}): 1601 (N=O).

CHAPTER FOUR

Molecular Behaviour:
Physical attributes of urea-hydrogen peroxide adducts

4.1 Introduction of Urea-Hydrogen Peroxide Adducts

The formation of urea-hydrogen peroxide (UHP) adducts from urea and hydrogen peroxide can be described by Equation 4.1. An energy requirement for UHP formation is indicated by the necessity to heat the system to push the equilibrium to the right (Eq. 4.1). In order to characterise the formation of the adduct, we must first distinguish between the bound and unbound states of the H_2O_2.

$$\text{Urea (aq)} + H_2O_2\text{(aq)} \rightleftharpoons \text{UHP(s)} \qquad 4.1$$

Unfortunately, when attempting to measure H_2O_2 or UHP it is difficult to distinguish between H_2O_2•urea and H_2O•urea. Both hydrogen peroxide and water display a similar hydrogen-bonding pattern with urea making it difficult to differentiate between them. This is a challenge for any hydrogen peroxide adducts, and is addressed in this chapter.

In addition to this equilibrium, effects such as the solubility of urea and UHP play an additional part in the adduct formation. Formation of UHP is achieved in an aqueous solution where urea is appreciably soluble (108 g/100 ml, 20 °C). Since this work concerns larger organic ureas that contain hydrophobic and aromatic groups, solubility becomes an issue in water. Solubility of these target compounds in organic solvents is also limited to polar solvents such as dimethylsulfoxide (DMSO), acetonitrile (MeCN), methanol (MeOH) and to some extent tetrahydrofuran (THF) and acetone.

Using the method described in Section 2.5.3 for the formation of adducts with an anhydrous THF:H_2O_2 solution, it is possible to add hydrogen peroxide in a non-aqueous form, reducing the amount of water in the reaction. The THF:H_2O_2 solution is in turn derived from anhydrous UHP, and exploits the low solubility of urea in THF to make an organic hydrogen peroxide solution. This decreases the interaction between water and the target organic ureas thus encouraging the formation of the desired adducts.

The competitive binding of water is largely overlooked in many perhydrates, as the characterisation is achieved by titrimetry or X-ray crystallography where it is not an issue. Lu[91] described a H_2O_2 content of 35.4% (w/w) in UHP by titrating it against standardised $KMnO_4$ in acid. Alternative analysis by thermal decomposition showed a mass loss of nearly 36% (w/w) of UHP at 85 °C; consistent with a 1:1 ratio.[194] Amino acids such as histidine,[195] serine,[98] adenine[196,197] and glycine[101] readily form perhydrates that are able to be characterised by X-ray crystallography.

To explore the characteristics of UHP, it first must be differentiated from the individual features of urea. Solid urea is a tightly packed network and has a melting point of 133 – 135 °C. It is expected that the melting point of UHP would be lower as it disrupts packing of the ordered structure.[198] However, melting of UHP does not take place in a straightforward manner. As the temperature rises, the complex dissociates into urea and H_2O_2, which implies decomposition of the solid. In these circumstances as decomposition of UHP proceeds, the amount of urea increases (Eq. 4.1). Composition of the melt can move towards pure urea resulting in the melt re-solidifying and the observed melting point skewed. Furthermore, as the temperature increases H_2O_2 decomposes into water and oxygen (Eq. 1.23). This essentially forms a ternary system of urea-UHP and water that reduces the eutectic temperature further than in the binary system of urea-UHP.[198] Consequently, measuring the melting point of hydrogen peroxide adducts is problematic and involves the products of both melting and decomposition of the complex.

4.1.1 Properties of Hydrogen Peroxide

Hydrogen peroxide is a strong oxidising agent that is routinely used in household and commercial processes as a bleach and antiseptic. Production of bulk hydrogen peroxide is predominantly by a cyclic auto-oxidation of alkylanthraquinones (Scheme 4.1).[199]

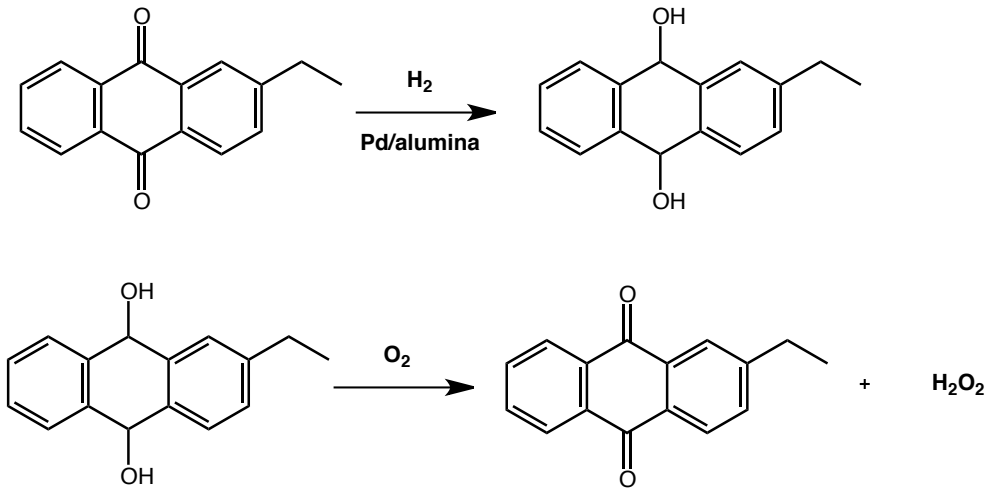

Scheme 4.1. Production of H_2O_2 by hydrogenation and auto-oxidation of 2-ethylanthraquinone.

Hydrogenation with a Pd/alumina catalyst forms an active catalytic species that undergoes auto-oxidation to furnish hydrogen peroxide along with regenerating the starting material.

Hydrogen peroxide exists as a non-planar molecule with a twisted or skew structure. It displays a large barrier to internal rotation of the O–O single bond due to repulsions exhibited by the lone pairs of the oxygen atoms (35.23 kJ/mol from skew to cis).[200] There is a relatively large difference in molecular structures between the gaseous and crystalline forms of H_2O_2 attributed to the effects of hydrogen bonding (Fig. 4.1). The crystalline structure exhibits hydrogen bonds between compounds of 2.78 Å in length extending in infinite helices around a 4-fold screw axis.[201]

With a boiling point in its pure form of 150.2 °C and a freezing point of -0.43 °C, hydrogen peroxide forms a miscible liquid with water. This eutectic mixture

exhibits freezing point depression and its density decreases with H_2O_2 concentration advancing to that of pure water. (eg. at 20 °C H_2O_2 has a density of 1.44 and 1.11 g ml^{-1} for pure and 30% respectively).[99]

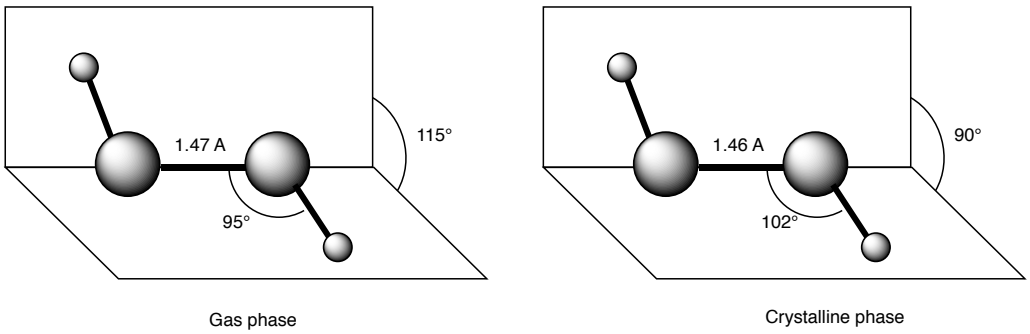

Fig. 4.1. Gas and crystalline structure of H_2O_2.

In aqueous solutions, hydrogen peroxide is more acidic than water with a pK_a of 11.75 as opposed to water with a pK_w of 14.1 at 20 °C.

$$H_2O_2 \rightleftharpoons H^+ + HO_2^- \qquad 4.2$$

In addition to acid dissociation, hydrogen peroxide can decompose into water and O_2 accelerated by trace impurities such as heavy metals.

$$2H_2O_2\,(aq) \rightarrow 2H_2O(l) + O_2\,(g) \qquad 1.23$$

ΔG^o = -224 kJ mol^{-1}

Contaminant-free containers must be used that do not promote the decomposition of H_2O_2. These materials include aluminium, pyrex-glass, quartz and a limited number of plastics. To ensure the elimination of trace metal impurities deionised or milliQ water is required when dealing with hydrogen peroxide materials.

In addition to the strong oxidising properties of H_2O_2, organic peroxides are known to have explosive properties. Each peroxy group correlates to one active oxygen atom. 'Active oxygen' is the term used to describe the amount of energy

content related to the compound whereby the more energy it has, the more hazardous it becomes. The theoretical amount of active oxygen can be described by

$$A[O]_{Theroretical}\ (\%) = [(16*p/m)]*100 \qquad 4.3$$

where p is the number of peroxy groups and m is the molecular weight of the pure peroxide.[202] As the binding strength of the adducts towards peroxide is uncertain, care must be taken when using peroxy-containing compound as the active oxygen content is initially unknown.

Acetone peroxide (TCAP) is an example of a compound that displays high active oxygen content. This cyclic tri-peroxide is susceptible to heat, friction and shock and is commonly used as a non-nitrogen containing explosive. A sample containing greater than 4 grams (1.2 L of O_2) of material will detonate on ignition where the rapid expansion of gas creates an explosion.

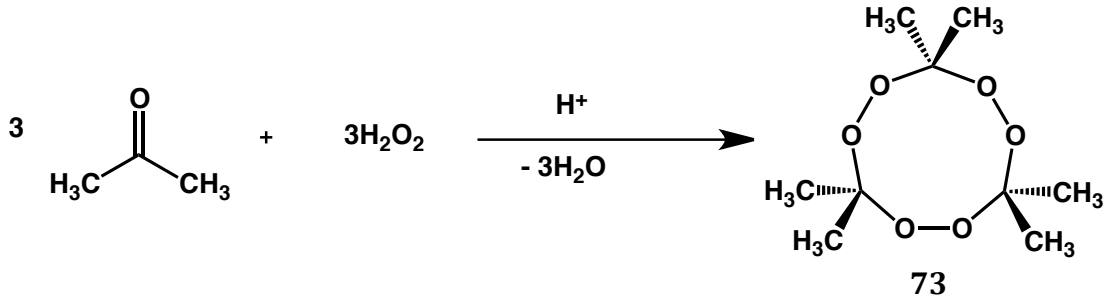

73

Scheme 4.2. Formation of cyclic tri-peroxide from acetone and hydrogen peroxide.

TCAP is formed by an acid-catalysed nucleophilic addition of acetone and hydrogen peroxide (Scheme 4.2). Although the monomer and dimer are possible, the angle strain of the internal bonds is not favoured. As a precaution, acetone was not used in any reaction or adduct formation which contains hydrogen peroxide, and adduct forming reactions were confined to small scale (<2 g).

4.1.2 Properties of alternative peroxide-containing adducts

Characterisation of a number of phosphine oxide-H_2O_2 adducts show distinct features in ^{31}P NMR spectroscopy in the solution and solid states. Differentiation is also possible in IR spectroscopy and single crystal X-ray analysis.[95] Deshielding of the phosphorus nucleus in the peroxide adduct results in a downfield shift from 44 ppm to 51 ppm, compared to phosphine oxide in ^{31}P NMR (Fig. 4.2). Although this is solvent dependent, it is clear there is a change in the phosphine oxide when complexed to H_2O_2.

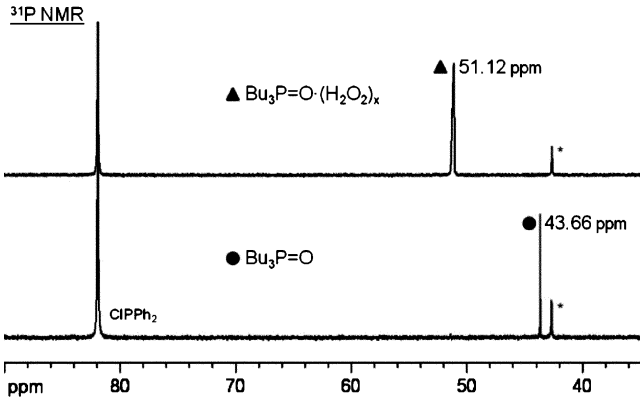

Fig. 4.2. ^{31}P NMR of $Bu_3P{=}O$ and $Bu_3P{=}O{\bullet}H_2O_2$ in C_6D_6 with $ClPPh_2$ as the standard. Asterisks denotes the oxidised standard, $ClPh_2P{=}O$, in the capillary. Reproduced from Ref.[95] with permission from The Royal Society of Chemistry.

Unfortunately as the target substituted urea adducts in the present study do not contain phosphorus atoms, ^{31}P NMR is unfeasible for this system. Urea does contain nitrogen atoms that can be used in nitrogen NMR.[204] ^{14}N is the most abundant isotope (99.6%). However its sensitivity is plagued by quadrupolar interactions that broaden the signal. An alternative isotope ^{15}N yields narrow lines although its low abundance (0.37%) requires an enriched sample for analysis. Enriching all the urea compounds with ^{15}N is unfeasible and costly, therefore was not used in the present study.

IR spectroscopy provides information on vibrational modes within a compound. A broad O-H stretch can be seen for the bound H_2O_2 in a solid sample, and exists at 3217 cm^{-1} for the $Bu_3P{=}O{\bullet}H_2O_2$ adduct. When this compound is allowed to partially decompose with heat, two additional broad O-H vibrational modes can

be observed at 3408 and 1647 cm^{-1}, attributed to the O-H stretch in H_2O and its associated bending mode respectively.[95] In a study on the $Ph_3P{=}O{\bullet}H_2O_2$ adduct, medium stretch at 2830 cm^{-1} was observed, which was assigned to the O-H stretching vibration of H_2O_2 lowered by strong hydrogen bonding.[203]

As part of the characterisation of the peroxide adduct, the equilibrium constant for each substituted urea-H_2O_2 adduct (U'HP) was required in the present study. The equilibrium constant defines that a high K value produces more adduct improving the binding of hydrogen peroxide within the proposed battery system.

$$\text{Urea}'(\text{aq}) + \text{H}_2\text{O}_2(\text{aq}) \rightleftharpoons \text{U}'\text{HP}(\text{aq}) \qquad 4.4$$

$$K = \frac{[\text{U}'\text{HP}(\text{aq})]}{[\text{Urea}'(\text{aq})]\,[\text{H}_2\text{O}_2(\text{aq})]} \qquad 4.5$$

(Urea' = substituted urea, U'HP = substituted urea hydrogen peroxide adduct)

Although determining the equilibrium constant for aqueous UHP was not novel, it was a useful starting point for developing methodology for the determination of the equilibrium complex of the new U'HP complexes.

4.2 Results and Discussion

This section commences with studies on urea-hydrogen peroxide before extending this work to characterise selected substituted urea adducts.

4.2.1 Binding Constant Analysis of Urea-Hydrogen Peroxide

4.2.1.1 NMR spectroscopy

^{1}H NMR spectroscopy has been widely used to investigate receptor-substrate interactions based on the difference in magnetic environments of the nuclei involved. Many recognition and sensor receptors use a urea moiety as the hydrogen-bond donor as it offers two parallel and adjacent N-H fragments suitable to establish interactions with anions. According to a review on hydrogen

bonding, this interaction can be considered as a “frozen” proton transfer from the receptor to the anion.[205] Therefore, the higher the acidity of the receptor and the more basic the anion, the greater the proton transfer. This leads to a more stable receptor anion complex.[206]

^{1}H NMR titration has been used to measure the interactions of the N-H protons of a substituted urea with anions.[207] Baggi showed the effect of adding increasing amounts of a neutral salt, $[Bu_4N]Cl$ to 1,3-di(pyridine-4-yl)urea.[206] Addition of Cl^- resulted in increased hydrogen bonding to the N-H proton resulting in a pronounced downfield shift (Fig. 4.3). The extent of the downfield shift is diminished after the addition of 1 equivalent of the anion. This displays the point of saturation providing stoichiometry of the complex.

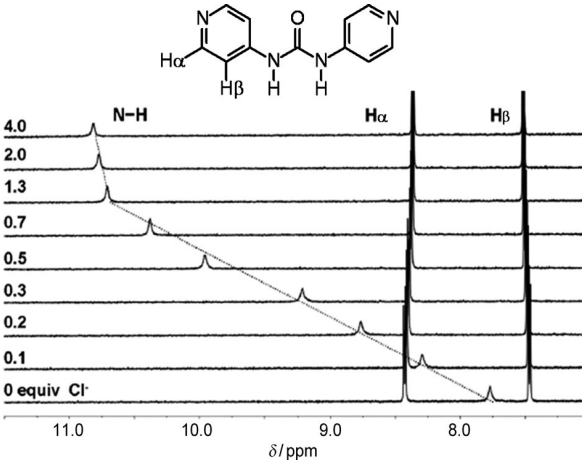

Fig. 4.3. Reproduced from Ref. [206] with permission of WILEY-VCH. Copyright 2011.

As stoichiometry and binding efficiency could be determined from these continuous titration methods, the initial approach in the present study was to use this methodology to analyse the interaction of urea and H_2O_2. The hydrogen peroxide source was a 30% solution in water (higher concentration solutions not being routinely available), so to avoid the use of multiple solvents; these experiments were performed in D_2O. Initial studies by another member of the research team attempted to evaluate the chemical shifts of either the N-H proton or the H_2O_2 proton in order to establish the interaction between donor and acceptor.[50] This was achieved by addition of aliquots of 30% aqueous H_2O_2 to a

1.0 mol kg^{-1} solution of urea in 10% D_2O/90% H_2O.[50] The results were not satisfactory due to the dominating effect of hydrogen-deuterium exchange between H_2O_2, urea, D_2O and H_2O. Introduction of H_2O/H_2O_2 affected the magnetic susceptibility of the medium, causing inconsistencies in the local magnetic field environment. Unfortunately, the alterations to chemical shifts caused by the change in the magnetic field were of a similar scale to the observed changes in chemical shift due to the H_2O_2-urea adduct, and an equilibrium constant could not be unambiguously determined.

As this interaction is fundamental to the system under study, it was crucial to find a way to evaluate binding. NMR is a convenient method that might permit a direct comparison of the binding strengths of the substituted ureas. While the concept of NMR titrations of urea and H_2O_2 seemed reasonable, it could not be realised due to differences in solubility of the substituted ureas in water. As urea in D_2O/H_2O did not produce a satisfactory response, a starting point for this investigation was by changing the solvent or substituting for another simple urea.

The second attempt to study the change in N-H chemical shift as a function of H_2O_2 concentration employed *d_4*-MeOD as solvent; this was selected due to the increased solubility of substituted ureas in methanol. Urea solutions with concentrations of 0.22, 0.47 and 0.96 M were investigated in the absence of H_2O_2, revealing a downfield trend in chemical shift on increasing urea concentration. This is consistent with self-association or dimerisation of urea N-H to the carbonyl functionality on a neighbouring urea. On addition of H_2O_2 (0.1 ml, 30%) to 0.7 ml samples of the 0.22, 0.47 and 0.96 M solutions of urea in *d_4*-MeOD, mole ratios of approximately 1:1, 1:3 and 1:6 of urea to H_2O_2 solutions were formed. Addition of H_2O_2 to the most concentrated urea solution resulted in a small change in the chemical shift of the N-H (0.002 ppm). The more dilute solutions displayed a larger change (Table 4.1). For comparison, a solution of H_2O_2 alone (0.1 ml, 30%) in MeOD, in the absence of urea, gave a peak at 10.729 ppm. Downfield shifts were observed for this H_2O_2 peak at each ratio of urea to peroxide with the greatest change in the 1:1 ratio (10.790 ppm). Interestingly,

when compared to a sample of commercial urea-hydrogen peroxide, which was assumed to have close to a 1:1 ratio, an upfield shift of 0.011 ppm was observed for H_2O_2.

Table 4.1. Chemical shifts of the N-H proton before and after addition of H_2O_2.

Ratio of Urea:H_2O_2	Before NH (ppm)	After NH (ppm)	After H_2O_2 (ppm)
0:1	-	-	10.729
1:1	5.725	5.727	10.790
1:3	5.707	5.715	10.758
1:6	5.695	5.710	10.741
UHP	-	5.717	10.718

These results suggest that both the N-H and H_2O_2 chemical shift values are dependent of the quantity of all possible hydrogen bonding interactions available. As commercial UHP is added as an anhydrous solid, the solution lacks the water provided by the 30% H_2O_2 solution. Consequently this reduces the possible hydrogen bonding interactions that would form between H_2O_2 and water with a resulting upfield move in the H_2O_2 chemical shift. Using this rationale, the additional urea in the 1:1 sample increases the quantity of hydrogen bonding with hydrogen peroxide, assisting the downfield shift in the H_2O_2 peak.

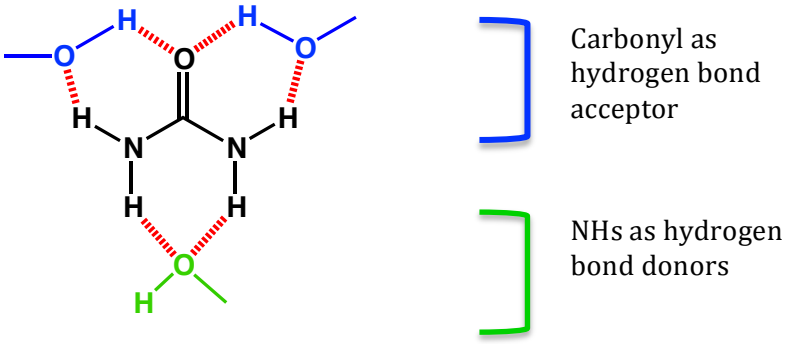

Fig. 4.4. Hydrogen bond donors and acceptors in urea.

As the magnitude of the downfield shift in H_2O_2 does not directly correlate to the downfield shift in the N-H protons of urea, it was proposed that hydrogen peroxide is also hydrogen bonding through the carbonyl oxygen (Fig. 4.4). This is not inconsistent with molecular modelling of urea-hydrogen peroxide where the favoured and lowest energy structure is where H_2O_2 forms an interaction with the C=O and a single N-H proton.[92] Unfortunately, these assumptions of binding configurations are *in vacuo* and have excluded the effects of MeOD and H_2O, which clearly is not accurate as these peaks also show fluctuations in the NMR spectra. Effectively the chemical shift of all species in solution is related to the total molarity whereby the larger the overall concentration, the more hydrogen bonding interactions are possible between all donor and acceptor species.

It appears that the present system is complicated by the presence of multiple hydrogen bond donors and acceptors. The chemical shift of the N-H of urea is not measured in isolation, but with H_2O_2 present. This is both a hydrogen bond acceptor through the oxygen lone pair and a donor through the OH bond. This problem is compounded by both solvents MeOD, H_2O and D_2O all possessing hydrogen bonding properties similar to that for H_2O_2. Anion binding systems measured in this way do not encounter this problem as the anions are usually introduced as a salt dissolved in an aprotic solvent.

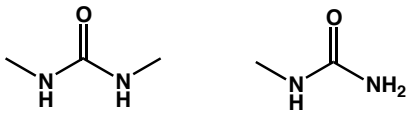

DMU **NMU**

Fig. 4.5. 1,3-Dimethylurea (DMU) and N-methylurea (NMU).

Further target ureas (Fig. 4.5) were investigated in the same manner, with an assumption that the methyl groups may act as a suitable indicator for NMR studies. The energy associated with rotation of the C-N bond is altered by addition of the methyl groups. If the *trans-trans* conformation is favoured in the 1,3-dimethylurea (DMU), as for DPU in Section 2.3.1.1, this would place the N-H protons in a parallel position. It is anticipated that this favours the dipole-

induced interactions through both urea protons (Fig. 4.6(a)) in preference to the disfavoured polarity of (b) (Fig. 4.6). Placing the N-H protons parallel reduces the opportunity for hydrogen peroxide to bond by the carbonyl and N-H proton.

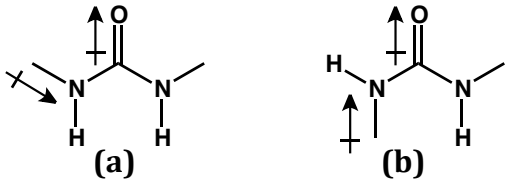

Fig. 4.6. Favoured dipole induced interaction (a) and disfavoured polarity (b).

1,3-Dimethylurea (DMU) was dissolved in 700 µl of D_2O (0.7 M) and a ^1H NMR spectrum was obtained after each subsequent aliquot of a 30% H_2O_2 solution (0 – 350 µl total in 50 µl aliquots) was added. The signal associated with the N-H protons were not discernible due to fast exchange and interestingly this was also found to be the case for the H_2O_2 protons. Consequently, the only changes observed are those for the methyl protons. An upfield shift of the methyl peaks infers progressive shielding of the methyl protons with increase in concentration of H_2O_2. It was proposed that upon hydrogen bonding the N-H bond lengthens with a concomitant increase in the dipole moment. The electrons of the nitrogen can be considered to be more localised on the nitrogen and this build up of electron density shields the adjacent methyl group (Fig. 4.7). However, a control experiment revealed that addition of H_2O alone (in the absence of hydrogen peroxide) shifted the methyl peaks downfield (Fig. A1). This suggests hydrogen bonding of water with the urea carbonyl lengthens the C=O bond thus making the carbon more partially positive (Fig. 4.7 (b)). This attracts the lone pair on the nitrogen therefore deshielding the adjacent methyl protons.

A further curious observation is that a second methyl peak is seen as a shoulder in both the DMU and N-methylurea (NMU) spectrum after *ca.* one equivalent of H_2O_2 has been added (Fig. A2). This is thought to be the different conformations of the ureas arising from the rotation of the C-N bond causing the methyl groups to exist in different environments.

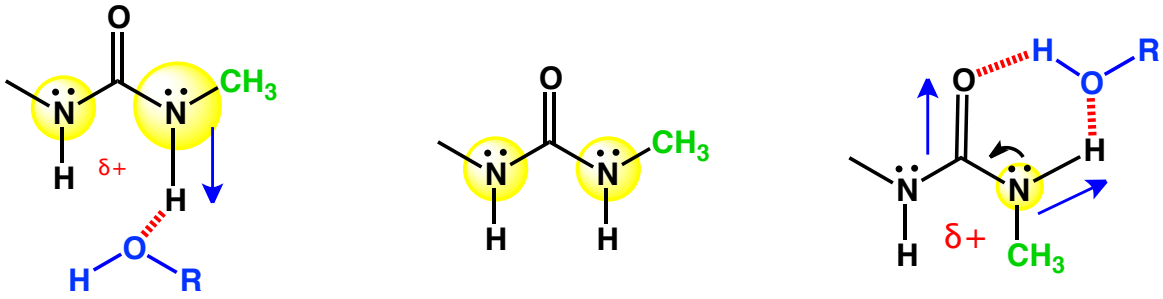

Fig. 4.7. (a) Hydrogen bonding showing lengthening of the NH bond, shielding the methyl protons (green) (b) Hydrogen bonding showing lengthening of the C=O and NH bonds, deshielding the methyl protons (green). Yellow spheres indicates an animation of the relative electron density of the nitrogen.

Furthermore, when the sample is heated to 50 °C in the absence of hydrogen peroxide, there is a significant downfield shift (~0.2 ppm) in the methyl peak. It is possible that that raising the temperature causes a change in conformation to the unfavoured *cis-trans* isomers or the *cis-cis* isomer of DMU.

In order to have an internal reference unaffected by hydrogen bonding and changes in sample concentration, a standard was used as a peak reference. Trimethylsilyl propanoic acid (tsp-d_4) is a water soluble reference commonly used as an internal standard for NMR.[208] Standards can also be affected by magnetic susceptibility of the medium caused by differences in solvent and solute composition. To minimise these effects tsp-d_4 was dissolved in D_2O and placed inside an inner capillary tube of a co-axial insert (capillary) as a reference at 0.00 ppm (Fig. 4.8).

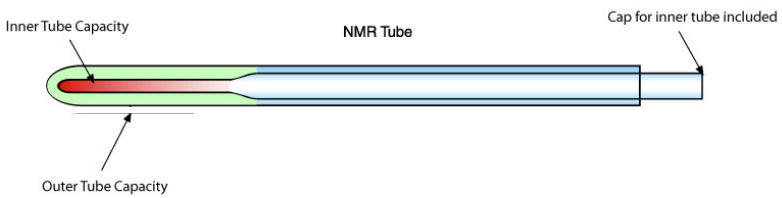

Fig. 4.8. Reproduced from www.wilmad-labglass.com/Products/WGS-5BL/.[209]

The addition of a capillary tube restricts the volume of sample that can be used and prevents simple cumulative addition of H_2O_2; the outer NMR tube simply cannot contain sufficient solvent. The capacity of the outer tube allows a maximum of 550 µl. Alternatively, multiple tubes with different mole ratios of DMU, H_2O_2 and H_2O were used (Table 4.2). The aim was to show if the presence of H_2O_2 and/or water displayed the same effect at high and low urea concentration. To accurately compare samples, controls were needed for each set of urea concentrations to measure the effect that hydrogen peroxide and/or water had on the urea NMR responses. The mole ratio given in Table 4.2 for H_2O does not include the solvent (D_2O) as we are just looking at changes from the original solution.

Table 4.2. Solutions with varying concentrations of DMU, H_2O_2 and H_2O for NMR.

Solution Number	[DMU] ($molL^{-1}$)	[H_2O_2] ($molL^{-1}$)	DMU:H_2O_2 ratio	[H_2O] ($molL^{-1}$)
1	0.9	0	1:0	0
2	0.9	0	1:0	0.9
3	0.9	0.2	1:0.22	0.8
4	5.7	0	1:0	0
5	4.6	0	1:0	10.1
6	4.6	1.8	1:0.35	8.0

Simply increasing the concentration of urea in the D_2O solution causes a dramatic shift in both the peak for H_2O (Fig. 4.9A) and the methyl groups of the urea (Fig. 4.9B). It is believed that the sharp peak at 4.78 ppm is the H_2O of the standard in the capillary tube. This peak barely shifts throughout these experiments and can be used as a secondary reference point (Fig. 4.9A).

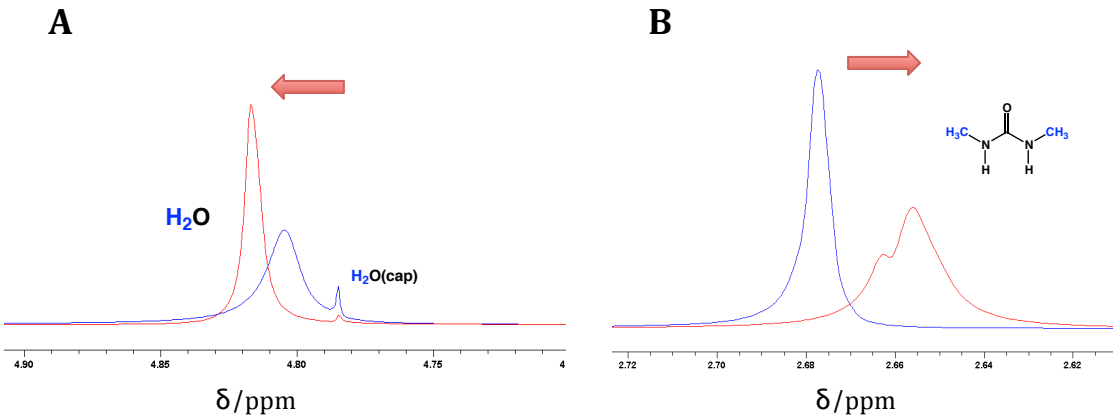

Fig. 4.9. NMR spectrum of solutions **1** (0.9 M blue) and **4** (5.7 M red).

Figure 4.9A shows that as the concentration of urea is increased so the shift for water moves to a lower field while Fig. 4.9B shows that the methyl group becomes more shielded. It is assumed that this is the consequence of additional hydrogen bonding of water with urea. Also self-association is more pronounced in the more concentrated solutions suggesting dimerisation lengthens the N-H bond increasing the polarity of the N-H bond and causing an increased shielding of the adjacent methyl group. Development of a shoulder on the methyl peak in the 5.7 M solution (Fig. 4.9B) is possibly due to changes in conformation of DPU that bring about two different peaks. Also at this concentration, a small peak at 5.87 ppm is likely to be the N-H protons involved in dimerisation of DMU, slowing down the rate of exchange and becoming discernible. As this is present in the hydrogen peroxide-free sample it is unable to be the 'frozen proton' scenario with an anion as discussed previously.

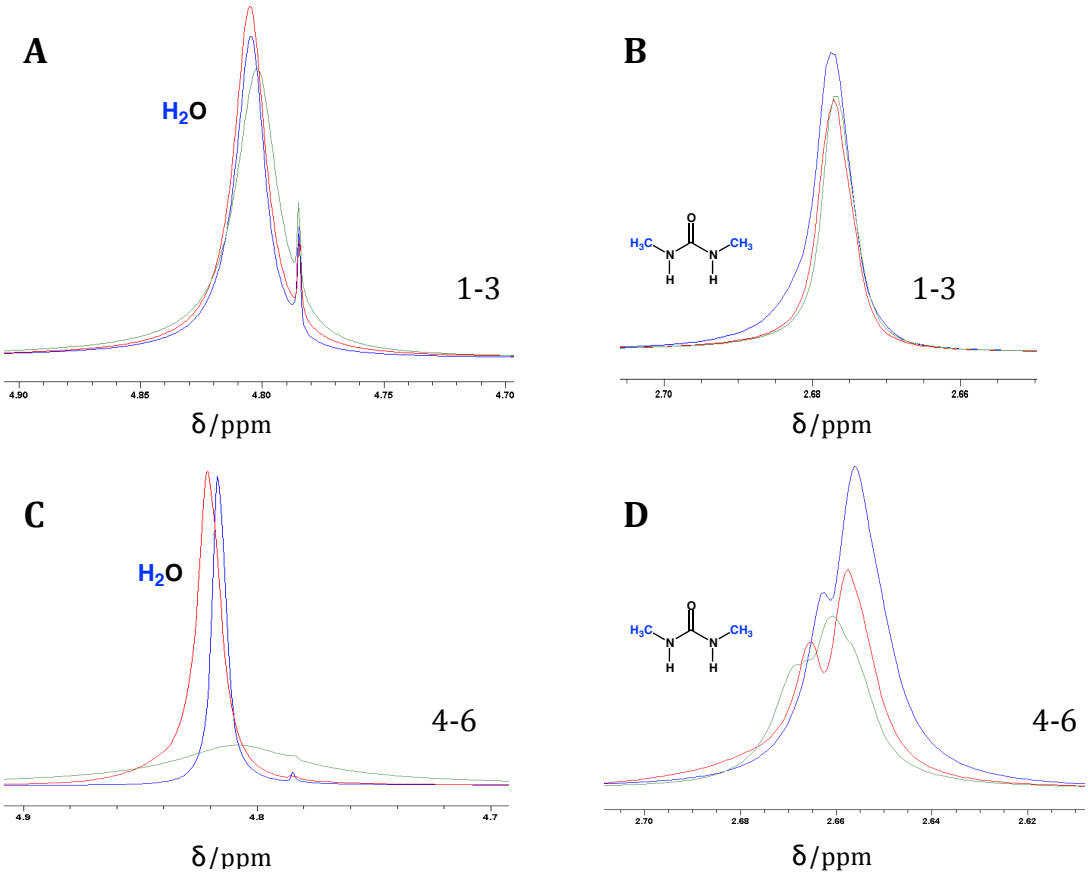

Fig. 4.10. A and B: Low concentration of DMU (0.9 mol L^{-1}), C and D: High concentration of DMU (4.6-5.7 mol L^{-1}). — Original solution — presence of water — presence of hydrogen peroxide corresponding to solutions in Table 4.2.

Furthermore, the two concentrations of DMU show different responses to the presence of aqueous H_2O_2. At the lower concentration (Fig. 4.10, 1-3 A and B) there is minimal change in chemical shift of the water or methyl peaks. In contrast, at the higher concentration of DMU, addition of H_2O_2 causes the water peak to broaden and the methyl peak to retain the shoulder and move downfield (Fig 4.10 4-6 C and D). The water peak broadens due to the hydrogen bond exchange occurring particularly with H_2O_2. This is more than just a concentration effect, as the [DMU] in solutions **5** and **6** is slightly less than that for solution **4**, although the difference between them is evident in the presence and absence of H_2O_2.

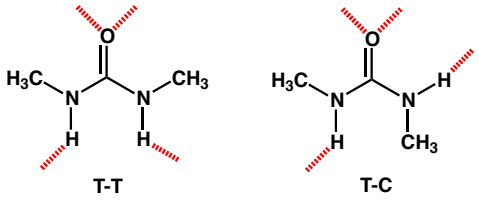

Fig. 4.11. *Trans-trans* and *trans-cis* formation of DMU.

Lecomte has shown that DMU can exist in two energetically similar conformations and that both of these contribute to anion binding.[210] In the present study, if a hydrogen bond acceptor interacts with the N-H of the *trans-trans* (Fig. 4.11) conformation, then it acts similarly to an anion receptor system lengthening the bond. If DMU exists in a *trans-cis* (Fig. 4.11) conformation then the carbonyl oxygen becomes the principal hydrogen bond acceptor, which upon coordination will cause deshielding of adjacent groups. It seems that under these conditions the change in chemical shift, specifically of the methyl protons, is not from a single conformation or binding orientation of the hydrogen bond donors and acceptors. A combination of effects, each with an associated influence on electron density in the urea and H_2O_2 molecule, are likely to be causing this variation.

A challenge with the present system arises from the dilute nature of hydrogen peroxide solutions and the need to avoid high concentrations due to stability and safety issues. Standard hydrogen peroxide is an approximately 30% solution in H_2O (9.76 M). Unlike other anion binding systems where 20-100 equivalents of anion to substrate ratios can be readily be studied, the present system is restricted by the requirement for hydrogen peroxide to be added in an aqueous solution. In addition, only 0.5 ml of solution is required in the NMR tube. By taking into account a minimal D_2O content of 10% is to be maintained for signal locking, this restricts the potential molarity of hydrogen peroxide obtainable.

While a relatively straightforward NMR titration was anticipated this was clearly shown not to be the case. Unfortunately, as this appears to be a dynamic situation, it has not been possible to distinguish between the conformations, binding interactions, dilution effects and chemical exchange in each sample.

Since this DMU/D_2O system was not going to be exploited directly in the New Cathode, further work was not pursued.

4.2.1.2 Isothermal Titration Calorimetry

In order to establish an association constant for UHP, alternative methods were applied. Isothermal titration calorimetry (ITC) measures the heat change that occurs when two molecules interact. This enables quantitative thermodynamic information from a single experiment. The methodology gives good results for protein-protein interactions,[211] macromolecular complex formation,[212] interactions of drugs with target biomolecule[213] and DNA with nanoparticles.[214] Simplistically, ITC involves the gradual addition of a ligand to the suspected host. The process of binding is either exo- or endothermic and the resulting change in temperature is measured by recording the energy output required to maintain a constant temperature with respect to a reference solution.[215] As the receptor becomes saturated, the power required to maintain the reference temperature tends to zero from which a binding isotherm (Fig. 4.12) can derive the binding enthalpy ΔH and equilibrium binding affinity K_a to give:

$$\Delta G^o = -RT \ln K_a \qquad 4.6$$

Where R is the gas constant (8.314 J K^{-1} mol^{-1}) and T is the temperature in Kelvin. From these parameters it is possible to determine Gibbs energy of binding, ΔG^o and an entropic contribution ($-T\Delta S$) drawn from Eqs. (4.6) and (4.7):

$$\Delta G^o = \Delta H^o - T\Delta S^o \qquad 4.7$$

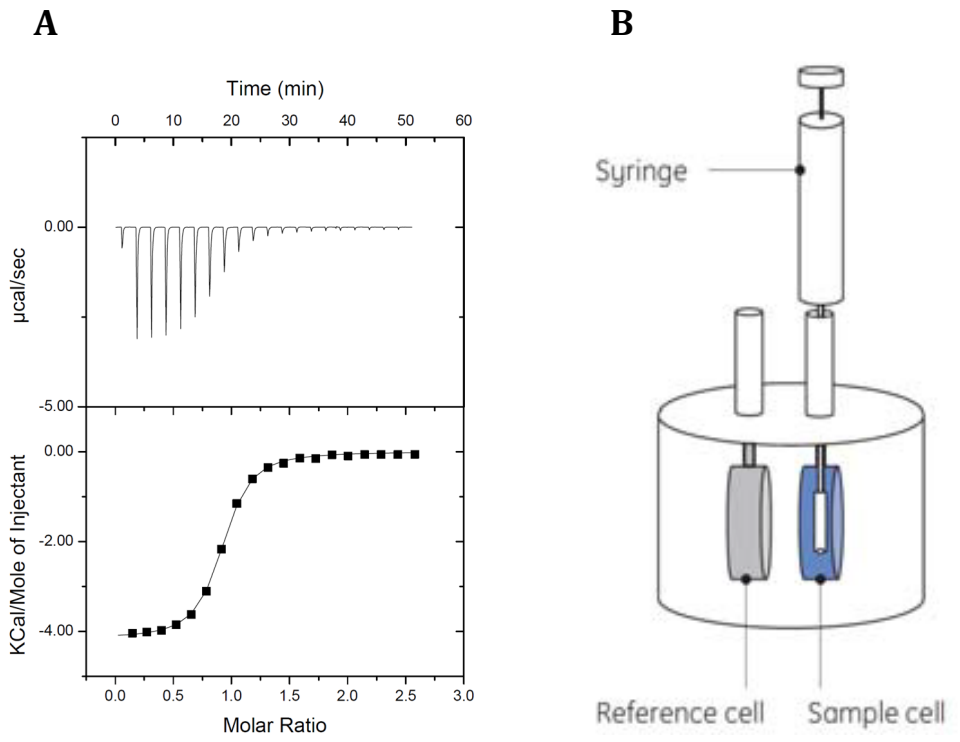

Fig. 4.12. A) Example of an ITC titration of EDTA (0.4 mM) with a $CaCl_2$ solution (5 mM) taken from reference[216]. B) Schematic representation of the components of an ITC system.

In an attempt to quantify the interaction between urea and hydrogen peroxide, ITC was performed in an aqueous system with the aim to use this methodology for binding assessment of the substituted ureas. An initial assessment was performed with the standard test kit of EDTA and $CaCl_2$ to ensure the instrument was functioning (Fig. 4.12). Following a simple washing procedure the sample cell was filled with approximately 250 µl of 0.5 mM solution of urea in purified water, and the reference cell with water. The removal of trapped bubbles, although difficult, is essential as this affects the thermodynamic parameters in the system.

As hydrogen peroxide is known to start disproportionating in the time necessary for stabilisation of the ITC cell (1-60mins), solutions were not prepared until immediately before being injected into the cell. Urea was used in the sample cell as its stability in solution allows the stabilisation of the differential power (DP) signal in the set up of the experiment. The initial experiment involved the gradual addition of a 50 mM solution of H_2O_2 to aqueous urea (0.5 mM). H_2O_2 was added in 18 portions and the energy to maintain a temperature of 25 °C recorded.

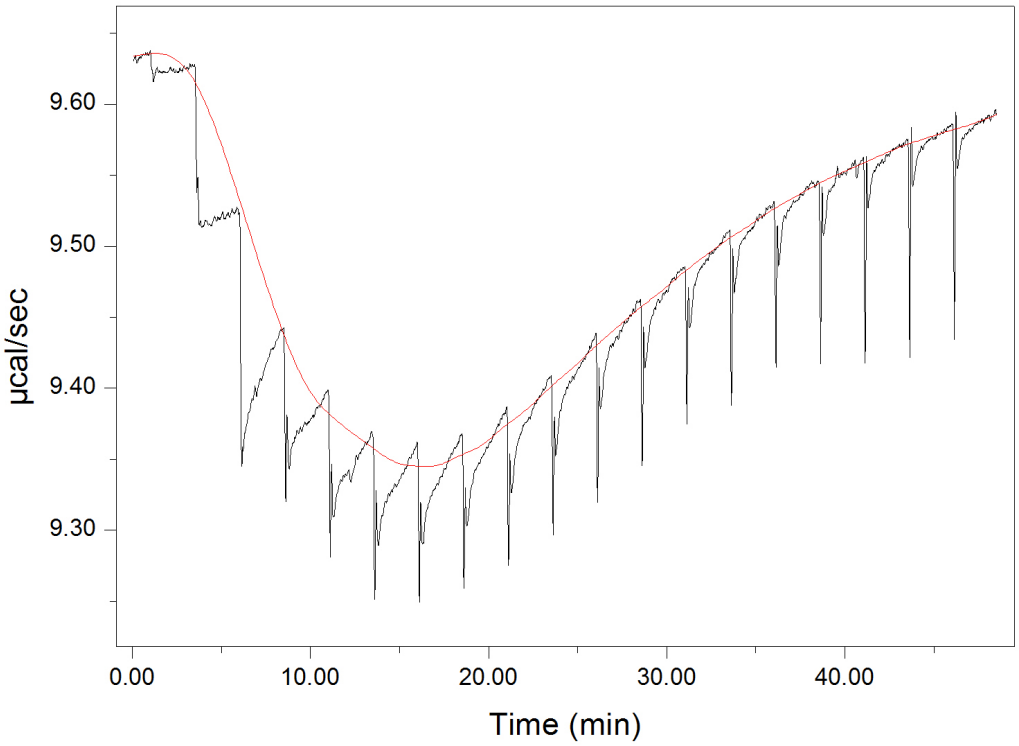

Fig. 4.13. ITC of the addition of 500 mM H_2O_2 to a 20 mM solution of urea.

The results showed some small exothermic peaks although several large spikes in power were observed likely due to air or O_2 bubbles. The very small peaks are a consequence of heat changes involved with dilution of the solution and have no correlation to the interaction of urea with peroxide. Similar peaks were observed in the absence of H_2O_2 when portions of water were added to the urea solution. It was thought that the solution may have been too dilute to show binding of urea with H_2O_2. However, increasing the concentration (20 mM urea

and 500 mM H_2O_2) and thoroughly degassing the solution still did not produce satisfactory results (Fig. 4.13). A combination of broad inconsistently sized peaks, a skewed baseline and variable power fluctuations produced results that could not be interpreted in terms of an equilibrium constant. Many ITC methods are quoted for the introduction of a guest molecule into a protein. This involves several non-covalent interactions such as ionic forces, hydrogen bonding and van der Waals interaction all with their associated energy values. The difference between proteins and the present system is the quantity of interactions in the formation of a host-guest complex or 'adduct'. The urea-hydrogen peroxide system has markedly fewer potential interactions and therefore the heat change, if any, is too small to be measurable under these ITC conditions. Furthermore, the potential need to heat mixtures of H_2O_2 and urea to 60 °C before adduct formation occurs may be problematical.

4.2.1.3 Thermogravimetric Analysis

Thermogravimetric analysis (TGA) is a form of thermal analysis that examines mass change as a function of temperature. Thermal events that afford change include desorption, absorption, sublimation, vaporisation, oxidation, reduction and decomposition.[217] Kinetic studies are also viable from this analytical method with the rate of mass loss associated with the rate of reaction. Thermogravimetric curves characterise thermal stability and physicochemical processes occurring in the sample.

An opposite approach was taken to the previous analytical techniques, as TGA analyses the decomposition of urea-hydrogen peroxide rather than its formation as in the NMR and ITC studies. There are many examples on the use of TGA for organic compounds, but very few on organic adducts, let alone peroxide adducts. Adams reported the analysis of hydrogen peroxide adducts of simple guanidinium salts by TGA.[218] Adducts were formed by slow recrystallization with H_2O_2 (30 or 50%) and showed a loss of mass below 140 °C corresponding to the total water and hydrogen peroxide content. In some instances this was achieved in two distinct stages, the first was gradual loss corresponding to H_2O (endothermic) followed by a second much sharper weight loss corresponding to

the exothermic loss of H_2O_2. Intriguingly, they accounted this weight loss to the formation of H_2O_2 vapour (Eq. 4.8). This evidence was achieved by a colorimetric test of the vapour with filter paper that was impregnated with titanium(IV), and showed a colour change in the presence of O_2^{2-}. It revealed the process involved was the evolution of H_2O_2 rather than instantaneous decomposition.

$$\text{salt} \cdot H_2O_2(s) \rightleftharpoons \text{salt}(s) + H_2O_2(g) \qquad 4.8$$

A 10 mg sample of commercially available urea-hydrogen peroxide was gradually heated (5 °C/min) under an inert atmosphere (N_2). At 50 °C the sample began to lose mass. A 47.5% decrease in mass was seen by 60 °C, which is greater than the total expected loss of H_2O_2 in pure urea-hydrogen peroxide at 36% (Fig. 4.14). This indicates that adsorbed water may also be present. However, the loss of water and H_2O_2 occur below the expected boiling point for the pure compounds at 100 and 150 °C respectively. It is unlikely the boiling point of H_2O has lowered to 50 °C, therefore decomposition of the hydrogen peroxide is more feasible. Decomposition of H_2O_2 is an exothermic process that liberates H_2O, O_2 and heat. The heat produced accelerates the decomposition process and is likely to start a thermal runaway or positive feedback loop. Additional thermal energy added to the system by H_2O_2 decomposition may assist in the vaporisation of water thus causing the loss of mass at 60 °C.

Sharp spikes in mass loss are of some concern as a popping sound could also be heard during the experiment consistent with a rapid expansion of gas. As vaporised hydrogen peroxide is highly dangerous and hazardous for the operator and equipment, it was decided to discontinue this method.

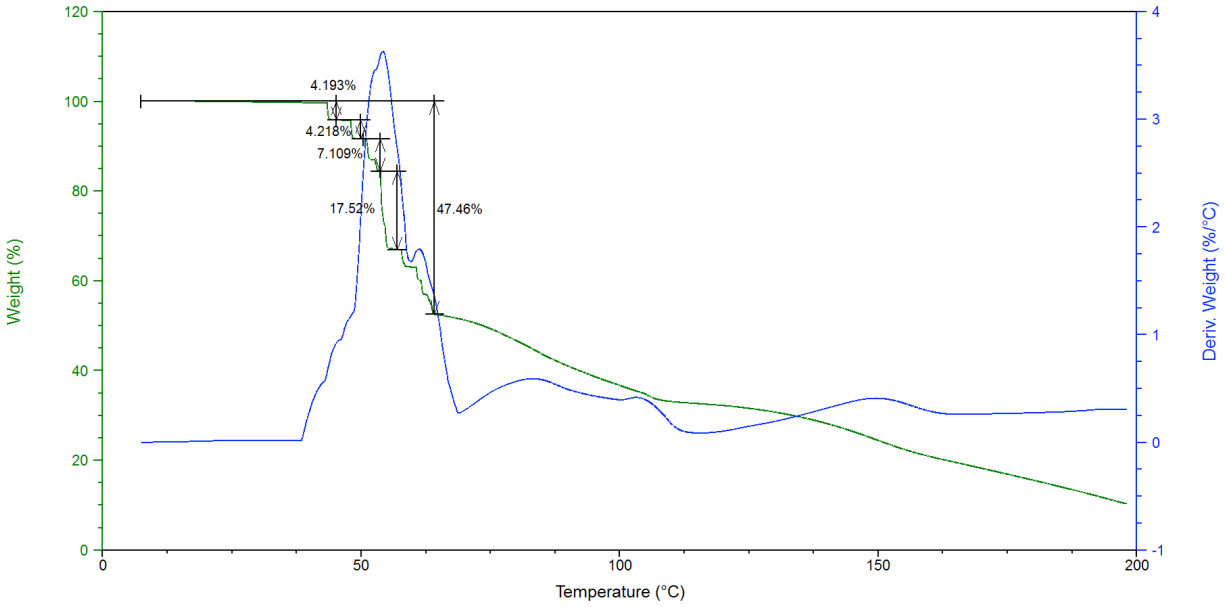

Fig. 4.14. TGA of UHP. Green line: percentage weight loss. Blue line: rate of loss.

4.2.2 Hydrogen peroxide identification in UHP

Determining a binding constant for the association of urea and hydrogen peroxide has proven difficult. Therefore, it was decided that investigation into the use of spectroscopic methods could be used to differentiate the adduct from its individual components.

A distinct difference between urea and the urea-hydrogen peroxide adduct could be seen by IR spectroscopy. The IR spectrum of urea is well established and in agreement with that determined in this study (Figure 4.15).[219-221] Table 4.3 lists the main peaks associated with urea and UHP.

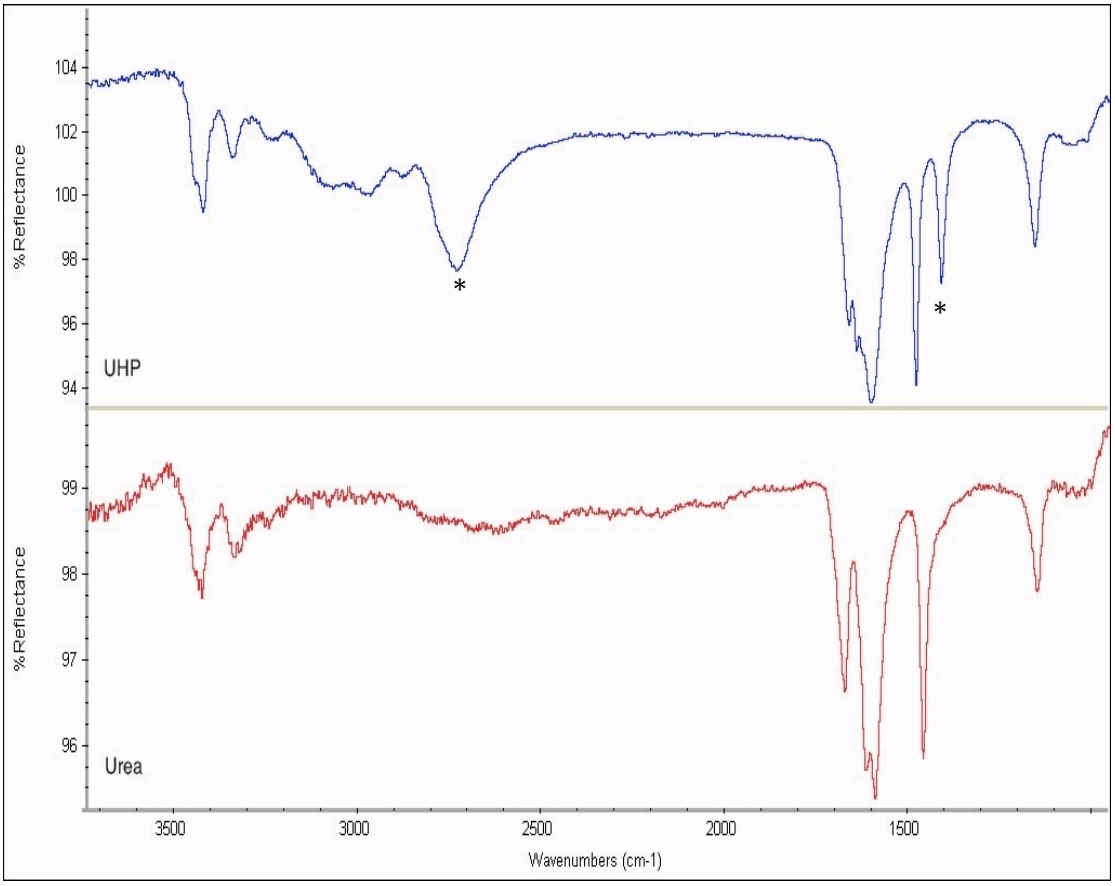

Fig. 4.15. ATR of urea (red; bottom) and urea-hydrogen peroxide (blue; top). (* are additional stretches in UHP)

Table 4.3. IR frequencies of Urea and UHP.

	Experimental Data (cm^{-1})	Literature Data (cm^{-1})	Assignment
Urea	3432	3440	(m) NH out-of-phase stretching
	3344	3320	(w) NH in-phase stretching
	1677	1685	(s) C=O stretch
	1620	1620	(s) NH bending
	1595	1608	(s) NH bending
	1464	1470	(s) C-N stretching
	1153	1155	(m) NH_2 rocking
UHP	2731		(m) O-H stretch (H-bonded)
	1413		(s) O-H symmetric bend
	900		(w) O-O stretch

The major difference between urea and urea-hydrogen peroxide is the addition of a large broad peak at 2731 cm^{-1}. It is proposed here that this is a consequence of strong hydrogen bonding between the hydrogen peroxide and the urea. This accounts for the decrease in energy of the vibrational state from the standard O-H stretch between 3400 - 3200 cm^{-1}. Earlier infrared studies on both liquid and vapour phase H_2O_2 suggest a different interpretation of the results. This peak was previously assigned as a combination of three fundamental modes.[222] In contrast to this strong evidence from the 1950s, an accompanying molecular modelling study to this work used density functional theory calculations on hydrogen peroxide interacting with different orientations of urea. This suggested than an O-H frequency was observed at 2826 cm^{-1} for the hydrogen bonding between the urea carbonyl and H_2O_2 (Fig. 4.16, as in structure 5 in Section 2.3.2.1). A new strong peak was visible at 1413 cm^{-1} and is believed to be an O-H bend. One final difference is the appearance of an O-O stretch at 900 cm^{-1} showing evidence of a peroxide bond.[195] Regardless of the correct interpretation of the band at 2800 cm^{-1}, these peaks only arise if hydrogen peroxide is present so it is characteristic of adduct formation of some description.

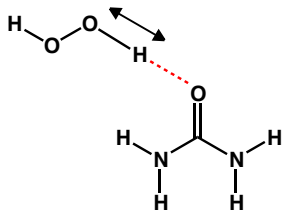

Fig. 4.16. Hydrogen bonding of H_2O_2 with the carbonyl of urea extending the O-H bond.

4.2.2.1 Quantitative titrations and UV-Vis Spectroscopy

Infrared spectroscopy gave qualitative data; it informs that H_2O_2 was present but does not reveal the quantity of H_2O_2 in the adduct or the strength of the binding between urea and hydrogen peroxide. To answer the first question attention was turned to redox titrations, which have been used for many decades as reliable methods for quantification of H_2O_2 and peroxy-containing compounds.

Iodometric titration is the generic redox titration method used to determine the amount of H_2O_2 in a solution.[223] In this process H_2O_2 is reacted with a source of acidic iodide to liberate iodine (Eq. 4.9). To ensure accuracy, a standardised sodium thiosulfate solution ($Na_2S_2O_3.5H_2O$) was used to titrate against the iodine to give a precise hydrogen peroxide concentration.

$$H_2O_2 + 2H^+ + 2I^- \rightleftharpoons I_2 + 2H_2O \qquad 4.9$$

As this reaction is relatively slow, two important sources of error must be taken into account. First, there is a small contribution from the loss of volatile iodine; therefore titrations were performed in a stoppered conical flask. Another error associated with iodometry is the oxidation of iodide by oxygen from the air (Eq. 4.10). As this is accelerated in acidic solutions, a small amount of sodium hydrogen carbonate was added to the flask displacing the air, before the iodide was added. Sodium hydrogen carbonate and acid generates CO_2, which is heavier than air, and pushes the oxygen-containing air out of the flask.

$$O_2 + 4H^+ + 4I^- \rightleftharpoons 2I_2 + 2H_2O \qquad 4.10$$

Although iodometry is a slow reaction and the method requires extra steps in order to obtain reliable results, it has advantages over other methods such as potassium permanganate titrations. These advantages include resistance to the contamination of stabilisers used in hydrogen peroxide solutions, such as boric and salicylic acid.[224]

Titration with potassium permanganate is an alternative method for the determination of hydrogen peroxide. A solution of potassium permanganate is standardised with sodium oxalate before being titrated with an acidic solution of aqueous hydrogen peroxide (Eq. 4.11).

$$2MnO_4^- + 5H_2O_2 + 6H^+ \rightleftharpoons 5O_2 + 2Mn^{2+} + 8H_2O \qquad 4.11$$

The reaction is quick and shows an immediate discolouration of the permanganate; furthermore it remains pink giving a distinct change from colourless when the end point is reached. However, a slow addition is necessary to reduce the possibility of producing a secondary reduction product MnO_2, which is an active catalyst for the decomposition of peroxide.[224] Throughout this research permanganometry was used not only to accurately measure the concentration of aqueous peroxide, but to measure the peroxide content in urea adducts in organic and aqueous solvents. All glassware was acid and base washed with HNO_3 and KOH in isopropanol to ensure any residual peroxide and heavy metals were removed.

Quantitative analysis of urea-hydrogen peroxide is feasible as the complex dissociates into its individual components in solution. Although urea-hydrogen peroxide is readily soluble in water, initial results showed large inconsistences when determining the hydrogen peroxide content. It was determined that the presence of urea was the cause of the problems. Permanganate can oxidise urea and this gives variable results.[225] The simplest method to separate urea and peroxide was to change the solvent to THF as urea is insoluble in this solvent and is easily removed by filtration. Separation was carried out by either filtration through fluted filter paper or centrifugation. A 1.5 ml sample was centrifuged at 15,000 rpm for 30 seconds. This leaves a THF:H_2O_2 solution where a 1 ml aliquot is titrated against standardised $KMnO_4$ to establish the hydrogen peroxide content. In a similar manner, the same mole percentage of urea was suspended in THF and the filtrate was titrated against $KMnO_4$ as a control. A second control considered was THF, as peroxides are a common, but hopefully low level, contaminant in ethereal solvents.

The average peroxide concentration was 1.028 M in the hydrogen peroxide:THF solution after accounting for peroxide impurities, although this does tend to vary slightly with each new solution. Assuming urea-hydrogen peroxide is a 1:1 complex, an average of 84% of the peroxide is released from the adduct into solution. The residue from the filtration was dried and a known mass was subject to colorimetric analysis with $KMnO_4$ (with H_2SO_4 and H_2O) in an effort to

account for the remaining hydrogen peroxide. The results varied between 10 - 15% giving overall peroxide values that surpassed the maximum amount of moles possible for a 1:1 complex. Regardless of the accuracy of the method, it shows that some H_2O_2 remains complexed to urea. For comparison, the same THF:H_2O_2 solution (from UHP) was analysed by iodometry to give a similar concentration (1.019 M) of peroxide to those determined by the permanganate titrations.

However, titrations are inconvenient, they are time consuming especially when standardisation is required before each run. A faster, more expedient method to measure hydrogen peroxide concentrations was required. To this end a spectroscopic method involving the determination of aqueous and organic peroxides with a titanium salt was investigated. This offers a potential fast and accurate method for determining the hydrogen peroxide concentrations to as low as 1 ppm. Adapting the method from Pobiner,[226] hydrogen peroxide is reacted with a titanium salt in H_2SO_4 to produce a titanium-peroxysulfate complex (Eq. 4.12/4.13). This yellow complex can be measured spectrophotometrically at 400 nm to give quantitative concentrations of hydrogen peroxide.

$$H_2O_2 \longrightarrow 2H^+ + O_2^{2-} \qquad 4.12$$

$$O_2^{2-} + Ti^{4+} + 2H_2SO_4 \longrightarrow [TiO_2(SO_4)_2]^{2-} + 4H^+ \qquad 4.13$$

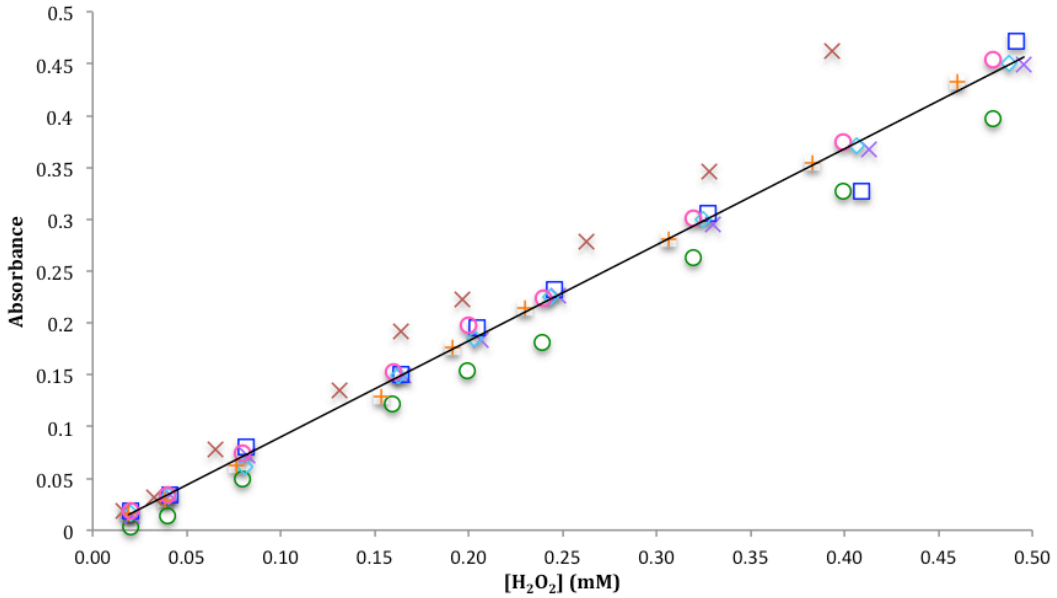

Fig. 4.17. Multiple series of absorbance maxima of known hydrogen peroxide concentrations at 400 nm. (Solid line = average).

Using permanganometry, a stock solution of known peroxide concentration was prepared. From this a series of dilute standards of concentration 0.02 – 0.5 mM was prepared. These were reacted with 5 ml of pre-prepared Ti^{4+} solution plus additional H_2SO_4 to ensure acidic disproportionation of H_2O_2, and the absorbance recorded at 400 nm. This gave a standard curve that could be used to determine the peroxide concentration spectroscopically (Fig. 4.17). To confirm the accuracy of this method, it was repeated multiple times and the average linear curve calculated. This was used for all further peroxide concentration determinations where A is the absorbance and x is the diluted concentration in mol L^{-1} (Eq 4.14).

$$A = 927.2 \pm 9.8\,x - 0.0027 \qquad 4.14$$

The concentration of H_2O_2 in our THF solution prepared from UHP was determined and compared to the initial titrations. Initially a sample of THF:H_2O_2 solution was reacted with Ti^{4+}. Following a procedure from Wolfe, the complex was extracted from the organic phase into the aqueous phase, until the organic layer was no longer yellow.[227] Unfortunately, this approach suffered from

emulsion formation and inconsistent absorbances. The more convenient method to obtain accurate results from the organic solution was to dilute 1 ml of the THF:H_2O_2 solution into water to give a 50-fold dilution. This dilutes the THF sufficiently such that it does not cause additional inconsistencies. Following dilution, the same preparation was used as the standard solution to form the yellow titanyl complex. A similar procedure was used to test THF as the control. Using the standard curve, an average of 1.021 M H_2O_2 was observed in the solution showing consistency through each method. However, without further refinement of the method this leads to a semi-quantitative technique at this point.

Table 4.4. Hydrogen peroxide concentration determination by various methods of a THF:H_2O_2 solution made from UHP.

	$KMnO_4$	Iodometry	Titanium
THF:H_2O_2	1.028 M	1.019 M	1.021 M

These three independent methods demonstrate confidence in the ability to test the accurate concentration of hydrogen peroxide in both aqueous and THF solutions.

4.2.2.2 Oxidation of Triphenylphosphine with UHP

It was of interest to determine how readily hydrogen peroxide dissociates from UHP and thus how much was "free" to react. A reaction oxidising triphenylphosphine (PPh_3) to triphenylphosphine oxide ($Ph_3P{=}O$) is known to occur with H_2O_2 as the oxidant.[228] This reaction is known to have a high conversion rate (>90%) therefore would be suitable for analytical analysis using urea-hydrogen peroxide as the source of H_2O_2 (Scheme 4.3). As PPh_3 can also be oxidised by atmospheric oxygen, it must be performed under inert conditions.

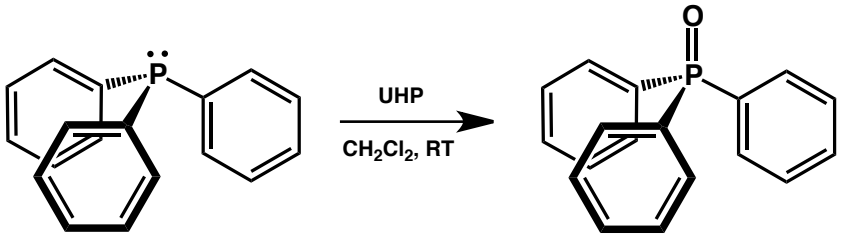

Scheme 4.3. Oxidation of triphenylphosphine with urea hydrogen peroxide.

The reaction was monitored by TLC or ^{1}H NMR in C_6D_6. Deuterated benzene is required to insure resolution of the peaks from starting material and product. Quantitative analysis of the integrals in ^{1}H NMR requires additional parameters such as uniform pulse excitation and broad band decoupling to assure the signal intensity is directly proportional to the number of nuclei responsible.[229] In an attempt to simplify analysis ^{31}P NMR was performed as it clearly differentiates between the product and reactant.

^{31}P NMR is less sensitive than ^{1}H NMR but more sensitive than ^{13}C due to the natural abundance of ^{31}P being 100%. ^{31}P NMR, like ^{1}H and ^{13}C, has spin-spin coupling with adjacent heteroatoms that cause the signal to split and the sensitivity to decrease. To simplify the spectrum, the adjacent nuclei may be decoupled to annul the spin coupling by applying a radiofrequency (RF) pulse greater than that of the Larmor frequency for the neighbouring nucleus. This increases the signal intensity and changes the integration. Another cause of increase in signal intensity is the nuclear Overhauser effect (nOe).[230] When a nucleus has been magnetically excited and its neighbour is at equilibrium, relaxation occurs between both nuclei. This changes the intensity of the nucleus that was at equilibrium. The smaller the physical distance between the two nuclei the greater the change this effect will have. Therefore, integration of a standard decoupled ^{31}P NMR spectrum is inaccurate due to the uneven enhancement of the signals. In order to obtain a quantitative spectrum inverse gated decoupling was used. A low power decoupling is applied during the acquisition of the FID (free induction decay) and turned off for the remaining cycle. This reduces the enhancement of the signal by nOe and with a long longitudinal relaxation time (T_1) can produce a quantitative ^{31}P integral.

In ^{31}P NMR the peaks for the phosphine and phosphine oxide are widely separated unlike in the ^{1}H NMR where the substrate and product signals overlap. This means correcting for differences in relaxation times is more readily achieved. Following an RF pulse, the nuclear spins do not return instantly to equilibrium; they relax according to a time constant T_1, where R is the rate of relaxation.

$$T_1 = 1/R \qquad 4.15$$

T_1 is dependent on the nuclear environment, temperature and solvent composition. Not allowing sufficient time for relaxation between pulse sequences will cause varied attenuation of signals leading in inaccurate integration. To correct for this a 90° pulse width is used to excite the spins whereby the total time between pulses is 4-5 x T_1 in order to have complete relaxation.[230] $Ph_3P{=}O$ relaxes more quickly than PPh_3 due to a difference in dipoles where dipole-dipole coupling assists relaxation of neighbouring nuclei. Therefore it is necessary to adjust for the extra time required for relaxation in the PPh_3. Using an inversion recovery pulse sequence, the magnetisation is inverted on the z-axis such that a second pulse gives a signal intensity proportional to the relaxation along the axis; positive for long and negative for short evolution times. The value of τ (tau) is directly related to T_1 through

$$T_1 = \tau_{null} / \ln 2 \qquad 4.16$$

In single scan experiments, τ is adjusted until a null intensity is found. For PPh_3, which requires the longest relaxation time, τ_{null} was 10 seconds. This gave T_1 as 14.4 seconds which is the time required for complete relaxation to allow for accurate signal intensity thus integration. Once the pulse sequence had been calibrated and proton decoupling enabled, the spectrum took only 4 scans to gain a sufficient signal. A $Ph_3P{=}O$ peak at 25.56 ppm integrated 4.5 times that of PPh_3 at -5.56 ppm (after normalisation). Taking into account the original number of moles of urea-hydrogen peroxide (0.156 mmol) and PPh_3 (0.193 mmol) used in the reaction, a total of 0.157 mmol $Ph_3P{=}O$ is formed. This gives a

100% conversion of PPh_3 to $Ph_3P=O$ within error, assuming UHP is a 1:1 ratio of urea to peroxide. Previously, a dissociation of only 84% of UHP into solution was observed. Therefore this reaction pushes the equilibrium to favour the dissociation by removing the H_2O_2 through oxidation of PPh_3. This methodology shows possible quantitative analysis of UHP that are assumed to be transferable to other H_2O_2 adducts.

$Ph_3P=O$, as described in Section 4.1.2 is able to form an adduct with H_2O_2. Although this was not taken this into consideration in the calculations, it has not been disregarded as an option in this reaction. It has been assumed that the dissociated H_2O_2 is more likely to act as an oxidant than to form aggregates with $Ph_3P=O$.

4.2.3 Determination of hydrogen peroxide content of substituted urea adducts

As methodologies had been established to measure the amount of peroxide in urea hydrogen peroxide adduct, these were then used to determine the H_2O_2 content of the substituted urea adducts.

The initial attempt to form a hydrogen peroxide adduct of urea **1** used a mixture of methanol and aqueous hydrogen peroxide (Scheme 4.4). The low solubility of **1** meant a large quantity of solvent was required, but this reduces the possibility of the adduct forming a precipitate. This makes the assumption that the adduct is a solid like urea-hydrogen peroxide. Therefore the solvent was removed under reduced pressure. Unfortunately this simply resulted in the urea precipitating and there was no evidence for the formation of an adduct. Changing the solvent to toluene permitted a more concentrated solution to be prepared. **1** (Phenylbutylurea, PBU) was stirred in dry toluene and cooled to 5 °C. Aqueous H_2O_2 (30%) was added slowly and the mixture was stirred at room temperature overnight before the solvent was removed under reduced pressure. To ensure the adduct was dry, the sample was placed in a pressurised glass oven at 110 °C for 30 minutes. This removed residual toluene, water and hopefully unbound hydrogen peroxide, without disturbing the bound hydrogen peroxide. A sample

of urea-hydrogen peroxide was also subjected to these same conditions and showed little decomposition.

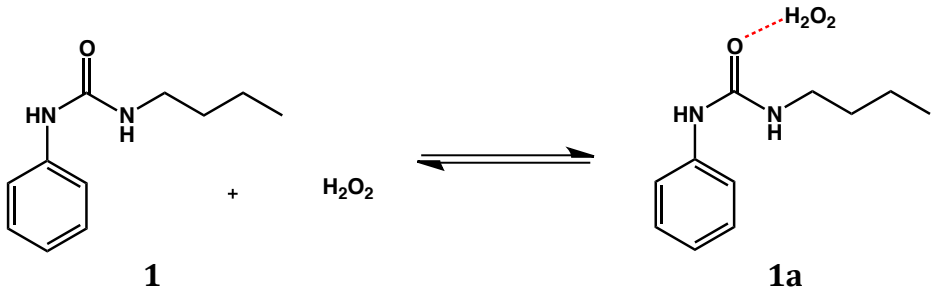

1 **1a**

Scheme 4.4. General reaction for adduct formation of **1a** from **1**. (Binding of H_2O_2 is shown generically without specifying binding sites). Compounds with '**a**' denote the H_2O_2 adduct.

Initially a rapid assay for the presence of hydrogen peroxide was sought. One of the simplest methods involved the use of peroxide test strips. A sample of **1a** was stirred in water for 1 hour to release the hydrogen peroxide before giving a positive reading with the test strips. Additional assessment by NMR in d_6-DMSO showed the presence of a small H_2O_2 peak at 10.2 ppm.

Direct titration of **1a** in an acidic solution with $KMnO_4$ was impossible as there was no well-defined colour change. The gradual discolouration of the pink solution at the equivalence point is characteristic of a competitive oxidation process of the organic material.[231] To determine if the urea (**1**) was responsible for this observation, the end solution was neutralised and extracted into EtOAc. The ^1H NMR spectrum displayed the original compound **1** in addition to multiple oxidation and degradation products. This result suggests that the $KMnO_4$ is being consumed in a side reaction and therefore the endpoint does not correlate to the amount of hydrogen peroxide. To eliminate this error the hydrogen peroxide from the adduct was extracted into water before performing the titration. Adduct **1a** (112 mg) was placed in 10 ml of water and vigorously stirred at room temperature for 1 hour. Approximately 1.5 ml of this solution was placed into an Eppendorf tube and centrifuged at 1,500 rpm for 30 seconds. As **1** is not soluble in water it forms a pellet at the bottom allowing separation of

the urea from the hydrogen peroxide. The supernatant (1 ml) was titrated with $KMnO_4$ to give a well-defined end point. This suggested that there was 8.6% w/w H_2O_2 in the adduct. This affords a ratio of approximately 2:1 PBU:H_2O_2, although this assumes that the unbound hydrogen peroxide was removed when forming the adduct. As there are uncertainties of how the substituted urea and H_2O_2 interact, the presence of residual hydrogen peroxide may be due to the amount of water trapped in the solid structure of the adduct. Trapped water can assist in making further hydrogen-bonding attachments to stabilise the hydrogen peroxide that is not directly bound to the urea moiety. These hydrogen bonds make it more challenging to remove the excess H_2O_2/H_2O. To remove this problem a non-aqueous hydrogen peroxide source was required. Thus a THF:H_2O_2 solution replaced the aqueous solution as the source of H_2O_2. Following unsuccessful attempts to form a precipitate or crystals through heating and cooling, **1a** was isolated by removal of the solvent. Initially, a 1:1 ratio of substituted urea to H_2O_2 was used, but unfortunately this compound did not survive the drying process as effectively as the previous method. Due to the volatility of THF it was left overnight on a standard vacuum line instead of using the low pressure oven. It was later established that this was too long and could account for the low hydrogen peroxide content. The test strips gave only a 0.025% or 7:1 (PBU:H_2O_2) ratio. In this case, titration with standardised $KMnO_4$ solution was not sufficiently sensitive. As there was so little hydrogen peroxide present, the associated errors would not have given accurate results. To confirm the presence of hydrogen peroxide, NMR in the Lewis basic solvent, d_6-DMSO, revealed a peak at 10.2 ppm. Interestingly, it also revealed a secondary peak at 5.40 ppm associated with a small amount of urea that was soluble in the THF solution from the original urea-hydrogen peroxide.

4.2.3.1 Quantitative titration, UV-Vis and NMR spectroscopy

Following initial attempts to form a substituted urea H_2O_2 adduct, it became evident that adduct formation was not straightforward. The formation of the adduct with an assumed 1:1 ratio was simply not producing the desired results. To increase the likelihood of forming the adduct, 5 equivalents of H_2O_2 (in THF:H_2O_2) was used to shift the equilibrium to the right to potentially form more

product (Scheme 4.4). Preliminary studies displayed this ratio as the most consistent and the maximum at which concentrating this solution would still be considered safe. Unfortunately this proposal had variations within itself. The THF:H_2O_2 solution exhibited unreliable hydrogen peroxide concentrations between each series of experiments. The nature of this variation was uncertain, however it was likely that it was due to either small impurities causing disproportionation of the hydrogen peroxide, or the length of time and temperature at which UHP was stirred in THF. All efforts were made to eliminate inconsistencies throughout, however differences in concentration of H_2O_2 caused variations in the volume of organic hydrogen peroxide solution between each series. Consequently this affected the amount of time under reduced pressure the samples were subjected to when removing the solvent. As it is assumed that when removing the solvent (THF) excess or unbound H_2O_2 is also being removed, time under vacuum may cause unavoidable variations.

To form **1a**, a solution of anhydrous hydrogen peroxide was stirred for 15 minutes with **1** (1 g) before the solvent was removed. To ensure the adduct was dry, the sample was placed in a low pressure vacuum oven at 80 °C for 90 mins. Assuming the mass of **1** remained the same, the average yield of **1a** was 82%. The large variation in hydrogen peroxide content found between samples (Table 4.5) could be due to the loss of H_2O_2 during the adduct formation process. Appreciable losses ranged from 10 – 60% of the initial H_2O_2 (according to mass) introduced. The variation confirms the complexity of the adduct forming reaction.

Taking a pragmatic approach, upon formation of **1a** multiple techniques were used to assess the H_2O_2 content of the adduct. These included: ^{1}H NMR in *d*$_6$-DMSO, titration with $KMnO_4$, UV-Vis determination and ^{31}P NMR of the oxidation of PPh_3. Using the same adduct sample, all four techniques were performed in parallel for each series. Proton NMR studies of **1a** in *d*$_6$-DMSO shows a direct comparison of integrals of H_2O_2 with the substituted urea. Extraction of hydrogen peroxide for $KMnO_4$ titration and visible spectroscopy was as described above. Each technique contained three replicates from the same

sample of water to ensure consistency. Oxidation of PPh_3 was performed by addition of 0, 10, 20, 30 or 40 mg (0.11 eq. – 0.46 eq. assuming a 1:1 adduct) of **1a** to 100 mg of PPh_3 in CH_2Cl_2. Following stirring for 1 hour under inert conditions; the solvent was removed and redissolved in deuterated DMSO for quantitative ^{31}P NMR analysis. The amount of auto-oxidation seen in the blank solution was removed from the remaining reactions in the series. All techniques were evaluated and expressed in terms of the ratio of **1** to H_2O_2 (Table 4.5).

Table 4.5. Calculated mole ratios of **1**:H_2O_2 from each analytical method repeated over 5 series. Ratios in brackets correspond to the maximum ratio due to complete oxidation of PPh_3.

Series	^{1}H NMR	$KMnO_4$ titration	UV/Vis spectroscopy	^{31}P NMR
1	**1:** 2.16	2.3 **1:** 2.5 2.8	2.1 **1:** 1.6 3.1	1.2 2.6 **1:** 2.5 2.3
2	**1:** 4.64	3.7 **1:** 3.2 3.8	3.5 **1:** 2.5 5.2	1.1 2.4 **1:** 2.6 2.5
3	**1:** 5.37	3.3 **1:** 2.8 2.5	3.7 **1:** 4.4 4.1	1.4 2.2 **1:** 2.5 (2.4)
4	**1:** 5.44	3.6 **1:** 3.3 3.2	2.7 **1:** 2.8 3.1	2.8 2.3 **1:** 3.2 (2.6)
5	**1:** 7.05	3.4 **1:** 3.3 3.5	2.5 **1:** 2.5 2.7	1.7 2.0 **1:** 2.9 (2.6)

The results suggest an adduct of some description is forming. However, the accuracy of determining the content of H_2O_2 in the solid compound is variable not only between each analysis method, but also the precision within analytical method itself. Despite efforts to restrict the variable of time under vacuum, it potentially is the problem that is causing discrepancies between each series. Of greater concern is the variability within one analytical technique. The titration with $KMnO_4$ and the UV/Vis spectroscopy methods use the same solution for extraction of the hydrogen peroxide from the adduct, therefore should give similar results. As the concentration of the H_2O_2 is low (0.16 – 0.29 mM), a greater effect is seen upon catalytic or non-catalytic disproportionation of H_2O_2. Despite these variations there is a degree of confidence that the adduct contains a 2 – 3 mole of H_2O_2 per urea. Unfortunately in some circumstances residual THF is present which poses the question, is it included in the adduct, such as in Fig. 2.13, or is the sample not sufficiently dry despite a thorough drying process? In the investigation of the formation of adduct **1a**, the results suggest that the adduct exists as a network of close hydrogen bonding interactions, rather than discrete substituted urea-peroxide units. This network may incorporate several binding orientations of not only substituted urea and H_2O_2 but also other solvents as well, giving a disordered structure. This could justify some variations between series as 'pockets' of material can occupy certain volumes of the material causing a non-uniform structure.

As these results are only preliminary, it shows some promise in the ability to measure H_2O_2, albeit not consistently at this stage. Further work would be required to reliably obtain consistent results, however it can be used as a tool to determine the formation of adducts and apply this to the library of compounds prepared in this study.

4.2.3.2 X-ray Crystallography and Mass Spectrometry

Growing crystals of the adduct suitable for X-ray crystallography proved challenging. To produce single crystals for analysis, techniques such as slow evaporation, vapour diffusion and multi-solvent evaporation were attempted. Unfortunately, all crystals analysed were simply composed of substituted urea

without the incorporation of H_2O_2. Crystals were obtained of just the substituted urea, however these compounds have already been reported in the literature. Potentially the single crystals do contain hydrogen peroxide. Unfortunately the arrangement of hydrogen peroxide in the crystal lattice is not uniform or consistent. Continual efforts have been made throughout this project to obtain a crystal structure of a hydrogen peroxide adduct compound as this would assist in the identification of the intermolecular interactions between the substituted urea and H_2O_2.

Characterisation of the adducts by mass spectrometry (ESI) was also attempted. Cationic peaks of $[M+H]^+$, $[M+Na]^+$ and $[M+K]^+$ were observed for ureas in urea-hydrogen peroxide and **1a**, although neither an adduct nor hydrogen peroxide peaks could be identified. This is not surprising as although ESI is a soft ionisation technique, the energy required to break an adduct into each component is much less than breaking a covalent bond.

4.2.3.3 IR analysis of adducts

Based on the results of Section 4.2.2, the most effective way to qualitatively identify formation of an adduct was by ATR. Using urea-hydrogen peroxide as an example, the additional vibrational mode at 2731 cm^{-1} has been identified as the lengthened O-H bond of peroxide when significant hydrogen bonding is occurring. As this was the only method to determine if the adducts had formed, the ATR was recorded for all the putative adduct samples (Table 4.6). It is noted that despite the possible assignment of this peak as an overtone of the hydrogen peroxide O-H vibration,[222] it clearly is not conclusive as other known hydrogen peroxide containing complexes do not show this peak.[232,233] Although in the event that it is the correct assignment, it still identifies that H_2O_2 is present in the solid urea adduct.

Table 4.6. Analysis and location of the O-H stretch in H_2O_2 of the synthesised adducts (R = phenyl). No binding indicated by ' – '.

Adduct	R'	O-H Binding (cm^{-1})
1a	$(CH_2)_3CH_3$	2820 (w)
2a	C_6H_5	2810
3a	$CH_2C_6H_5$	2801
6a	$C(CH_3)_3$	-
7a	H	2846
8a	OH	2982, 2876
9a	C_6H_3-3,5-CF_3	2798
10a	C_6H_4-*p*-CF_3	2809
11a	C_6F_5	2814
12a	C_6H_4-*p*-NO_2	2789
13a	C_6H_4-*m*-NO_2	2798 (mult)
14a	C_6H_4-*o*-NO_2	2798 (mult)
15a	C_6H_4-*p*-N=N-Ph	2792
16a	C_6H_4-*p*-I	2981, 2878
17a	C_6H_4-*p*-Cl	2983, 2877
18a	C_6H_4-*p*-CO_2H	2811 (w)
19a	C_6H_4-*p*-CH_3	2808
20a	C_6H_3-2,6-CH_3	2809
21a	C_6H_2–2,4,6-CH_3	2810 (w)
22a	C_6H_4-*p*-NH_2	-
23a	C_6H_4-*p*-OCH_3	2787 (vw)
24a	C_6H_4-*p*-OAlk	-
25a	Butyl phenylcarbamate	2872 (vw)
26a	Methyl phenylcarbamate	2799
27a	N-butyl-benzamide	-
28a	N-butyl-4-methylbenzensulfonamide	2775
29a	N-phenylmethanesulfonamide	2973, 2874
74a	Nitrobenzene	2810
75a	2-hydroxybenzimidazole	2806

Stretching frequencies associated with H-bonding are proposed to undergo a shift to a lower frequency in comparison to the free molecule. In particular, the hydrogen peroxide O-H bond is elongated causing the stretching frequency to be red shifted upon H-bonding. The degree of red shift is directly correlated to the strength and length of a bond and hence its force constant. The stronger bonds have a higher force constant and vibrate at higher frequencies. Therefore, it is assumed here that the lower the wavenumber, such as 2731 cm^{-1} in urea-hydrogen peroxide, shows shorter H-bond distance between H_2O_2 and urea giving a more stable complex.

The red shift of this O-H bond in ureas containing an electron withdrawing group varies from 2798 – 2983 cm^{-1}. As described in Section 2.5.1 the deshielding of the N-H protons creates a partially positive region that was proposed would be the area that forms the interaction with the H_2O_2 oxygen. This hypothesis assumes that this is the only point of contact between the H_2O_2 and the N-H from the urea. However this is unlikely as nitrobenzene (**74a**) revealed a similar red-shifted peak at 2810 cm^{-1} suggestive of an O-H H_2O_2 stretch. Binding of the hydrogen peroxide to a nitro group indicates that alternative binding modes in the library of substituted ureas must be considered. A lower frequency stretch is present in diphenylurea (**2a**) that has no additional functional groups on the urea or phenyl moiety therefore implying the mode of binding is not simple. Compounds **13a** and **14a** contain both a nitro and urea moiety and despite being weaker than **2a**, present multiple peaks in this region suggesting interaction of H_2O_2 with both functionalities.

Electron donating substituents give a notably less intense IR stretch, if any at all. In contrast, the halide substituted adducts (**16a** and **17a**) and hydroxylurea (**8a**) form two additional peaks opposed to one. It is not unreasonable to assume that either A) one H_2O_2 molecule is forming two hydrogen bonds of different strengths thus causing variability in the O-H bond stretch or B) two H_2O_2 molecules are binding to the substituted urea in distinct orientations and strength.

Previously, it was noted that the carbonyl in the urea is capable of accepting a hydrogen bond from H_2O_2. The carbonyl stretch in IR is very prominent due to its large dipole moment, and small changes in crystal structure or hydrogen bonding can significantly change the frequency of the C=O stretch. If it were involved in the binding to H_2O_2 a shift in the absorbance to a lower frequency would be expected. Surprisingly, no such change is seen in any spectra. Fluctuations in frequency of 0–5 cm^{-1} is the extent of change between the carbonyl stretch in the substituted urea and the associated H_2O_2 adduct.

Calculations suggests the phenyl butylurea (**1**) will not form a stable adduct with H_2O_2.[49] It was proposed that the conformational freedom associated with the butyl chain hindered the ability to form a stable structure. For comparative purposes, 2-hydroxybenzimidazole (**75**) a cyclic urea with less flexibility than **1**, was prepared as an adduct and subjected to IR analysis. Interestingly, in addition to the peak at 2806 cm^{-1}, it appears that the carbonyl stretch has red-shifted from 1712 to 1631 cm^{-1} (Fig. 4.18). A stronger and broader peak at 1361 cm^{-1} indicates the presence of the O-H symmetric bend as seen in the UHP adduct earlier (Figure 4.15). This evidence suggests that the limited flexibility and fixed orientation of the cyclic urea promotes intermolecular interactions between the carbonyl and hydrogen peroxide. However the assistance of the adjacent N-H protons remains unknown.

Ultimately, ATR can be used to show the presence of H_2O_2 in an adduct sample. Furthermore, it was proposed that due to the increased intensity of the peak at *ca.* 2800 cm^{-1} in the electron-withdrawing ureas, hydrogen peroxide forms a stronger hydrogen bond and thus a more stable adduct. Similar to UHP, this technique does not indicate the quantity of H_2O_2 or enable analysis of a binding constant for the adducts.

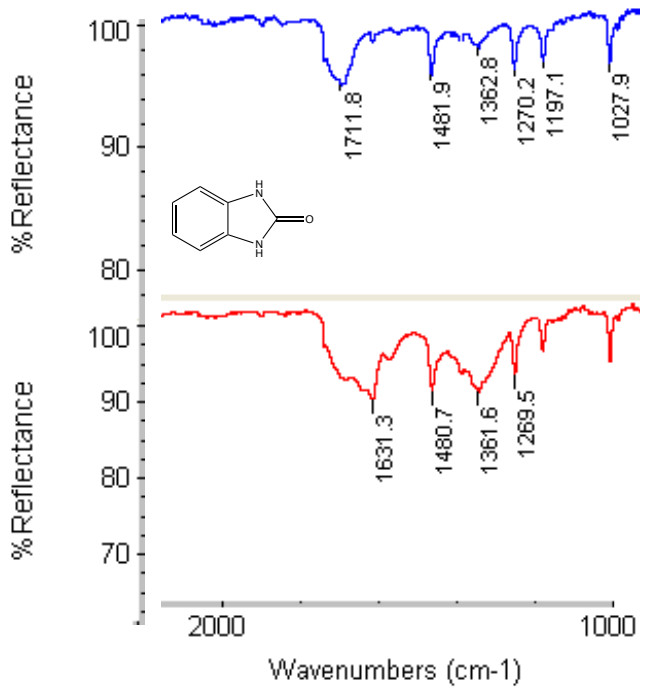

Fig. 4.18. ATR spectra of 2-hydroxybenzimidazole (**75**) (top) and its H_2O_2 adduct (**75a**) (bottom).

From these results, the most promising binder would be a derivative of 2-hydroxybenzimidazole. The fixed orientation of the urea moiety promotes interactions of the carbonyl with hydrogen peroxide with possible assistance from the adjacent N-H protons. Adding an electron-withdrawing substituent on the phenyl ring may assist the strength of binding as demonstrated in the above examples. The question then becomes if hydrogen peroxide is also binding to the substituent (-NO_2 etc.), is this sufficiently strong enough to immobilise H_2O_2 and prevent self-discharge of the battery cathode system.

4.2.4 Binding constant analysis in substituted ureas

4.2.4.1 NMR Spectroscopy

After determining which ureas led to the formation of adducts, the next stage was to evaluate binding constants. ^{1}H NMR had previously been abandoned as a method for obtaining K_a for urea interactions with H_2O_2 due to the large amount of hydrogen-deuterium exchange with the solvent. It was proposed that with the larger, more hydrophobic substituted ureas in this second study the exchange

process would be slowed sufficiently for meaningful results to be obtained from the substituted groups as well as the N-H protons. The ^{1}H NMR chemical shift when forming a hydrogen bond is related to the strength of the bond. Generally, the stronger the bond, the more deshielded the proton. As hydrogen bonds can be formed and broken within the NMR timescale, only an average of peaks is anticipated, rather than two distinct peaks of the hydrogen bonded and non-hydrogen bonded protons.

The substituted ureas show poor solubility in water and limited solubility in methanol, therefore a different deuterated solvent was required. Preliminary ^{1}H NMR spectra of **1** were collected in *d*$_6$-DMSO hence this was the starting point for future experiments. DMSO is a polar aprotic solvent that reduces the extent of exchange between solvent and compound. The systematic addition of a hydrogen peroxide solution of known concentration allows the change in chemical shift attributable to H_2O_2 binding to be used to calculate the binding constant by extrapolation of the data. As water interferes with these interactions an organic hydrogen peroxide solution; THF:H_2O_2 of known concentration (see Section 2.5.3) was titrated with the substituted urea.

The titration was performed at 25 °C where **1** (10 mg, 0.052 mmol) was dissolved in *d*$_6$-DMSO (700 µl) and a solution of THF:H_2O_2 was added in aliquots to give a total of 0, 50, 100, 150, 200 and 400 µl of H_2O_2 solution in the sample tube (0 – 0.4 mmol). Unexpectedly, ^{1}H NMR only showed a broadening of the key peaks: H_2O_2, H_2O and N-H. To test whether this correlated with the addition of H_2O_2, two controls were also performed, the first adding only water and the second only THF. In both the control experiments and the titration with THF:H_2O_2, shielding of the both N-H peaks of the urea was evident. On addition of the same volume of water, the H_2O peak shifted dramatically from 3.38 to 4.33 ppm after adding 400 µl. This was not surprising as the exchange of water peaks is generally very fast, thus only an average response was observed. The downfield shift is attributed to an increase in hydrogen bonding when additional water is added. Interestingly, there was little change in the substituents of PBU on addition of any of the solutions. This suggests that the DMSO is forming its

own strong interactions with PBU and the addition of water, H_2O_2, or THF is unable to displace the DMSO from the substituted urea. With each addition it is more likely that changes in chemical shift of the N-H protons are predominantly due to a dilution effect, rather than specific interactions. Although this does not necessarily mean there was no H_2O_2 binding, it simply reflects the requirement for an unbiased standard as all spectra were calibrated to the DMSO peak at 2.5 ppm.

As seen with the simple ureas and the titration method above, concentration of the analytes is important to chemical shift. As aliquots are successively added to the mixture both the H_2O_2 and substituted urea concentrations are changing. The method was therefore changed such that the amount of THF:H_2O_2 was kept constant, and the amount of **1** increased from 0 – 40 mg (0 – 0.25 mmol) in the sample. A mixture of THF:H_2O_2 and d_8-THF was used in the sample tube at a great excess and THF:H_2O_2 in the capillary tube as a standard. In practical terms, for each titration point following the initial sample of 0 mg of substituted urea, the capillary tube was removed and the remaining solution was tipped into a pre-weighed solid sample of substituted urea which was dissolved and re-inserted into the sample tube. Comparing each spectrum showed the first sign of a change in chemical shift in H_2O_2 whereby a prominent downfield shift of 0.2 ppm was visible in response to an increase of 0.25 mmol of **1.** A second peak was also visible where it appeared as a broad shoulder (Fig. 4.19). It is proposed that the two peaks correspond to the H_2O_2 inside the capillary and in the outer tube. The aromatic and butyl protons negligibly shifted although a slight downfield shift could be seen in both N-H protons, residual urea (from urea-hydrogen peroxide) and water peaks.

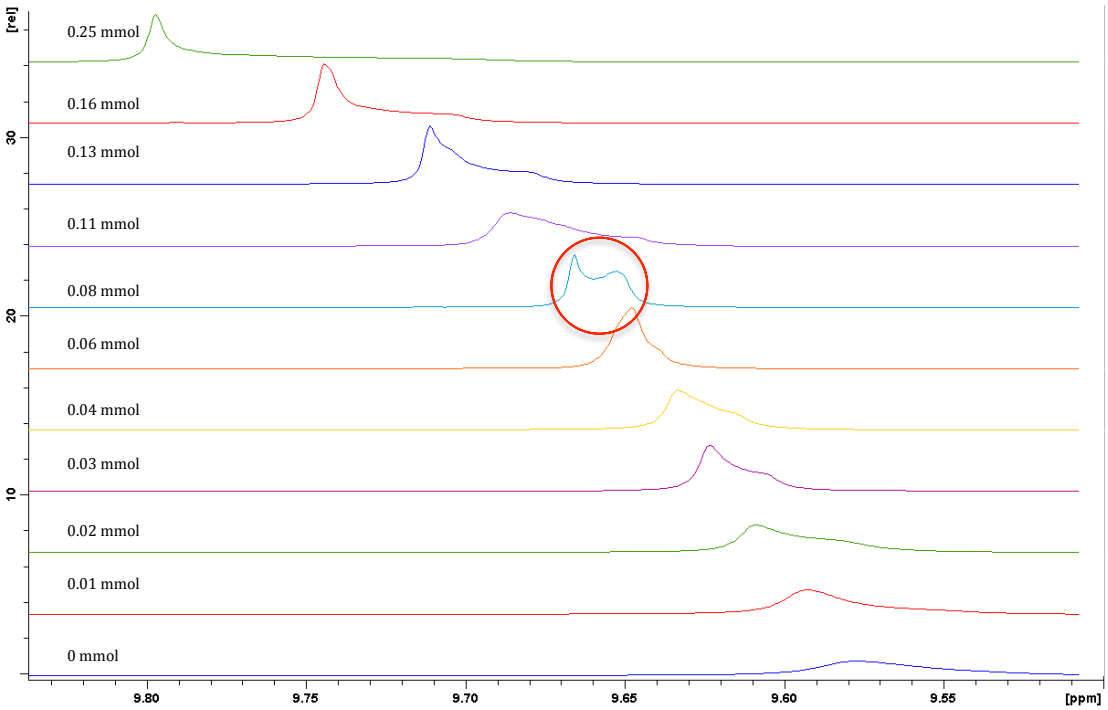

Fig. 4.19. Initial ^{1}H NMR studies of H_2O_2 with PBU.

Unfortunately, this method had an inherent error in that solvent was lost during the transfer steps and this effects the concentration. As the experiment deals with such small concentrations of **1** this had an adverse effect not only on concentration but also the volume in the sample tube and this severely limits the accuracy of the results.

To try to minimise these inaccuracies the titration method was further optimised. Having previously determined that the H_2O_2 concentration could not be increased and transfer errors marred the alternative method, the increase of substituted urea concentration was achieved by using a separate sample and NMR tube for each concentration. In these experiments the interaction between DPU (**2**) and H_2O_2 was studied. The move away from PBU (**1**) was as a result of the IR studies and the calculations discussed in Section 4.2.3.2. PBU was exhibiting weak binding while DPU (**2**) showed a strong peak at 2810 cm^{-1}.

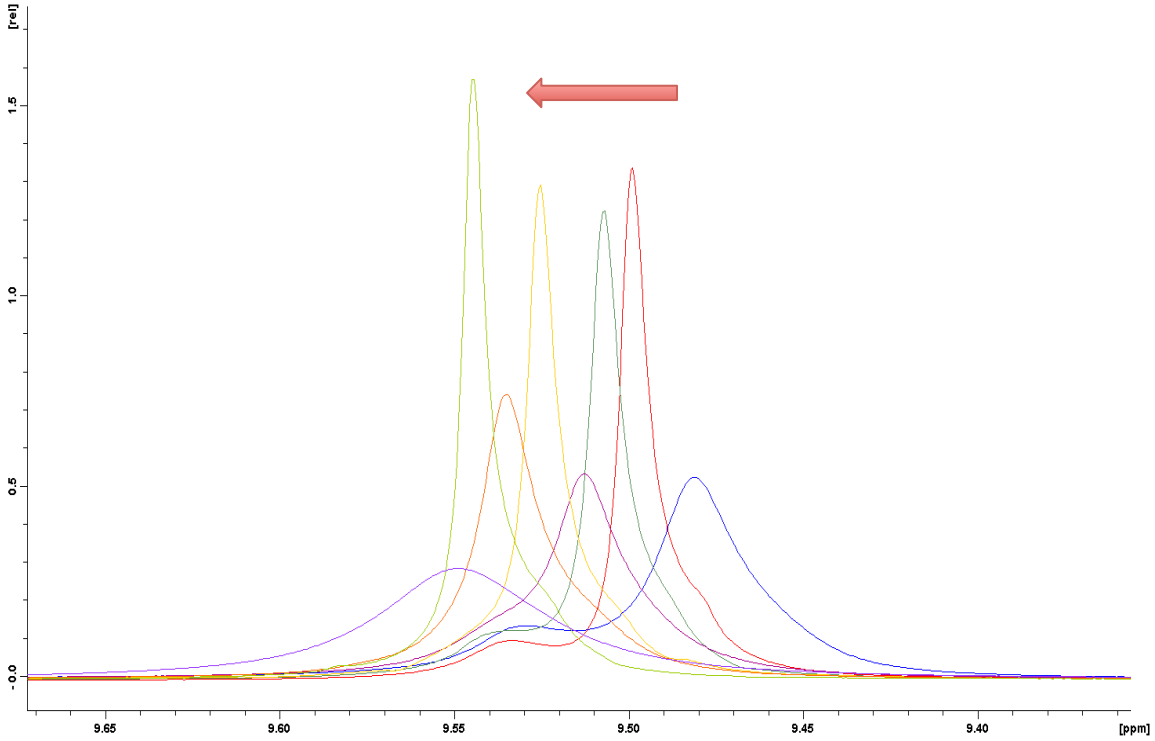

Fig. 4.20. 15 – 110 mM of **2** with THF:H_2O_2 (578 mM) in d_8-THF. Arrow indicates increasing concentration. Capillary: THF:H_2O_2 (small downfield peak).

First the solubility limit of **2** was much lower in THF than **1** with a limit of 14 mg in a 600 µl sample (110 mM). This dramatically affected the ratio of substituted urea/H_2O_2 that could be achieved in these experiments, with an upper limit of 0.19 when keeping the H_2O_2 concentration constant. Solutions of DPU with concentrations 15 – 110 mM, had a standard amount of THF:H_2O_2 (578 mM) in each sample. The capillary contained THF:H_2O_2, while the sample tube was a 1:1 mixture of THF:H_2O_2 and d_8-THF. Calibrating the THF peak in the capillary to 1.79 ppm, a clear downfield shift of H_2O_2 was seen in the bulk solution from 9.48 to 9.55 ppm with a small shoulder seen further downfield in the lower concentrations of DPU (Fig. 4.20). It was presumed that this shoulder was the H_2O_2 in the capillary and that the change in the large peak was due to the interaction with **2**. This was confirmed experimentally by a control experiment in the absence of **2** (Fig. A3). Additional downfield shifts are also present in the residual substituted urea and H_2O that are also present in these solutions,

although it is unclear whether this is due to an increase in self-association or an explicit interaction with **2**.

Table 4.7. Chemical shift of the N-H proton in **2** in the presence and absence (control) of H_2O_2.

[**2**]	NH (H_2O_2) ppm	NH (control) ppm	Difference ppm
15 mM	8.07	7.78	0.29
31 mM	8.06	7.78	0.28
47 mM	8.06	7.78	0.28
63 mM	8.05	7.79	0.26
78 mM	8.05	7.82	0.23
94 mM	8.05	7.83	0.22
110 mM	8.05	7.83	0.22

A control experiment was performed under identical conditions except in the absence of hydrogen peroxide. This showed a downfield shift in the N-H signal, which is in contrast to the experiment containing H_2O_2 where the N-H signal shifted slightly upfield (Table 4.7). In this control titration the N-H proton showed little change until 60 mM DPU, therefore suggesting that this is the concentration of which self-association becomes prominent (Fig. 4.21). Ultimately this change is so small that it may be within the experimental error. However it is possible that the N-H forms hydrogen bonds with a carbonyl from another molecule of DPU thus deshielding the proton.

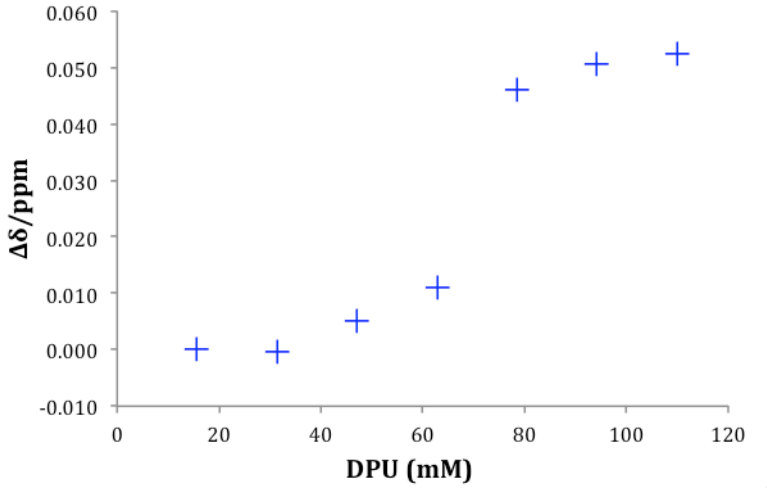

Fig. 4.21. Change in chemical shift of the N-H proton in DPU with increasing concentration of DPU (in the absence of H_2O_2) suggesting self-association.

In the 15 mM DPU solutions, the N-H signal showed a difference of 0.29 ppm in the presence and absence of H_2O_2 (Fig. 4.22). A similar shift of 0.22 ppm was observed in the 110 mM solution (Fig. 4.23). It can be concluded from this data that the presence of H_2O_2 makes an immediate and significant change in chemical shift of the N-H proton, making it challenging to measure the initial change. It is clear that the presence of H_2O_2 immediately forms interactions with DPU. Increasing the concentration of the substituted urea has less of an effect on DPU than in the absence of H_2O_2 where self-association is dominant.

Another noticeable change in Fig. 4.22 is the deshielding of H_2O, which could be attributed to the additional hydrogen bonding opportunities with the addition of hydrogen peroxide. This appears to be a trend throughout all NMR titrations performed. To remove equilibration time as a variant, a spectrum was taken at various time intervals over a 60 minute period after adding H_2O_2 to the sample tube. As no deviations could be seen, it was concluded that the system reaches equilibrium almost immediately, or within the time it takes to lock and shim the sample (*ca.* 5 minutes)

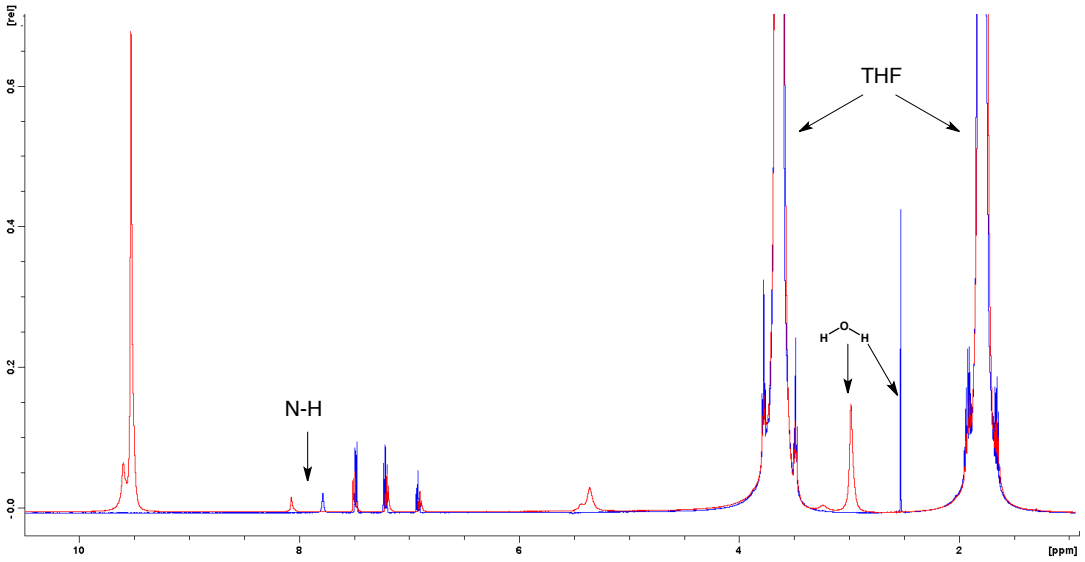

Fig. 4.22. Comparison of 15 mM **2** in the presence of H_2O_2 (red) and absence (blue) in d_8-THF. Capillary: THF:H_2O_2.

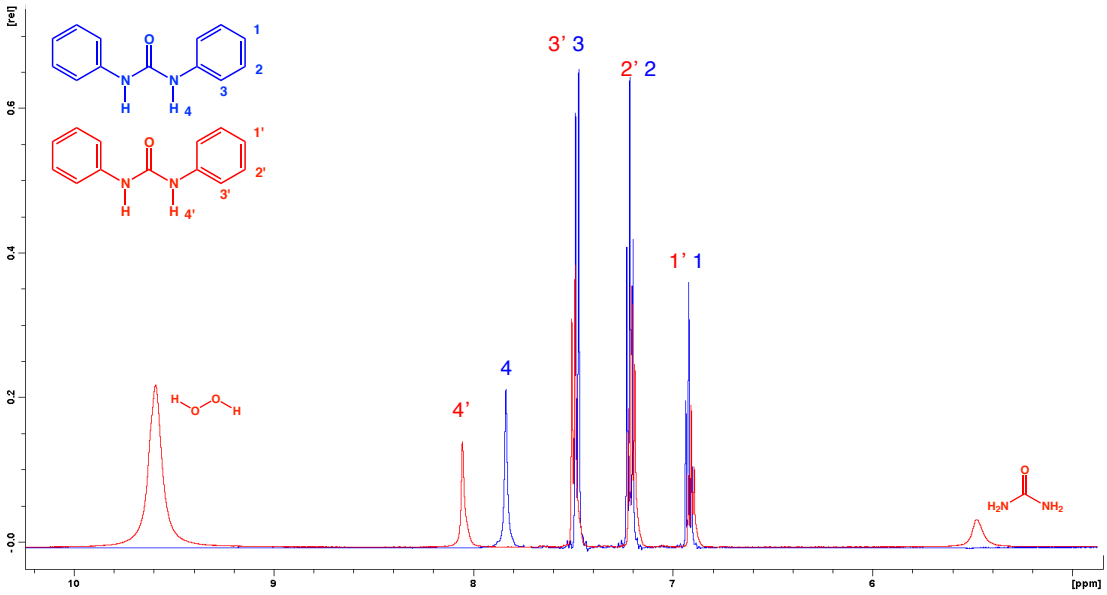

Fig. 4.23. Comparison of 110 mM **2** in the presence of H_2O_2 (red) and absence (blue) in 1:1 THF:d_8-THF. No capillary.

The ^{1}H NMR titrations above (Fig. 4.20/4.22) were all calibrated to the THF peak in the capillary tube. On further analysis of the H_2O_2 signal it was clear that the H_2O_2 peak in the capillary was not at a consistent chemical shift. Therefore the H_2O_2 peak in the capillary (9.59 ppm) was used to align each spectrum (Fig. 4.24). The variation in chemical shift of H_2O_2 between the capillary and bulk

solution could be due to differences in the medium environment. However it can be assumed that this peak from the H_2O_2 in the capillary remains constant.

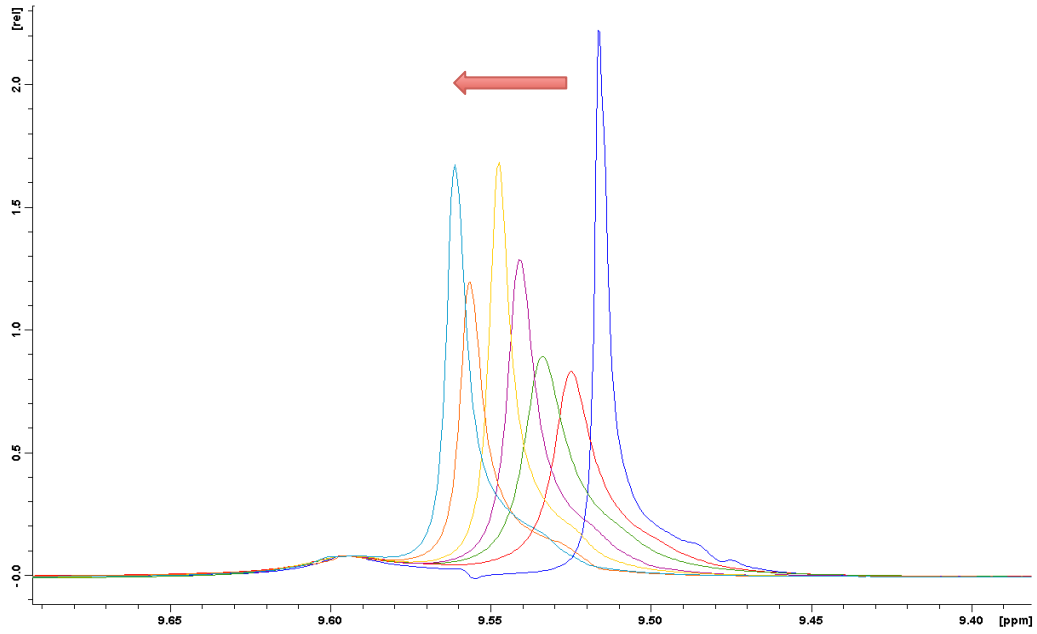

Fig. 4.24. 15 – 110 mM of **2** with THF:H_2O_2 (560 mM) in d_8-THF. Capillary: THF:H_2O_2 (calibrated to capillary H_2O_2). Arrow: direction of increasing [**2**].

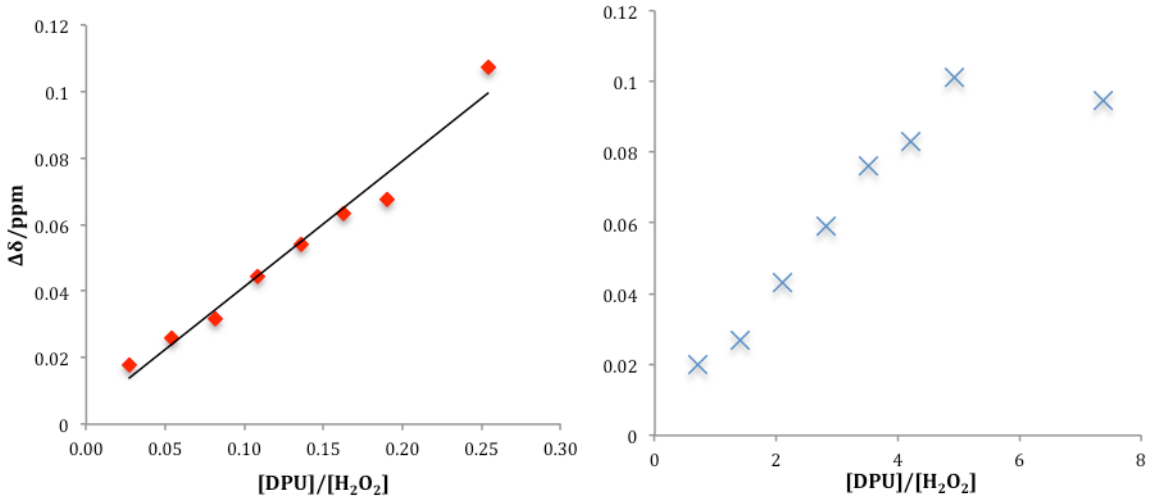

Fig. 4.25. Chemical shift of H_2O_2 in response to increasing ratio of [**2**]/[H_2O_2]. Ratio of [DPU]/[H_2O_2]: < 0.3 (Left), >0.3 (Right).

In the series of samples, a downfield shift was still evident in the bulk H_2O_2 after calibration, giving a linear correlation between changes in chemical shift to the ratio of **2** with H_2O_2 (Fig. 4.25:Left). This correlation is seen at a substituted urea/H_2O_2 ratio less than 1, where the amount of hydrogen peroxide is greater that that of **2**. In order to determine the subtle interaction between urea and H_2O_2, this ratio was increased above 1 to give an excess of urea. This was achieved by diluting the THF:H_2O_2 solution with THF, and provided solutions with 0.7 – 7.4 mole excess of urea (Fig. 4.25:Right). Again this showed a linear relationship but showed a saturation point of a 5 mole excess of urea above which no further changes in H_2O_2 were observed. As this does not align with the previous data (Fig. 4.26), it suggests the change in chemical shift of H_2O_2 is dependent on hydrogen peroxide concentration.

To demonstrate this point further, the different H_2O_2 concentrations not only gave a different starting value but the magnitude of the change in chemical shift was dependent of the initial H_2O_2 concentration (Fig. 4.27). In the original hydrogen peroxide series experiments, the H_2O_2 concentration was 578 mM (9.516 ppm) compared to the dilute series of 22 mM (9.367 ppm).

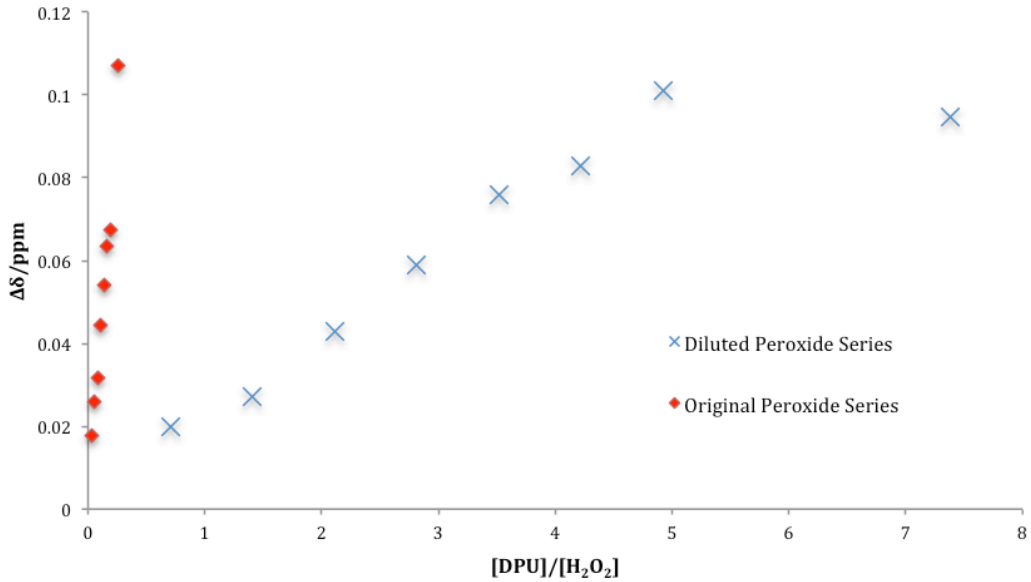

Fig. 4.26. Chemical shift of H_2O_2 in response to [**2**]/[H_2O_2] ratio in the original (578 mM) and diluted (22 mM) H_2O_2 series.

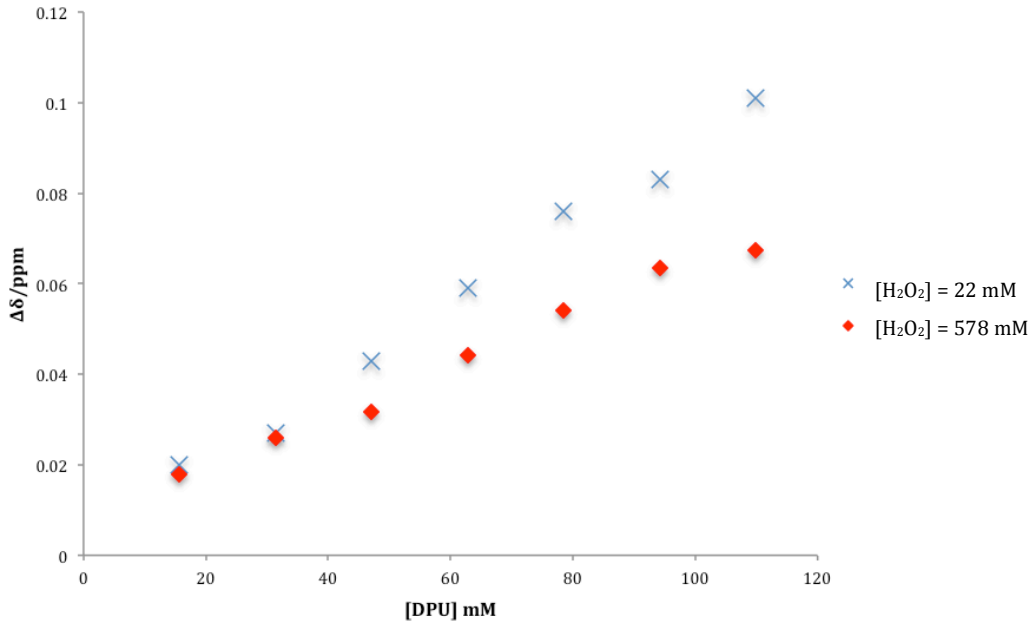

Fig. 4.27. Change in chemical shift of H_2O_2 at 22 and 578 mM in reponse to [**2**] (mM).

Although this is not unexpected due to the increased proportion of intermolecular hydrogen bonding of H_2O_2 in the higher concentrated sample, it does highlight the fundamental challenge when attempting to find a binding constant. As the complexation of substituted urea and hydrogen peroxide has a rapid exchange of the bound and unbound state compared to the NMR time scale, the peaks assigned to the free and complexed host or guest parts are fixed. Assuming H_2O_2 is the host (as it is kept constant), the peak appears as a weighted average chemical shift between the free host and complexed host. As the concentration of H_2O_2 is constant, δ is the observed chemical shift and δ_H and δ_C are the chemical shifts of the free host and complexed host respectively (Fig. 4.28).

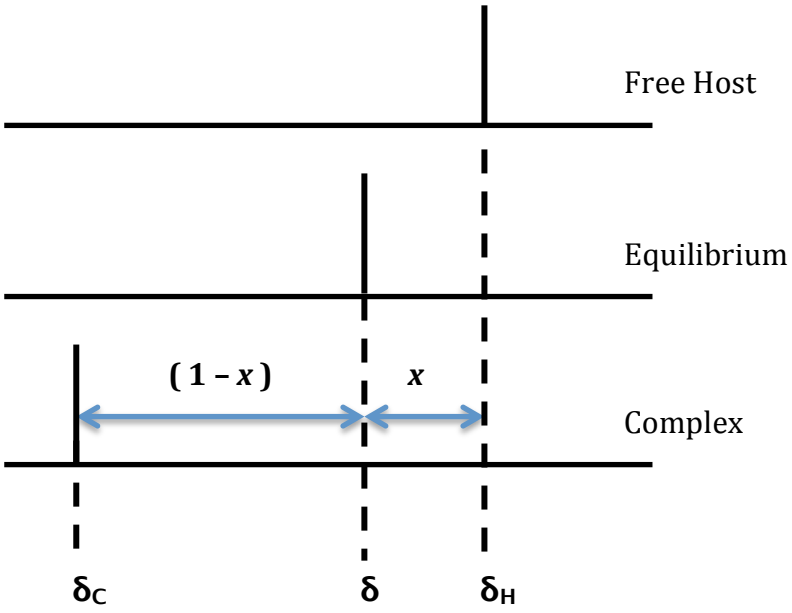

Fig. 4.28. Representative NMR spectra for fast exchange of the complexation showing a correlation of host to guest ratio.

The chemical shift data of H_2O_2 may be interpreted as an average whereby the difference of further change is determined by the ratio of bound to unbound H_2O_2, not only to **2** but also with other hydrogen bonding donors and acceptors. As H_2O_2 contains exchangeable protons, the rate at which these protons exchange can also influence the chemical shift. Slow exchange exhibits a population-weighted average therefore since the kinetics of each exchanging proton are not known, it is possible that the observed chemical shift is an average of bound and unbound H_2O_2 as well as for the exchange rates.

To find the equilibrium constant *K*, one must first find the stoichiometry of the host-guest system and thus the concentration of the complex. In this case, the observed chemical shift can be placed into Eqs. 4.17 and 4.18, and rearranged to find [C] where [C] is the concentration of the complex at equilibrium, $[H]_t$ is the total concentration of the host at the initial stage and *a* is the stoichiometry.[234]

$$\delta = \delta_H \,.\; (1 - x) + \delta_C \,.\, x \qquad 4.17$$

where $x = \frac{a\,.\,[C]}{[H]_t}$

so that $$[C] = \frac{1}{a}\,.\frac{\delta - \delta_H}{\delta_C - \delta_H}\,.\,[H]_t \qquad 4.18$$

Unfortunately, it was not possible to determine the chemical shift of the complex, δ_C and extrapolation of the data is unable to give an accurate stoichiometry. As Eq. 4.17 assumes that $a(\delta_C - \delta_H)$ is constant, it means that $[C]$ is proportional to the initial concentration multiplied by the difference between the observed chemical shift and the chemical shift of the host ($[H]_t\,(\delta - \delta_H)$). This is in alignment with the experimental observations that the observed chemical shift of H_2O_2 was related to the initial H_2O_2 concentration.

The large downfield proton shifts (~0.3 ppm) of water and residual urea (~0.2 ppm) remained prominent in the sample solution and can be attributed to changes in the solvent medium. This suggests they are forming their own hydrogen bonds with the guest in addition to the changes in permeability and volume magnetic susceptibility that can cause small fluctuations in local magnetic field. A correction can be made with Eq. 4.19 if the magnetic susceptibility of the reference solution and sample are known.[235]

$$\delta_{corr} = \delta_{obs} + \frac{2\pi}{3}(\chi_o^{ref} - \chi_S) \qquad 4.19$$

where δ_{corr} is the corrected chemical shift, δ_{obs} is the observed chemical shift and χ_o^{ref} and χ_S are the volume magnetic susceptibility of the reference solution and sample solution respectively. As we are only interested in the relative value of the chemical shift in each of the samples, it would be too time consuming to determine the magnetic susceptibility of each solution. Consequently, while there is awareness of the potential difference this study did not proceed further into this correction.

NOESY experiments were conducted on the most concentrated DPU/H_2O_2 sample. This was able to differentiate between a true nOe peak that involved the

transfer of nuclear spin polarisation through space, and exchange peaks. The exchange peaks were observed for residual urea, H_2O_2 and H_2O which all have exchangeable protons. For protons that are not within 2 – 3 covalent bonds of each other, the NOESY spectra displays cross peaks if they are within 5 - 6 Å of one another. This spectrum revealed that the aromatic protons are close to each other and to the N-H. Interestingly the H_{ortho} has a small NOESY peak associated with H_2O_2 (Fig. 4.29).

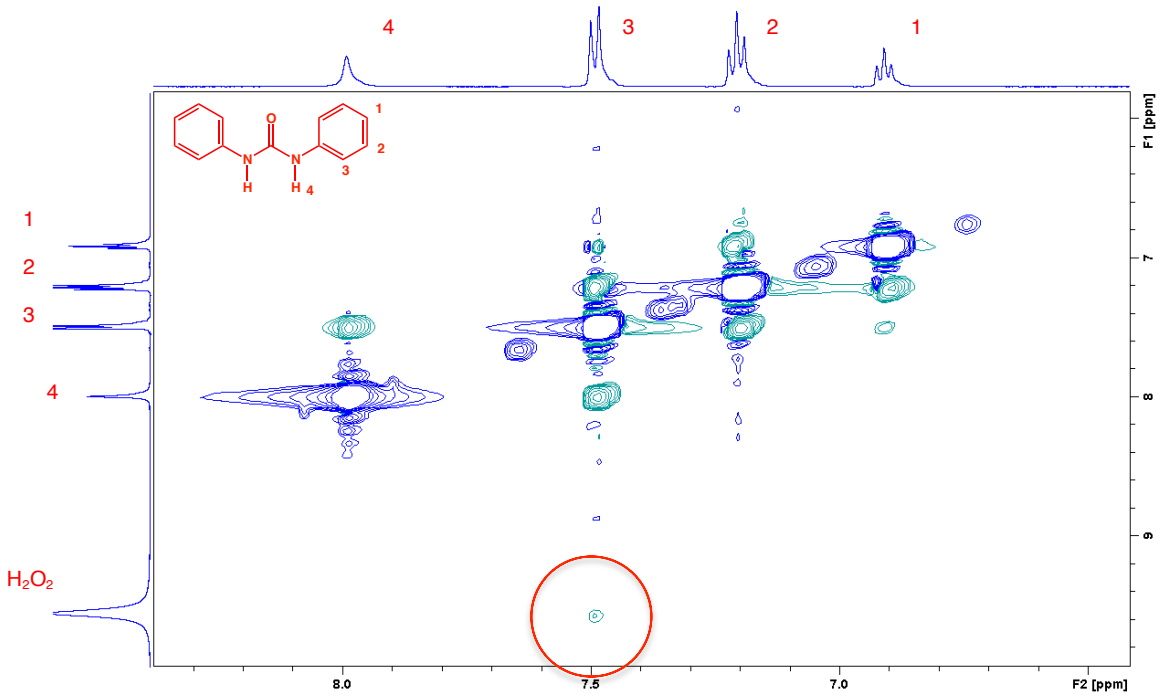

Fig. 4.29. NOESY spectra of **2** with H_2O_2 in THF/d_8-THF. Red circle represents the NOESY interaction between H_2O_2 and H_{Ortho} of diphenylurea.

If DPU exists in the trans conformation as suggested previously, H_2O_2 is able to bind to the carbonyl oxygen or the N-H, which would explain the proximity to the ortho proton (Fig. 4.30). This gives further evidence along with deshielding of the N-H proton compared to in the absence of H_2O_2. A ^{13}C spectrum at each DPU concentration revealed no noticeable change in chemical shift. A shift in the carbonyl oxygen had been anticipated upon binding of H_2O_2 but there is insignificant shift observed(<0.1 ppm) between the 15 mM and 110 mM sample.

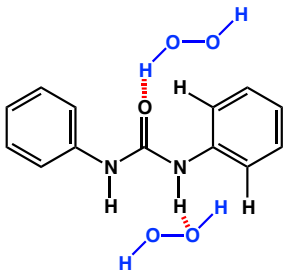

Fig. 4.30. Possible binding scenario where the ortho proton on the aromatic ring of DPU (**2**) is in close proximity to H_2O_2 and would give a nOe response in a NOESY spectrum.

It is extremely difficult to assign the changes in chemical shift of each solute to a specific interaction. This is highlighted by the ability of multi-site exchange in each compound. Not only does exchange occur at different sites, it occurs at different rates. This kinetic discrepancy forms a matrix that is highly complex as the peaks observed are averages and the extent to how much one form is occupied depends on the rate it undergoes exchange. Mathematical systems have been established for non-exchanging system (Ernst)[236,237], two-site system and in recent years a three-site system.[238] Unfortunately, in the present system, taking into account all exchangeable protons, 10 potential sites are available: two N-H protons on the substituted urea, four on the residual urea and two each for peroxide and water.

Other considerations in this system include contributions of magnetic anisotropy from the benzene ring, rate of tumbling and the spectral density function J (ν) which not only effects chemical shift but also the shape of peaks. Subsequently, this method was abandoned due to numerous variations and uncontrollable discrepancies that were unable to be resolved.

4.2.4.2 UV-Vis Spectroscopy

UV-Vis spectroscopy is a valuable technique for compounds with π electrons or non-bonding (n) electrons that absorb energy in the form of visible or UV light. This allows excitation to a higher energy anti-bonding molecular orbital. The

smaller the energy gap between the HOMO and LUMO, the longer the wavelength of light absorbed on excitation. These energy levels can vary depending on delocalisation within the molecule and the external solvent polarity. In anion-recognition studies, the addition of the anion stabilises the excited form of the receptor lowering the energy gap causing the absorption bands to be red shifted to a longer wavelength.[239] In an attempt to evaluate a binding constant we investigated the change in absorbance between the free receptor and the complex of azo dye **15**. Azo dyes are useful molecules in UV/visible spectroscopy especially aryl azo dyes where the increase in delocalisation reduces the energy gap between the HOMO and LUMO. The gap is lowered sufficiently that such compounds emit/absorb in the visible range giving rise to coloured solutions. It is essential that we worked within visible wavelengths as UV light causes the homolytic scission of the O-O bond in peroxide to form hydroxyl radicals (Scheme 4.5).

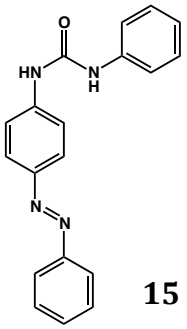

15

$$H_2O_2 \xrightarrow{h\nu} HO\bullet + \bullet OH$$

Scheme 4.5. Cleavage of hydrogen peroxide into two hydroxyl radicals by UV light.

As the hydroxyl radical is a strong oxidising agent with an oxidation potential of 2.8 eV, it is able to destroy the chromophoric structure of aryl azo dyes.[240] Although the rate of destruction is dependent on the auxiliary groups attached to the aromatic ring, this system cannot be evaluated in the UV region without the possibility of destroying or changing the original solution.

The UV-vis absorption spectrum of **15** presents two characteristic bands corresponding to π-π* and n-π* electronic transitions at 366 and 435 nm respectively (Fig. 4.31). The absorption band at 366 nm is very intense with a molar extinction coefficient, ε, of 16,772 M^{-1} cm^{-1} assumed to be from the *trans* isomer.[241] Unfortunately this lies in the UV region of the spectrum and is

inappropriate for this study. Consequently focus was shifted to the smaller n-π* transition at 435 nm (ε = 2,078 M^{-1} cm^{-1}) presumed to be the *cis* isomer as this transition is not allowed in the *trans* form due to symmetry rules.[241] The *trans*-azo dye isomerises to the *cis*-isomer by irradiation at short wavelengths.[242] This is a reversible reaction as the *trans* isomer can be recovered by irradiation at a longer wavelength or by heating. Absorption peaks corresponding to both isomers are evident thus it is concluded that a mixture of *trans* and *cis* isomers are present.[242] Photochemical interconversion may be present in this system, however it was assumed that the H_2O_2 would complex in preference to the urea moiety and not the azo moiety. Therefore the inversion and rotation of the azo functionality is irrelevant so long as the compound remains delocalised. Furthermore there are possible transitions that originate from the carbonyl π and non-bonding electrons and the nitrogen non-bonding electrons, although as these are higher energy transitions they are found in the UV region at 232 and 203 nm respectively (Fig. 4.32).

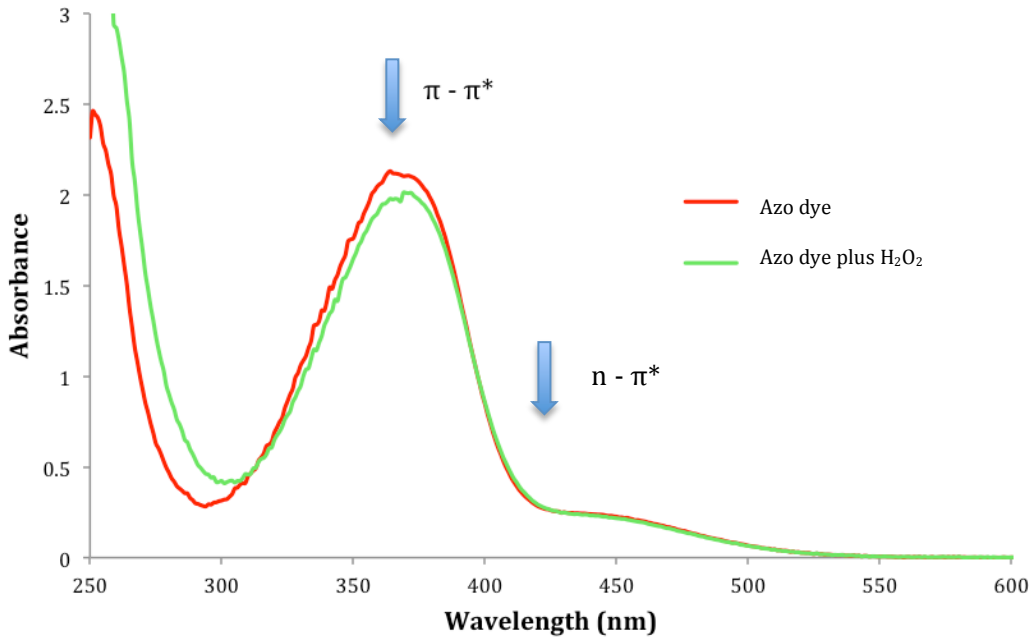

Fig. 4.31. UV-vis absorption spectrum of compound **15** (1.27 x 10^{-4} M) and **15** plus 100 µl THF:H_2O_2 (0.99 M) in THF. Sample discarded after single use.

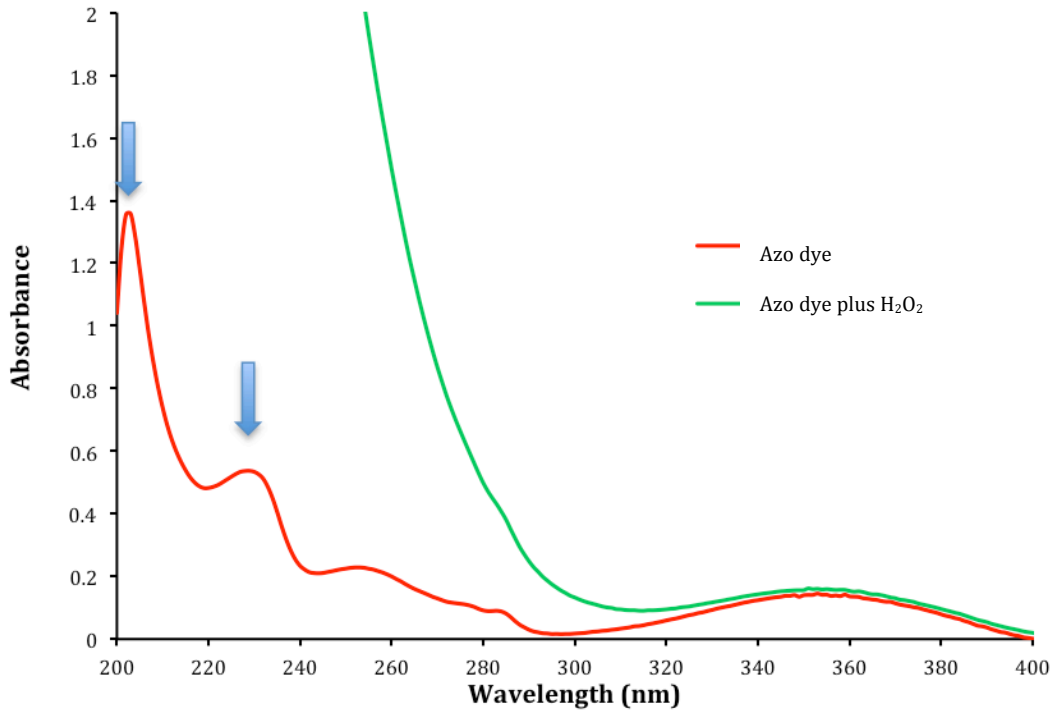

Fig. 4.32. UV-Vis absorption spectrum of compound **15** (red) and **15** plus an excess of H_2O_2 from 400 – 200 nm in THF. Sample discarded after single use.

In an attempt to demonstrate that H_2O_2 has a significant effect on the colour of the dye, an adduct was prepared using the THF:H_2O_2 method, assuring to saturate it with H_2O_2. Following removal of the solvent, the originally yellow solid became bright orange (Fig. 4.33) and also showed a new IR peak at 2789 cm^{-1} suggestive of H_2O_2 binding. The orange solid returned to yellow after two days standing at room temperature, showing a non-destructive and equilibrium-like process. Despite the fact that a colour change is evident, how the colour change arises remains unknown. This naked-eye colorimetric detection only occurs when the solid was isolated and not in solution suggesting that the interaction must be forced. This experiment suggests adduct formation is occurring but it provides no data as to where binding has occurred.

Fig. 4.33. Azo dye **15** (right) and azo dye **15** with H_2O_2 (left).

To commence a more detailed assessment, a visible spectrophotometric titration was performed on **15** (1.27×10^{-4} mol L^{-1}) from 700–390 nm in THF. Subsequent aliquots of a THF:H_2O_2 (0.99 mol L^{-1}) solution were added and a spectrum recorded at each titration point (16 – 140 mM).

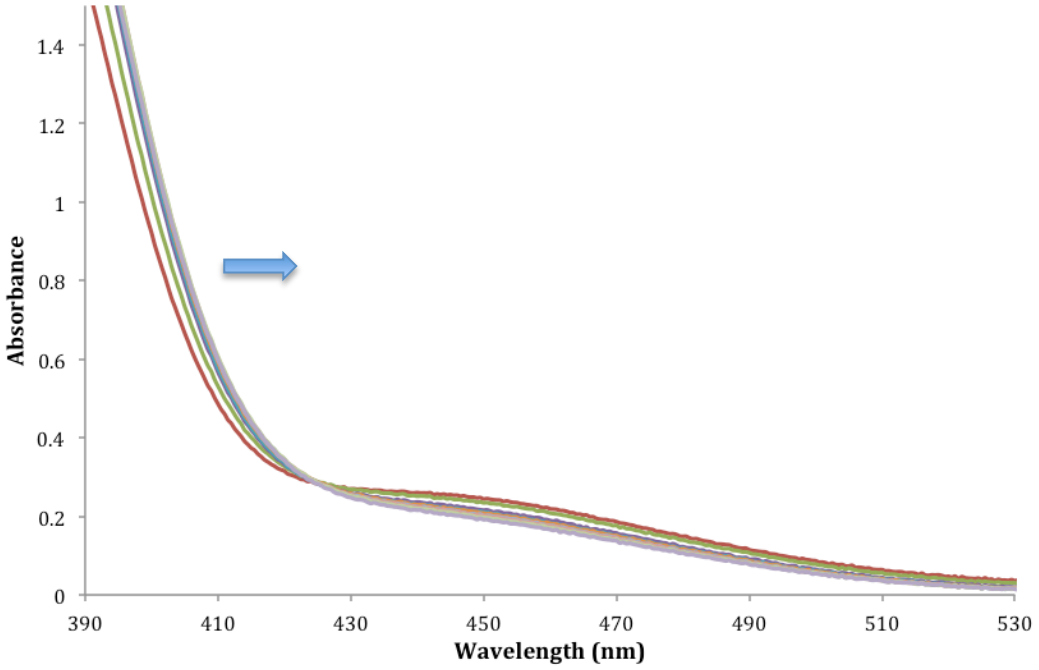

Fig. 4.34. UV-vis absorption spectrum of compound **15** (1.27×10^{-4} M) and **15** plus THF:H_2O_2 (0.99 M) from 16 – 140 mM in THF. Direction of arrow indicates increasing concentration of THF:H_2O_2.

From these results it can be proposed that a slight red shift of the large peak at 364 nm is observed due to the shift of the tail end of the absorption peak (Fig. 4.34). Consequently this tail end moves into the visible region therefore is absorbing in the violet to blue region. This could account for the transmission of a more orange colour. This is arguably the result of a change in energy of the π-π* transition of the carbonyl through interactions with H_2O_2. However, it could

also be a consequence of the change in π-π* of the azo moiety. As was established earlier, the carbonyl absorption peak is at much higher energy, therefore it could only affect this system through changes in delocalisation. Ultimately, as this displays only a minimal bathochromic shift it might simply be the result of solvent effects. Addition of hydrogen peroxide increases the polarity of the solvent which stabilises the π* excited state. Unlike the anion binding examples[87,212,239,243-245], this is a non-specific interaction as opposed to a precise interaction in complexation or adduct formation. A small hyperchromic effect associated with the n-π* transition in the azo moiety at 435 nm was also observed, which can also be linked to polarity and solvent effects.

An alternative chromophore was attached to the urea moiety (**77**) in the hope of forming a more sensitive hydrogen peroxide receptor. Napthalimide sensors are strongly coloured with a λ_{max} of 415 nm recorded for the free sensor (**77**) in DMSO.[131] Using an aprotic solvent the dye was tested by colorimetric visualisation in THF. The initial colour was yellow and on addition of THF:H_2O_2 remained yellow. In contrast, adding aqueous NaOH caused an immediate colour change to purple/red that returns to yellow on addition of acid. After the addition of H_2O_2 to a new sample of **77** it takes significantly more NaOH to visualise a colorimetric change. This is perhaps not surprising as H_2O_2 has a lower pK_a and is likely to be deprotonated before the substituted urea. Just as previously, addition of a small amount of acid returns the solution to the original yellow colour.

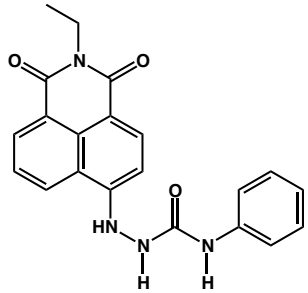

Fig. 4.35. Compound **77**. (Synthesis given in Experimental Section 2.6)

Analysis of the spectral changes by UV-visible spectroscopy was able to demonstrate these changes in terms of changes in electronic transitions. In

particular, as the N-H is incorporated in the chromogenic subunit, the negatively charged anion, or in the present case hydrogen bonding, modifies the dipole associated with the charge-transfer transition leading to changes in the absorption spectra.[246] In THF the extinction coefficient was determined to be 10,225 $M^{-1}cm^{-1}$ for the charge-transfer transition for which it had a λ_{max} of 386 nm (Fig. 4.36).

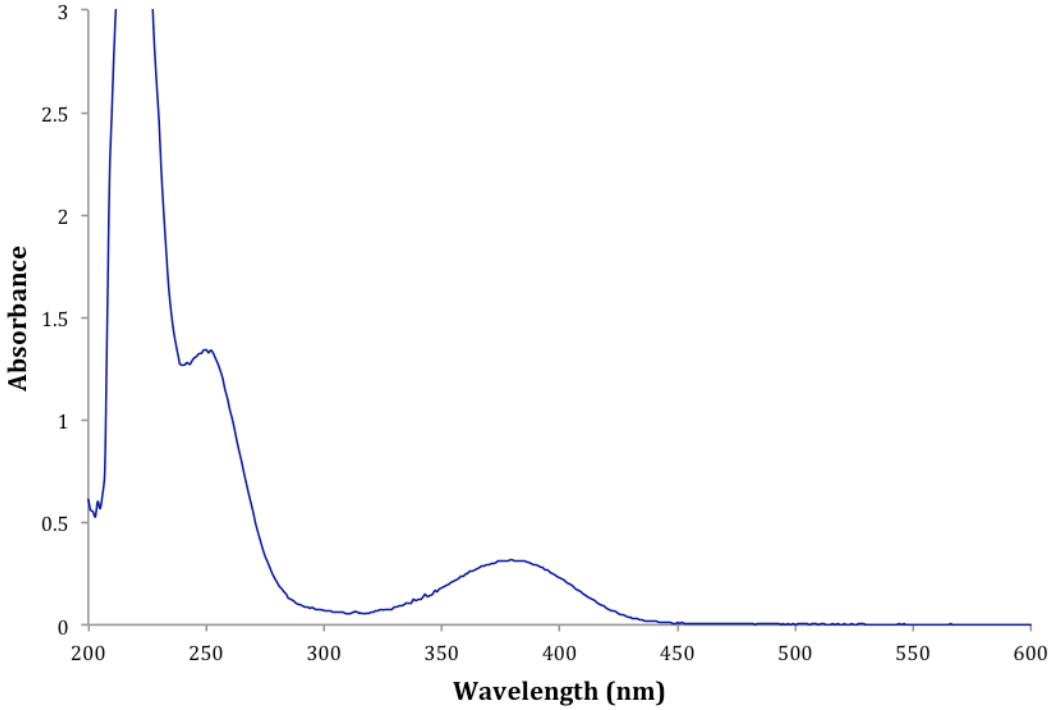

Fig. 4.36. UV-vis absorption spectrum of compound **77** (0.03 mM) in THF.

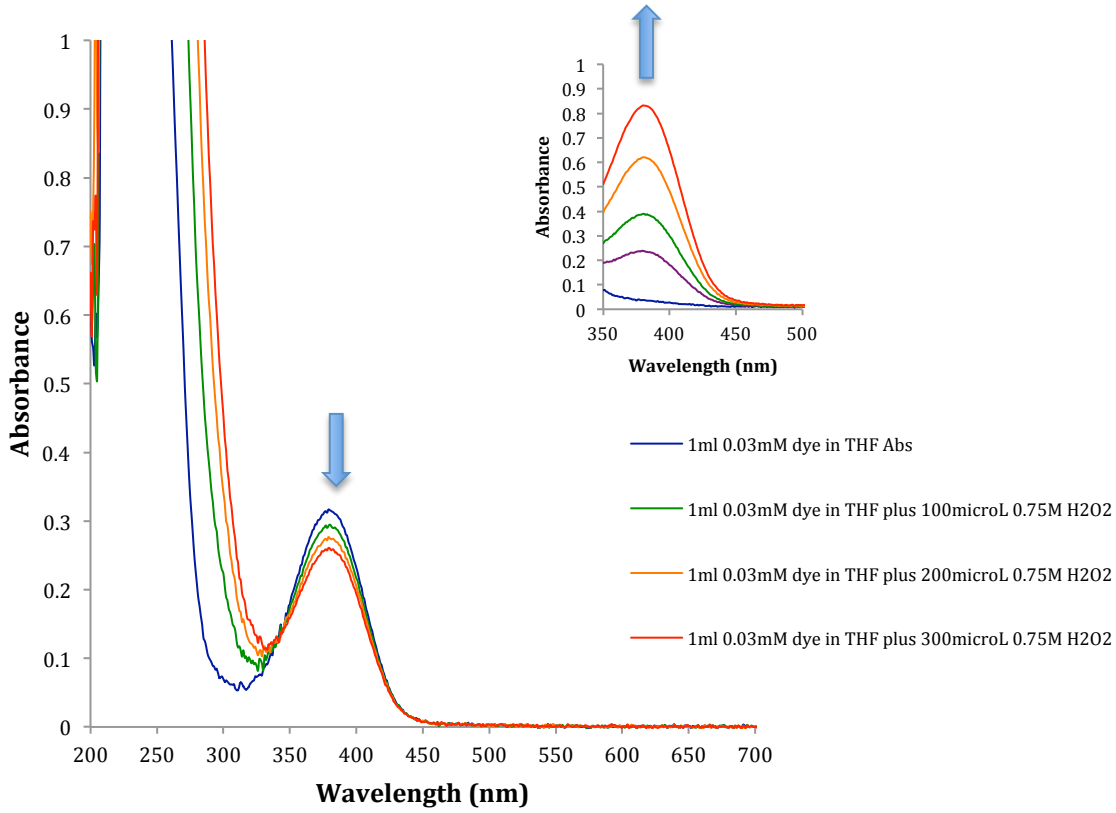

Fig. 4.37. UV-vis absorption spectrum of compound **77** (0.03 mM) in THF with aliquots of THF:H_2O_2 (0.75 M) from 0 – 7500 equivalents (Arrow is increasing aliquots). Inset: 1 ml 0.75 M THF:H_2O_2 with 5, 10, 15 20 µL (3.4 mM) dye. (Arrow indicates increasing dye).

Further analysis of these spectral changes demonstrates that the charge-transfer absorption band has not significantly changed and its reduction in intensity is directly due to dilution factors (Fig. 4.37). In comparison, upon addition of 2 M NaOH two new bands arose centred at 353 and 515 nm (Fig. 4.38). This was accompanied by the collapse of the λ_{max} band at 386 nm. Subsequently, the addition of H_2O_2 and NaOH to the napthalimide dye also exhibited a similar collapse, and the peak at 515 nm seen in NaOH alone, was slightly red shifted to a longer wavelength band at 530 nm. This observation has been recognised for various other napthalimides and other urea-based sensors where, if the added anion is sufficiently basic, it will deprotonate the acidic urea proton.[131,239,243,247] This result suggests that hydroxide is responsible for deprotonation of one N-H in the substituted urea moiety. However, unlike titration with fluoride or excess hydroxide as described in the paper by Esteban-Gomez *et al.*[246] with a

napthalimide derivative, the second deprotonation does not occur as the absorption band at a longer wavelength (~600 nm) is absent.

$$LH_2 + OH^- \rightleftharpoons [LH]^- + H_2O \qquad 4.20$$

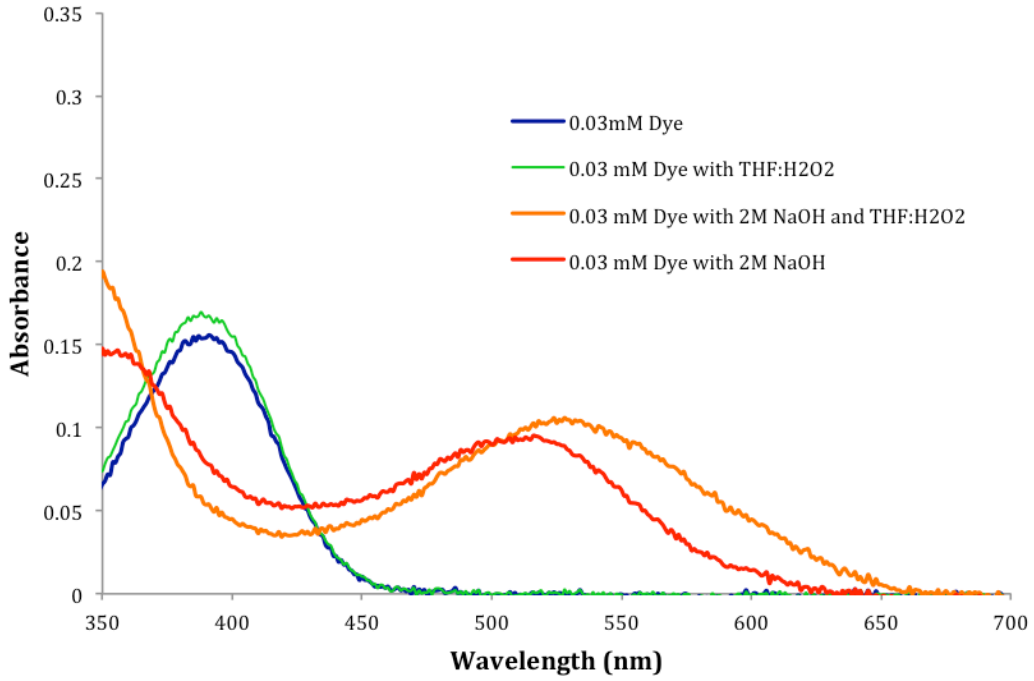

Fig. 4.38. UV-vis absorption spectrum of compound **77** (0.03 mM) in THF with the addition of THF:H_2O_2 (0.75 M), 2M NaOH and THF:H_2O_2 and 2M NaOH. Where L is the napthalimide ligand.

Solvent–solute interactions influence the stability of $[LH]^-$. As hydroxide does not deprotonate the second N-H in the presence or absence of H_2O_2, it suggests that the solvent is stabilising the $[LH]^-$ in instead of forming the unstable dianion $[L]^{2-}$. However, the bathochromic shift in the presence of hydrogen peroxide indicates secondary hydrogen bonding, suggesting that HO_2^- binds to the dye in a unique manner in which it is unable to achieve in the absence of base. By taking the above results into consideration, it is unlikely that a binding constant for H_2O_2 with compound **77** can be evaluated.

Molecular Behaviour:
Molecular interactions of the regeneration catalyst

4.3 Introduction

Chapter 3 discussed the synthesis of compounds containing the TEMPO subunit and related nitroxides. TEMPO has attracted significant attention over the past decade given its ability to undergo one-electron oxidation and reduction to give the oxoammonium and hydroxylamine species respectively. Similarly, the interconversion of TEMPO derivatives is well known and is the basis for many applications. In addition to redox coupling, many nitroxides undergo disproportionation to the corresponding hydroxylamine and nitrone. TEMPO does not spontaneously undergo disproportionation as the α-methyl groups protect the radical. Instead protonation is required before disproportionation will occur. This produces the hydroxylamine and *N*-oxoammonium cation (Scheme 4.6). The kinetic profile and disproportionation of TEMPO has been thoroughly studied in recent years, in particular in acidic conditions.[248,249]

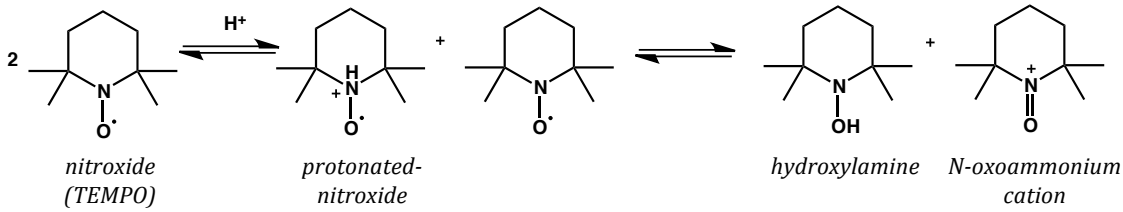

Scheme 4.6. Acid-catalysed disproportionation of TEMPO.

In the acid-catalysed disproportionation of TEMPO, the rate-determining step is the electron transfer from TEMPO to the protonated nitroxyl.[250] In highly acidic conditions the rate of comproportionation (k_{-1}) is negligible in comparison to k_1, however on neutralisation of the products, a near quantitative amount of the starting radical is possible pushing the equilibrium to the left (Scheme 4.7). The efficiency of this reverse reaction is dependent on the stability of the hydroxylamine and oxoammonium cation.

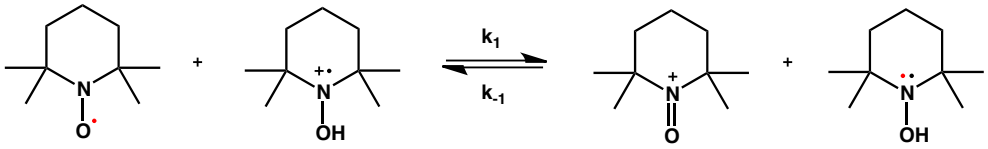

Scheme 4.7. Equilibrium denoting decomposition (k_1) and comproportionation (k_{-1}).

Golubev has proposed decomposition or auto-oxidation of oxoammonium salts in neutral media (Scheme 4.8).[251] Although the investigation involved the 4-oxo-TEMPO species, the initial mechanism involves the same principles allowing similarities to be drawn with TEMPO. The hydrolysis of the *N*-oxoammonium salt to form TEMPO and a hydroxyl radical is presumed to use a hydroxide ion as the reducing agent.

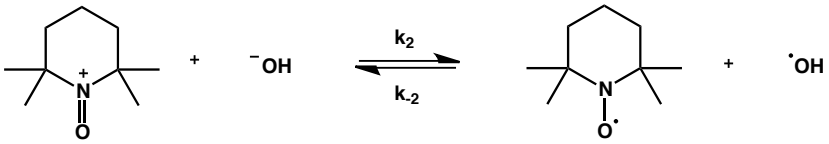

Scheme 4.8. Oxidation of hydroxide ion with oxoammonium salt.

The equilibrium constant calculated from using the reduction potentials (Eq. 4.20) of the oxoammonium cation (0.75 V)[158,252] and the hydroxy radical (1.89 V)[253] is very small (Eq. 4.21).

$$E_{cell} = E°_{cell} - (RT/nF)\ln K \qquad 4.20$$

$$K_1 = \frac{k_2}{k_{-2}} \approx 5 \text{ x } 10^{-20} \qquad 4.21$$

This implies that the electron transfer from the hydroxide ion to the oxoammonium cation is negligibly small. An alternative mechanism suggests the formation of an intermediate hydroperoxide species. This involves a nucleophilic attack on the electronegative nitrogen, as opposed to the oxygen to form a reactive complex.[254,251] On further reaction with hydroxide and comproportionation with a second oxoammonium cation, the nitroxyl radical is re-formed along with hydrogen peroxide (Scheme 4.9). Comproportionation is

pH-dependent and the reaction occurs quickly in neutral and basic media and more slowly in acidic solutions. Although this is a potential mechanism of the decomposition of oxoammonium salts in basic media, it has yet to be supported experimentally.

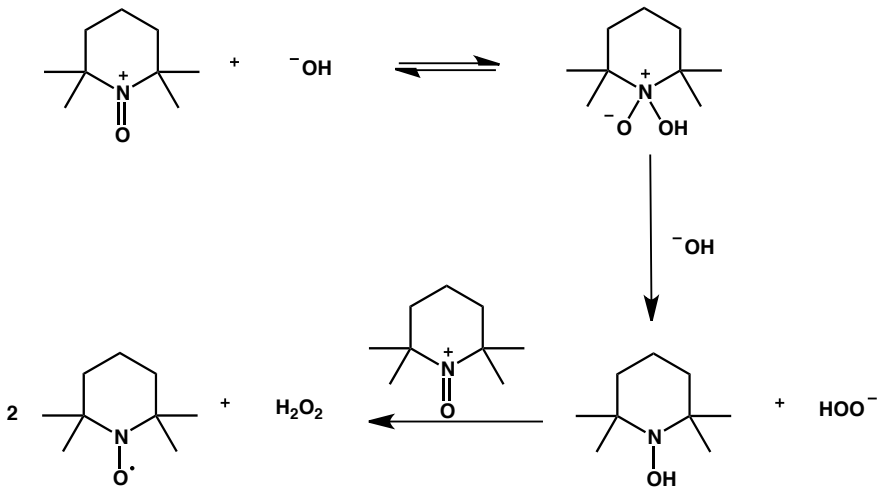

Scheme 4.9. Alternative mechanism to the oxidation of hydroxide ions with an oxoammonium cation.

In either case, the reaction of the oxoammonium cation with hydroxide ions yields the nitroxide and hydrogen peroxide. This is the focus of the present investigation. To further confound this complicated system, H_2O_2 can be oxidised by the oxoammonium cation in neutral and alkaline media (Scheme 4.10). Evidence for this was obtained electrochemically where the oxoammonium salt was embedded in a carbon paste electrode and oxidised H_2O_2 under anodic conditions.[255] This further reduces the amount not only of oxoammonium catalyst available but measureable H_2O_2 in the system.

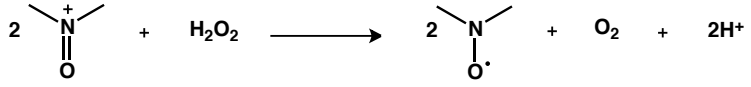

Scheme 4.10. Potential side reaction where hydrogen peroxide is oxidised by an oxoammonium cation.

The kinetic and thermodynamic stability of TEMPO and its derivatives is not solely controlled by disproportionation. Nitroxides are able to abstract a hydrogen atom from molecules with labile hydrogen to form the corresponding hydroxylamine. In contrast this N-OH species has a low bond dissociation of 299.2 kJ mol^{-1}, thus the O-H bond can be easily abstracted to reform the nitroxide. This is the basis for antioxidant applications as abstracting this hydrogen can quench reactive radicals, leaving a less reactive nitroxide radical in its place.

Hydrogen abstraction involved in the hydrogen atom transfer process between two similar molecules can be described as either a one-step, concerted electron transfer process (CEP) or a two-step process consisting of electron transfer (oxidation/reduction) and protonation (Scheme 4.11). In the case of self-exchange, these reaction pathways can be differentiated by pK_a and redox potential to ultimately give the same product.

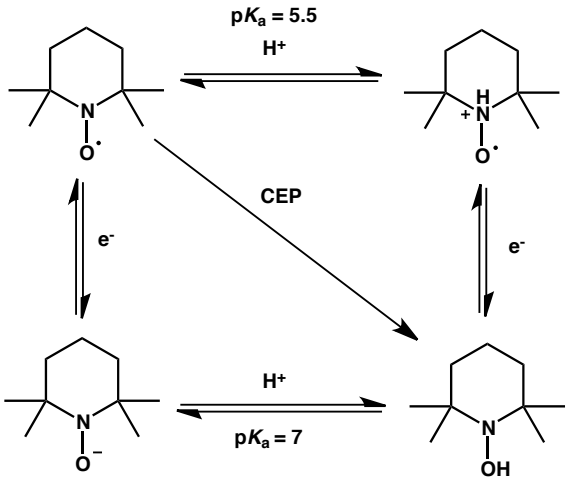

Scheme 4.11. Hydrogen abstraction by concerted electron transfer (CEP) or by oxidation/reduction and protonation.

In a thorough practical and computational study on the hydrogen-atom transfer between TEMPO compounds, it was established that transfer predominantly proceeds through CEP.[256] Intermediate states, TEMPO- and TEMPO-$H^{\bullet+}$, have potentials higher than the Erying barrier $\Delta G^{\ddagger}$ < 84 kJ mol^{-1} therefore are energetically unfavoured pathways. The kinetics of this exchange were

demonstrated through pseudo-self-exchange of two different TEMPO derivatives. For the reaction of TEMPO-H and 4-oxo-TEMPO•, activation energies and H/D kinetic isotope effects suggest tunnelling is important for exchange.[256]

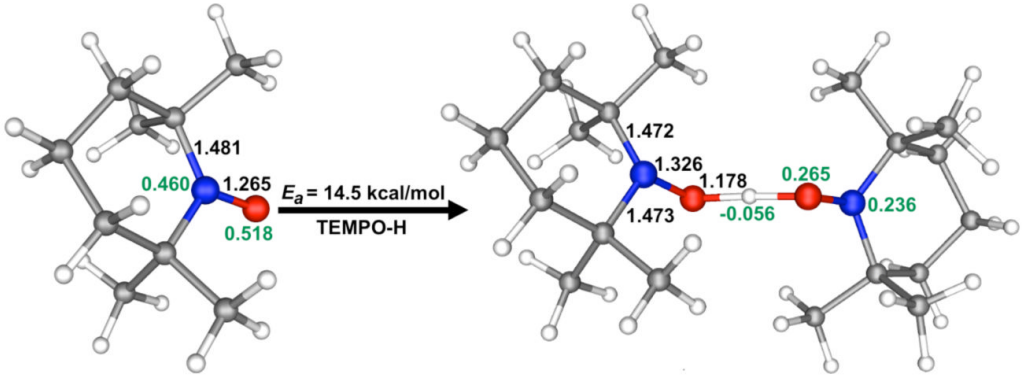

Fig. 4.39. Activation energies (61 kJ mol^{-1}) for TEMPO, and the transition structure for hydrogen self-exchange (HAT) with the corresponding hydroxylamine. Reprinted with permission from Wu.[256] Copyright 2009 American Chemical Society.

Fast electron exchange can also occur between TEMPO and the oxoammonium cation (Scheme 4.12). This exchange occurs more rapidly than the NMR timescale leading to significant broadening and absence of some peaks in the ^{13}C NMR spectra.[249] Ma *et al.* observed this exchange through different signal intensities in EPR. The oxoammonium cation is EPR silent, however in the presence of a small quantity of TEMPO a signal can be seen in a dilute oxoammonium solution. As the concentration of oxoammonium cation increases so this signal significantly broadens and decreases in height as a result of the electron exchange.[249]

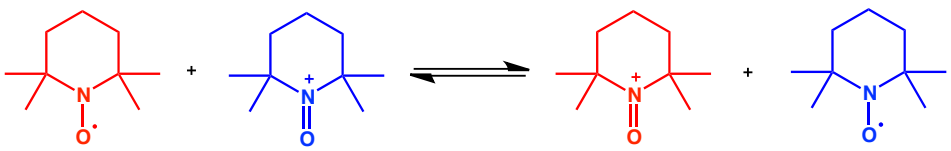

Scheme 4.12. Fast electron exchange between TEMPO and the oxoammonium cation.

Furthermore, the rate constant of this exchange is dominated by solvent dynamics. A 'friction' effect controls the longitudinal relaxation time of the solvent thereby perturbing the observed rate constant in this adiabatic system.[161]

Thermal decomposition of TEMPO at 150 °C is possible in solvents that have H-donating capacity. This reduces the nitroxide to a hydroxylamine and an amine. Whereas in solvents that lack H-donating capacity, TEMPO is stable until higher temperatures (>230 °C) where hydrogen abstraction then becomes dominant. TEMPO is able to abstract a hydrogen atom from another TEMPO molecule followed by fragmentation to give a methyl radical and the corresponding nitroxide (Scheme 4.13).

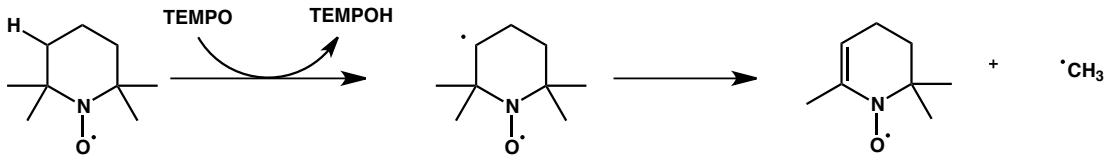

Scheme 4.13. Abstraction of hydrogen from TEMPO at high temperatures.

Since the present work does not involve elevated temperatures, this type of mechanism can be ruled out. However, in TEMPO-derived compounds additional substituents on the piperidine ring may alter the basicity of hydrogen, making this H-abstraction process more significant.

It is clear that TEMPO derivative systems are complex, as various reactions and equilibriums exist between all associated species. This project does not set out to identify the mechanisms and kinetics of the proposed system, however it did require knowledge of the range of potential pathways. The following section outlines preliminary studies into the complexity associated with oxidation of nitroxides and the molecular dynamics of the oxoammonium catalyst in solution.

4.4 Results and Discussion

4.4.1 Oxidation of complex nitroxides

Progressing from the initial objectives, outlined in Section 3.61, to use a hydrophobic form of TEMPO (**42**) to oxidise hydroxide ions in a biphasic system, the oxidised form of the alkylated-TEMPO was required. This oxidation of nitroxide **42** to the oxoammonium cation **43** proved to be more challenging than first expected. In contrast to the simple oxidation of TEMPO, which produced one clear product, oxidation of **42** formed multiple products.

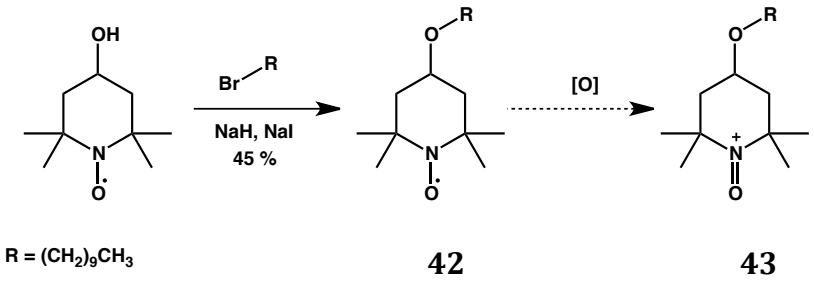

Scheme 3.13. Alkylation followed by oxidation of 4-hydroxy-TEMPO.

Initially the alkylated TEMPO was oxidised with Br_2 in a hexane and DCE mixture in accordance with the procedure outlined in Section 3.6.1, resulting in the formation of a dark brown sticky oil, which was problematic to work with. Mass spectrometry (ESI) of the salt showed a larger proportion of the peak at 312 m/z in comparison to the radical and hydroxylamine forms at 313 and 314 m/z respectively. Although **42** and **43** have the same mass, the difference is that **42** must be protonated in order to become a charged species and traverse the mass spectrometry chamber to the detector. Compound **43** is already charged and therefore will remain as the initial molecular mass. Although this is inclusive due to the possibility of oxidation of both the nitroxide and hydroxylamine in the spectrometer, the increase in the relative intensity of the oxoammonium peak (312 m/z) peak compared to that observed in the starting material supports the formation of desired product. Analysis of the ^{1}H NMR spectrum was in accord with the formation of **43**; the peaks had sharpened suggesting the sample was no longer paramagnetic (Fig. A4). However, at room temperature the molecule

appears to exist in two conformations as indicated by the appearance of two distinct sets of methyl peaks (four methyl peaks in total). As the ring is a saturated heterocycle, axial and equatorial substituents give rise to non-equivalent protons. The 6-membered ring can exist as two inter-convertible conformations.[257] While it could be assumed that **43** exists in two different chair conformations, this seems unlikely, as one would place the bulky alkyl group in an axial orientation giving rise to destabilising 1,3-diaxial interactions with the methyl groups. An alternative is that a boat-like conformation is accessible and this maintains a pseudo-equatorial alkyl chain (Scheme 4.14).

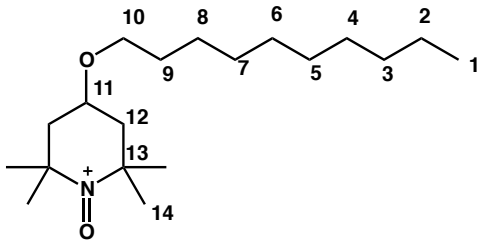

Fig. 4.40. Numbering system for oxoammonium **43**.

It is evident by correlation with ^{13}C, COSY, DEPT 135 and HMQC NMR spectral data in $CDCl_3$, that there are 4 methyl peaks (*14*-C*H*$_3$) (Fig. A4). Integration of the data suggests these peaks are attributable to each axial and equatorial orientation of both conformations. There is slight ambiguity concerning the alkyl chain, as it appears both conformations have similar chemical shifts. ^{13}C NMR of (**43**) shows the presence of two similar compounds, although only one set of alkyl peaks from carbons 1-7 (Fig, 4.40). It is proposed that at room temperature the alkyl chain is able to rotate in both conformations, so an average peak is observed for these carbon and proton peaks. As the temperature is increased the ring system can undergo ring-flipping. When the temperature was increased to 50 °C no coalescence was seen for the ring substituents. As the $CDCl_3$ solvent has a relatively low upper temperature limit, d_6-DMSO was utilised for wider temperature range studies.

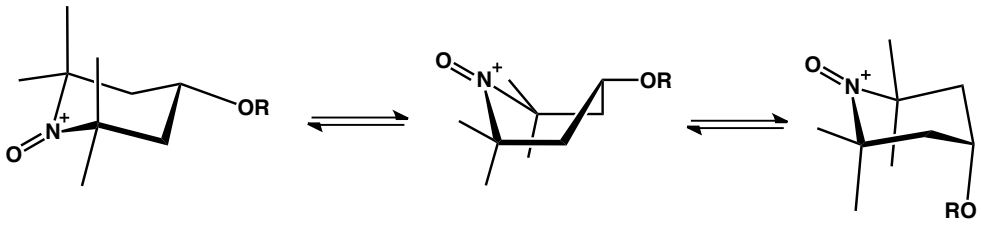

Scheme 4.14. Ring-flipping equilibrium through a boat conformation intermediate. Hydrogens omitted for clarity.

Oxidation of the alkyl-TEMPO radical (**42**) with bromine produced two distinct products consistently in a 1:1 ratio when analysed by ^{1}H NMR in d_6-DMSO (Fig. 4.41). These two compounds differ dramatically in chemical shifts for the methyl peaks, however the alkyl chain peaks remains similar. One set of axial and equatorial methyl peaks is between 1.60–1.65 ppm whereas the second set is downfield at 2.45–2.63 ppm. In contrast to the previous results, these peaks appear to differ considerably to the two compounds thought to be related by ring-flipping. Also, two extra doublets at 4.27 and 4.07 ppm would suggest deshielding of the internal ring CH_2 protons, which are correlated to the downfield methyl peaks by 2D COSY. Attempted purification and separation of the two compounds using column chromatography, recrystallization, salt metathesis and two-solvent precipitation all failed. It is proposed that the products were the oxoammonium salt and the protonated hydroxylamine species.

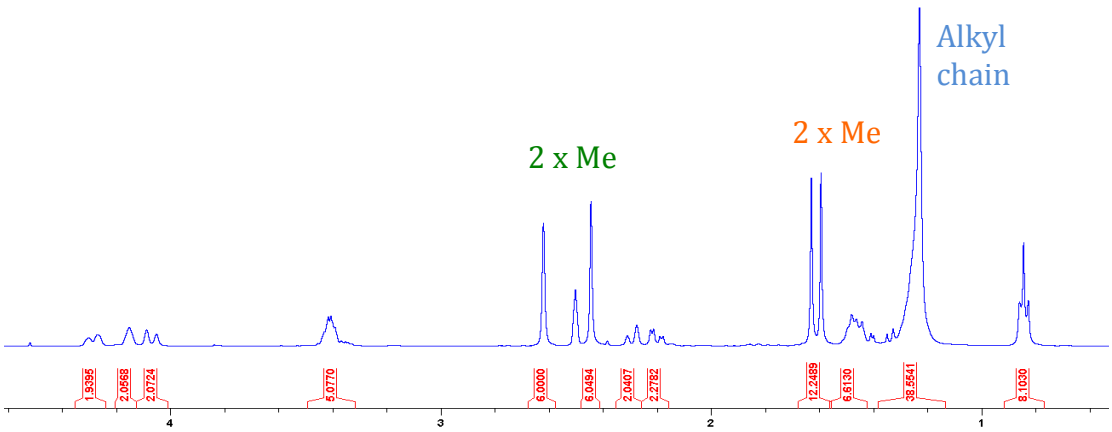

Fig. 4.41. ^{1}H NMR of compound **43** in d_6-DMSO.

In an attempt to identify the new species, the alkylated radical was reduced to either the hydroxylamine with ascorbic acid or was fully reduced with $SnCl_2$ to

give the amine. Comparison of the NMR spectra of these compounds with the spectra of the mixture showed no correlation (Fig. A5). Addition of trifluoroacetic acid (TFA) protonated both species for further comparison. Despite the fact that protonation shifted the protons associated with the piperidine ring downfield, the spectra did not correspond to the unknown species in the oxidised compound. If it is assumed that one of the sets of methyl peaks corresponds to the oxoammonium, the second species which is always present in a 1:1 ratio does not correspond to any of the remaining 5 options (Fig. 4.42, Left). This raises further questions as to which is the correct identification of the oxoammonium species in the original experiments analysed in $CDCl_3$.

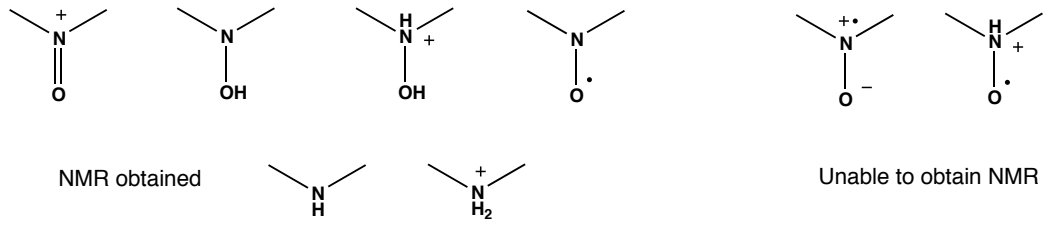

Fig. 4.42. Different possibilities of the unknown species seen in the oxidation of **42**. NMR obtained species compared in A5.

Potential alternative side products arising from substitution of the bromine onto the alkyl chain or onto the ring have been dismissed. A product with a higher mass indicating the substitution of single bromine at 391 *m*/z was absent in MS thus confirming the unlikeliness of this pathway to occur either on the alkyl chain or on the ring.

The possibility of a ring opening process to give a nitroso (N=O) moiety and a positively charged carbocation is thought to be unfavourable although possible.[249] Ma *et al.* observed a small amount of degradation products after heating to 100 °C, therefore it seems unlikely that this degradation pathway is operating in the present case.

Subsequent to the above analyses reports that the oxoammonium salt was capable of oxidising DMSO were located.[258] The products of the reaction have not been identified, however this may account for the additional peaks seen only in this solvent.

There was a possibility that the oxidation reaction caused the displacement of the alkyl chain by S_N2 substitution with bromide at the α-alkyl carbon 10 (Fig. 4.40). To eliminate this possibility, the *t*-butyl ester analogue **78** was synthesised, as this molecule should be incapable of following this decomposition pathway (Scheme 4.15).

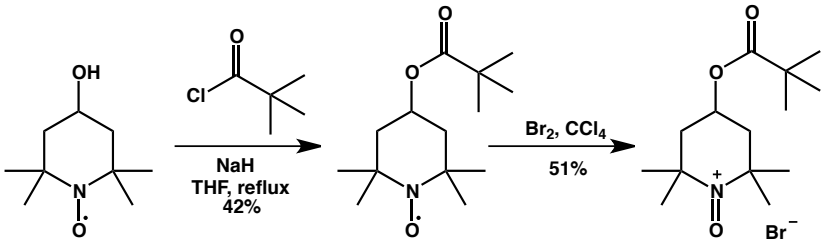

78 **79**

Scheme 4.15. Nucleophilic addition of 4-hydroxy-TEMPO to give nitroxide **78**. Oxidation with bromine in CCl_4 to give oxoammonium cation **79**.

Unlike the alkylated derivative **43**, oxidation of **78** with bromine gave a dark orange precipitate. However, upon addition of 0.75 and 3 equivalents of bromine, ^{1}H NMR again shows that two sets of methyl peaks remain in a 1:1 ratio. This confirms that neither of the as yet unidentified products were the consequence of ether cleavage; unfortunately this does not assist with the confirmation or identity of the compounds.

As many species of TEMPO derivatives are in equilibrium with each other, the presence of two compounds might not be an issue and a reaction may well shift the equilibrium to favour formation of the oxoammonium cation. To test this hypothesis, the 1:1 mixture of compounds **79** was reacted with one equivalent of benzyl alcohol (Scheme 4.16). It was assumed that the oxoammonium salt would

oxidise this alcohol.[144,162,254,259] If this were so then a decline or removal of the peaks associated with the oxoammonium cation would be expected as it oxidises the benzyl alcohol to benzaldehyde. Surprisingly, 80% of the benzyl alcohol was converted to the aldehyde, despite the starting reagent consisting of a 1:1 mixture of two compounds. Furthermore, the mixture of two compounds was converted into a third distinct species whose ^{1}H NMR bore a resemblance to the spectrum of the protonated hydroxylamine species (+NH-OH). This suggests that the two unknown compounds are either 1) in equilibrium with the oxoammonium species which causes the oxidation, or 2) they are both oxidants that give a common by-product upon oxidation of benzyl alcohol. Of some concern, this also suggests that the unknown species are simply the result of oxidation of DMSO when analysed by NMR, and the original product was in fact the oxoammonium salt.

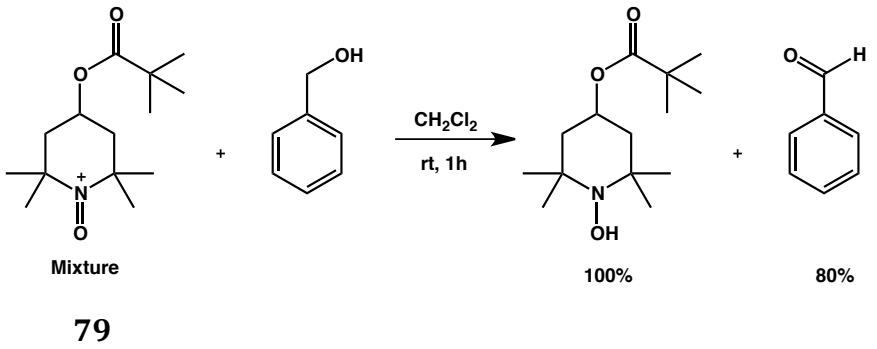

79

Scheme 4.16. Unidentified mixture of oxoammonium salt **79** oxidising benzyl alcohol to benzaldehyde.

In an analogous reaction, oxoammonium salt **43** was reacted with one equivalent of benzyl alcohol (Scheme 4.17). In this instance only 28% of the benzyl alcohol was converted to the aldehyde. As almost all of the oxoammonium mixture had been converted into a third species, it shows strong evidence that a side reaction was occurring. Nitroxide disproportionation is well-known under acidic conditions, while the reverse process, comproportionation of an oxoammonium and hydroxylamine species, occurs under neutral conditions. Thus it is possible that the oxidation of benzyl alcohol

forms the hydroxylamine that can then undergo comproportionation with the reactant. This would reduce the amount of active reagent in solution and cause the low yield.

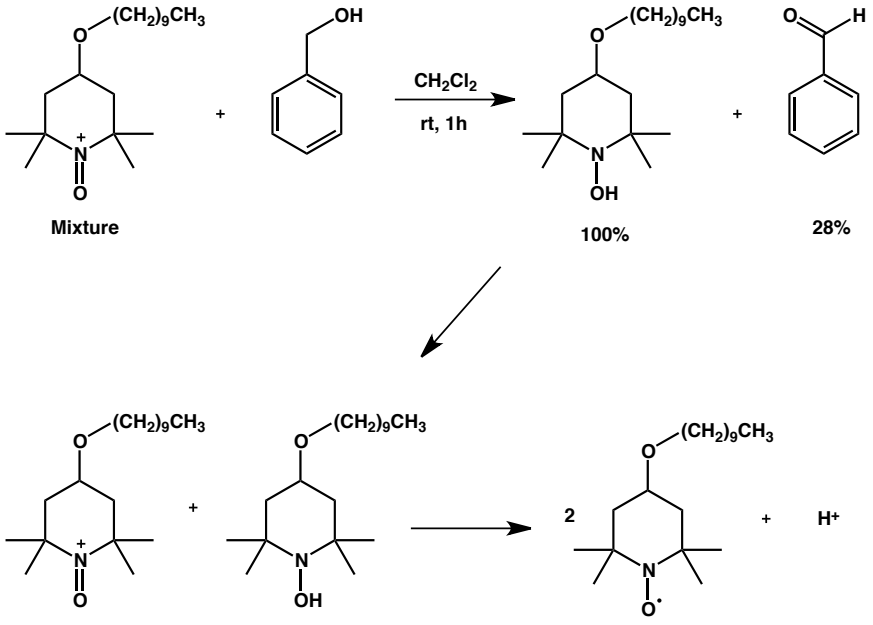

Scheme 4.17. Oxidation of benzyl alcohol with oxoammonium salt **43**. Potential comproportionation of the hydroxylamine product with a second oxoammonium cation.

The ultimate objective for this initial stage in development of the catalyst for recharging of the New Cathode only requires stoichiometric amounts of material to oxidise a hydroxide ion to form hydrogen peroxide. The requirement to fully identify and characterise the multi-compound product is unnecessary, and due to the complexity is a large project worthy of a separate study. As the mixture is able to oxidise the benzyl alcohol, it is assumed here that it is a catalytically active material, despite not having established its exact composition.

4.4.2 Biphasic system to quantify hydrogen peroxide production

A biphasic system has been proposed as a method to quantify the amount of hydrogen peroxide generated from the oxidation of hydroxide ions. Many

biphasic systems are based on H_2O_2 as the catalyst such as the hydroxylation of benzene to phenol in an aqueous and ionic liquid system.[260] The two phases consist of an organic layer and a basic aqueous layer. As shown in Chapter 3.6.1 the oxoammonium salt can give a false positive reading when trying to identify the presence of H_2O_2. This biphasic system separates the organic catalyst from the hydrogen peroxide to allow for unambiguous detection. The hydrophobic alkylated oxoammonium salt **43** is assumed to reside entirely in the organic CH_2Cl_2 layer (5 ml) where the amount of material can be controlled between experiments. It was imperative that a solvent with low hydrogen-donating ability was used to limit potential abstraction of a hydrogen atom as a side-reaction (as in Scheme 4.13). Ideally, the solvent should have a higher density than water to facilitate the simple removal of aliquots of the aqueous phase for analysis. Although CH_2Cl_2 is relatively volatile, it is one of the few solvents that does not form mixtures with water hence it can be assumed that a well-defined separation between the layers will be maintained. In this biphasic set up, the aqueous layer and source of hydroxide ions was a 2 M NaOH solution (5 ml). *Tert*-butylammonium hydroxide (TBAH) (0.5 ml of a 60% v/v solution) was employed as a phase transfer catalyst (PTC) to assist with the passage of hydroxide ions into the organic layer where it was anticipated that they would be oxidised to form hydrogen peroxide. The use of a PTC accelerates the reaction by allowing greater mixing of substrate (OH^-) and reagent (**43**). The two-phase approach used in this experiment is analogous to that found at the surface of an electrode (Fig. 4.44). The interface formed at the liquid-liquid boundary was used here to mimic that of a solid-liquid boundary in an electrode. To maximise the interfacial area the solutions were vigorously stirred and shaken.

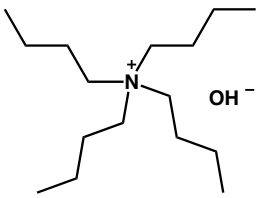

Fig. 4.43. *Tert*-butylammonium hydroxide, TBAH.

The mechanism for the one-electron oxidation of hydroxide is unknown, although several competing theories have been proposed. The first involves direct electron transfer from the hydroxide ion to the oxoammonium cation.[251] The resulting hydroxyl radical then dimerises to form a new oxygen-oxygen bond and thus hydrogen peroxide (Scheme 4.18). The low equilibrium constant and the short half-life of hydroxyl radicals cause great concern for its validity.

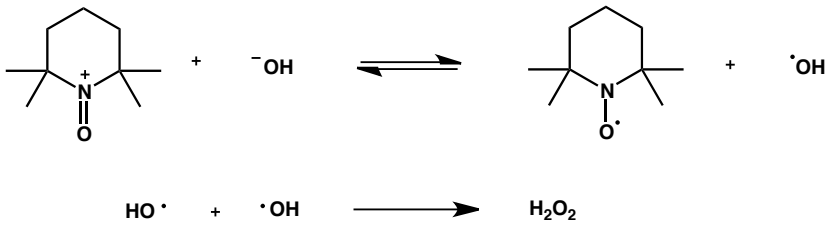

Scheme 4.18. Oxidation of hydroxide ions with an oxoammonium cation followed by dimerisation of two hydroxyl radicals forms H_2O_2.

The second proposed mechanism involves is the nucleophilic attack of the hydroxide to form the hydroperoxide intermediate followed by loss of hydroperoxy anion (Scheme 4.9).[251,254] A second equivalent of oxoammonium is required to comproportionate with the hydroxylamine to give the nitroxide radical and H_2O_2. As both mechanisms involve 2 equivalents of oxoammonium salt and hydroxide, they have identical stoichiometry. Ultimately, when the catalyst is bound onto an electrode surface, it is effectively stationary thus comproportionation will not be able to occur. Mechanism 2 may therefore require a larger oxidising potential to reform the oxoammonium cation from the hydroxylamine species rather than the 1 electron process from the nitroxide radical. However as these initial experiments are performed in solution it needs to be considered as a potential pathway.

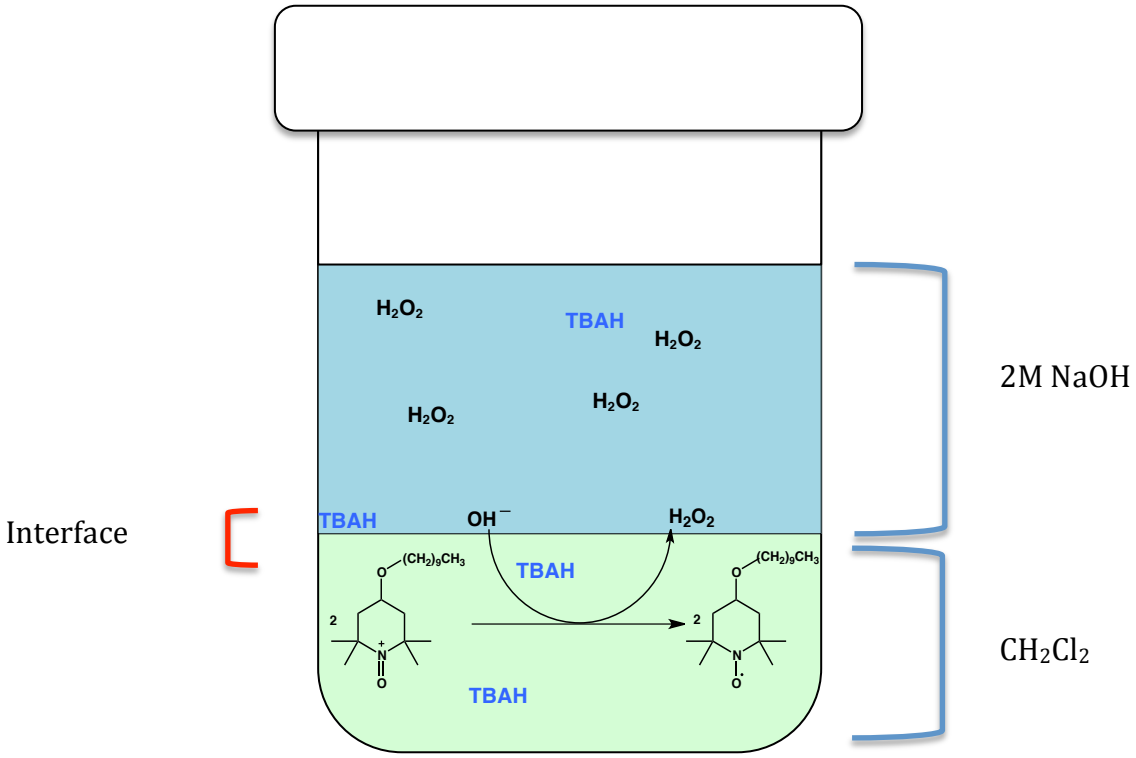

Fig. 4.44. Illustrative representative of the biphasic experiment set up.

This experiment was intended to be a 'proof of concept' and qualitative only; few attempts were made to minimise or limit many sources of error. The assumptions made in this experimental design included:

- Oxoammonium **43** is insoluble in water and freely soluble in CH_2Cl_2
- H_2O_2 is substantially more soluble in water than in CH_2Cl_2
- The dimerisation of the nitroxide radical and hydroxyl radical does not take place
- The extent of disproportionation of H_2O_2 is minimal over the time frame of the experiments
- The oxoammonium salt does not react with H_2O_2, or is at least physically separated from H_2O_2
- H_2O_2 formation is dependent on concentration of reactants

$$\text{rate} = k[\text{+N=O}][OH^-]$$

As the amount of hydroxide ions reaching the catalyst is dependent on the efficiency of the PTC, the main focus is on the reaction order with respect to the +N=O species. To obtain a measurable concentration of H_2O_2, it was calculated that approximately 0.75 g (~2 mmol) of **43** would be required. Following combination of all reactants, the vial was sealed and shaken (IKA-Vibrax-VXR, IKA-Labortechnik) for the required time. The reaction was sampled periodically by halting the shaking and allowing the solvents to separate before removing an aliquot from the aqueous layer well away from the liquid-liquid interface. A preliminary test using the peroxide test strips was performed on each sample. For accurate analysis the aliquot required the pH to be within the range that the specified by the test strip manufacturers (pH 5-7). This was achieved with addition of a citric acid solution, upon which this dilution was factored in to give an approximate concentration (Table 4.8). As the test strips only give qualitative responses of 0, 0.5, 2, 5, 10, 15 and 25 mgL^{-1} of H_2O_2, the accuracy of the measurements at each time point is low. However, despite this, the results unambiguously identified that the concentration of H_2O_2 was increasing over 1 to 75 minutes. By 90 minutes, no further H_2O_2 was formed and the slight decrease in concentration may well indicate its decomposition.

The maximum concentration observed indicates only 5.9% of the quantity of H_2O_2 that could be formed assuming a 2:1 ratio of oxoammonium cation to H_2O_2. In addition to this it was also noted that the temperature of the mixture rose from the ambient 18 °C to 22 °C and was directed related to the speed and length of stirring. As the vessel was sealed to ensure a closed system, shaking at 2000 rpm not only raised the temperature, but also the pressure in the system. Occasional small leakages of solvent escaped the vial on opening, which may well have led to a variation in volume and therefore concentration.

Table 4.8. Test strip determination of H_2O_2 concentration in biphasic system with **43** as the oxidant.

Time (min)	H_2O_2 test strips ($mg\ L^{-1}$)	Sample Conc. (mM)	Aliquot Conc. (mM)	Moles in vial (μmol)	Percentage of total possible H_2O_2 (%)
0	0	0.000	0.00	0.0	0.00
1	2	0.059	0.29	1.6	0.17
5	2	0.059	0.29	1.6	0.17
10	2	0.059	0.29	1.5	0.16
20	5	0.147	0.73	3.8	0.40
30	10	0.294	1.47	7.5	0.78
45	25	0.735	3.31	16.5	1.72
60	25	0.735	5.88	28.8	3.00
75	25	0.735	11.76	57.0	5.94
90	25	0.735	11.76	56.7	5.90

Sample: Combined aliquot and citric acid. Aliquot: Volume taken from vial.

Maximum number of H_2O_2 moles possible: 961 μmol (Based on the total amount of oxoammonium salt)

To ensure that the H_2O_2 formed was not from the solvent or other sources, control tests were performed for the milliQ water, NaOH solution, citric acid solution, CH_2Cl_2 and the PTC. These revealed that no H_2O_2 was present in the initial reagents and that no reagent caused a false positive.

This preliminary set of semi-quantitative results is of significance not only for the overall goals of the project (the recharging process for the New Cathode) but also to provide confirmation of the first reports of Endo[152] which others have failed to reproduce.[251]

To obtain a more accurate understanding of the development of H_2O_2 in the biphasic system, a more sensitive and quantitative approach was taken. In this approach an aliquot was combined with a titanium sulfate solution to form the titanium peroxy sulfate complex. Following the methodology outlined in Section 4.2.2 the concentration of H_2O_2 can be determined from the absorbance at 400 nm. Compound **43** (0.752 mg, 0.192 mmol) was used in the biphasic system analogous to the experimental design above. At each selected time period two aliquots were taken from the aqueous phase; 20 μL to test with the peroxide test strips and 100 μL required to react with titanium sulfate (first requiring dilution). The concentration of H_2O_2 obtained for each time period was converted into number of moles of H_2O_2. This allowed the amount of H_2O_2 that was removed to be accounted for in subsequent calculations. This included consideration of the reduction in volume of the aqueous layer throughout the progression of the experiment.

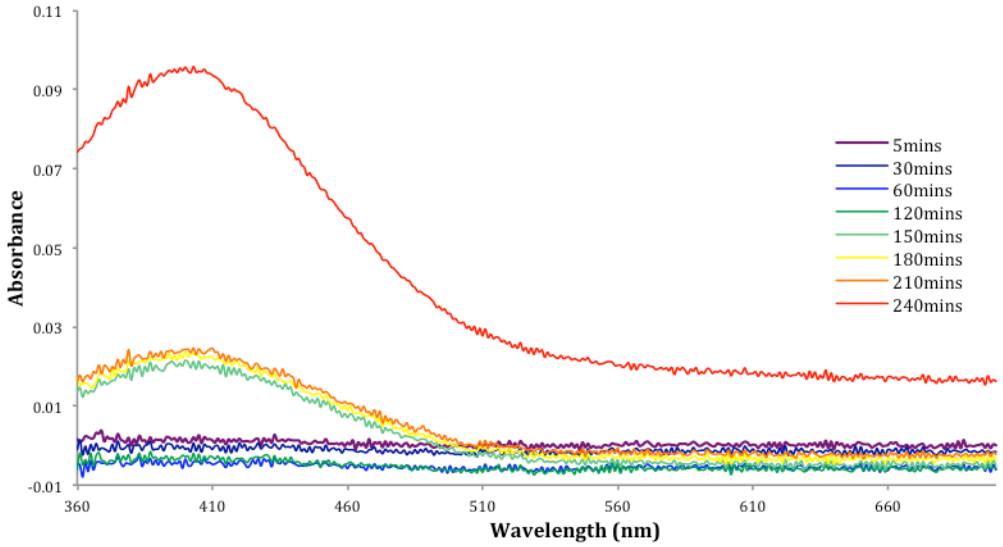

Fig. 4.45. UV-visible spectrum of the titanium complex with peroxide from aqueous phase (5 minutes – 4 hours).

Analysis by UV/Vis spectroscopy revealed a delay in H_2O_2 production of 2.5 hours suggesting either 1) the kinetics of the reaction are slow, 2) transfer of hydroxide ions by the PTC into the organic layer is slow or 3) this is simply the limit of detection at the initial low concentrations (Fig. 4.45). It does however show a gradual increase in the formation of H_2O_2 with time. Taking into account all H_2O_2 removed for analysis as well as the H_2O_2 remaining in the biphasic solution, a total of 10.7 mM H_2O_2 (56 µmol) was produced. When compared to the test strips that were analysed in parallel, a considerable difference is observed (Fig. 4.46).

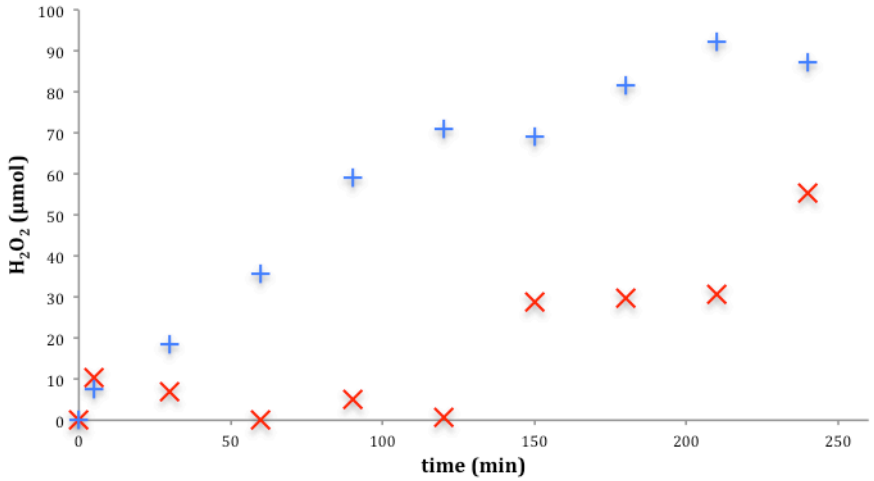

Fig. 4.46. Amount of H_2O_2 produced measured by both H_2O_2 test strips (blue cross) and by UV-Vis determination (red cross) over 4 hours.

An almost linear response is observed for the test strips up to 2 hours, in contrast to the spectroscopy method, which during this time shows little production of H_2O_2. Despite the inconsistency, both methods show an increase in H_2O_2 production over the course of the experiment. Based on the H_2O_2 produced, the oxoammonium salt has a turnover value of 5.8 and 9.1% of the maximum number of moles possible according to UV/Vis spectroscopy and test strips respectively. This is not inconsistent with the value of 5.9% seen previously for the test strips alone.

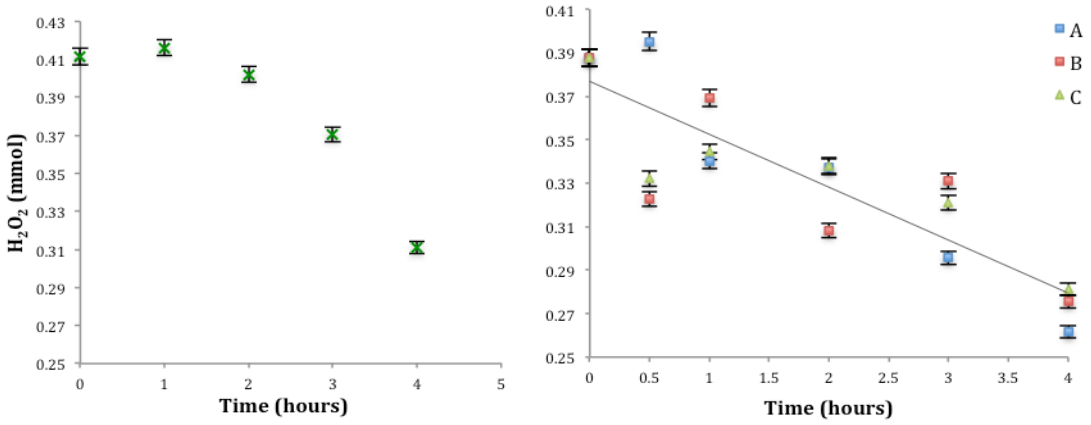

Fig. 4.47. Biphasic disproportionation of H_2O_2 in H_2O (left) and 2M NaOH (right) over 4 hours. Values from UV/Vis spectrophotometric data at 400 nm. (Displaying triplicate data A-C).

As H_2O_2 is known to undergo disproportionation, it was assumed that this may have an influence on the results, especially over the time scale of the experiment. To measure the rate of disproportionation in this system, the same experimental design was used however the oxoammonium salt was omitted and a known amount of H_2O_2 was used. In the absence of NaOH in Fig. 4.47 (left), a progressive decrease for H_2O_2 was observed with an acceleration of disproportionation with time. However, in the presence of NaOH large discrepancies are seen throughout each series of experiments (Fig. 4.47 right, A-C). A decreasing trend can be established although in a more linear response than in the absence of NaOH. However both display a loss in H_2O_2 of *ca.* 25% after 4 hours. If it is assumed that the concentration of H_2O_2 does not effect its rate of disproportionation (i.e. a zero partial order), the observed production of H_2O_2 (Fig. 4.46) is 25% less than the actual amount of H_2O_2 produced in this 4 hour time period. This increases the turnover of the oxoammonium species to 7.3 and 11.4%.

These preliminary results strongly suggest that the oxoammonium species **43** can generate H_2O_2 from hydroxide. It does warrant further investigation into the kinetics and rate of the reaction however that is beyond the scope of this project.

4.4.3 Nitroxide Reactions

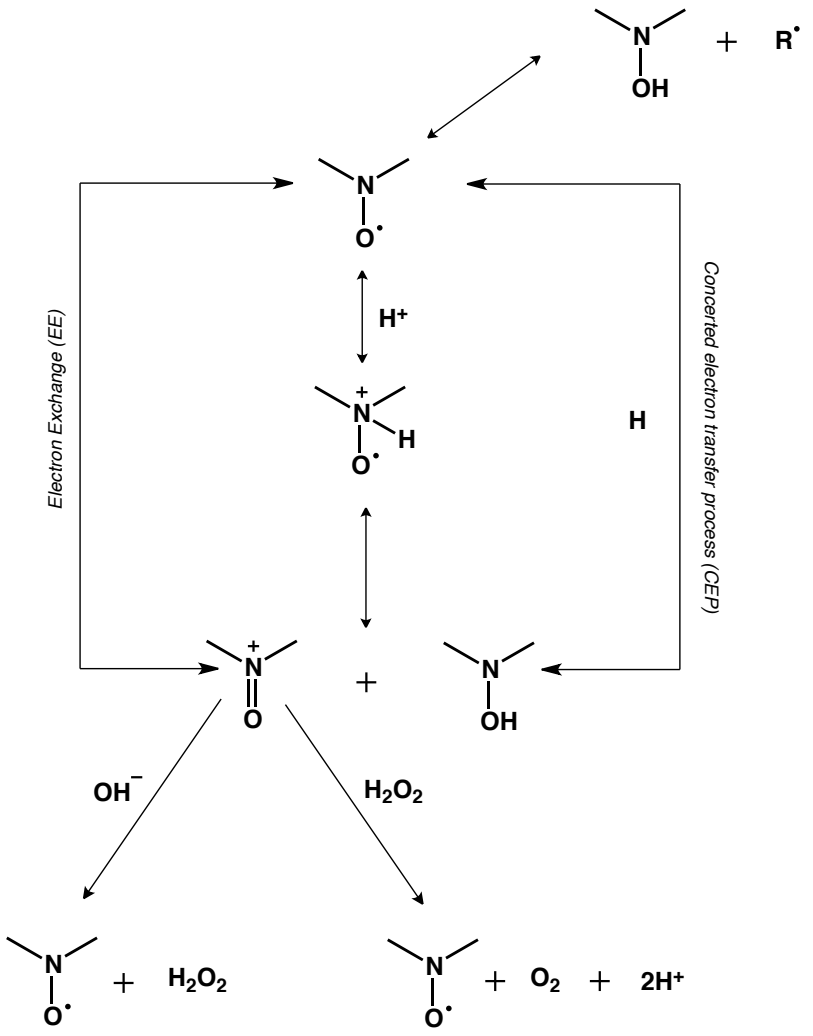

Fig. 4.48. Overview of the potential processes of the nitroxide-based species possible in the present system. Likely reversible processes are indicated by double-headed arrows.

Figure 4.48 combines all the potential processes of the nitroxide-based species that could occur in the present system. In addition to these pathways are the redox reactions for each species and their ability to be oxidised and reduced. Accurate determination and detection of each species in isolation has proved difficult due to the multiple pathways that can alter or remove any target species. In the example of the oxoammonium cation, rapid electron exchange in solution produces the nitroxide free radical, which causes discrepancies in the

assessment of the molecule by NMR and mass spectrometry. Additionally in a basic solution comproportionation with a hydroxylamine can also form the nitroxide radical. The ability of the nitroxide free radical to abstract a hydrogen from a solvent was also observed. Decolouration of the solution was observed and this is characteristic of loss of the radical species. It is unclear if the radical abstracts a hydrogen from the solvent or traces of water.

In the desired reaction for the New Cathode recharging process, the oxoammonium cation is required to oxidise hydroxide to form H_2O_2. The results of this preliminary study suggest that this reaction is occurring, albeit with low yields. An alternative pathway that was not investigated in this study is the further oxidation of H_2O_2 by a second oxoammonium cation. This will not only reduce the amount of H_2O_2 and catalyst in solution, but will produce O_2 that would decrease the efficiency of a battery incorporating the New Cathode. It is uncertain whether this reaction occurs under the anticipated alkaline conditions for a battery and consequently this will need to be investigated at a later stage.

The results obtained are in a solution-based system where the mechanisms and kinetics will differ to surface-based chemistries. When the catalyst is attached to a surface it potentially may aid the formation of H_2O_2, as the catalyst will be unable, or less able, to undergo reaction pathways that require two compounds to be in close proximity (disproportionation/comproportionation).

CHAPTER FIVE

Physical and Chemical Analysis of Surfaces

5.1 Introduction

The focus of this chapter is to report the physical characterisation of low (<0.2 cm^2) and high surface area (>0.1 m^2) electrode materials. There are two objectives to this work. The first is to demonstrate attachment of the previously synthesised compounds (reported in Chapters 2 and 3) onto electrode surfaces. The second is to establish a methodology to assess the electrocatalytic formation of H_2O_2 on an electrode surface.

Two methodologies were used to attach the new compounds to the surfaces: adsorption (physisorption) and chemical attachment (chemisorption). Physisorption is generally described as the reversible adsorption to a surface by van der Waals interactions. The electronic structure of the molecule is minimally disturbed upon adsorption and does not involve an activation energy barrier. In contrast chemisorption is the direct covalent bond attachment of a molecular fragment to the surface. An activation energy is usually required to form a new valence bond with the surface. Chemisorption is a feature in heterogeneous catalysis processes.

In this project the proposed cathode is carbon-based and a range of carbon-based electrodes will be reported here. It is noted that many commercially-available carbon materials (developed for a variety of purposes) also contain other constituents. These may prove to be deleterious in this project given the propensity for H_2O_2 to decompose in the presence of a wide range of materials. One measure of the 'non-carbon' content of carbon materials is the non-combustible 'ash' content comprising of Na, K, Ca, Si, Fe, Al and V. Consequently, low-ash carbons are desired in the longer term project, although less pure materials remain useful in the preliminary method development reported here.

Carbon exists in several allotropes of which we are interested in ones that vary in sp^2 and sp^3-hybridised atoms. This variety allows different physical and chemical properties of allotropes that are of significant technological importance, in particular for electrochemistry.[261,262] Of particular interest in this thesis are glassy carbons, amorphous carbon powder and carbon fibre felts.

Glassy carbon (GC) is one of the most widely used materials in electrochemistry research primarily due to its good electrical conductivity and wide potential window (with respect to oxidation and reduction of typical electrolyte systems). The proposed structure by Jenkins and Kawamura is a disordered form of incomplete graphitising carbon predominantly containing sp^2-hybridised carbon atoms.[263]

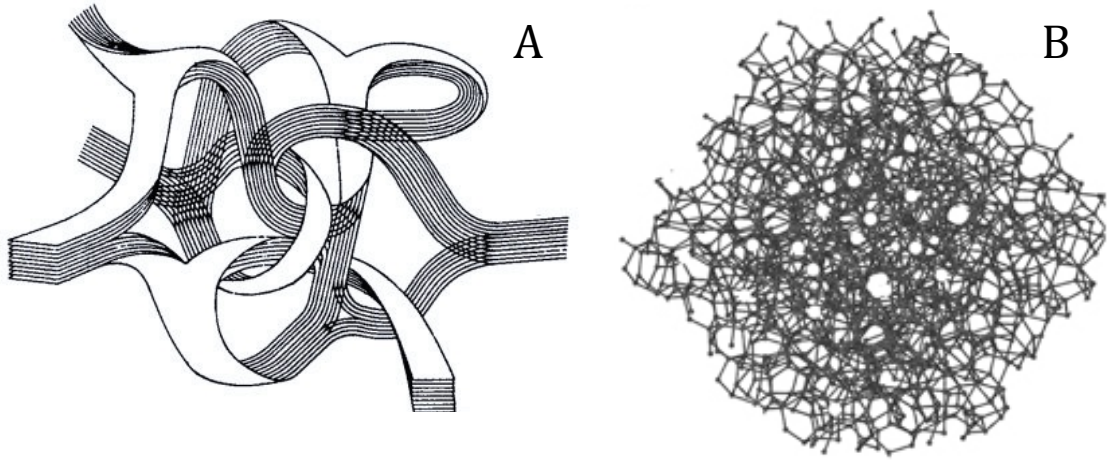

Fig. 5.1. Glassy carbon according to the model proposed by Jenkins. Image A adapted from Jenkins[263], Copyright 1971, Nature Publishing Group; and image B reproduced from Wang [264], Copyright 2014, Nature Publishing Group.

The 3-dimensional structure is understood to be a complex network of interwoven ribbons that are cross-linked throughout the network by covalent carbon-carbon bonds. GC is known to contain various oxygen functional groups, particularly distributed at the edge–plane sites. As GC surfaces can become deactivated with respect to electrochemical response (attributable to the available adsorption sites) over time and repeated use, mechanical polishing is routinely employed to restore the surface by removing the impurities and

adsorbents blocking the possible sites.[265] Polishing was achieved using a polishing kit, with a Rayon cloth and 0.3 μm aluminium slurry (PINE Research Instrumentation, NC, USA).

Amorphous carbon is a disordered combination of sp^2 and sp^3-hybridised carbon atoms, often with hydrogen atoms attached to the dangling π-bonds at carbon sheet edges.[262] In contrast, graphite consists of infinite sheets of graphene stacked parallel sheets containing only sp^2-hybridised carbon atoms. Graphite electrode materials are available in a range of ordered structures from highly oriented pyrolytic graphite (HOPG) to less ordered polycrystalline graphite.[262] The ordered structure allows the incorporation of hydrogen and oxygen-containing groups, particularly at edge planes.

Carbon fibres in carbon felts exhibit a range of order and crystallite size. Individual fibres can consist of concentric cylinders of graphene planes (as in multiple walled carbon nanotubes) or collections of randomly oriented graphitic planes. These may be arranged in both ordered graphitic regions, or turbostratic regions where the planes of carbon are folded or crumpled together.[266] This is discussed further in Section 5.3.2.

In each of these presentations of carbon, the functionalisation of the surface was achieved by the same methodology. Following pioneering work by Pinson in 1992,[48] diazonium coupling with a surface has become a standard approach to modification of a surface. Most methods use electrochemical means to induce attachment. In these approaches, a solution-based radical species is generated at the electrode or substrate surface by reduction or oxidation of a suitable precursor of the molecular fragment to be attached. This radical couples to the surface of the electrode through formation of a covalent bond with carbon atoms on the electrode surface.[267] The most widely utilised reaction is the reduction of an aryl diazonium to form an aryl radical, which then forms a new chemical bond to the surface (Scheme 5.1).

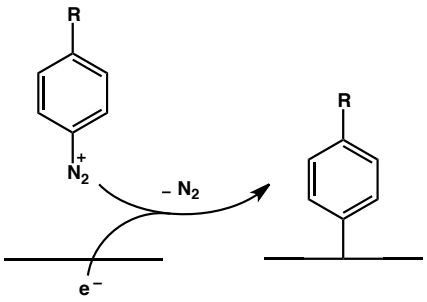

Scheme 5.1. Diazonium coupling with a surface.

Coupling of aryl radicals via aryl diazonium salts have many advantages over other methods including:

- Prior activation of the surface is not usually required
- Ease of preparation of the diazonium salts in gram quantities
- Ambient reaction and electrochemical coupling conditions
- The production of innocuous N_2 during the grafting process
- The ability to couple a wide range of functionalities on the electrode surface through the ready functionalisation of the aromatic ring

Diazonium coupling is also an attractive modification process since it avoids the use of oxidative conditions, which can alter the surface of the carbon substrate. Oxidising these surfaces may lead to superficial oxygenated groups (carboxylic, quinone, ketone or hydroxyl). Such oxidised carbon surfaces have been shown to lead to large background currents in many electrochemical applications.[48]

Diazonium salts can undergo either homolytic or heterolytic bond cleavage of the C-N bond (Fig. 5.2).[268] The particular combination of solvent, counterion and reducing agent influence whether cleavage of the diazonium group will be by homolytic or heterolytic fashion.[268]

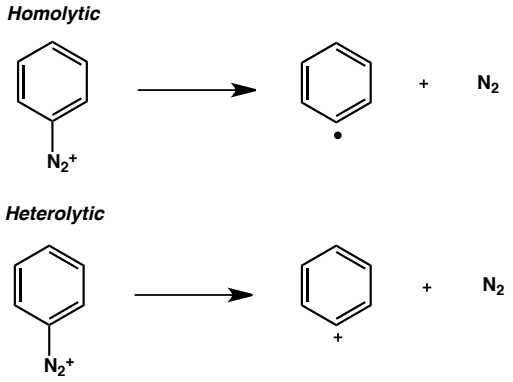

Fig. 5.2. Homolytic and heterolytic cleavage of an aryl diazonium salt.

Conditions are selected with the aim to promote homolytic cleavage to form the aryl radical species. Homolytic cleavage is rapidly followed by addition of the radical to the surface of the electrode substrate. This process suggests that distinct monolayers of the attached molecular fragment should form on an electrode. However, there is difficulty in controlling the extent of the reaction, as aryl radicals will attach not only the original electrode surface, but also to already-grafted aryl layers (Fig. 5.3).[191]

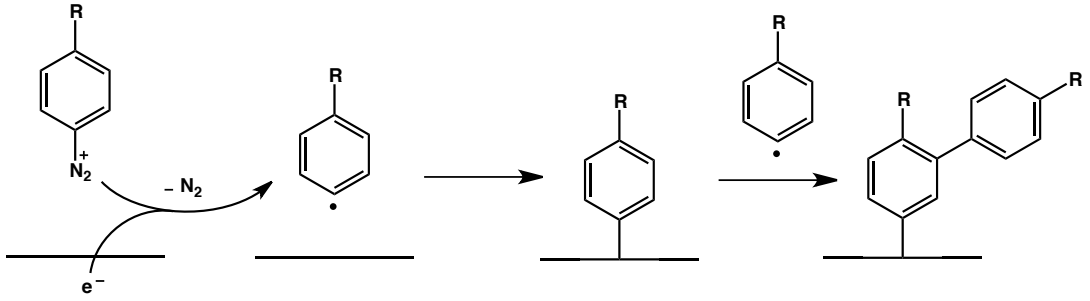

Fig. 5.3. Homolytic cleavage of an aryl diazonium rapidly followed by addition of the radical onto a surface. It is possible that a second aryl radical can attach to the already grafted aryl-layer.

Two factors promote the one-electron reduction of the diazonium salt at the carbon surface:

i) the diazonium salt is adsorbed prior to its reduction[269] and

ii) despite the fact that aryl radicals can be further reduced electrochemically, this is found to occur at a more negative potential

than that for the reduction of the diazonium cation. Even if large cathodic potentials are applied, as the attachment occurs rapidly, most of the radical is covalently bound by the time the potential is sufficiently negative to make this further reduction.

It is possible to control the thickness of the aryl layer by controlling the charge passed during the grafting by control of electrolysis time and current. As might be anticipated, a higher concentration of the diazonium salt solution and a more cathodic grafting potential can increase the surface concentration of grafted material.

5.2 Instrumentation

This chapter reports preliminary studies on low surface area electrodes, followed by the characterisation of higher surface area materials. Throughout this chapter analysis will include; cyclic voltammetry, chronopotentiometry, chronoamperometry, FTIR, solid-state NMR, atomic absorption spectroscopy, Raman spectroscopy, scanning electron microscope (SEM) and microanalysis.

5.2.1 Potentiostatic Equipment

An Autolab Potentiostat Galvanostat PGSTAT30 ADC 164 accompanied by GPES software (Eco Chemie B.V. Utrecht, The Netherlands, Ver. 4.9) was used to control the electrochemical experiments performed in this study.

An MSRX speed control (PINE Instrument Company, NC, USA) was used to control the rotation speed of the shaft in the analytical rotator (model AFMSRXE 1402, PINE Instrument Company, NC, USA). This rotator was used in conjunction with a rotating disc electrode to form a hydrodynamically-controlled working electrode in some cases.

The electrochemical cells consisted of three electrodes, in general, the working electrode (WE), reference electrode (RE) and counter electrode (CE). The potential of the working electrode is controlled by the potentiostat that either fixes or scans the potential difference between the WE and RE through altering

the current flowing through the WE and CE in chronoamperometry (CA) or cyclic voltammetry (CV) experiments. The reference electrode is an invariant potentiometric probe against which the change in potential of the WE is measured. The CE is driven by the potentiostatic circuit to balance the faradaic process at the WE however in the opposite direction (e.g. if oxidation occurs at the WE, reduction will occur at the CE). Typically the process at the CE does not influence the process at the WE due to the small currents observed in these systems.

The supporting electrolyte employed in each experiment was based on the solubility of the electroactive species, the redox activity and solvent properties. A 0.1 M tetrabutylammonium hexafluorophosphate (NBu_4PF_6) electrolyte in acetonitrile (MeCN) was used for the majority of the electrochemical analyses and grafting of organic compounds. Work with grafted electrodes or H_2O_2 solutions required an aqueous 0.1 M phosphate buffer (pH = 7.0 to 8.0) or KOH (0.1 to 1.0 M) electrolyte. Since dissolved oxygen has the potential to interfere with measurements in this system, the supporting electrolyte was purged with argon or nitrogen prior to experiments. In the case of the rotating electrode systems, adhered O_2 bubbles arising from H_2O_2 decomposition (which are likely to decrease the working area of the electrode and disrupt the hydrodynamic flow across the electrode) were removed by rotating the WE at 1000 rpm briefly (2-5 s) immediately prior to each experiment.

Processes at the working electrode are of most interest. In this study the predominant working electrode was carbon based; glassy carbon microelectrodes, glassy carbon macro-electrodes and carbon felt.

5.2.1.1 Microelectrodes

Microelectrode systems were used to minimize artefacts associated with ohmic potential drop. The small working areas of microelectrodes (ME) generate extremely small currents (typically of the order of nanoamperes), thus, *iR* potential drop is minimised. A glassy carbon microelectrode (GCME) with diameter 10 μm was employed as the WE for preliminary experiments

(Bioanalytica Stystems Inc., Indiana, USA). Microelectrodes with dimensions (1-10 μm) significantly less than the Nernst layer thickness (0.1 to 1.5 mm) are capable of exhibiting hemispherical diffusion-controlled mass-transport. This offers a significant advantage over electrodes with larger dimensions in that the electrochemical response is not dependent on stirring or fluid flow of the electrolyte solution and steady-state responses proportional to the reactant concentration are observed (provided the system is not operating under electron-transfer control) (Eq. 5.1).[270] The steady-state current is given by

$$i = 4nFDcr \qquad 5.1$$

where n is the number of electrons transferred per molecule, F is the Faraday constant, D is the diffusion coefficient, c is the bulk concentration of the electroactive species and r is the radius of the electrode. As the microelectrode system results in very low currents (typically nanoamperes) all measurements were performed in a Faraday cage to minimise noise from external electrical interferences.

5.2.1.2. Macroelectrodes

In such experiments where either a low concentration was used or an electroactive species was grafted on the surface, in order to obtain a satisfactory response a glassy carbon macroelectrode with diameter 0.3 mm was used.

5.2.1.3. Rotating Disk Electrode

A glassy carbon rotating disk electrode (RDE) with geometric area of 0.1963 cm^2 was used for the CV and CA experiments. RDEs are a controlled mass-transport electrode system where a disk-shaped working electrode material is embedded in a cylinder of insulating material (Fig. 5.4a). The cylinder is inserted into the solution with only a circular surface of the disc exposed (Fig. 5.4b). Rotation speeds were in the range of 0 – 1500 rpm in this study and were controlled by a synchronous controllable speed motor that rotated with constant angular velocity at a perpendicular axis to the planar disk surface.

Rotation rates higher than 1500 rpm are not available in this system; rotation at higher rates leads to Reynolds numbers indicative of the likelihood of turbulent flow.

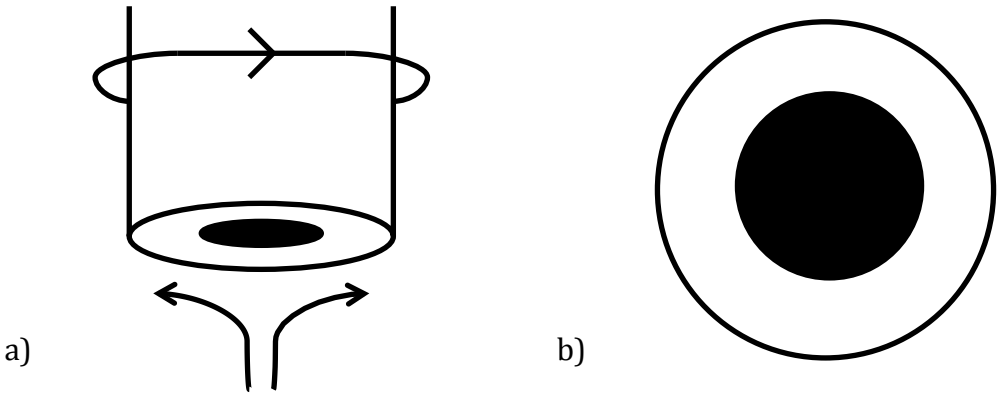

Fig. 5.4. a) Schematic diagram of a RDE showing the rotation of the cylinder and induced direction of electrolyte towards the disc surface b) Bottom view of the RDE with the inner circle the disc surface.

Rotation increases the flow of electrolyte from the bulk solution to the face of the disk by centrifugal force or forced diffusion in a laminar flow. The current response has been derived according to Fick's first law and the Nernst diffusion layer concept as in Eq. 5.2.

$$i = \frac{nFD(c_b - c_s)}{\delta} \qquad 5.2$$

Where i is the current density, n the number of electrons transferred in the reaction, F is the Faraday constant (96,485 C mol^{-1}), D is the diffusion coefficient of the electroactive species, c_b and c_s are the species concentrations of the bulk and surface respectively, and δ is the thickness of the Nernst diffusion layer.

A limiting current density, i_L, is reached when the surface concentration effectively becomes zero, $c_s = 0$. Substitution into Eq. 5.3 gives the relationship for limiting current density.

$$I_L = \frac{nFDc_b}{\delta} \qquad 5.3$$

Under laminar flow conditions in a liquid medium of kinematic viscosity *v*, the thickness of the diffusion layer decreases with increasing angular velocity as described by Levich. Incorporation of the viscosity and angular velocity into Eq. 5.3 provides the limiting current as a function of rotation rate for a RDE (Eq 5.4).

$$I_L = 0.620\, nFD^{2/3}\omega^{1/2}v^{-1/6}c_b \qquad 5.4$$

Consequently, under mass transport it is anticipated that the limiting current will be proportional to the square root of the angular velocity.

5.2.1.4. Carbon Felt Electrodes

The carbon felt was supplied by ArcActive of Christchurch, NZ (sample CF014). It is understood that this material was formed (elsewhere) through the pyrolysis of polyacrylonitrile (PAN) felt (Fig. 5.5).

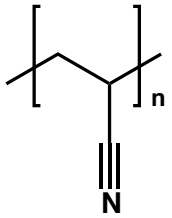

Fig. 5.5. Polyacrylonitrile polymer.

This material was supplied in sheets 15.4 cm x 60.5 cm and 3 mm in thickness. The measured gravimetric density (using the outer dimensions of the sheets) is 0.144 g cm^{-3} indicating that a substantial fraction of the felt is 'void volume'. The fibres constituting the felt tended to be in a random pattern, presumably as result of the original PAN felt-making process.

To prepare a carbon felt WE, the felt was cut into 2.0 cm (*h*) x 1.5 cm (*w*) x 0.3 cm (*d*) electrodes and connected to the electrochemical system by conductive carbon rods (Fig. 5.6B/C). Two pieces of carbon rod, approximately 2 and 3 cm long were joined together in a pincer like manner with a rubber band (Fig. 5.6A). The longer of the rods was attached to the alligator clip analogous to that for a regular static electrode and the assembly immersed in the electrolyte (Fig. 5.6D).

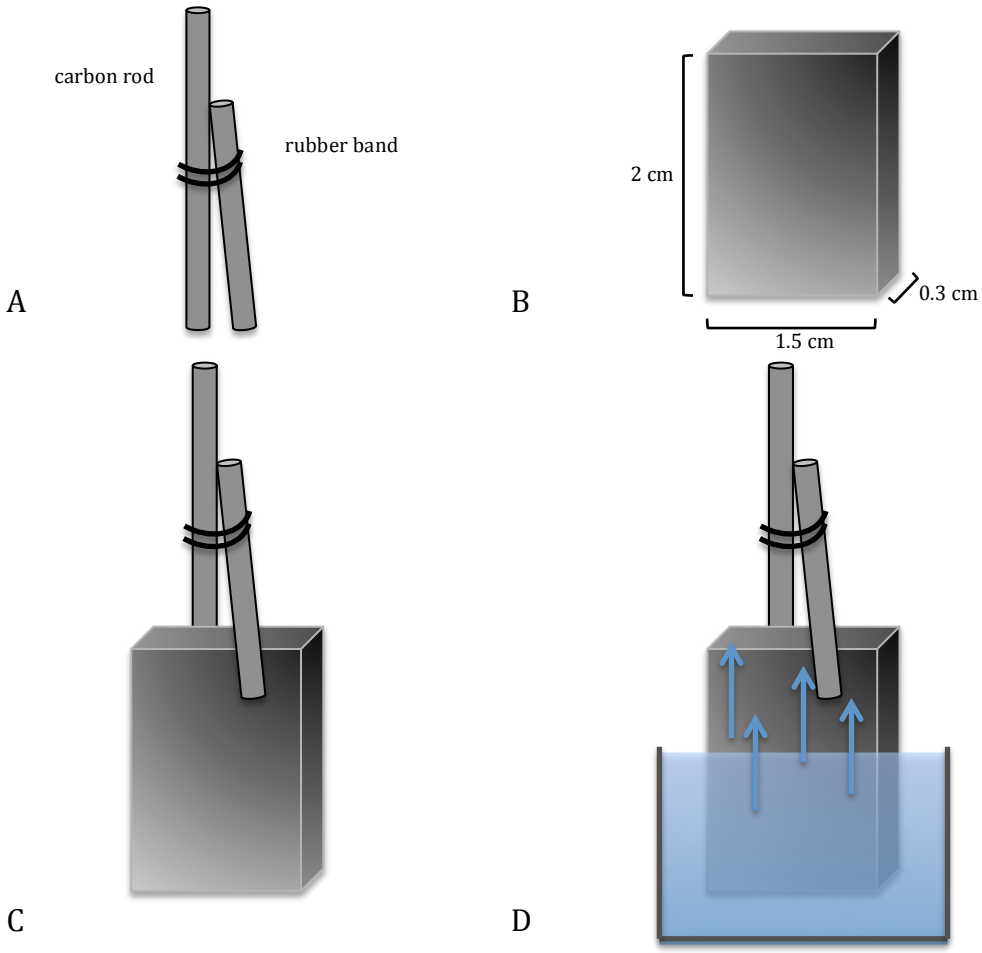

Fig. 5.6. Set up of carbon felt as the WE.

It was not necessary to fully immerse the felt into the solution as capillary action in the porous felt allowed the entire area to become wet over time.

5.2.2 Analytical Techniques

5.2.2.1. Cyclic Voltammetry

Cyclic Voltammetry (CV) is a potential-controlled technique where the potential of the WE is scanned linearly with respect to time from an initial value E_i to a final value E_f at a constant rate (mV s^{-1}). Once the final potential is reached the scan may be reversed to complete the cycle. This technique offers prompt location of the redox potentials for electroactive species. It may involve a single cycle or repeated numerous times to provide both qualitative and quantitative information regarding the electrochemical processes that are occurring at the electrode surface.

5.3 Results and Discussion

5.3.1. Grafting of Simple Diazoniums

To illustrate the technique of electrochemical grafting to a carbon electrode, a simple and well-known diazonium was used. Standard diazotisation conditions were used to synthesise 4-nitrobenzenediazonium tetrafluoroborate from 4−nitroaniline (see experimental section 2.6). A 10 mM solution of 4−nitrobenzenediazonium in MeCN (0.1 M NBu_4PF_6) underwent electroreduction upon potential cycling from +0.6 to −0.75 V *vs.* Ag/Ag^+ on a glassy carbon electrode. Fig. 5.7 presents the cyclic voltammogram which shows a broad irreversible wave on the first cathodic scan. Subsequent cycles show a marked decrease in current corresponding to diazonium coupling. This is ascribed to the blocking of further access of diazonium cations to the surface. Once the electrode had been carefully rinsed to ensure removal of any material not chemically grafted, a characteristic reversible wave of the nitro group can be seen on scanning to −1.50 V *vs.* Ag/Ag^+ in pure aprotic electrolyte (MeCN) (Fig. A6). The integrated current of this reduction peak in MeCN was used to calculate a current density of 0.24 mC cm^{-2}; this is assumed to correspond to the quantity of nitro groups in electrochemical communication with the electrode surface. The calculated surface concentration of the GC modified with nitrophenyl groups was 2.5 x 10^{-9} mol cm^{-2}. Pinson *et al.* determined a surface coverage (Γ)

for the grafted 4-nitrophenyl on glassy carbon of $\Gamma = 1.4 \times 10^{-9}$ mol cm^{-2}.[271] This suggests that more than one layer has formed, or that the surface has a roughness factor greater than unity. Despite the possibility that several layers may have formed, this demonstrates the technique of attaching an organic diazonium salt onto a carbon electrode.

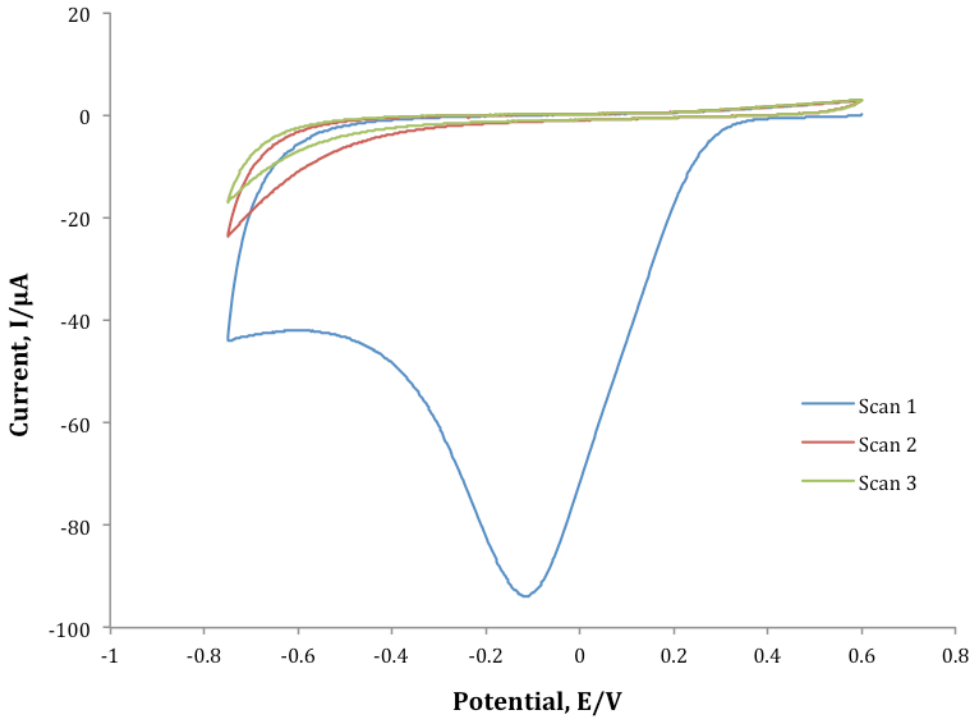

Fig. 5.7. First three cyclic voltammograms from +0.6 to -0.75 V *vs.* Ag/Ag^+ for the attachment of 10 mM 4-nitrobenzene diazonium tetrafluoroborate in MeCN (0.1 M NBu_4PF_6) with a GC macroelectrode. (Pt CE, Ag RE).

5.3.2 Physical and Chemical Attachment on High Surface Area Carbon Materials

In order to obtain a high storage capacity in the battery cell, a high surface area carbon substrate is required. Standard graphite samples generally range between 5 – 100 m^2/g, which is considerably lower than that for the aim of this overall project where at least 1000 $m^2\,g^{-1}$ is necessary for a final electrode system. Two distinct types of carbon substrates were used for this study; carbon powder and carbon felt. The carbon powder provides an initial substrate to with appreciable surface area; the carbon felt has a lower surface area and primarily serves as a

macroscopic (with dimensions >10 cm x >10 cm) current collector in a final battery electrode. While the latter material serves this current collecting role (as opposed to directly being involved in the charge-discharge electrochemical reactions), it was also investigated as a substrate for grafting.

Two different carbon powders derived from coal and are steam activated to give surface areas of 1000 m^2/g (Activated Carbon Technologies Pty Ltd, Australia) were investigated. The determination of the carbon felt material (ArcActive Technologies Limited) is described in Section 5.3.4 and was shown to be 0.41-0.42 $m^2\ g^{-1}$.

5.3.2.1. Carbon Powders

The main focus of physical and chemical attachment on high surface area carbon powders were performed on the 1000 m^2/g sample (PS1000). Substituted ureas were attached either by physical adsorption (physisorption) or chemical attachment (chemisorption) through diazonium coupling with the surface. Physical attachment of compounds to the surface is achieved through van der Waals interactions or π-stacking attractions. It was thought prudent to determine whether physisorption would yield similar properties to that for the covalently bound compounds. If so, this would remove the necessity for chemical attachment and the accompanying precursor synthetic steps. In addition, when the adsorbed material is placed in an aqueous solution, we must assume that the substituted groups are sufficiently insoluble to enable the urea to remain physically attached to the substrate when presented to the electrolyte.

In order to estimate the quantity of diphenylurea (DPU) required to cover the surface of the carbon an assumption of the size of a DPU molecule was made. This included the notion that to complete a monolayer each DPU will reside in a flat, planar–like arrangement on the substrate surface and occupy approximately a 0.4 x 1.2 nm rectangular area (0.48 $nm^2\ molecule^{-1}$). This estimated area was calculated from average bond angles and lengths for DPU reposing in a *trans* conformation. To find the mass of any compound that will fully occupy the

substrate (assuming a surface roughness of unity) the surface area of PS1000 must be taken into account. At 1000 m^2 g^{-1} it is equivalent to 10^{21} nm^2 g^{-1}, consequently the mass of DPU anticipated to adsorb on the carbon surface, m_s, is given by

$$m_s = \frac{10^{21}\ \mathrm{nm^2 g^{-1}} \cdot M_r}{0.48\ \mathrm{nm^2\ molecule^{-1}} \cdot N_A} \qquad 5.5$$

where M_r is the molecular weight (212 g mol^{-1}) of the adsorbed molecule and N_A is Avogadro's constant (mol^{-1}).

This analysis estimates a loading of 0.734 g DPU to cover the surface of 1 g of PS1000 substrate. Scaling down to suitable working amounts, the carbon was first dried in a 50 °C glass vacuum oven (BUCHI Labortechnik AG, B-585) for 5 hours before 100 mg was weighed into a vial. The appropriate ratio of DPU (73.4 mg) was dissolved in methanol/acetone mixture (4:1 v/v) and added to make a suspension with the carbon where it was maintained stirring at room temperature for 1 hour. Following careful removal of the solvent under reduced pressure (with no heating) the carbon remained a very black powder in presentation and no visible signs of white urea aggregates were discernable visually. The modified carbon was placed back into the vacuum oven at 50 °C for a further 2 hours before analysis of the material.

Chemical attachment was achieved by diazonium coupling of a DPU precursor (Fig. 5.8) with the carbon powder. This forms a strong covalent bond from the aromatic ring in the substituted urea to the surface. This would potentially result in DPU orienting perpendicular to the surface rather than planar as in the physisorbed case due to the constraints of the covalent bond with the surface.

Complexities exist when diazonium coupling with dispersed carbon powders as there is no contiguous electrical pathway available. However, Murphy *et al.* have shown that discrete carbon particles can participate in diazonium attachment.[272] The process is less well understood than the original Pinson method, but is

assumed to involved the abstraction of an electron from the bulk of the carbon particle to initiate the formation of the aryl radical. Consequently, the carbon surface appears to be able to act as a mild reductant spontaneously transferring electrons to initiate the grafting process. The grafting yield appears to depend on the willingness of the carbon substrate to donate an electron to the acceptor levels of the diazonium cation. In addition the kinetics at carbon surfaces has a strong non-linear dependence on sp^2 content presumably due to the higher level of energy associated with sp^2 electrons, specifically in the p-orbital.[273]

It has been suggested that under thermal conditions heterolytic cleavage of the C-N_2^+ gives rise to an alternative pathway of covalent attachment of aryldiazonium at surfaces.[272,273] However, the distinction between the two pathways was not required for the overall project.

Two aryldiazonium salts were prepared for spontaneous attachment to carbon **1**; 4-(3-phenylureido)benzendiazonium and 4-nitrobenzenediazonium (Fig. 5.8). The simple nitrobenzene compound was selected since it displays well-characterised and strong spectroscopic and electrochemical responses and offers the potential to demonstrate the efficiency of the non-electrode method and for subsequent comparison with the attachment of DPU.

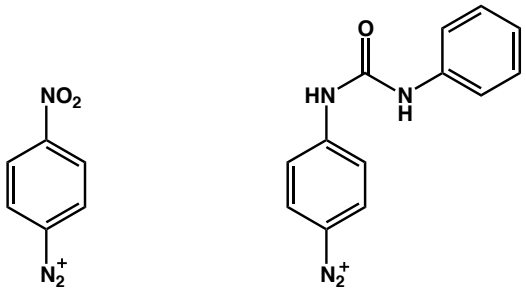

Fig. 5.8. 4-Nitrobenzenediazonium (**38**) and 4-(3-phenylureido) benzendiazonium (**35**).

Spontaneous diazonium attachment was achieved using two different methods for preparation of the diazonium salt species. In the first, 4-nitroaniline was diazotised in an aqueous solution (see Experimental Section 2.6) and after the required reaction time (1 hour) the appropriate amount of carbon powder was

added (assumed 100% reaction of the diazonium). In the second method, the isolated diazonium salt (**38**) was dissolved in H_2O before addition of the carbon. This carbon suspension was vigorously stirred at rt overnight, during the early stages of which gas evolution and bubble formation was evident. It should be noted that gas evolution (presumed to be N_2) is not fully diagnostic of success given this could be due to self-dimerisation or surface impurity. Following sonication for 3 x 10 minutes the suspension was centrifuged at 4000 rpm for 20 minutes to a) form a pellet of modified carbon and b) release unreacted material into the supernatant liquid. Once the supernatant liquid was discarded, the pellet was redistributed in acetone and the centrifugation process repeated. The pellet was redistributed in fresh acetone before being transferred to a new flask where the solvent was removed under vacuum.

The verification of attachment of the diazonium-coupled material proved challenging. As DPU is not electrochemically active, an assessment of the surface by electrochemical techniques is not available. Alternative verification methods such as spectroscopy and microanalytical techniques were employed to assess the grafting of the compounds to the carbon powder. These outcomes are outlined below.

5.3.2.2. Raman and FTIR Analysis

Raman spectroscopy provides a vibrational spectrum of a molecule as a result of inelastic scattering of intense, quasi-monochromatic incident light that is usually suppled by a laser. A classical model describes Raman scattering arising from polarisation of a molecule's electron cloud, whilst the molecular vibrations modulate the electron distribution. The difference between the frequency of incident light and the frequency of molecular vibrations (both positive and negative) is described as Raman scattering. Each molecular vibration generates a unique difference frequency and the intensity of the Raman scattering is determined by the change in polarisability as the nuclei oscillate.

The Raman microscope used at Massey University, Palmerston North is a locally-designed and assembled confocal system with an Olympus IX70 inverted

microscope as the platform. The spectrograph is a Princeton Instruments Acton LS 785 with a 1200 g/mm grating while the detector used was a Princeton Instruments PIXIS:400 with a 1340 x 400 CCD array. The laser source is a 30 mW single-mode 785 nm diode laser (Warsash Scientific). Rejection of Rayleigh scattered light is achieved using Volume Bragg Gratings from OptiGrate Ltd (Orlando, FL, USA).

To apply Raman spectroscopy to the analysis of the grafted carbon materials a reference spectrum of DPU was collected (Fig. 5.9). The main diagnostic features discernible from this spectrum are the carbonyl stretch of the urea at 1640 cm^{-1} and the strong ring stretch, breathing and wagging at 1589, 1296, 998, 915 and 893 cm^{-1} which are comparable to those reported for DPU in the literature.[274] In addition to these observations, high intensity low frequency modes below 100 cm^{-1} are tentatively assigned to lattice movements between entire molecules/planes in the crystal lattice of DPU. These are potential features for establishing the physical and chemical attachment of DPU to the high surface area carbon.

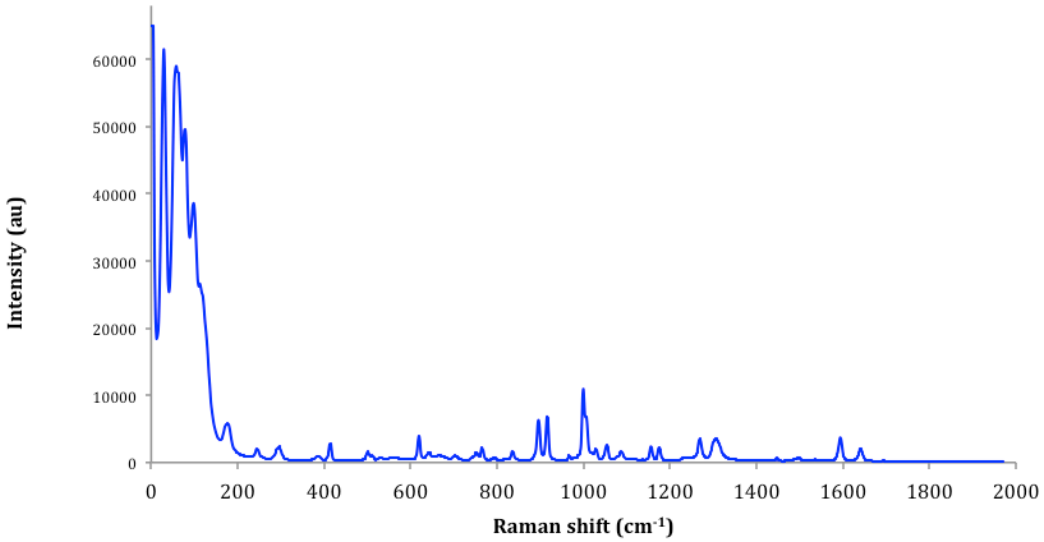

Fig. 5.9. Raman Spectroscopy of solid DPU (40x objective, 30 s integration, 4 mW at sample).

Raman spectroscopy is highly sensitive to bond configurations of carbon atoms in carbon-based materials.[275] This arises from the strong dependence of their physical properties on the ratio of sp^2 (graphite-like) and sp^3 (diamond-like) bonds.[276] The spectrum for disordered graphite generally exhibits two modes, the G peak at *ca.* 1520 – 1600 cm^{-1} and the D band at *ca.* 1350 cm^{-1}. The D band arises from breathing vibrations of sp^2 carbon rings or ring-like structural units and is activated in the presence of disorder, thus is absent in perfect graphite.[275] The peak width, especially of the D band, is correlated to a distribution of clusters that have different orders and dimensions. The Raman spectra of PS1000 gives a broad D band at 1298 cm^{-1} with a small shoulder G band at about 1580 cm^{-1} (Fig. 5.10). This is characteristic of a very disordered amorphous carbon with little graphitic structure. The DPU adsorbed carbon displayed a similar spectrum to the crystalline DPU with the exception of a broad peak at 1300 cm^{-1} assigned to the D band of the amorphous carbon material. Unfortunately in the spectrum of the chemically attached DPU carbon, only the peaks associated with the carbon were visible. This suggests that the amount of material bound to the surface is insignificant for detection through this method. This was also the case for chemically attached 4-nitrobenzene. The electrochemical analysis showed that grafting gives approximately mono-layer coverage on a GC electrode. This is therefore only a small number of molecules present in the scattering volume and without substantial enhancement of the Raman scattering intensity, it is likely that the scattering intensity of the adsorbed molecules is not sufficient to be seen above the noise level.

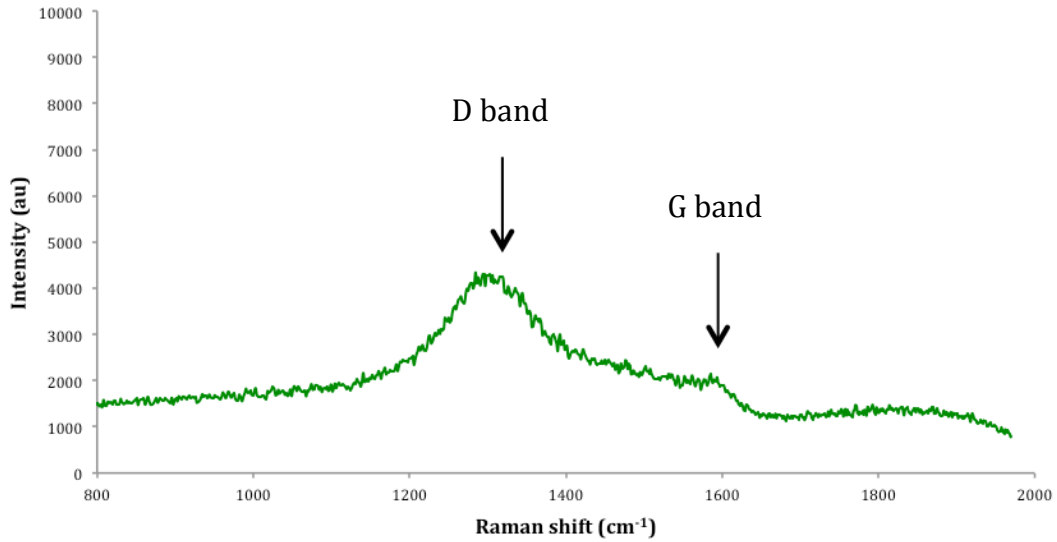

Fig. 5.10. Raman spectra of PS1000.

In conjunction with Raman, ATR-FTIR spectroscopy was performed on these carbon materials as they are both probe vibrational motion. Similarly to that for Raman, there is a poor signal-to-noise response that does not permit detailed analysis. Rather, it is suggestive of small surface coverages for the chemically attached compounds. As the beam will only pass through *ca.* 1 μm of the sample, the concentration of the putatively attached compounds is very small in comparison to the large surface area of the amorphous carbon. Therefore in order to successfully use both these spectroscopic techniques, a larger surface coverage is required to be able to draw reasonable conclusions.

5.3.2.3. Solid state-NMR spectroscopy

Solid state (ss) NMR spectroscopy is an alternative to solution state spectroscopy where solubility in a solvent is an issue. It is a technique that complements X-ray crystallography, electron microscopy as well as solution state methods. Ss-NMR is similar to classical liquid-state NMR except compounds in the solid state are unable to tumble in solution. This tumbling leads to an average anisotropic association that ultimately can be neglected in the timescale of solution-state NMR. These anisotropic interactions are distance and orientation dependent and therefore have a significant influence in ss-NMR. The use of magic angle spinning (MAS) orientates the sample with respect to the magnetic field. The interactions on the nuclear spin such as dipolar, chemical shift anisotropy and quadrupolar

interactions are time-dependent interactions so that introducing MAS permits these to be averaged. This gives rise to a much sharper signal and enables structural determination of the solid material by the isotropic value.[277]

Ss-NMR was performed with MAS on PS1000 and the chemically attached DPU carbon. PS1000 contained very little hydrogen and according to the proton spectrum, the carbon is highly ordered. In contrast, the DPU sample had a significantly higher quantity of hydrogen than the original carbon material and the carbon is not as ordered. A ^{13}C spectrum in the DPU sample showed a single extremely broad peak. This indicates the presence of metal ions (with unpaired electrons) in the sample as paramagnetic species reduce the magnetisation relaxation times, which appears as broadening of peaks in the frequency domain. Overall, these experiments demonstrate that the chemical attachment of DPU onto the carbon induce changes in the ss-NMR spectrum. Despite the fact that the spectrum may not have distinct chemical shift values, it does help establish components such as residual metal ions in the carbon powder.

5.3.2.4. Metal ion content – Fe Analysis

The interference of metal ions in the ss-NMR response provoked a more thorough investigation of the metal content in the carbon powders. Once the substituted ureas are attached to the high surface area carbon, the intention would be to test its ability to bind H_2O_2. As H_2O_2 is catalytically reduced in the presence of metal ions it is essential to establish whether this is a potential problem in further analysis. A small sample of PS1000 was placed in an Eppendorf tube where approximately 1 ml of 30% H_2O_2 was added. After attempting to wet all the carbon by flicking the tube, violent bubbling was visible (Fig. 5.11) and heat evolution was evident that persisted for several minutes. This exothermic reaction is not inconsistent with the catalytic decomposition of H_2O_2. In an attempt to first remove metal constituents from the surface the carbon was washed with 2 M HCl and dried before retesting. However, the reaction with H_2O_2 had only changed negligibly after pre-treatment with acid. Pre-treatment of the carbon with either H_2O_2 or fuming HNO_3 (refluxing) also produced an exothermic reaction on subsequent addition of H_2O_2. It was proposed that the pre-treatment

of the carbon may well remove some of the metals content, but that a sufficient amount still remained at or near the surface to promote H_2O_2 decomposition.

Fig. 5.11. PS1000 with *ca.* 1ml of 30% H_2O_2. Bubbling persisted for several minutes.

Adsorption of DPU on PS1000 in a surface area coverage ratio of 1:0.5, 1, 1.5, 3 and 4 (carbon:DPU) gave decreasing reactivity towards H_2O_2 decomposition with increasing amount of urea. This implies the urea is covering the surface sufficiently to reduce the contact of H_2O_2 with surface metal ions or is trapping the H_2O_2 as intended.

Iron is routinely found in graphitic materials. This was confirmed in the case of PS1000 by atomic absorption spectroscopy (AAS) analysis. A sample of PS1000 was placed in a round bottom Pyrex flask and cooled in ice before adding fuming HNO_3 dropwise. The suspension was heated to reflux at 90 °C for 2 days before centrifuged at 7000 rpm on a fixed rotor for 20 minutes. The dark brown solution was carefully removed and the pellet rinsed with water and repeated. The combined supernatant solutions were filtered and diluted to a known volume and compared with a series of standards by AAS (GBC Scientific Equipment, XPLORAA 2A). It was found that the extractable Fe content using this method was 0.4% w/w in PS1000. This was compared with the total Fe content determined by microanalytical combustion analysis (Campbell Microanalytical Laboratory, University of Otago) where it was established that PS1000 had a content of 4.9% w/w.

5.3.2.5. Scanning Electron Microscopy

Scanning Electron Microscopy (SEM) employs a focused beam of electrons that interact with atoms in the sample to generate a secondary electron signal that can be detected to give an image that displays characteristics of the solid material. These signals effectively provide a high magnification image of a sample and hence reveal information about morphology, texture, composition and orientation of the material.

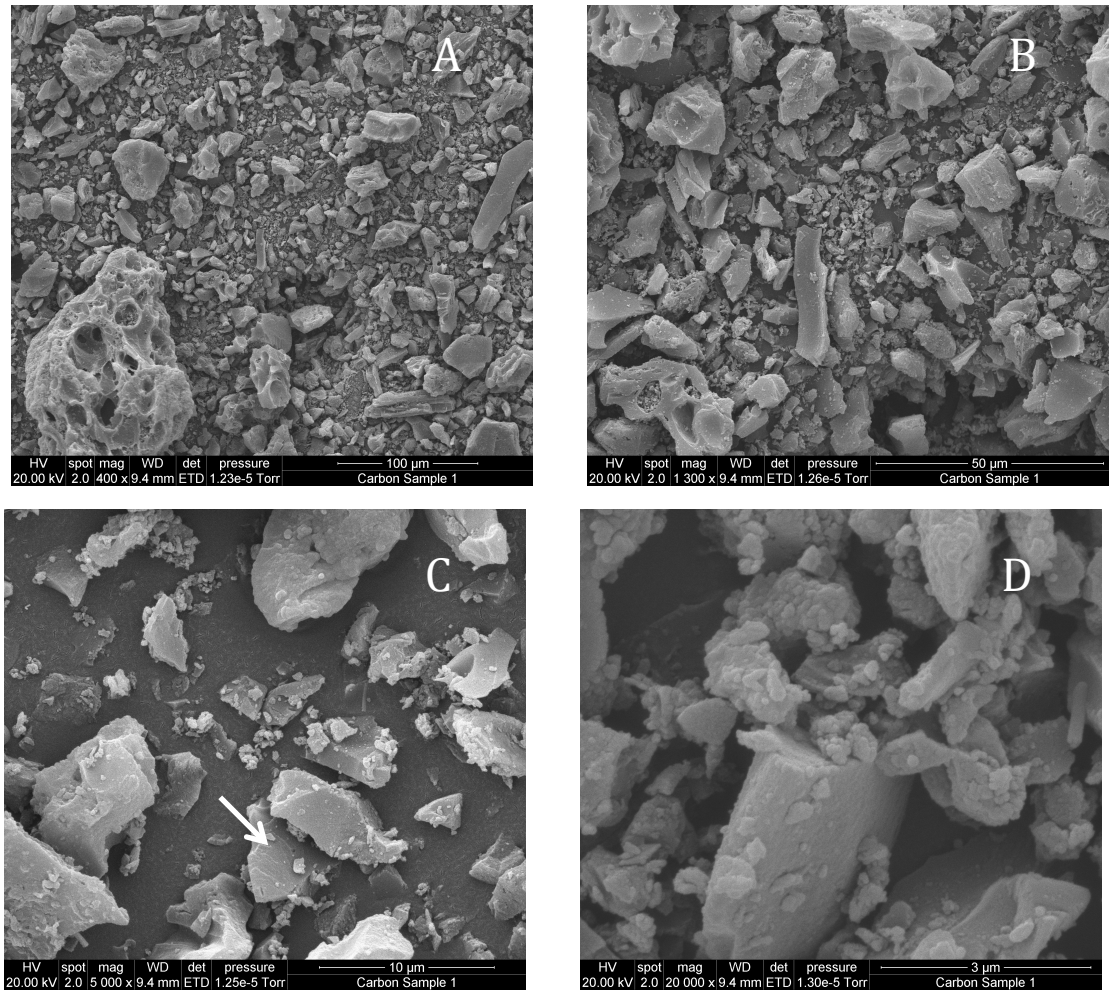

Fig. 5.12. SEM images of PS1000 at 400 (A), 1300 (B), 5000 (C) and 20,000 (D) x magnification.

Figure 5.12 displays SEM images of the original carbon powder over a range of magnifications. Image A shows a variety of particle sizes and shapes with evidence of larger aggregates greater than 100 µm in diameter. In particular, the largest fragment contains craters and holes greater in size than some smaller fragments. At a higher magnification, image B displays angular shards, giving the

appearance of a flat surface on some of the particles. These shards are consistent with the physical nature of the milling process that produces a fine powder from the granular starting compound.

The higher magnifications in image C and D show irregular-shaped nodules present on the surface of some of the non-uniform structures, whereas the angular shards appear flatter and in some cases very smooth. Image C displays a layered texture (arrow) on a shard which could possibly indicate areas of the ordered graphite indicated by Raman spectroscopy to be present in this sample to a small degree.

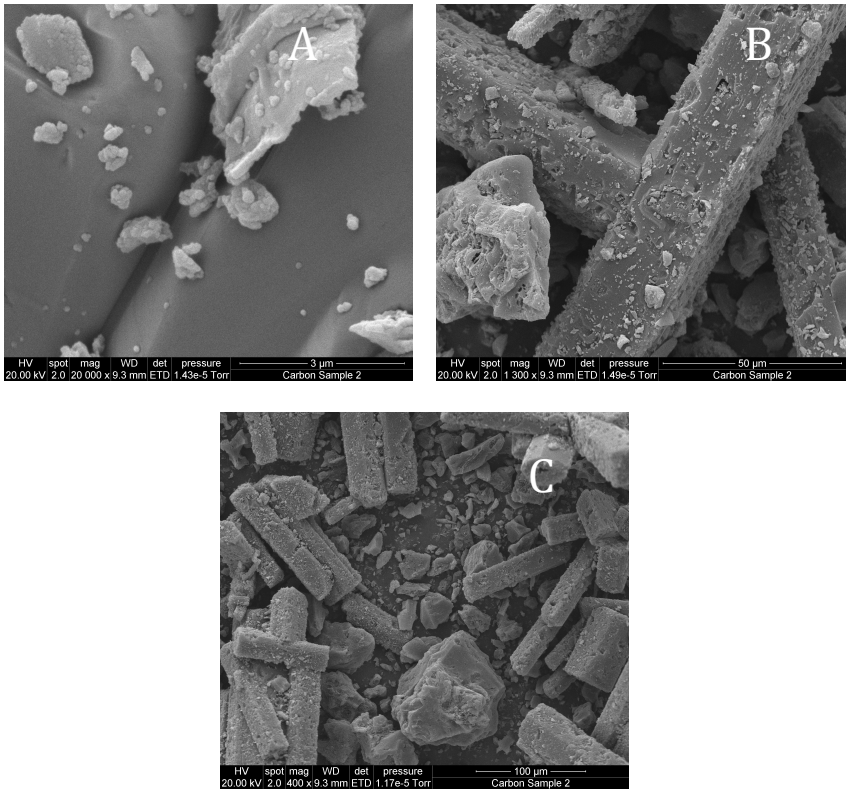

Fig. 5.13. SEM images of the adsorbed DPU material on PS1000 at 20,000 (A), 1300 (B) and 400 (C) x magnification.

Large crystalline structures were evident for the adsorbed DPU material with SEM. Rectangular crystals, which in some images were over 300 µm in length, were interlaced with the carbon particulates. Contrary to the initial aim of adsorbing layers of DPU to provide a coating on the surface of the carbon, it

appears that DPU has aggregated to form the discrete particles adhered to the substrate carbon particulates (Fig. 5.13). These images are not inconsistent with data from Raman spectroscopy, which indicated that DPU was aggregating to an extent so that spectra were similar to those for bulk crystalline DPU.

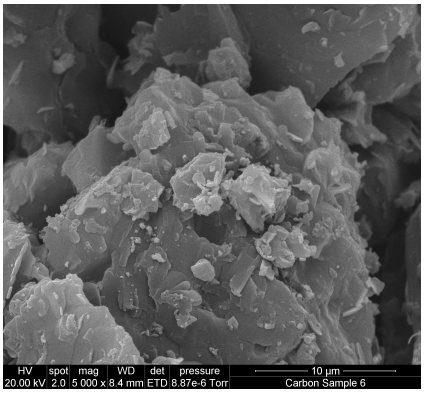

Fig. 5.14. Adsorption of hexadecylurea to PS1000.

Adsorption of hexadecylurea (**5**) to PS1000 however resulted in small planar crystals on the carbon substrate particulates as evident in Fig. 5.14. The alkyl chain in hexadeclyurea is anticipated to have a large degree of flexibility and therefore it is expected to have substantially different crystal packing dynamics from DPU. One could also argue that crystal packing would be encouraged by the hydrophobic interaction of the alkyl chains. In addition, it is noted that this material floats on water (the DPU-coated carbon does not), rather than forming a suspension like the original carbon. This presumably is due to hydrophobic nature of the long alkyl chain. In turn this suggests that the carbon particles have a direct interaction with the urea moieties and the alkyl chains are projected away from the surface of the substrate.

Carbon pre-treated with H_2O_2 and HNO_3 (in attempts to remove iron content, described in Section 5.3.2.4 was also subjected to SEM (Fig. A7). A slight increase in surface roughness was seen, accompanying oxidation of the surface by these reagents.

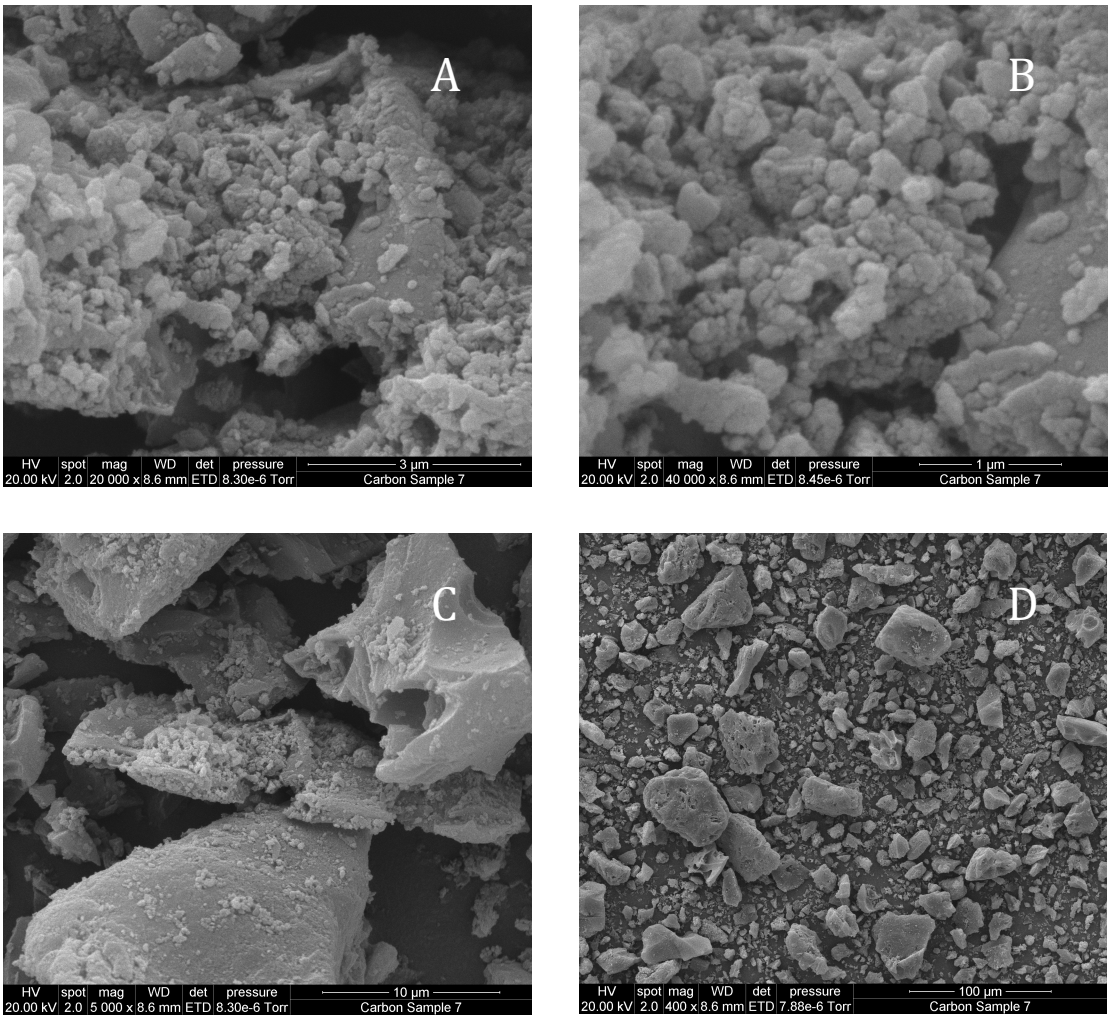

Fig. 5.15. Chemical attachment of 4-nitrophenyl to PS1000 at 20,000 (A), 40,000 (B), 5000 (C) and 400 (D) x magnifications.

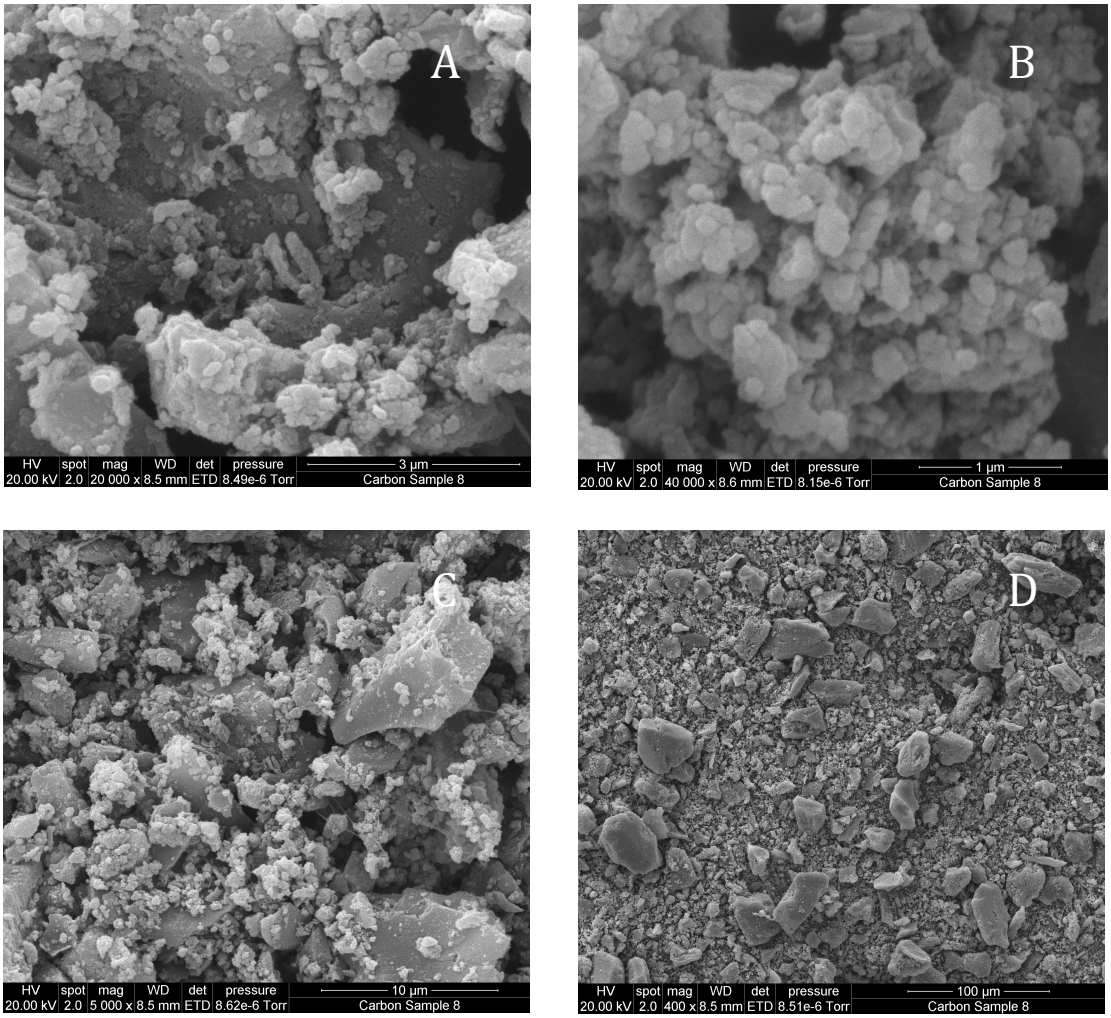

Fig. 5.16. Chemical attachment of DPU to PS1000 at 20,000 (A), 40,000 (B), 5000 (C) and 400 (D) x magnifications.

Chemical attachment of both 4-nitrophenyl (Fig. 5.15) and DPU (Fig. 5.16) substantially alters the morphology of the carbon material. In both cases the higher magnification images show significantly more nodular and rougher surfaces than the original carbon particulates (Fig. 5.12). Given that the process is reliant on spontaneous diazonium coupling, the probability of a multilayer is high, especially in the case for DPU, since once bound to the surface, it has a second aromatic ring available for attachment to additional DPU aryl radical species. Uneven coupling could result in formation of multiple layers in one area, consistent with the nodular features in the SEM images. This is particularly apparent in Fig. 5.16C where scatterings of small features on the carbon particles can be observed.

A dilemma arises in this analysis, if these particulates are multiple layers of diazonium-coupled DPU species, the question then becomes why has it not been confirmed by other spectroscopic methods (Raman, FTIR)? It is also recognised that the SEM images are always a small snapshot over a very small area of the material tested; these might not be representative of the entire sample.

In an attempt to quantify the amount of chemically attached 4-nitrophenyl and DPU samples were sent for microanalytical combustion analysis (Campbell Microanalytical Laboratory, Otago University). Table 5.1 lists the carbon, hydrogen and nitrogen composition for each sample. The *ca*. 20% w/w unaccounted for composition is attributed to oxygen, iron and other elements in the PS1000 sample.

Table 5.1 Percentage of atoms in carbon powder samples. (Corrected percentage showing contribution from attached material).

	% C	% H	% N
PS1000	78.23	1.25	<0.3
4-Nitrobenzene	70.90	1.52	0.72 (0.42)
DPU	67.27	1.81	2.93 (2.63)

In the PS1000 sample the amount of nitrogen was below the detection limit for this technique. Focusing on the increase in nitrogen and assuming all of this is due to the urea moieties adhered to the carbon samples, the amount of grafted compound on the modified substrate is approximately 3.6% w/w and 19.7% w/w for 4-nitrophenyl and DPU respectively. However, this does disregard the possibility of an azo group –N=N- present on the surface in the multilayers. An azo group is formed when the diazonium species is involved in aromatic

electrophilic substitution with an activated or electron rich aromatic ring that is already grafted as opposed to homolytic radical attachment. However, this is substantially at odds with the decrease in carbon content after grafting both 4-nitrophenyl and DPU. There are two potential causes for this. The first is that the grafting process results in a greater degree of oxygen functionalities on the carbon substrate. The second is that the grafting conditions lead to uptake of spectator species (e.g. BF_4^-) resulting in a greater level of ash content and/or species with elements not selected for analysis.

In this work, preliminary investigations are reported for the attachment of substituted ureas onto the surface of a high surface area carbon powders. The optimisation of the efficiency of the reaction has not been reported and will require further studies. However it has been shown that reaction time, reduction potential of the diazonium salt, concentration and solvent can effect the final coverage and morphology of the grafted material.[269,273] Little is understood about how the composition of carbon substrates affect the structure of the modified substrates. It has been suggested that a two-stage model represents the mechanism for grafting (Scheme 5.2).[269] The first step involves the reversible adsorption of the aryldiazonium where the adsorbate accepts an electron from the surface. The second step involves the elimination of nitrogen followed by the covalent bond formation of the molecule with the surface.

Scheme 5.2. Two-stage model representing the mechanism for grafting of an aryldiazonium to a surface.

It is not unreasonable to expect a larger chemisorption rate constant, k_{ch}, for a carbon substrate that has a higher degree of sp^2 character, such as graphite or graphene, especially at graphitic edges. Carbon surfaces that are better electron donors adsorb the diazonium more rapidly and with higher yields.[269] Changing to a sp^3-rich carbon alters the kinetics such that the chemisorption rate constant,

k_{ch}, is smaller to the extent that it may become the rate-determining step. According to Jayasundara,[269] their classification of a hydrogen-doped insulating carbon has approximately 17% sp^2 content and 40-57% H content. On comparison of this hydrogen-doped carbon with Raman spectroscopy, PS1000 has similar if not slightly lower sp^2 content. However, analysis by ss-NMR (Section 5.3.2.3) is consistent with minimal hydrogen being present. This leads to the proposition that PS1000 is a disordered carbon structure with high sp^3/sp^2 content and relatively little hydrogen (together with a high Fe content). As it is minimally graphitic, the kinetics of adsorption (Step 1, Scheme 5.2) can be modelled with a reversible Langmuir adsorption isotherm. In contrast carbon surfaces that perform better as electron donors (graphitic) adsorb the diazonium species more rapidly and therefore do not follow a Langmuir isotherm.[269] Additional factors in the adsorption of aryldiazonium cations that might also play a role in attachment include hydrophobic effects or preferential orientation at the interface. As DPU has a second aromatic ring, it might enable extra van der Waal interactions at the surface thus stabilising the adsorbed aryldiazonium promoting dediazonation and chemisorption.

5.3.3. Electrochemistry of H_2O_2 on Low Surface Area Electrodes

To evaluate the ability of the substituted urea on a surface to bind H_2O_2, an electrochemical approach was taken. The assumption for this experiment is that if the urea is able to bind H_2O_2 from a known [H_2O_2] solution it should lower the bulk H_2O_2 concentration. This in turn can be observed using electrochemical detection of the bulk H_2O_2 concentration and thus a difference in current will be observed according to

$$H_2O_2 + 2H^+ + 2e^- \rightarrow 2H_2O \qquad 5.6$$

5.3.3.1. Chronoamperometry

Chronoamperometry involves the change of potential of the WE in a single step from a value at which little or no Faradaic current occurs, to a potential where the current response can be measured as a function of time. In this study the

potential was stepped between +100 mV to -600 mV vs Ag/AgCl on a glassy carbon microelectrode where the reduction of H_2O_2 is detectable. This step sequence was 10 s at 100 mV followed by 30 s at -600 mV at the end of which a steady state current was observed. A series of 5 potential step sequences were recorded and the current averaged over the last 1 s.

The most significant feature of this method is that the rate of reduction attains a steady-state that is controlled by hemispherical diffusion of [H_2O_2] to the electrode surface as given by Eq. 5.1.

An initial attempt to include a substituted urea to the system was through the addition of water-insoluble hexadecylurea (**5**) to an aqueous H_2O_2 solution with vigorous stirring before taking measurements. Unfortunately this did not result in a dispersion of the urea and this insoluble material coated the electrode to form an insulating layer and prevented current flow. High surface area carbon with diphenylurea (**2**) physisorbed onto the surface (prepared as in Section 5.3.2) was used instead. The relationship between limiting current and bulk [H_2O_2] was established for this system. Known quantities of H_2O_2 premixed in 0.1 M phosphate buffer were successively added into a temperature-controlled (20 °C) water-jacketed cell containing a GC microelectrode (WE), Ag/AgCl (RE), Pt (CE) electrodes and 0.1 M phosphate buffer at pH 7.2.

Fig. 5.17 displays the chronoamperometric responses for a range of [H_2O_2] from 0 – 1.5 mM in the buffer following a step from +100 mV to -600 mV vs Ag/AgCl. A steady-state of reduction of H_2O_2 is observed 15 s after the step potential to -600 mV in each case. The response was analysed by averaging the data over the last second in each case.

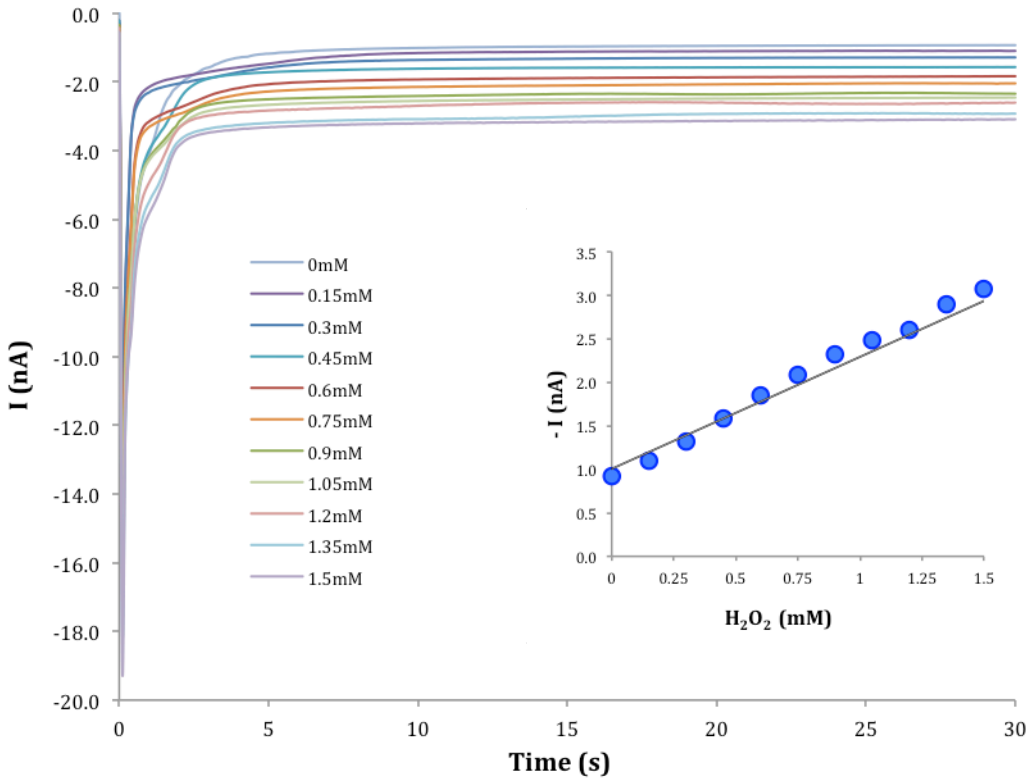

Fig. 5.17. Transient current response for potential steps between +100 to -600 mV vs Ag/AgCl with a static glassy carbon microelectrode at 20 °C for the reduction of H_2O_2 over a range of concentrations from 0 – 1.5 mM. Inset: steady-state currents as a function of $[H_2O_2]$.

Fig. 5.17 (inset) shows the steady state response of a static glassy carbon electrode for a range of bulk $[H_2O_2]$ for the displayed transients 0 – 1.5 mM. A linear dependence is observed for these limiting currents at this concentration range. Fig. 5.18 displays the steady-state responses at higher concentrations (0 – 15 mM) where a non-linearity in concentration-dependence is observed.

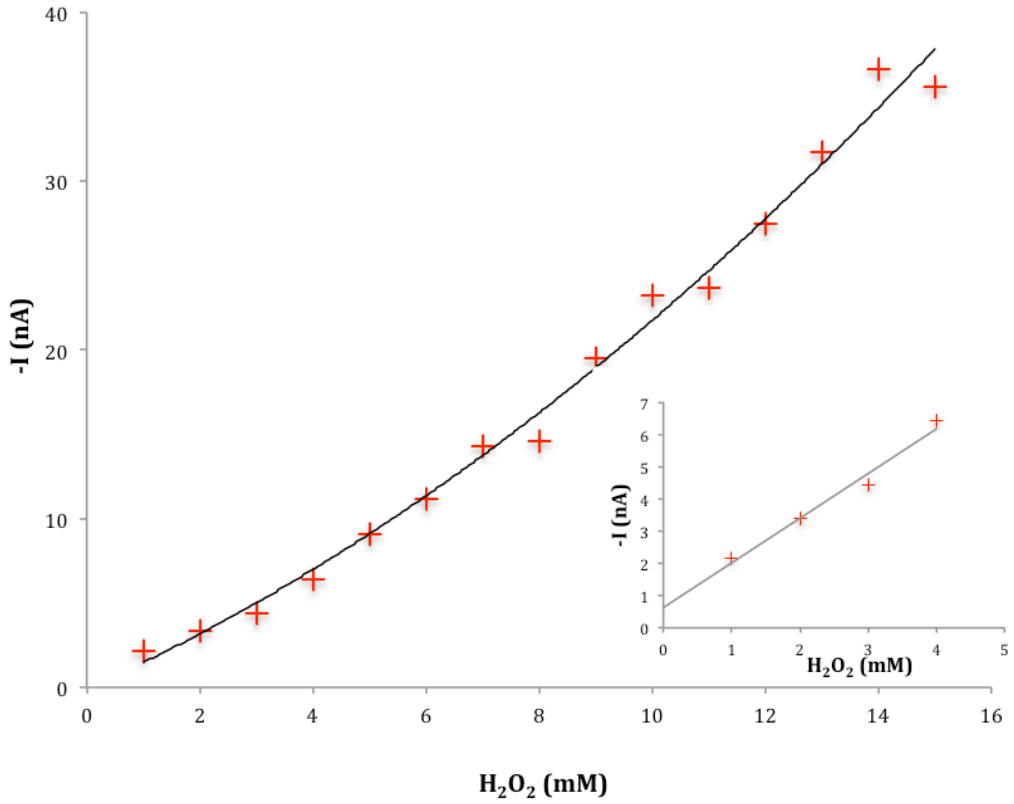

Fig. 5.18. Steady-state current response for potential steps between +100 to -600 mV vs Ag/AgCl with a static glassy carbon microelectrode at 20 °C for the reduction of H_2O_2 over a range of concentrations from 0 – 15 mM. Inset: steady-state currents with $[H_2O_2]$.

A linear dependence on $[H_2O_2]$ is observed up to 4 mM, but this dependence becomes progressively curved as the $[H_2O_2]$ increases. This demonstrates that a suitable maximum concentration of 4 mM H_2O_2 can be used if a linear correlation of limiting current is desired.

Following this response calibration, a control experiment using 100 mg of PS1000 was suspended in 10 ml 0.1 M phosphate buffer at pH 7.2 and was subjected to successive additions of known quantities of H_2O_2 premixed in buffer.

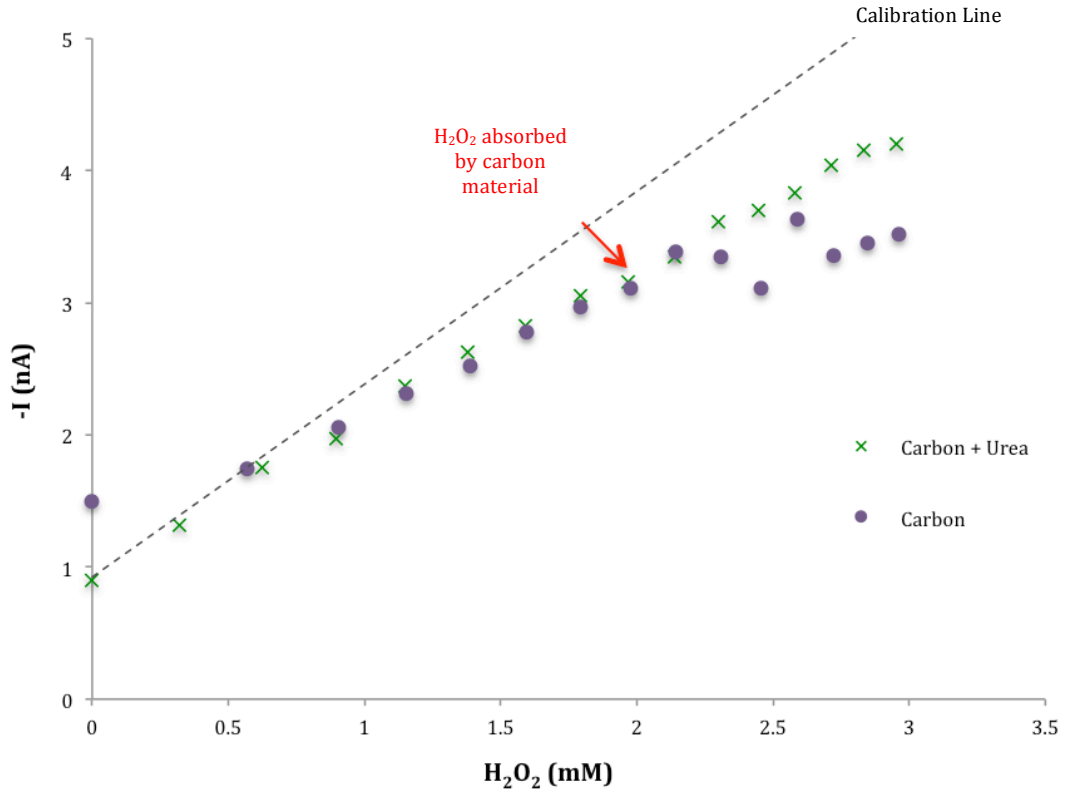

Fig. 5.19. Steady-state current response of [H_2O_2] with PS1000 (purple circle) and adsorbed DPU PS1000 (green cross) against a standard curve (dashed line) with no carbon powder present.

The data presented in Fig. 5.19 demonstrates that the presence of uncoated carbon particulates leads to lower currents than expected. This suggests that the uncoated carbon either exhibits some degree of adsorbancy of H_2O_2 or initiates decomposition of H_2O_2. If lowering of [H_2O_2] is due to adsorption then in hindsight this might have been anticipated given the high surface area of the substrate. Based on the size of H_2O_2 molecules, 0.12 mol of this species would be required to close pack onto 1 g of the carbon at 1000 $m^2\ g^{-1}$. The 4 mM H_2O_2 solution, however, only contained a total of 0.09 mmol H_2O_2 but showed a response *ca*. 15% lower than that expected. Consequently, this extent limits the utility of this experiment considerably.

Interestingly, a sample of adsorbed diphenylurea on the high surface area carbon did not lower the [H_2O_2] to any more than the carbon substrate alone.

This is not inconsistent with the SEM images (Section 5.3.2.5) of the carbon and diphenylurea adsorbed carbon which suggested a deposition of isolated crystals of DPU rather than formation of a coherent thin layer. DPU deposited in a crystalline phase reduces the number of urea entities in contact with the solution for binding. Indeed, the majority of DPU molecules are occluded in this case.

5.3.4 Characteristics and Electrochemical Response of Carbon Felt

Carbon felt is a three-dimensional fibre structure derived from the pyrolysis of either polyacyronitrile (PAN) or rayon (cellulose polymer). Carbon felts show potential over other carbon materials in synthesis,[278] energy storage and environmental recovery applications.[279] Carbon felt excels with respect to high tensile strength, low thermal expansion and in practical terms as they do not require the addition of exogenous materials to form an electrically conductive substrate when used as an electrode. Given earlier issues with iron content in carbon powders the Fe content was determined by microanalysis. This demonstrated that the Fe content was less than the detection limit of 0.3% w/w. Since the felt is prepared from the pyrolysis of a polymer, rather than from plant or coal derived material as in the case of carbon powders, it is not surprising that there is negligible Fe content. The Raman spectrum of the felt shows a broad D-band with a very weak G-band (spectra provided in Fig. A8) characteristic of a disordered amorphous carbon with little graphitic structure.

The three dimensional structure allows electrolysis of the solution inside and outside the outer dimensions of the felt structure and pathways combine to give appreciable current densities, especially in high surface felts.[280] From a kinetic point of view, the process will become controlled by convection-diffusion mass transport from the bulk solution to the outer surface area of the felt. Under these conditions, the limiting current density must now include the electrode volume, V_e (based on the outer dimensions of the felt), in combination with the specific surface area, A_e ($m^2\ m^{-3}$) and the diffusion coefficient, D, as given in Eq. 5.7.

$$i_L = nFDA_eV_ec \quad 5.7$$

where *i* is the limiting current density, *n* is the number of electrons transferred in the electrochemical process, *F* is Faraday's constant and *c* is the concentration of the electroactive species. Therefore it is important to characterise the physical and structural properties of the felt.

5.3.4.1. Surface Area Determination

Two methods were used to analyse the surface area of the carbon felt. First, a Brunauer-Emmett-Theory (BET) isotherm was performed through physical adsorption of nitrogen gas molecules onto the felt surface at 77K. This provided a specific surface area of between 0.41-0.42 m^2/g, which is considerably lower than anticipated. This suggests that the felt is substantially non-porous and the surface area is simply the accumulation of the surface area of the individual fibres.

The second method involved the electrochemical assembly described in Section 5.2.1.4. Reduction of $[Fe(CN)_6]^{3-}$ was used in an attempt to quantify the surface area of the felt. A section of felt with dimensions 1.2 x 2.3 x 0.3 cm was placed in an aqueous solution of 0.5 mM $[Fe(CN)_6]^{3-}$ in a pH 7 phosphate buffer. This 133.3 mg rectangular prism shaped working electrode had an outer surface area of 7.62 cm^2 and volume of 0.83 cm^3. If the individual carbon fibres have density similar to that for graphite (typically 2.09 to 2.23 g cm^{-3})[281-284] then this implies a non-carbon 'void' fraction of *ca.* 0.93 for this felt material.

The peak currents for the anodic and cathodic waves increase with increasing scan rates. It was proposed by Kato that in the early stages of the anodic and cathodic waves potential scan the current is controlled by the internal diffusion of $[Fe(CN)_6]^{3-}$ or $[Fe(CN)_6]^{4-}$ inside the felt matrix.[280] In contrast, the currents after the peak responses are more likely to be dominated by mass transfer from the bulk solution towards the outer surface of the electrode. Similar systems

have shown that external diffusion towards the electrode as well as internal diffusion from within the matrix of the carbon both significantly contribute to the currents observed.[280] It is also affected by the ratio of area to volume A/V where diffusion towards an electrode from the bulk becomes dominant at higher ratios.

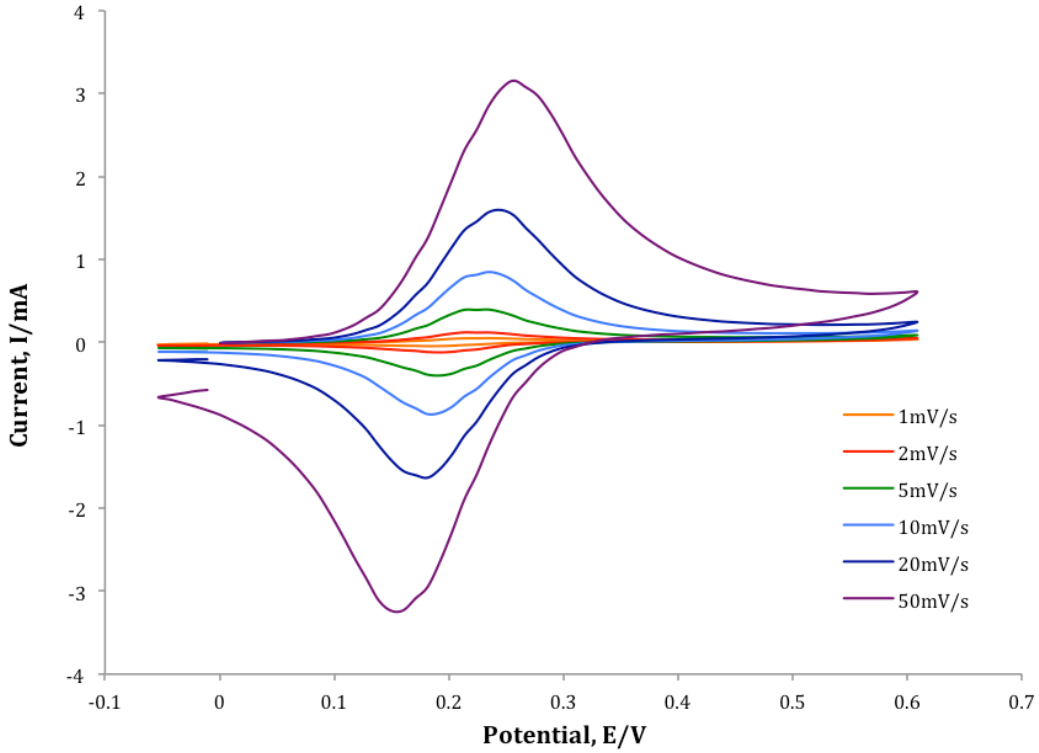

Fig. 5.20. Cyclic voltammogram of 0.5 mM $[Fe(CN)_6]^{3-}$ with a carbon felt electrode at v = 1 to 50 mVs^{-1}.

Chronoamperometry was carried out for the reduction of 0.5 mM $[Fe(CN)_6]^{3-}$ at -0.2 V *vs.* Ag/AgCl following an equilibrium time of 10 seconds. Chronoamperometric responses are expected to follow the Cottrell equation

$$i = \frac{nFAc\sqrt{D}}{\sqrt{\pi t}} \qquad 5.8$$

so that a plot of $it^{1/2}$ should approach a constant value.

A felt electrode measuring 1.4 x 2.1 x 0.3 cm with a mass of 135.6 mg was used. The current was observed to approach a constant value over 50 s. The time dependence of total outer surface and inner surface current, i_{total}, was plotted as the product of $-i_{total}t^{1/2}$ as a function of t (Fig. 5.21).

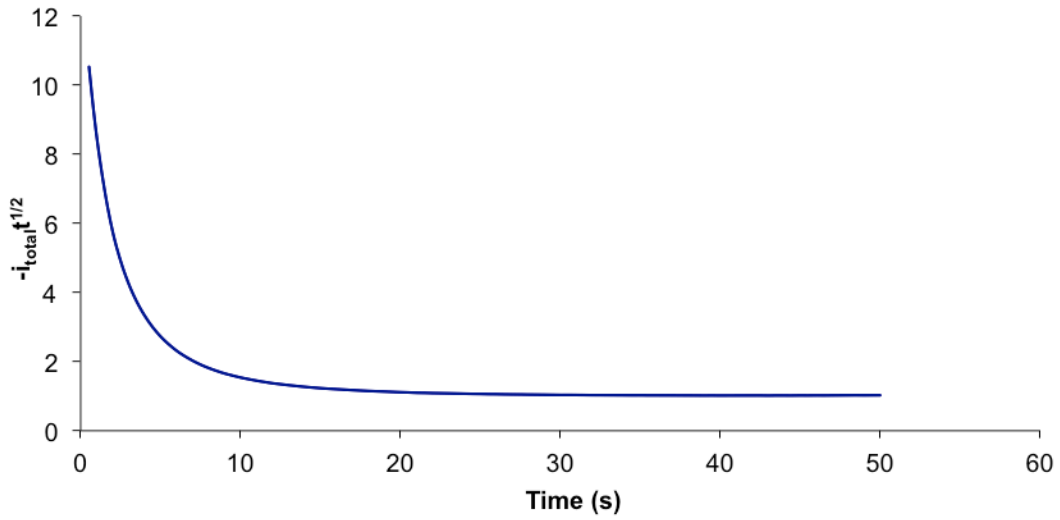

Fig. 5.21. Chronoamperometry of the carbon felt at -0.2 V *vs.* Ag/AgCl plotted as $-i_{total}t^{1/2}$ against time for the response of 0.5 mM $[Fe(CN)_6]^{3-}$ in pH 7 phosphate buffer.

Given that that $i_{total}t^{1/2}$ approaches a constant value of 1.02 mA $s^{-1/2}$ it is not inconsistent with the current in this potential region being controlled by linear diffusion of the electroactive species, in particular from the bulk solution to the outer surface area of the felt. Using this value for the limiting value for $i_{total}t^{1/2}$ and a diffusion coefficient for $[Fe(CN)_6]^{3-}$ of 7.6 x 10^{-6} cm^2 s^{-1} an effective outer surface area of 13.7 cm^2 is inferred using Eq. 5.8.[280]

$$i_{total}t^{1/2} = nFA_{out}(D/\pi)^{1/2}c_{[Fe(CN)_6]^{3-}} \qquad 5.8$$

The projected surface area of the rectangular prismatic felt is 7.98 cm^2. Given that the Cottrell equation infers a larger surface area indicates that $[Fe(CN)_6]^{3-}$ is able to penetrate into the felt to a certain depth. This is not inconsistent with the high void fraction calculated earlier. Kato[280] has determined the current attributable to internal electrolysis of an electroactive species in a porous

electrode, i_{in}, by subtracting the diffusion-limited current from the total current. The time-dependence of i_{in} in these cases is such that it approaches zero. A simplified model of this diffusion was derived by Kato and can be expressed by

$$\ln i_{in} = -\frac{\pi^2 D t}{l^2} + \ln \frac{4nFA_{in}D}{l} c_{[Fe(CN)_6]^{3-}} \qquad 5.9$$

with l representing the average distance between carbon fibers and A_{in} is the effective surface area of the fibres constituting the carbon felt electrode.

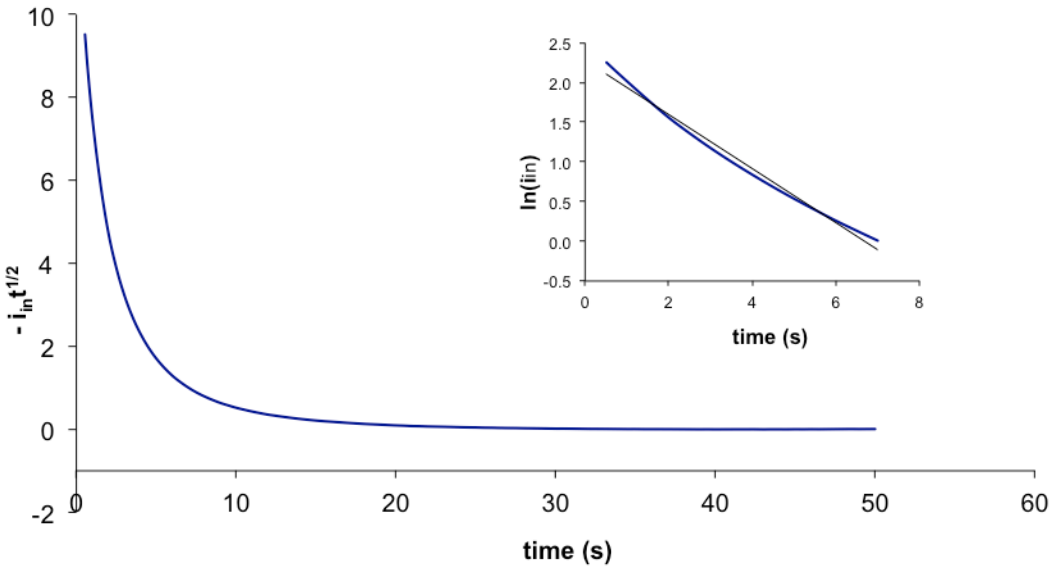

Fig. 5.22. Chronoamperometry of the carbon felt at -0.2 V plotted as $-i_{in}t^{1/2}$ with subtraction of the diffusion limited current, against time for the response of 0.5 mM $[Fe(CN)_6]^{3-}$ in pH 7 phosphate buffer. Inset: ln(i_{in}) against time.

The plot of ln(i_{in}) against time yields a linear relationship with a slope (0.3406 s^{-1}) that can be inserted into the first term of Eq. 5.9 providing a value for l of 148 µm. Combining this with the observed intercept (2.28) and the second term of Eq. 5.9 provides an effective surface area of 97.6 cm^2 and a specific surface area of 0.072 m^2 g^{-1}. This inferred electrochemically available surface area is substantially lower than the 0.41-0.42 m^2 g^{-1} found by BET analysis for physisorption of gas phase N_2 molecules. This might suggest a high degree of porosity of the fibres, but that these pores have dimensions too small

for admittance of the solvated $[Fe(CN)_6]^{3-}$ anions. Alternatively, if the surface was negatively charged, the $[Fe(CN)_6]^{3-}$ anions would be repelled resulting in a lower observed surface area.

SEM images of the carbon felt show randomly dispersed fibres that are cylindrically shaped with a range of diameters (Fig. 5.23). The fibres have shallow grooves (*ca.* 100 nm in width and depth) along the long axes and with occasional small nodules (*ca.* 100 nm) on the surface. The space between the fibres is large and consistent with the void faction of 0.93 calculated earlier. The Cottrell analysis determined an average distance between fibres of 148 μm. This is consistent with the spacing observed in Fig. 5.23.

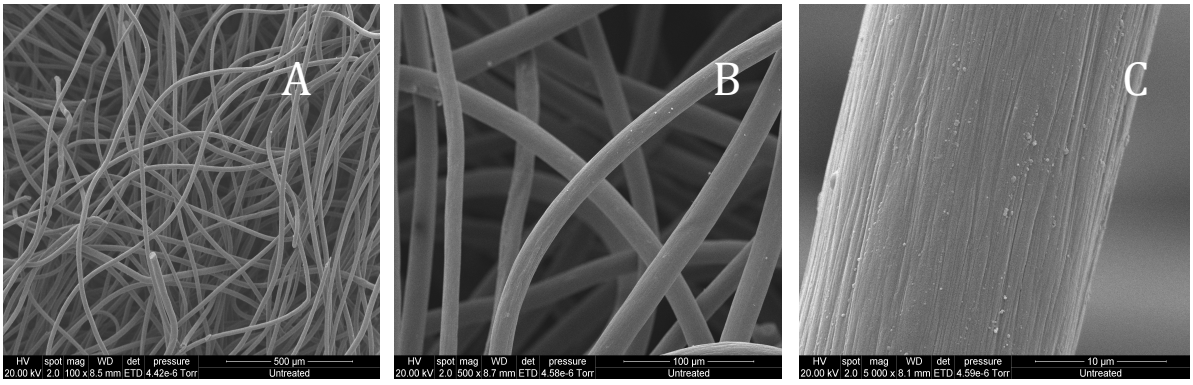

Fig. 5.23. SEM images of carbon felt at 100 (A), 500 (B) and 5000 (C) x magnification.

Additional methods to obtain surface area might be applied in future studies should more precise data be required. These include filamentary analog procedure, [285] permeametry,[286] and mercury porosimetry.[287]

5.3.4.2. Electrochemistry of felt with H_2O_2

The low surface area of the felt clarifies that it is inappropriate for use as a primary carbon substrate for the proposed cathode. As outlined in Section 1.5 the carbon felt is anticipated to have a role in providing physical support and electrochemical communication for higher surface area carbon powders, in turn

modified with the appropriate binder or catalyst compound. Since the felt will form part of the final cathode, a preliminary assessment of the response of this material with respect to the electrochemistry with H_2O_2, electrolyte and grafting processes.

Chronopotentiometry was selected as the technique for providing a preliminary indication of the capability of the felt to participate in the electrochemical reduction of H_2O_2. Any participation would not likely provide a significant contribution to the charge and discharge currents for a finished electrode given the low surface area of the felt. Indeed, in future it may be found preferable that this substrate (with the primary purpose of carrying current) should not participate in the cathode reactions. This is the case for example in the metallic lead current-carrying grid in lead-dioxide cathodes in lead-acid batteries where participation of metallic lead results in deleterious positive-grid corrosion. [288]

In the chronopotentiometry technique (also known as galvanostatic control) a constant current *i*, is applied to the electrode to cause an electroactive species to be reduced (in this case). The potential of the electrode moves to values characteristic of the redox couple and varies with time as the concentration of the couple changes at the electrode surface. [289] After the concentration of the species drops to zero at the surface, the flux of species to the electrode is insufficient resulting in the drop of the electrode potential to more negative values (conversely, more positive potentials for an oxidation process).

The susceptibility of the felt to electrochemical oxidation and reduction in the electrolyte in the absence of H_2O_2 was first evaluated. Chronoamperometric oxidising and reducing tests were performed on the carbon felt electrode in a 1 M KOH solutions in the absence of H_2O_2.

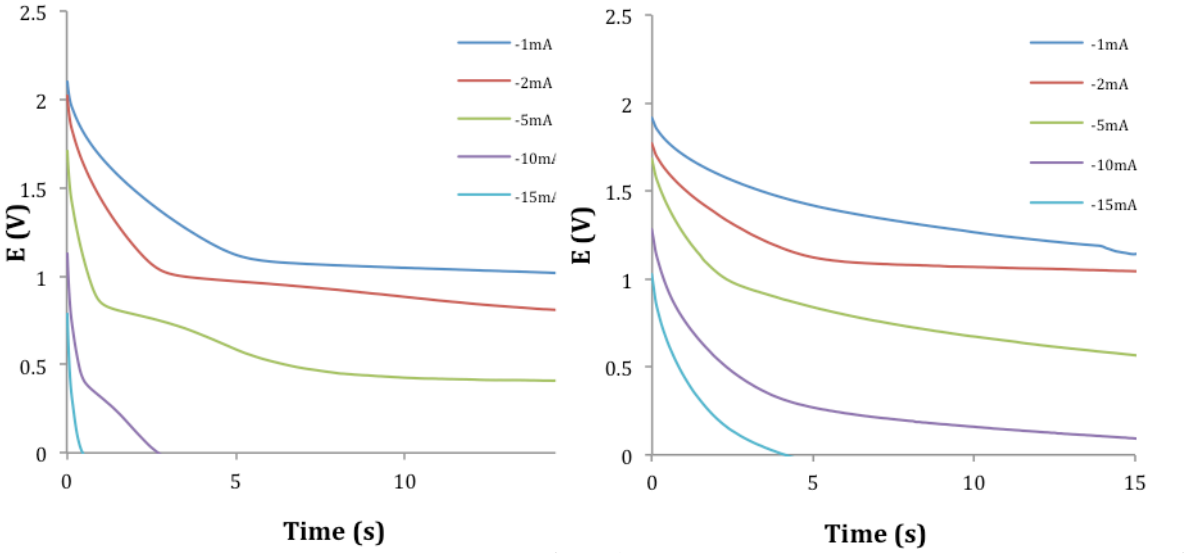

Fig. 5.24. Chronopotentiometry of the carbon felt before treatment (left) and after -100 mA for 60 sec then 100 mA for 60 sec (right) from -1 mA to -15 mA in 1 M KOH.

Currents from -1 mA to -15 mA were applied immediately following either oxidation at 100 mA for 1000 sec or reduction at -100 mA for 1000 seconds. These data are provided in Fig. 5.24. Following oxidation treatment of the felt, the colour of the electrolyte was found to become dark yellow/brown in colour. This suggests that some of the solid carbon fibre substrate had formed soluble species. Mass spectrometry of this solution produced peaks at 158, 179 and 214 m/z which is not inconsistent with oxidation compounds from the pyrolysis of PAN. The pyrolysis process is understood to include cyclisation and dehydrogenation reactions that ultimately lead to oxidation products remaining in the product if the final dehydrogenation is incomplete (Fig. 5.25).[290,291] In an alkaline electrolyte the dangling or edge oxidation products may be cleaved by the oxidising conditions with assistance from hydroxide ions.

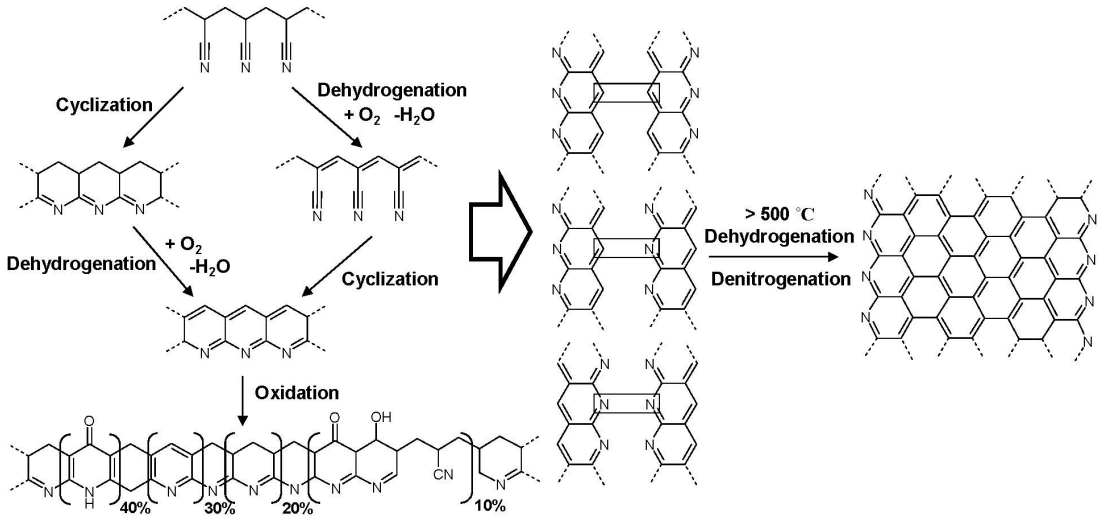

Fig. 5.25. Process of the pyrolysis of PAN. Image adapted from website: www.cmu.edu/maty/materials/Nanostructured-materials/carbon-nanostructures.html.

When the oxidised felt was placed in a new solution of electrolyte, the potential response was similar to that before oxidation. Observing the felt after reduction showed that it was now coated with a light grey/blue material. Further investigation would be required to establish what this material is. This modified felt when placed in a new electrolyte solution appears to be electrochemically inactive in this media. This suggests that before this type of carbon felt be employed in a final battery cathode that detailed studies be undertaken to establish the stability of the material in the particular battery electrolyte to be used. Oxidation to form soluble species will lead to structural failure and may interfere with the battery anode, while reduction to form passivating layers will negate the utility of the material.

Using carbon felt as an electrode (2.0 x 1.0 x 0.3 cm), chronopotentiometry was performed in 50 mM H_2O_2 in a 1 M KOH electrolyte. A zinc electrode was used as both the reference and counter electrode. This combination of zinc anode and KOH electrolyte is representative of the possibilities that an H_2O_2-based cathode might be combined with in a finished battery. The imposed galvanostatic currents ranged from -1 to -25 mA (Fig. 5.26). Currents greater in magnitude to -25 mA could not be attained due to mass-transport limitations. A pre-treatment

was applied in order to obtain consistent results; a +5 mA constant current was applied for 5 seconds before each cathodic excursion.

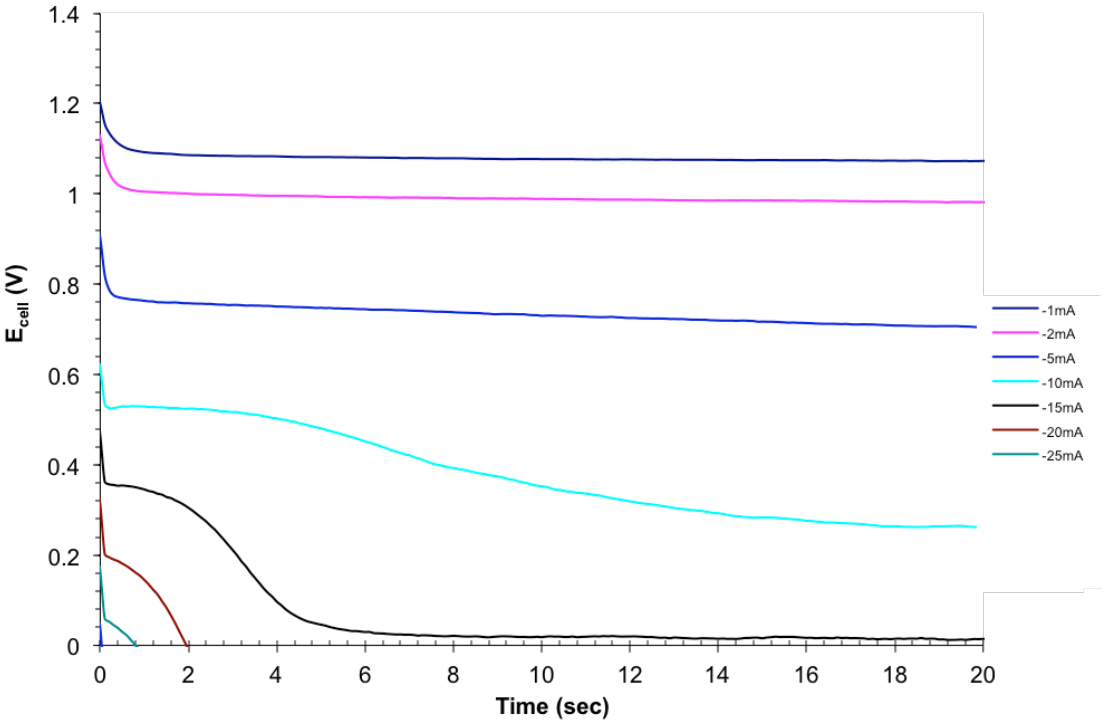

Fig. 5.26. Chronopotentiometry of the carbon felt in 50 mM H_2O_2 with a pre-treatment at 5 mA for 5 seconds.

As expected the greater the magnitude of the current, the more rapidly the concentration of H_2O_2 becomes zero at the electrode surface with a consequent decrease in cell potential following which a pseudo-steady-state is observed. At a -2 mA discharge a steady-state polarisation of *ca.* 200 mV is observed from the open circuit current of *ca.* 1.2 V. This total current represents a low current density of only *ca*. 20 μA cm^{-2} for the carbon fibre substrate (given the electrochemically available surface area of 0.072 m^2 g^{-1} and mass of 120 mg). This suggest that the carbon fibre substrate should not be considered as a likely contributor for the total discharge current on a final cathode based on H_2O_2 reduction.

5.3.4.3. Functionalisation of Carbon Felt

The ability of the carbon felt to participate in the electrochemical grafting reactions was assessed. Grafting of the high surface area carbon powders could be contemplated on dispersions of these powders (as in Section 5.3.2.1) or on fully assembled electrodes (carbon powders bound to a carbon fibre substrate). If it is to take place by the latter approach then the fibre support may well be exposed to the grafting conditions. This may offer advantages including: a slight increase in H_2O_2 binding or generation sites; the potential for blocking fibre surface sites for competing reactions or disadvantages (e.g. passivation of the fibre surface).

In an attempt to functionalise the surface of the carbon felt, 4-nitrobenzenediazonium tetrafluoroborate (**38**) was attached via electrochemical diazonium attachment in a stirred solution. Stirring of the salt solution is essential to ensure flow of the electroactive species into the fibre matrix. A 0.2 M solution of the diazonium salt in a 0.1 M NBu_4PF_6 solution in MeCN was used to graft onto a 2 x 1 cm felt using aluminium foil as the CE and Ag wire as the RE. Aluminium foil was used as a ready means to form a disposable appreciable surface area counter electrode. Addition of ferrocene was used as a reference in the non-aqueous electrolyte. The one-electron oxidation of ferrocene (Fc) to the ferrocenium cation (Fc^+) is a standard in electrochemistry with a redox potential of 0.50 V vs SCE. The RE was calibrated against the ferrocene/ferrocenium couple after the displayed voltammograms were collected. 10 scans were performed at 50mV/s from +0.11 to -1.23 V *vs.* Fc/Fc^+ to show a broad reduction wave of the diazonium characteristic of grafting process. This wave was not as pronounced as the smaller surface area electrodes; instead it is very broad typical of a large surface area response (Fig. 5.27).

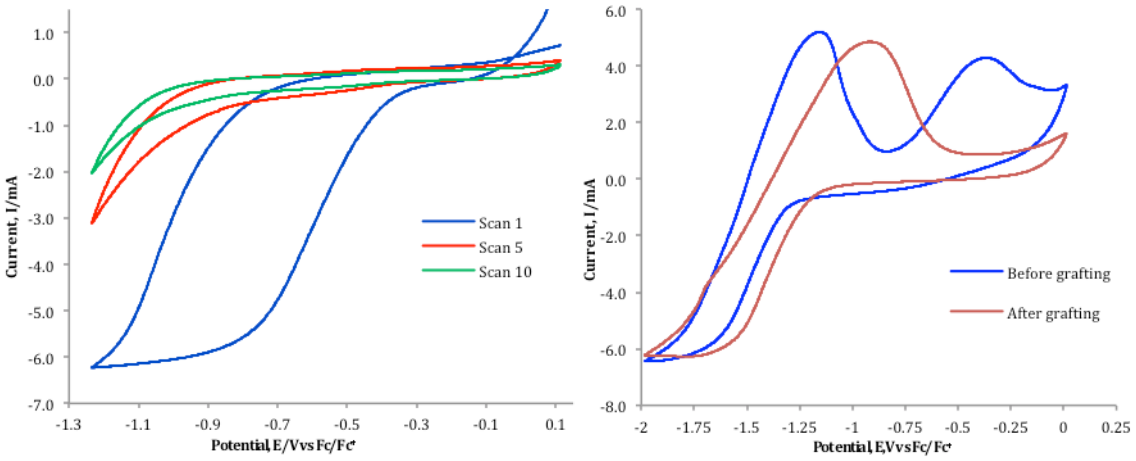

Fig. 5.27. Electrochemical attachment of 4-nitrobenzenediazonium in 0.1 M NBu_4PF_6 in MeCN, scanning potentials from +0.11 to -1.23 V *vs.* Fc/Fc^+ at 50 mV/s. Showing scans 1,5 and10 (left). 0.1 M NBu_4PF_6 solution in MeCN before and after grafting (right).

The difference in the CV in electrolyte from 0.0 to -2.0 V before and after grafting is pronounced (Fig. 5.27). It is uncertain whether the voltammogram in just electrolyte shows redox of the electrolyte itself, or other material on the surface. In particular, the broad oxidation wave at -0.5 V *vs.* Fc/Fc^+ is no longer evident after the grafting process. In an aprotic solvent such as MeCN, reduction of the NO_2 to the radical ion should be observed at -1.28 V.[292] However, this reversible reaction is not discernible on the modified felt and therefore there is no confirmation of the grafting procedure having taken place under these conditions. The response of the modified felt towards ferrocene as an electrochemical probe was examined in 0.1 M NBu_4PF_6 in MeCN (Fig. 5.28). The electrochemical response from 1 mM ferrocene was not totally suppressed. This is consistent with only partial grafting of 4-nitrobenzene to the felt surface.

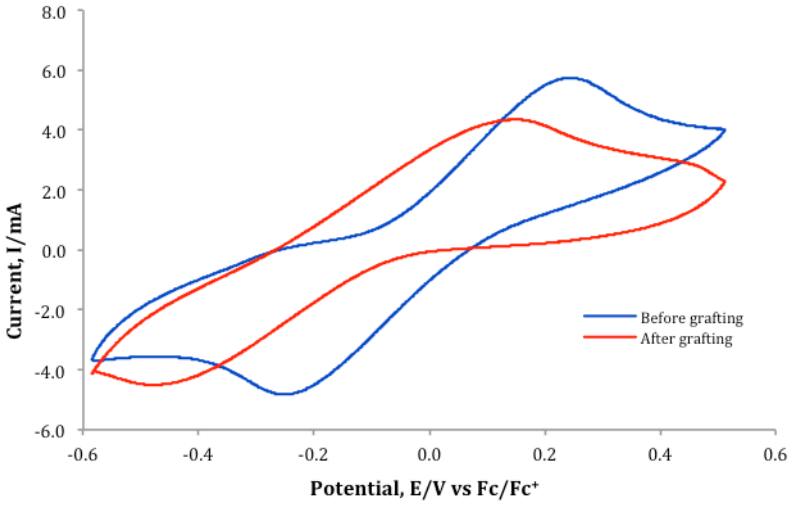

Fig. 5.28. Cyclic voltammograms recorded in 0.1 M NBu_4PF_6 containing 1 mM ferrocene on carbon felt before grafting (blue) and the carbon felt after grafting with 4-nitrobenzenediazonium (red). Scan rate: 50 mVs^{-1}.

ATR-FTIR spectra of the modified carbon felt did not show characteristic peaks for 4-nitrobenzene. This is likely due to either limited coverage of the grafted material or the small percentage of grafted material relative to the carbon fibre substrate.

5.3.5 Electrochemistry of Nitroxides on Low Surface Area Electrodes

Cyclic voltammetry was used as the main electrochemical technique employed in the grafting of nitroxides to a glassy carbon electrode. This technique provides a ready means for obtaining an overview of the oxidation and reduction potentials of the nitroxides and is used to provide evidence of diazonium attachment.

5.3.5.1. Electrochemistry of solutions of TEMPO derivatives

The aim of this section was to attach nitroxide species to a carbon surface and provide preliminary evidence of their use as an electrocatalyst for H_2O_2 formation. Initially, electrochemistry of the solution species was performed to find the oxidation potentials of the nitroxide moieties.

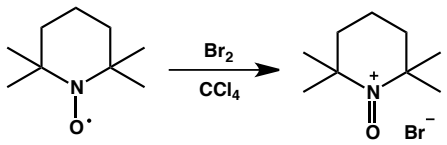

Scheme 5.3. Oxidation of TEMPO with bromine in solution.

TEMPO was oxidised with bromine to furnish a bright red precipitate of the oxoammonium salt (see Section 3.8 for synthesis). The oxoammonium salt was dissolved in MeCN and subjected to electrochemical analysis. Fig. 5.29 shows the electrochemical response for both TEMPO and the TEMPO salt at GC microelectrodes. The oxidation of the nitroxide radical occurs at potentials more anodic (positive) than 0.2 V to form the TEMPO salt at the electrode. Solutions of the pre-prepared TEMPO salt demonstrate reduction to regenerate TEMPO at potentials more cathodic (negative) than 0.2 V. It is noted that the TEMPO salt demonstrates oxidation at potentials more positive than 0.5 V whereas TEMPO salts formed from oxidation of TEMPO at the electrode do not. Multiple oxidation products are possible and include but are not limited to multiple radical species and the subsequent dimerisation product (Scheme 5.4). It is also not unreasonable to propose the oxidation of the hydroxylamine (N-OH) species. The products of this oxidation process have not been identified in this work.

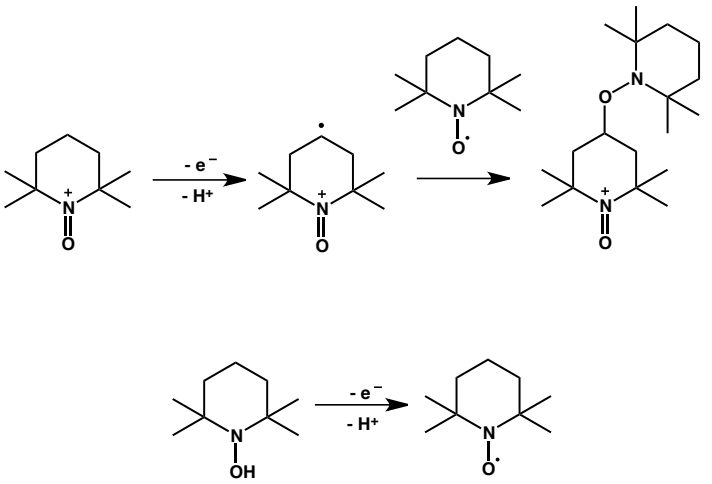

Scheme 5.4. Potential for dimerisation of TEMPO (top) and oxidation of hydroxylamine (bottom) to occur.

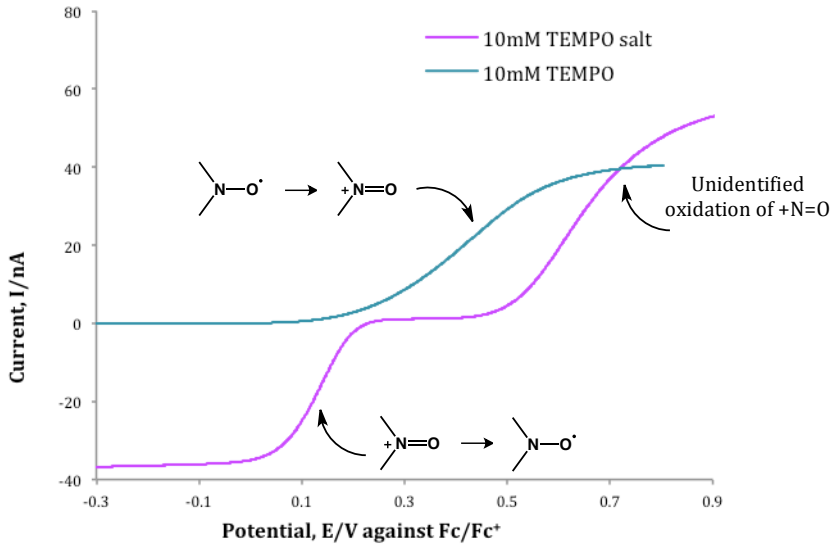

Fig. 5.29. 10 mM TEMPO salt (reverse scan) and 10 mM TEMPO in 0.1 M NBu_4PF_6 in MeCN at 100 mV/s on a GC microelectrode.

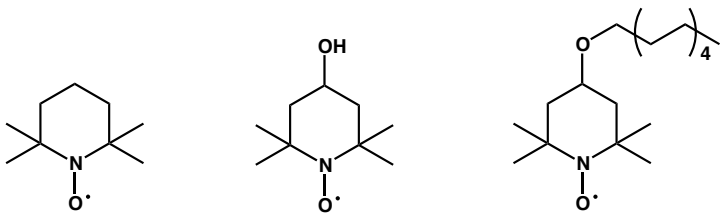

TEMPO 4-OH-TEMPO Alk-TEMPO

The electrochemical oxidation of three nitroxides, TEMPO, 4-OH-TEMPO and alkylated-TEMPO (Alk-TEMPO) on a GC microelectrode in 0.1 M NBu_4PF_6 in MeCN was examined. Figure 5.30 shows the anodic sweeps at 10 mV/s for the GC microelectrode in electrolyte with a 10 mM solution of each of the nitroxides against Ag wire RE with potential quoted with respect to the Fc/Fc^+ couple. In each case a distinct single oxidation wave is observed. These are assumed to be due to the oxidation of the nitroxide radical to the corresponding oxoammonium species (N–O• to +N=O). As expected for the electrochemistry of solution species at microelectrodes current peaks are not observed; rather the current attains a steady state value. A limiting current plateau is observed for each species at potentials more anodic than 0.4 V vs Fc/Fc^+. The onset of oxidation in TEMPO occurs at approximately 0.0 V and reaches the limiting current by 0.2 V, whereas oxidation of 4-OH-TEMPO and Alk-TEMPO commences at *ca.* 0.2 V reaching a limit by 0.4 V. The half-wave potentials are 0.18 V, 0.26 V and 0.30 V vs Fc/Fc^+

for TEMPO, 4-OH-TEMPO and Alk-TEMPO respectively. This is expected due to an increase in stabilisation of the cationic species by H, OH and OC_6H_{13} substituents respectively.[293] The limiting current of each species tends to decrease in order TEMPO > 4-OH-TEMPO > Alk-TEMPO as the size of the compound increases. This likely due to a progressive decrease in diffusion coefficient associated with an increase in hydrodynamic radii with the increasing size of the TEMPO substituents.

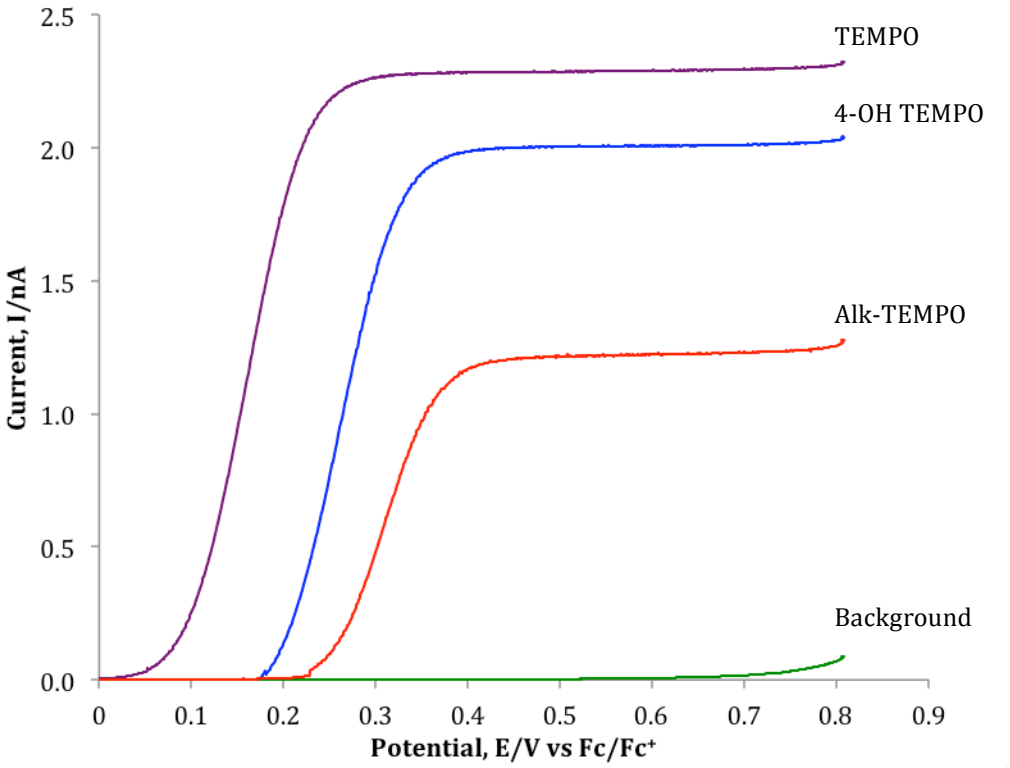

Fig. 5.30. 10 mM nitroxides samples on a GC microelectrode in 0.1 M NBu_4PF_6 in MeCN. Potentials quoted with respect to the Fc/Fc^+ couple. Anodic sweep shown only for clarity. Sweep rate 10 mV/s.

While it was of interest to establish the electrochemistry of these nitroxides, a more applied approach was required for the progression of next stage of the overall project. Before grafting the diazonium-containing nitroxides to the surface, a CV was obtained of the two related compounds: amido-TEMPO (**76**) and TMIO (**60**). These compounds contain TEMPO or TEMPO-like N-O• functionalities attached to an aryl ring. Both compounds were synthesised

without the amine or diazonium functionality required for attachment in an attempt to simplify the species and isolate the nitroxide redox couple in electrochemical characterisation (see Experimental section for details). In particular, the effect of including aryl groups in the N-O• containing species needed to be established. These two compounds provide the opportunity for this without adding further complexity associated with the amine functionality.

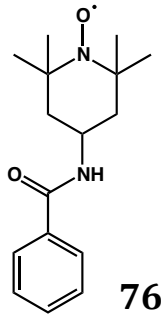

76

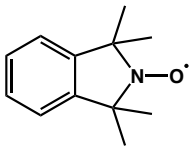

60

Amido-TEMPO TMIO

Fig. 5.31. Amido-TEMPO and TMIO.

The onset of oxidation for amido-TEMPO (**76**) occurs at approximately 0.2 V and reaches a limiting current by 0.4 V vs Fc/Fc^+(Fig. 5.32). The oxidation of TMIO (**60**) commences at *ca.* 0.3 V reaching a limit by 0.6 V. The half-wave potentials are 0.32 V and 0.45 V vs Fc/Fc^+ for amido-TEMPO and TMIO respectively, which are slightly higher than the simple TEMPO derivatives in Fig. 5.30. TMIO displays a limiting current higher than all nitroxides investigated suggesting a larger diffusion coefficient.

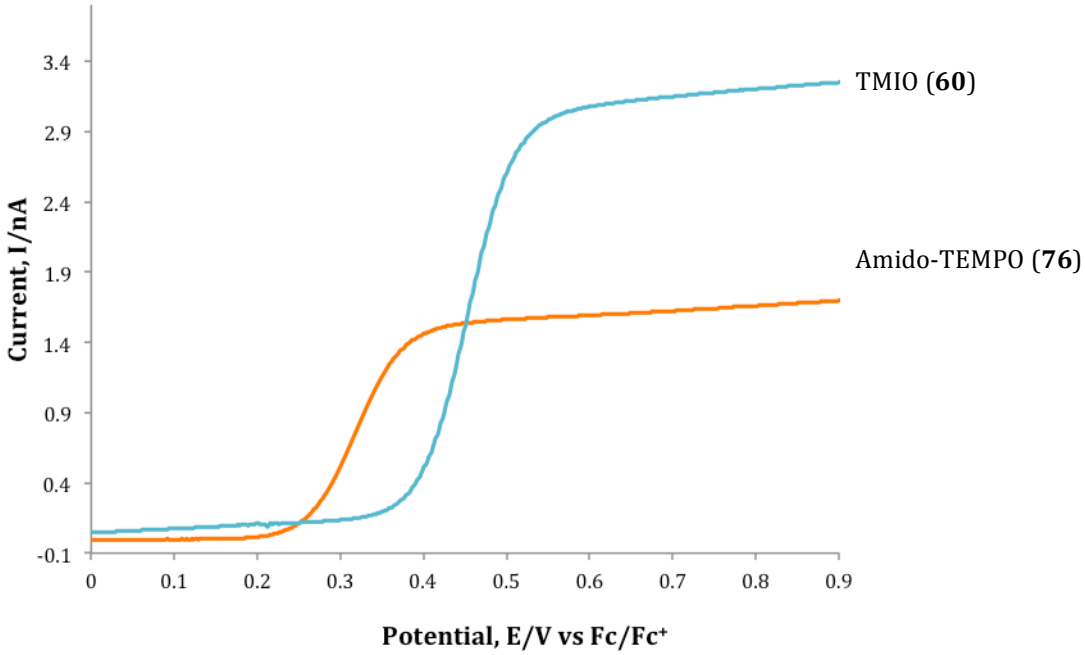

Fig. 5.32. 10 mM nitroxides (**76** and **60**) on a GC microelectrode in 0.1 M NBu_4PF_6 in MeCN. Potentials quoted with respect to the Fc/Fc^+ couple. Anodic sweep shown only for clarity. Sweep rate 20 mV/s.

5.3.5.2. Attachment of complex nitroxides derivatives to surfaces

It was recognised that there were two distinct pathways to attaching nitroxide species to an electrode surface. The first, as typified by the diazonium coupling method is to fully assemble the target molecule for attachment with a suitable aryl amine group that can be converted to a diazonium salt. Subsequent departure of N_2 allows attachment of the aryl radical to the surface of the carbon electrode substrate. A second method is to attach a suitable linker group to the surface and then perform chemistry on this new functionality to assemble the final grafted molecule. The latter process, while potentially involving more steps for the electrode assembly offers the potential advantage of controlling the loading of material onto the surface.

Preliminary work on both methodologies is reported below. In the latter case the initial stages of the 'click chemistry' methodology is introduced. In the diazonium method the attachment is achieved and carried through to demonstrating the electrochemical activity of the tethered N-O• containing species to produce the target H_2O_2.

5.3.5.2.1. 'Click' Chemistry

'Click' chemistry[121,184-186,294] was used to modify a silyl protected aryl functionality grafted to the surface by the diazonium method (Fig. 5.33). The silyl-protected alkyne was selected since it reportedly prevents unwanted addition to grafted aromatic rings. The silyl functionalities are sufficiently large to prevent this reaction pathway and distinct monolayers of diazonium grafting are observed.[190,191,294] The synthesis of (**72**) is described in Chapter 3.7.3.4.

The silyl group can be cleaved after grafting, in this case to leave a reactive ethynylaryl functionality, which participates in 'click' chemistry to form the final tethered molecular species on the electrode surface (Fig. 5.34).

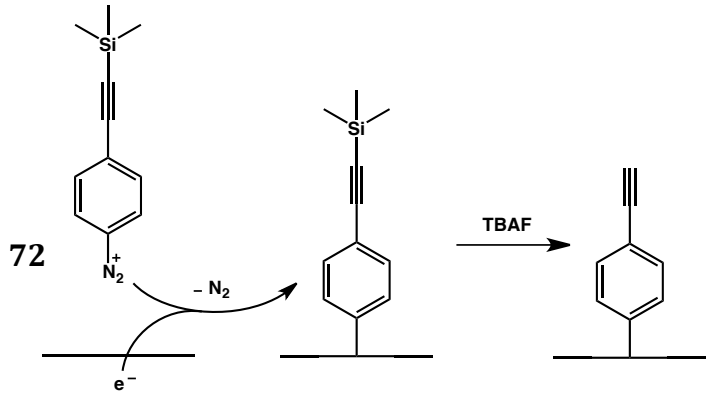

TMS-Eth-Ar

Fig. 5.33. Illustration of TMS diazonium attachment to a surface followed by deprotection with TBAF to give a reactive alkyne.

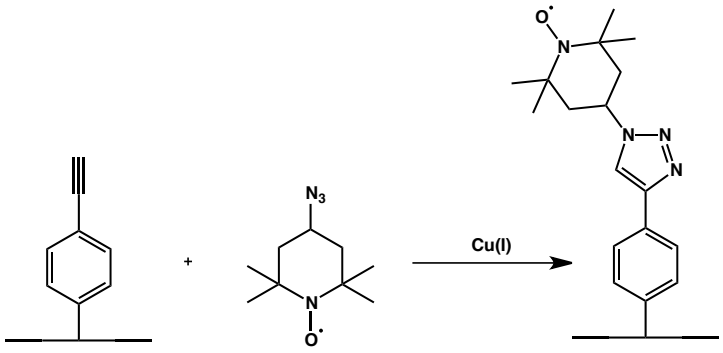

Fig. 5.34. 'Click' chemistry of a terminal alkyne on a surface with 4-azido-TEMPO to give a triazole linker.

Attachment of TMS-Eth-ArN_2^+ was performed in a 10 mM solution of MeCN (0.1 M NBu_4PF_6) and the potential cycled between +0.6 V to -0.75 V for 10 cycles (Fig. 5.36). The characteristic reduction peak for diazonium coupling was seen at -0.05 V in the first cycle and rapidly decreased with each scan thereafter. This indicates that the surface is progressively becoming less able to take up further aryl radical species and a monolayer forms.

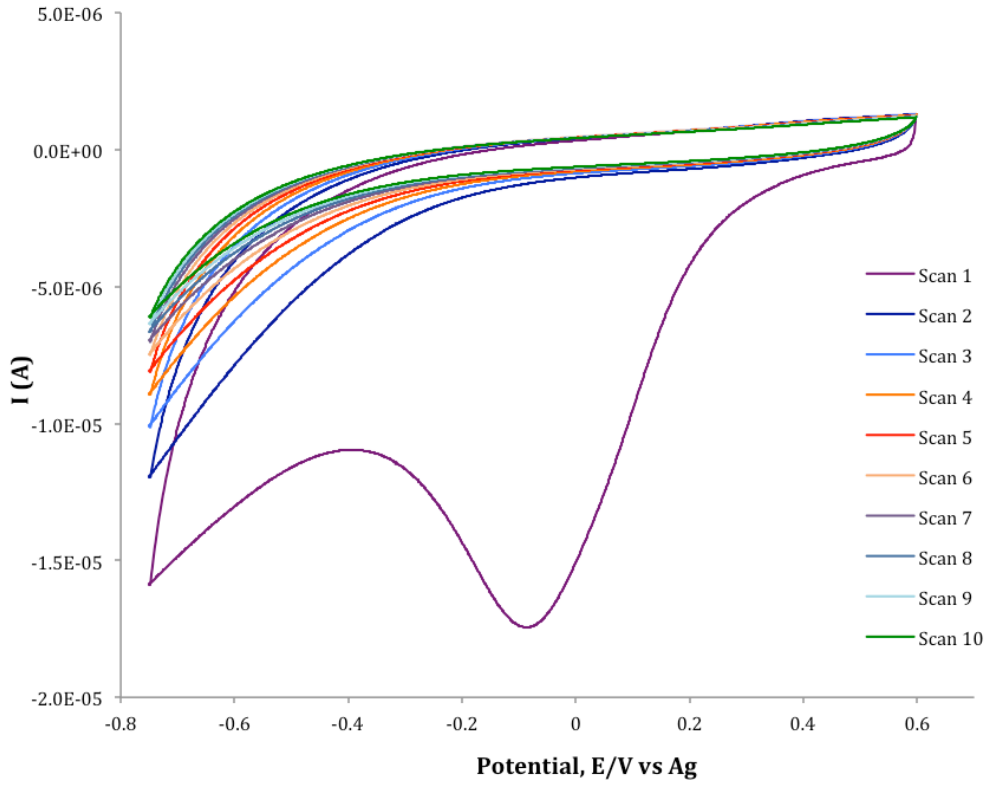

Fig. 5.35. TMS diazonium attachment. Cyclic scans 1 – 10 from +0.6 to -0.75V. Sweep rate 50 mV/s. 0.1 M NBu_4PF_6 in MeCN. Ag wire is + 0.413 with respect to Fc/Fc^+ couple.

The blocking properties of the TMS-Eth-Ar layer were characterised by recording the CV of the oxidation of ferrocene in MeCN. Electroactive species in solution can assist in the characterisation of the deposited layers by examining the differences in permeation of the molecules through the layer of the modified surface.[187] A CV was recorded between 0.0 to 0.7 V on a glassy carbon macroelectrode before any modifications were performed and following the grafting of TMS-Eth-ArN_2^+ (Fig. 5.36). A ferrocene redox couple was observed in the bare electrode prior to grafting. Following electrografting, the peak

associated with ferrocene is not discernable. This suggests blockage of the electrode with respect to electrochemistry of ferrocene.

Deprotection through removal of the silyl group was achieved by immersing the TMS-Eth-Ar grafted electrode in a stirring solution of 0.1 M tetra-n-butylammonium fluoride (TBAF) in THF for 30 minutes. This left a reactive ethynylaryl moiety available for further functionalisation. Following thorough rinsing with MeCN and drying under argon, the electrode was returned to a ferrocene solution.

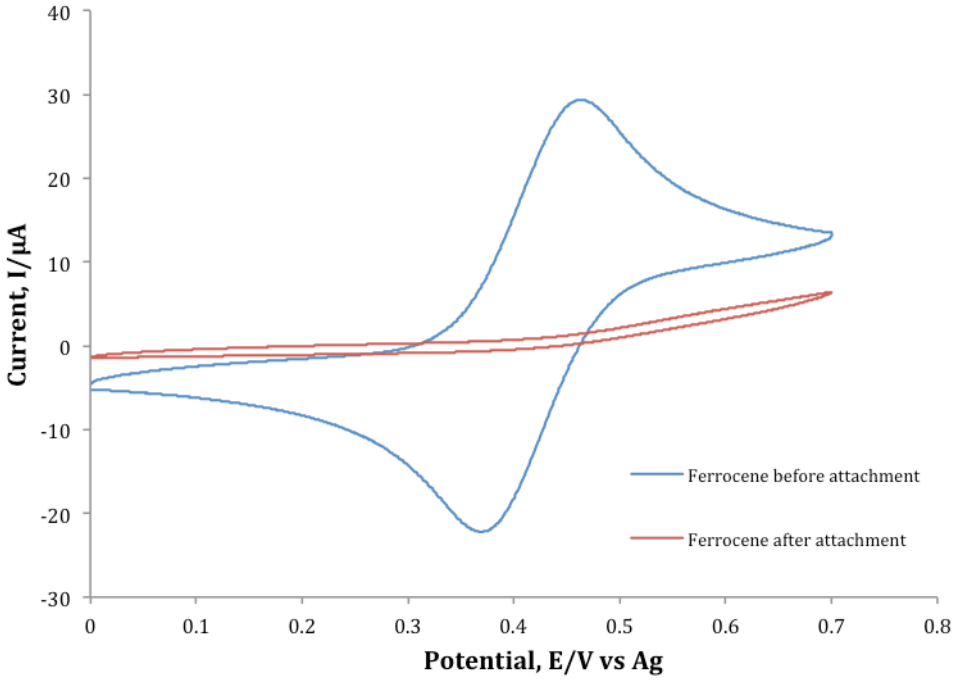

Fig. 5.36. CV of 1 mM Ferrocene in 0.1 M NBu_4PF_6 in MeCN with bare GC macroelectrode (blue) and after diazonium attachment (red). Sweep rate 100 mV/s.

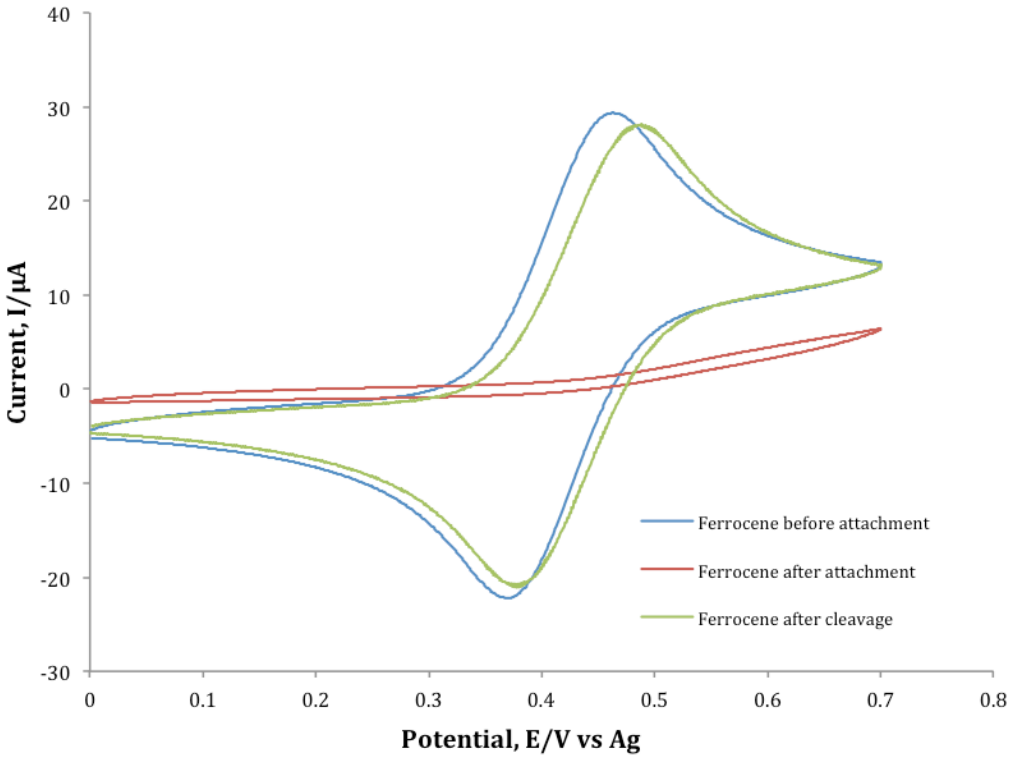

Fig. 5.37. CV of 1 mM Ferrocene in 0.1 M NBu_4PF_6 in MeCN with bare GC macroelectrode (blue), after diazonium attachment (red) and following deprotection of the silyl group (green). Sweep rate 100 mV/s.

The reappearance of the ferrocene redox couple (albeit shifted anodically by *ca*. 15 mV) suggests that the deprotection was successful (Fig. 5.37). The curve displays a slightly larger peak-to–peak potential separation than for the bare electrode suggesting the electroactive species traverses through an alternative channel.[187,295] This is consistent with the reported behaviour of a modified surface containing nanometric pinholes that permits ferrocene to freely reach the electrode surface, rather than simply loss of material from the surface.[190,294] In addition, as the size of the surface layer is smaller, it presents a very low barrier to charge transfer between molecules in solution and the surface.[191]

Post-functionalisation of the surface is achieved by 'click' chemistry in solution to incorporate the catalytic portion of the molecule (Fig. 5.38). 'Click' chemistry enables a wide range of functionally complex structures to be immobilised on a surface; in this case a stable radical.[296] Conditions for Cu(I)-catalysed Huisgen

1,3-dipolar cycloaddition ('click') were determined in Section 3.7.3 using phenylacetylene as the surface analogue. It was determined that the best method for combination of phenylacetylene and azido-TEMPO used Cu(II) as the catalytic source, with reduction by ascorbic acid in a $EtOH/H_2O$ solution. Following cleavage of the silyl protecting group, the electrode was placed into the stirred solution overnight. Unfortunately, analysis by CV in standard electrolyte the following day failed to produce a nitroxide peak in the anticipated potential region. On reflection it was thought that the nitroxide had been reduced by ascorbic acid and may be present as the hydroxylamine (N-OH) form. Therefore, attempted electrochemical cycling of the potential was undertaken to re-oxidise the hydroxylamine to form the nitroxide/oxoammonium redox couple. This, however, proved unsuccessful and it is suggested that reaction pathways that avoid the possibility of the hydroxylamine species should be avoided.

Further investigations were made into the conditions for post-modification of the electrode surfaces by 'click' chemistry. The use of Cu(I) is generally avoided in sensitive catalytic reactions such as the present case, due to ease of its oxidation to Cu(II).[186] However, an alternative reported method employs an excess of Cu(I) in place of Cu(II) as the catalyst. As the reducing agent is not necessary in the reaction, this offers the possibility of retention of the nitroxide functionality. The alkyne functionalised electrode was stirred overnight in a thoroughly degassed solution of 5 mM azido-TEMPO (**56**) and 25 mM CuI in MeCN. Following rinsing with MeCN and drying under argon, the electrode was placed back into the 0.1 M NBu_4PF_6 in MeCN electrolyte. Figure 5.38 shows the response of the modified electrode in comparison to the blank GC electrode. First, a change in the reduction of the electrolyte is seen below -0.5 V, with the absence of an oxidation peak. Secondly, a broad oxidation peak is seen at around +0.8 V suggestive of a nitroxide-type oxidation that is now present on the surface.

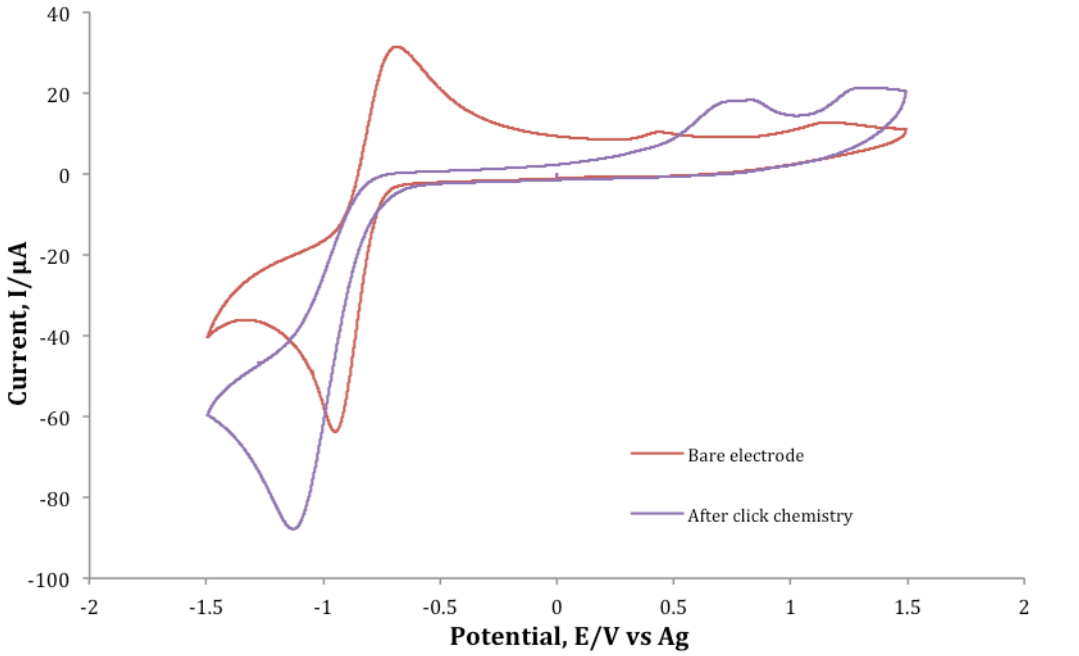

Fig. 5.38. CV in 0.1 M NBu_4PF_6 in MeCN on a bare GC electrode and following 'click' chemistry of 4-azido-TEMPO (**56**) on the modified electrode. Sweep rate 100 mV/s.

The redox couple for ferrocene was also obtained after the 'click' reaction, although as a much broader voltammogram than that for a bare electrode. Figure 5.39 shows a much larger peak-to-peak separation (217 mV) with comparison to the bare electrode (77 mV) and the modified electrode after cleavage (95 mV). This suggests that post-functionalistion has altered the electrode such that it has affected the permeation properties of ferrocene accessing the electrochemically–active surface. Although this does not confirm the presence of the triazole product, it shows that the surface has changed sufficiently after performing 'click' chemistry. Further analysis was required to accurately define the product on the GC surface.

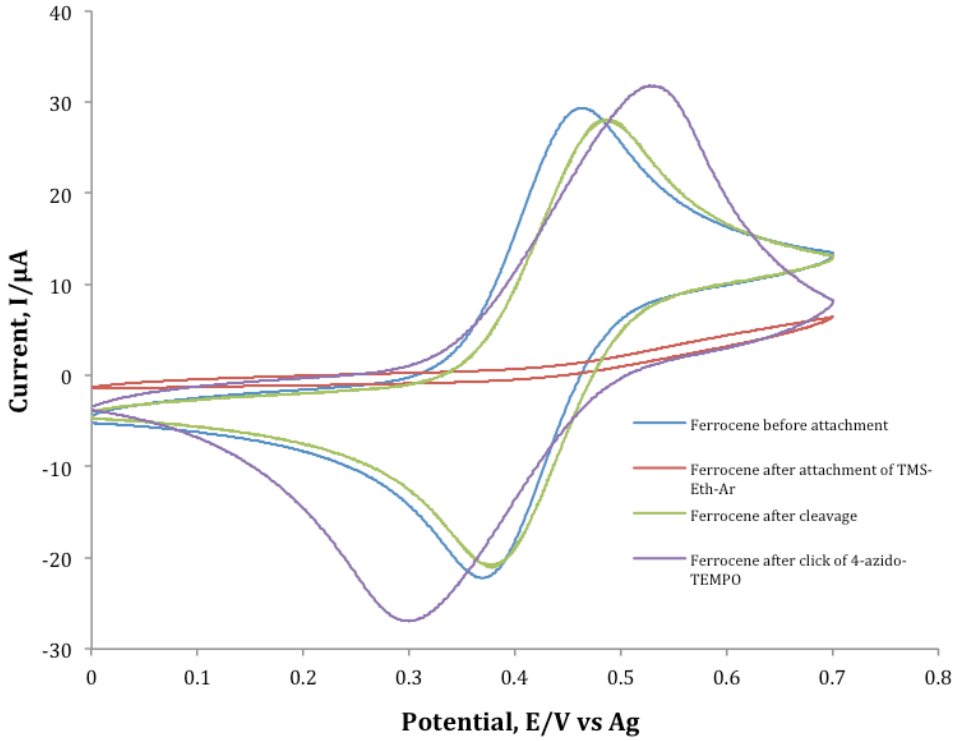

Fig. 5.39. CV of ferrocene before (bare electrode), after attachment of the TMS group, after cleavage of the silyl group and following 'click' chemistry. 0.1 M NBu_4PF_6 in MeCN. Sweep rate 100 mV/s.

5.3.5.2.2 Amido-TEMPO

The diazonium attachment of a complex nitroxide onto a surface at this initial stage was first performed on diazotised amido-TEMPO (**62**). Grafting of amido-TEMPO was by reduction of the corresponding diazonium salt at a GC electrode. As the stability of the diazonium species is questionable under these conditions, a new sample was always synthesised immediately before grafting. Grafting was achieved in a 10 mM solution of the diazonium salt in MeCN with 0.1 M NBu_4PF_6 and potential scanning from +0.75 to -0.6 V *vs.* Ag/Ag^+ at 20 mV/s. A broad irreversible peak was seen at –0.2 V characteristic of diazonium attachment (not shown).

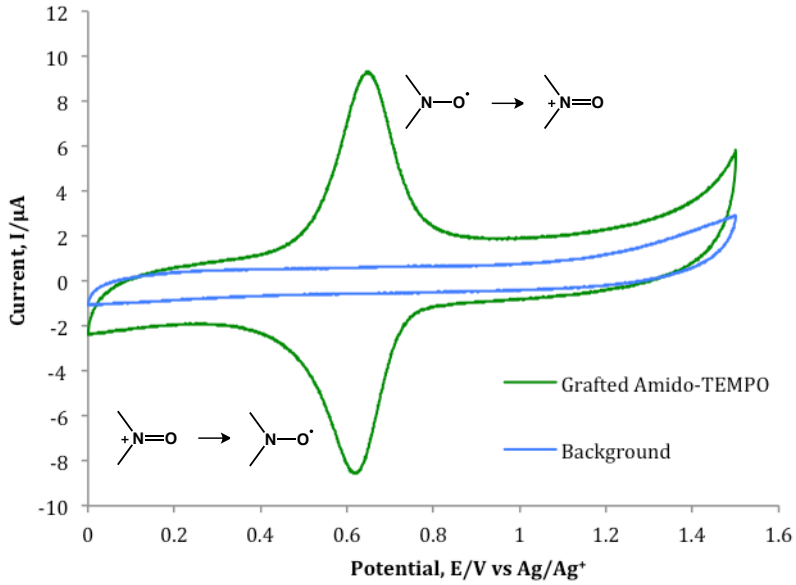

Fig. 5.40. CV of the grafted amido-TEMPO formed by attachment of **62** in MeCN (0.1 M NBu_4PF_6). Sweep rate 100 mV/s.

After repetitive cycling (up to 20 scans) to complete diazonium attachment, a reversible system attributed to the nitroxide/oxoammonium cation redox couple reaches a maximum (Fig. 5.40). In contrast to the solution state, the separation of peaks is 20 mV, characteristic of a chemically-bound species. The integration of the voltametric signal gives a surface coverage of 6.4 x 10^{-10} mol cm^{-2} (assuming a 1-electron process), which corresponds to slightly more than a close-packed monolayer calculated for a similar ($(CH_2)_7$-Amido-TEMPO) structure (5.0 x 10^{-10} mol cm^{-2}).[165,297] It is possible that the surface species exists in the hydroxylamine form (N-OH) and the cycling between 0 and 1 V can restore the nitroxide/oxoammonium redox couple.[165] However the intensity of the signal was not enhanced upon repetitive cycling suggesting that the species already exists in the redox active form. Once grafted, this material remains on the surface unchanged for several days after either being stored in MeCN or stored out of the solution in air.

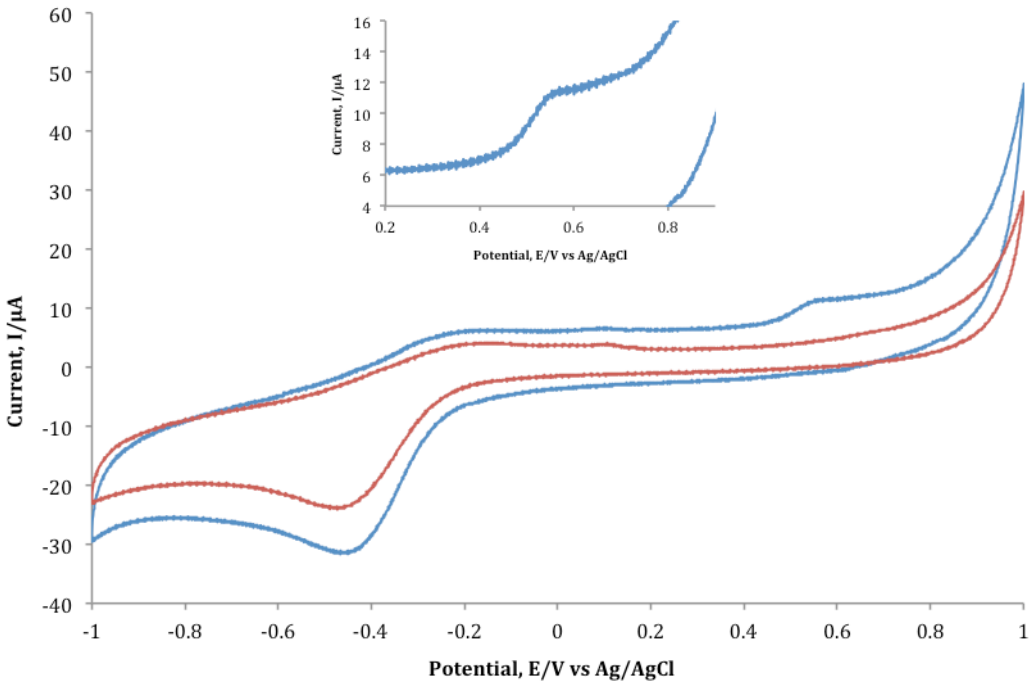

Fig. 5.41. Oxidation of grafted amido-TEMPO (formed by attachment of **62**) in 1M KOH. Bare GC electrode (red). Grafted GC electrode (blue). Inset: Nitroxide oxidation peak. Sweep rate 100 mV/s.

Figure 5.41 shows the cyclic voltammogram of the grafted GC electrode in an aqueous KOH electrolyte. The anodic sweep displays a peak at 0.59 V proposed to be the oxidation of the nitroxide (see inset) although the reduction peak appears to be absent. Integration of this peak area yields a surface coverage of 2.1 x 10^{-10} mol cm^{-2}, a 68% reduction compared to the electrode in MeCN showing a difference in response in this aqueous electrolyte. A large increase in current is seen at potentials more positive than +0.8 V vs Ag/Ag^{+} suggesting over-oxidation of the oxoammonium salt or the oxidation of the electrolyte. The absence of a reduction peak is not inconsistent with the ability of the oxoammonium species to oxidise hydroxide ions to form hydrogen peroxide.

5.3.5.3. Electrochemical production of H_2O_2 by nitroxide catalyst

In an attempt to measure the proposed oxidation of hydroxide ions, an electrochemical setup was used which incorporated the grafted electrode and a secondary electrode to measure the hydrogen peroxide production.

A rotating ring disk electrode (RRDE) was employed that utilised a secondary electrode, in this case platinum, to electrochemically probe the product flowing away from the disk electrode. The catalyst (nitroxide) was immobilised on the surface of the GC disk (0.1963 cm^2) surrounded by a Pt ring electrode (1 mm ring width, 0.11 cm^2) separated by an insulating material (Fig. 5.42).

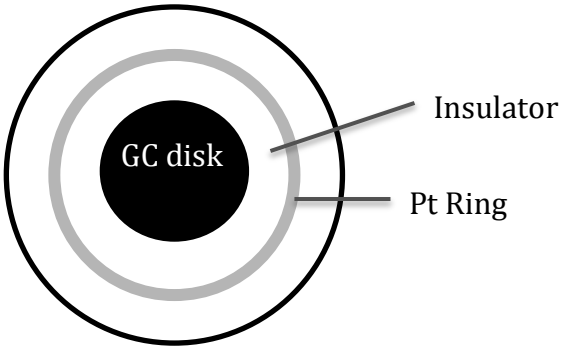

Fig. 5.42. Representative diagram of a RRDE used in this set up.

The hydrodynamics of the rotating disc allow the hydrogen peroxide formed during the reaction at the central modified GC disk surface to flow outwards towards the ring electrode at which a separate electrochemical response can be obtained. The oxidation of H_2O_2 at Pt surfaces was selected as the probe process.[298] Figure 5.43 shows the electrochemical response for the Pt ring electrode to H_2O_2 over a wide potential range. A steady-state response of the oxidation of H_2O_2 was achieved at +500 mV *vs.* Ag/AgCl before further oxidation of the electrolyte and the aqueous electrolyte become dominant at potentials more positive than 1 V. As expected at each rotation rate the current exhibits linear dependence on [H_2O_2] at concentrations lower than 10 mM. It is noted that there exists the option to use the electrochemical reduction of H_2O_2 instead of the selected oxidation process, however these conditions are less well known.

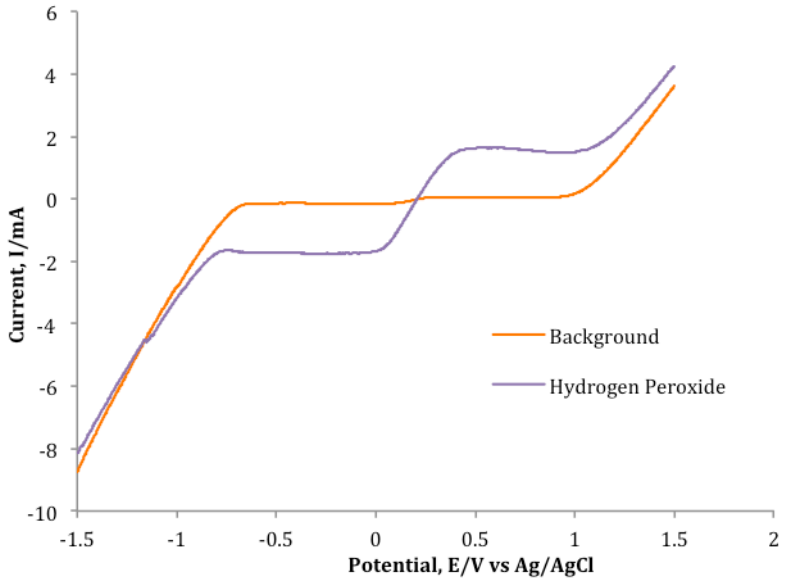

Fig. 5.43. Response of a Pt ring electrode to 1 M KOH electrolyte alone (orange) and in presence of *ca.* 100 mM H_2O_2 (purple) over both oxidation and reduction potential regions at 1000 rpm.

In subsequent ring disk experiments a potential of +500 mV *vs.* Ag/AgCl was employed to observe the oxidation of H_2O_2 at the Pt ring surface. This ensures that a steady-state current associated with H_2O_2 is reported and there is minimal current associated with oxidation of the electrolyte

Prior to analysing the material at the ring, the effect of KOH, multiple potential ranges and scans were addressed on the amido-TEMPO modified GC rotating disk electrode. Rotating the disk in 0.1 M and 1 M KOH for several hours did not appear to affect the grafted material when placed back into MeCN and compared with previous CVs. However, following performing multiple scans over a range of potentials, and over a period of a day, it was noted that the peak intensity of the nitroxide couple had decreased (Fig. 5.44).

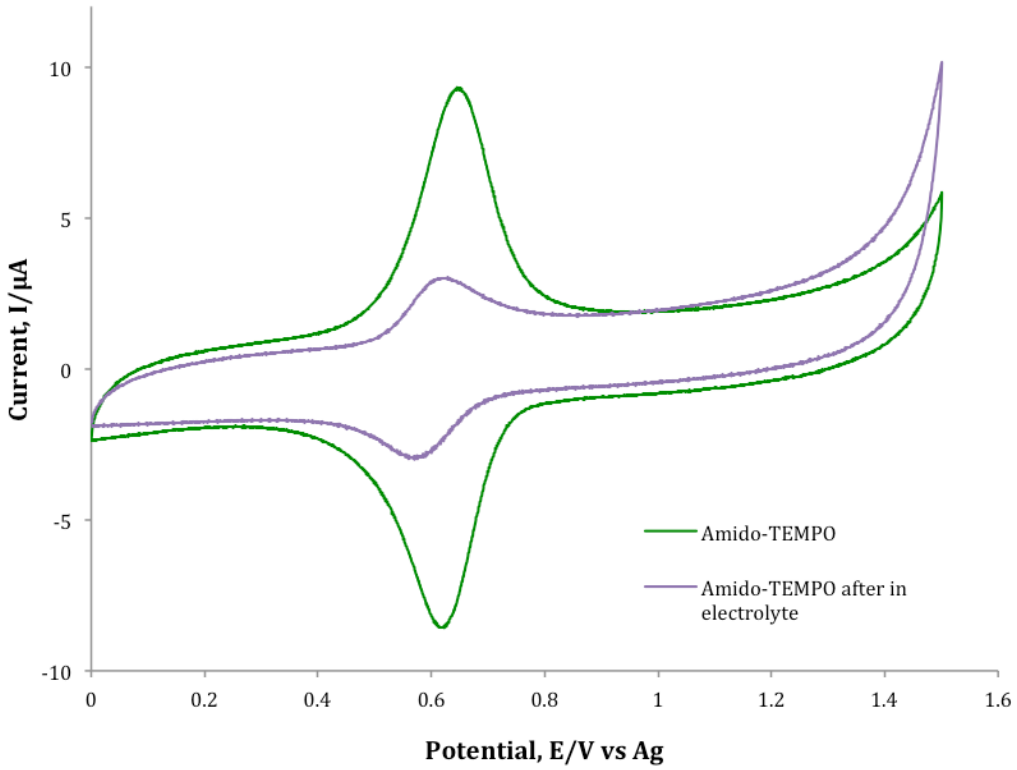

Fig. 5.44. CV of modified GC electrode immediately after grafting with amido-TEMPO (**62**) and after a days work in 1 M KOH.

There are a number of possible reasons for the reduced redox response of the nitroxide. These include fouling of the surface, addition of a by-product that restricts the response or the removal of the material on the surface. For example, Kibena *et al.* has shown the exfoliation of aryl layers on a glassy carbon surface by hydroxy radicals.[299] Although the production of hydroxy radicals in that case was from the photolysis of H_2O_2, it was demonstrated that the response of a redox probe $[Fe(CN)_6]^{4-}$ on the grafted GC electrode returned following irradiation. Caution was noted in this paper as the grafted compounds contained azo groups that are known to degrade with hydroxy radicals. However the site of exfoliation is unknown and this should be considered in future work. It was hypothesised in the present study that to decrease the amount of degradation by the hydroxyl radicals, an increase in KOH concentration from 0.1 M to 1 M might assist in the rate of dimerisation to H_2O_2.

The potential of the amido-TEMPO modified GC disk was set at +600 mV *vs.* Ag/AgCl to ensure constant oxidation of the nitroxide, and the potential of the Pt ring was set at +500 mV *vs.* Ag/AgCl. Using the bipotentiostat mode of the

Autolab potentiostat, chronoamperometry was performed on the RRDE system stepping the modified GC disk from the open circuit potential (0 mV for 20 seconds) to +600 mV for 150 sec. The nitroxide on the disk acts as an electrocatalyst by constantly oxidising to the reactive oxoammonium cation. This reactive species is understood to oxidise hydroxide ions to hydroxyl radicals with reformation of the nitroxide species in an electrodeless process (i.e. no current will be detected).

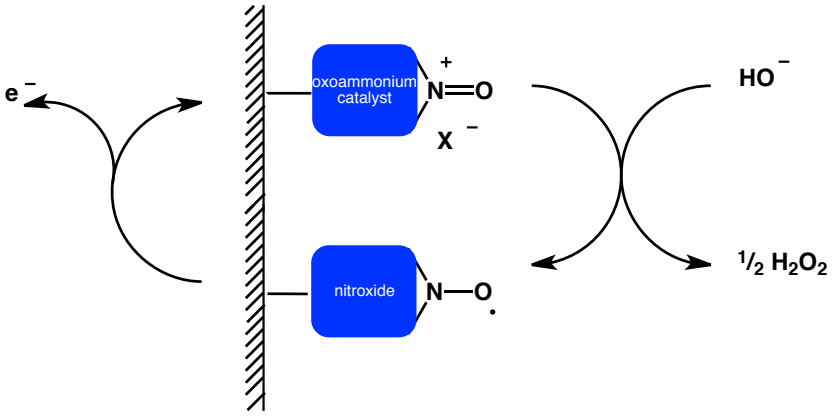

Fig. 3.5. Proposed system for catalytic regeneration of H_2O_2.

Two hydroxyl radicals dimerise in order to produce each soluble H_2O_2 molecule that then will flow radially away from the central disk electrode to be detected electrochemically at the ring electrode. The capture efficiency of the Pt ring to collect the product is approximately 75% (PINE Instrument Company) so that the current observed for H_2O_2 oxidation will be lower than that observed at the disk electrode for generation of the oxoammonium cation.

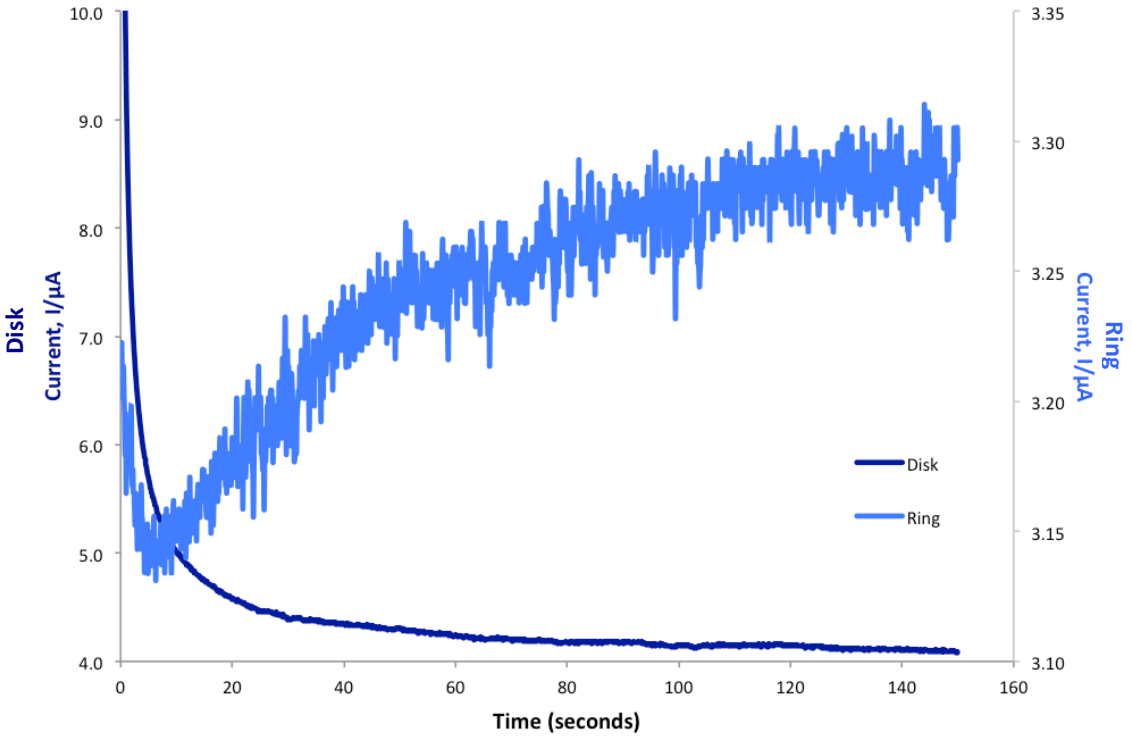

Fig. 5.45. Bipotentiostat response at an amido-TEMPO grafted GC disk electrode (left hand y-axis) and the resulting electrochemical response to the generated H_2O_2 at a platinum ring electrode (right hand y-axis) in 1 M KOH. GC electrode at +600 mV *vs.* Ag/AgCl, Pt electrode at +600 mV *vs.* Ag/AgCl, RRDE rotation rate 400 rpm.

Figure 5.45 demonstrates the response of the Pt ring to the oxidation of the nitroxide on the disk to produce H_2O_2 at a rotation rate of 400 rpm. The disk decreases in current over time until a steady state is reached (4.1 µA) where the rate of oxidation of the nitroxide is in equilibrium with the reverse reduction reaction by hydroxide. In response to this oxidation a slow increase is seen at the ring following an initial lag period of 4 seconds. This is assumed to be the oxidation of H_2O_2 produced from the catalytic reaction at the disk. The time delay suggests a dependence on the ability of the hydroxy radicals to dimerise to form H_2O_2. The noise associated with the platinum ring in Fig. 5.45 is likely due to a faulty connection of the brush with the rotator shaft. The grafted material under these conditions has the potential to become dislodged from the disk surface. As the ring is set at a potential that oxidises the nitroxide, this material can enhance the observed current on the ring electrode. However, a current

response of *ca.* 3 μA is observed at the ring for excess of 150 s and according to the surface coverage of amido-TEMPO, loss of all grafted material would only produce a response at this current for less than 4 seconds (Fig. 5.46).

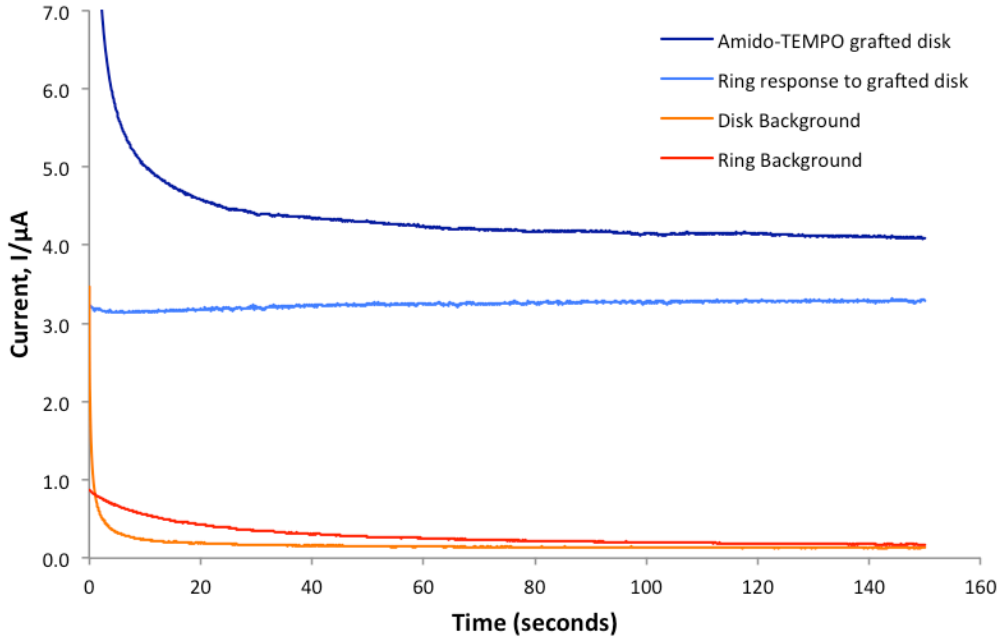

Fig. 5.46. Bipotentiostat response of an amido-TEMPO grafted GC disk electrode and the resulting electrochemical response to the generated H_2O_2 at a platinum electrode against a bare GC disk electrode and the complementary platinum ring response in 1 M KOH. GC electrode at +600 mV *vs.* Ag/AgCl, Pt electrode at +600 mV *vs.* Ag/AgCl, RRDE rotation rate 400 rpm.

In terms of the limiting current shown by the amido-TEMPO grafted GC disk, a current density of 0.21 A m^{-2} was observed. With a carbon substrate such as the PS1000 at 1000 m^2 g^{-1}, the rechargeability of the nitroxide electrocatalyst is promising at 210 A g^{-1}.

The detailed mechanistic analysis of this likely potential-, concentration- and rotation rate-dependent response is beyond the scope of the present study. However, a preliminary investigation into the effect of rotation rate suggested no clear rotational dependence on the current produced at the ring. It had been considered here that at the faster rotation rates, the concentration of the

hydroxyl radicals might decrease at the disk and hence lower the quantities of H_2O_2. Figure 5.47 shows the rotational rate-dependence of the system over the range 0-400 rpm. The increase in both ring currents suggests that the enhanced removal of hydroxyl radicals at higher rotation rates is not taking place. Rotation rates higher than 400 rpm provided no further substantial increase in response at either electrode.

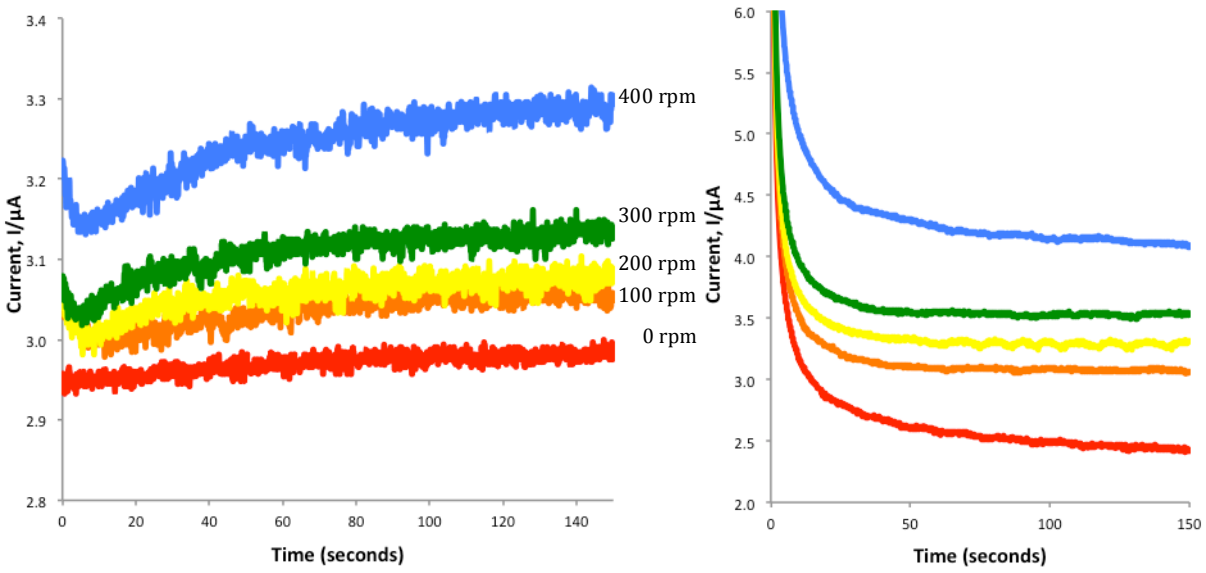

Fig. 5.47. Bipotentiostat response at an amido-TEMPO grafted GC disk electrode (right hand plot) and the resulting electrochemical response to the generated H_2O_2 at a platinum ring electrode (left hand plot) at RRDE for rotation rates 0-400 rpm in 1 M KOH. GC electrode at +600 mV *vs.* Ag/AgCl, Pt electrode at +600 mV *vs.* Ag/AgCl.

A similar trend was seen in the disk where an increasing trend in steady state current was seen for increases in rotation rate to 400 rpm representative of more hydroxide reaching the surface with regeneration the nitroxide species. At higher rotation rates (not shown) there was no distinct pattern suggesting that the rate of electron transfer from the hydroxide ion to the oxoammonium cation at the surface may be a factor in observed current. In the absence of the grafted nitroxide, there were very small currents produced at the ring and the disk, characteristic of background currents.

An in-depth discussion on the production of H_2O_2 in this system is not possible without further investigation into the kinetics of the reaction. The system is likely to be extremely complicated with multiple side reactions and species that must be considered. This includes the possibility of the oxoammonium cation further reacting with H_2O_2 and its radical form ($HO_2^{\bullet}$) to produce the nitroxide species.[300] It has also been proposed by others that hydroxyl radicals could react with the nitroxide radicals to form a NOOH intermediate before collapsing to the oxoammonium and hydroxide ion (Scheme 5.5).[301] This creates an alternative pathway for oxidation to the reactive species that is not measureable by current flow through the electrode

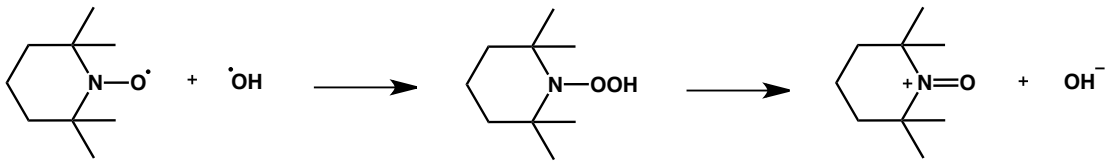

Scheme 5.5. Potential reaction of TEMPO with a hydroxyl radical.

A number of unresolved factors in this research will form the basis of further studies. However, these initial findings suggest that the production of H_2O_2 from KOH with an oxoammonium cation catalyst has been successfully demonstrated. This novel idea is the basis of the rechargeable system and was one of the main objectives of the overall project.

CHAPTER SIX

Conclusions

6.1 Conclusions

This thesis provides an insight into the fundamental concepts required to form a rechargeable electrochemical storage device without the need for a metal-centred redox couple. Utilising hydrogen peroxide as the electroactive species, this 'New Cathode' was proposed to operate in an aqueous battery system. This required the immobilisation of H_2O_2 to prevent self-discharge together with means for regeneration of the electroactive species.

Although the construction of the device was not within the scope of this project, the chemical and electrochemical analysis of potential compounds were evaluated at a molecular level. In particular, the synthesis and molecular behaviour of a 'binder' that will immobilise hydrogen peroxide, and a 'catalyst' to reform hydrogen peroxide during recharge of the battery. Additionally, the binding of these compounds to a surface was also evaluated.

This work demonstrated the synthesis of a variety of substituted ureas that were proposed to form immobilising adducts with hydrogen peroxide. Initial studies to evaluate binding employed substituted ureas in the solution phase. The molecules were initially prepared from benzoic acid, a relatively inexpensive and commercially available starting material applicable for use on an industrial scale. Utilising the Curtius rearrangement to form phenylisocyanate, a di-substituted urea was formed from the reaction of the isocyanate with a primary amine. As this route was facile and convenient, a library of di-substituted ureas was synthesised. These compounds contained electron donating (-OCH_3, -NH_2, -CH_3), electron withdrawing (-NO_2, -CF_3, -Cl), hydrophobic (alkyl chains) and bulky (-C(CH_3)) groups to preliminary assess the interaction of the family of urea derivatives with H_2O_2. Synthetic challenges, in particular the synthesis of 1-hydroxy-3-phenylurea (**8**), required modified conditions that afforded much

lower yields. Additionally, amines containing an electron-withdrawing group were less reactive due to decreased nucleophilicity of the aromatic amine. In contrast, electron-donating amines were more reactive giving almost quantitative yields. Consequently, this work demonstrates the ability to synthesise ureas with a variety of functional groups using this method.

In the crystal structure of the model compound urea-hydrogen peroxide demonstrated by Chia Si Lu,[91] H_2O_2 interacts with the N-H protons on the urea. ^{1}H NMR assessment of N-H protons (d_6-DMSO) in the di-substituted ureas showed deshielding in the presence of an electron withdrawing group and shielding with electron donating groups. This is not unexpected, however it provides a point of difference when assessing where hydrogen peroxide will interact. Analysis of the interactions between substituted ureas with H_2O_2 proved difficult, predominantly due to the inability to work with a single solvent system in which both the urea and the H_2O_2 are readily soluble. Initial qualitative assessment by ^{1}H NMR was abandoned due to the ability for multi-site exchange between the urea, H_2O_2, H_2O and solvent. A downfield trend of the H_2O_2 peak was observed upon an increasing amount of diphenylurea. However, the change in chemical shift associated with this interaction and the inability to unambiguously identify the maximum chemical shift of the adduct when complexed prevented evaluation of a binding constant.

Evaluation of a urea-containing chromophore by UV/Visible spectroscopy to evaluate the interaction also proved challenging and therefore was abandoned. H_2O_2 produces hydroxy radicals under UV radiation that either removes or irreversibly alters the chromophore. Spectral changes in the visible region were minimal on the addition of H_2O_2, reflecting potential issues such as limited H_2O_2 concentration and concerns about forming the adduct in solution.

Using a different approach the H_2O_2 content in solid adducts was evaluated using analytical techniques. An organic hydrogen peroxide solution was utilised to prepare the substituted urea•H_2O_2 adduct, decreasing the problematic competitive binding of H_2O. The removal of the organic solvent (THF) forced the

formation of a substituted urea adduct. A quantitative approach using ATR-FTIR was established to be the leading methodology to identify the presence of H_2O_2. This identified a potential red-shift of the hydrogen peroxide O-H bond in response to hydrogen bonding with the substituted urea. Initial analysis showed an increase in intensity of this peak in compounds with an electron withdrawing group. Two peaks were observed in a number of compounds suggesting the additional functionality on the urea could also be contributing to binding of H_2O_2. However this method was not able to distinguish the strength of binding, orientation of binding or the amount of hydrogen peroxide bound for each substituted urea.

Detailed characterisation of the butylphenylurea•H_2O_2 adduct by ^1H NMR, titration with $KMnO_4$, UV/Visible spectroscopy and an oxidation reaction with triphenylphosphine, revealed that an adduct with H_2O_2/butylphenylurea ratio of approximately 2-3 was formed. Although this was a preliminary study and some variation in molar ratio was observed, there is a strong degree of confidence that solid hydrogen peroxide adducts are formed. This methodology can now be applied to the range of hydrogen peroxide adducts. These findings suggest that adduct formation is not confined to formation of 1:1 hydrogen peroxide:urea derivative adducts as is the case for the adduct formed between urea and H_2O_2 (UHP). The inability to form crystals for any of the range of adducts meant that X-ray crystallography could not be performed.

Preliminary studies of attachment of the substituted urea were performed on a high surface area carbon powder (1000 m^2/g). The high surface area carbon was required in order to obtain a theoretical specific capacity in a range necessary for this system to be viable as a stationary battery. Analysis of the carbon powder (PS1000) by Raman spectroscopy revealed a broad D band and small G band characteristic of a very disordered amorphous carbon with little graphitic structure. Solid state-NMR spectroscopy indicated the presence of metal ions in the sample. Iron analysis by atomic absorption spectroscopy and microanalytical combustion gave a high percentage of aqueous acid extractable (0.4% w/w) and total (4.9% w/w) Fe content in the carbon powder sample. This proved to be

deleterious since trace metal impurities catalyse the decomposition of H_2O_2 thus preventing preliminary assessment of the adducts on the modified carbon powder.

Attachment of substituted ureas to the carbon powder was achieved by physical adsorption (physisorption) and by chemical attachment (chemisorption). Diphenylurea was used for the majority of the attachment experiments as it was selected as a baseline molecule when comparing with the range of substituted ureas. Physical adsorption was achieved through van der Waals interactions and π-stacking of diphenylurea. Comparison of the Raman spectra and SEM images revealed aggregation of the urea derivatives to form discrete crystalline layers rather than coating the surface. In an attempt to evaluate the interaction of H_2O_2 with diphenylurea, chronoamperometry was performed on this physisorbed carbon material. The transient current response at a static glassy carbon electrode was measured from 0 – 3 mM H_2O_2 in the absence of PS1000, untreated PS1000 and the diphenylurea physisorbed material. These results suggested the carbon had some degree of adsorbancy of H_2O_2, however the addition of the adsorbed diphenylurea did not increase the adsorbancy of H_2O_2 to any greater extent, suggesting minimal binding. This to some extent was not unexpected as the surface area of available urea binding sites was decreased through the majority of the urea molecules being located within crystal aggregates rather than at a solid-solution interface.

Chemical attachment of urea derivatives was achieved through diazonium coupling of a diphenylurea precursor with the carbon powder. This forms a covalent bond from the aromatic ring of the substituted urea to the carbon surface. In contrast to electrochemical grafting techniques where a reducing potential induces attachment, the method adopted in this study relied on the carbon surface acting as a mild reductant spontaneously transferring electrons to affect the grafting process. Spontaneous diazonium attachment of 4-nitrobenzenediazonium and 4-(3-phenylureido)benzenediazonium was demonstrated. Verification of attachment was challenging since diphenylurea is not electrochemically active; therefore assessment of the surface by

electrochemical techniques was not available. Quantitative analysis by Raman and FTIR spectroscopy was unsuccessful and suggested only a small surface coverage of the chemically attached compounds. However, the morphology of the carbon material has been substantially altered in both the diazonium-coupled powders. SEM images revealed a more nodular and rougher surface than the original carbon particulates. This is not inconsistent with the ability of these compounds to form isolated multilayers due to spontaneous attachment with another coupling partner. Microanalysis provided a quantitative analysis of the percentage of carbon, nitrogen and hydrogen in the sample. In particular, an increase in nitrogen from PS1000 to the grafted material was ascribed to the chemically tethered compounds. The amount of material on the modified substrate was found to be 3.6% w/w and 19.7% w/w for 4-nitrophenyl and diphenylurea respectively. This shows promising results and completes one of the initial targets for the overall project this study formed part of for the attachment of a H_2O_2 'binder' to a carbon substrate.

As an alternative carbon substrate, functionalisation of carbon felt was also investigated. The selected carbon felt had been formed from the pyrolysis of polyacrylonitrile to leave an open three-dimensional structure. The specific surface area of the felt was determined by BET (0.41-0.42 m^2/g) and electrochemical analysis with $Fe(CN)_6^{3-}$ (0.072 m^2/g). The marked difference for the two techniques is not inconsistent with high porosity of the fibres, but the dimensions of these pores are too small for accessibility of solvated species in electrochemical determination but sufficiently large for accessibility of N_2 molecules in BET analysis. The low surface area of the felt made it inadequate as the primary carbon substrate. However it may provide physical and conductive support for higher surface carbon powders. A preliminary assessment of the response to the electrochemistry of H_2O_2 suggested the carbon fibre should not be considered a likely contributor for the total discharge current in the final cathode. However if the felt is the physical support within the cathode it may be subjected to grafting conditions during processing and electrode formation. Electrochemical grafting of 4-nitrobenzenediazonium onto the felt showed

promising results. However, a more thorough investigation needs to be undertaken.

Two key steps were achieved in this section of work; implementation of a synthetic strategy to prepare target compounds and demonstration of the attachment of these compounds to high surface area carbons. Although both of these steps were not optimised, methods were established that are applicable to most of the synthesised substituted ureas. Evaluating the interaction of the substituted ureas with H_2O_2 was more challenging. Ultimately the binding constant of adduct formation in solution was not obtainable by the methods undertaken. This does not mean that there is no interaction; it simply highlights the inability to measure it in isolation. The results did suggest that adducts were forming between H_2O_2 and the substituted ureas in which the amount of hydrogen peroxide could be quantified. This supports the principal requirement for a substituted urea to immobilise H_2O_2 and is encouraging for future work.

The second aspect to this project was the synthesis of a nitroxide/oxoammonium species and evaluation of its catalytic ability to produce hydrogen peroxide from hydroxide ions. Nitroxides have been frequently used for the oxidation of alcohols, however very little is known about its use in the oxidation of hydroxide ions. In general, the isolation of the active oxoammonium catalyst has been inferred by most, and the present work has demonstrated the complexity of the reaction mechanism.

In this study it has been shown that the oxidation product of TEMPO (oxoammonium) interferes with the detection of H_2O_2 due to its strong oxidising properties. Therefore a biphasic system was employed to differentiate between the catalyst and H_2O_2. A derivative of TEMPO was synthesised and following oxidation with bromine was insoluble in aqueous solutions but soluble in an organic solvent immiscible in water. Sodium hydroxide was introduced into the system with a phase transfer catalyst to allow the transfer of hydroxide ions from the aqueous phase to the TEMPO derivative catalyst in the organic phase. Vigorous stirring for 4 hours produced an aqueous H_2O_2 solution (6-9%, mole%)

by spectrophotometric determination when complexed with a Ti^{4+} salt. This oxidation of hydroxide to H_2O_2 demonstrates the potential for further studies towards developing a surface attached catalyst in an electrode system.

The synthetic procedure of the 'catalyst' was demonstrated for five different nitroxide species with the intention of coupling to a surface. In contrast to the general procedure for substituted urea synthesis, each nitroxide species required its own synthetic procedure. The catalyst design involved three sections; linker, tuner and catalytic moiety. The five proposed molecules varied in the linker and tuner to assist with determining a combination that promoted the catalytic ability of the nitroxide moiety. In the attempt to form a diazonium salt required for coupling to a surface from an amine precursor, two compounds decomposed and were thus inappropriate for further utilisation in this project. Of the remaining three compounds, two were electrochemically grafted onto a glassy carbon surface. Of particular interest was the amido-TEMPO structure where a surface coverage of 6.4×10^{-10} mol cm^{-2} suggested formation of a close-packed monolayer. Using bi-potentiostat control in KOH solution, this TEMPO derivative-coated carbon electrode was held at a potential that continually oxidises the nitroxide and a Pt ring electrode was held at a potential to oxidise the catalytically formed H_2O_2. Following an initial lag time of 4 seconds, the Pt ring responded to the process occurring at the disk, strongly suggesting H_2O_2 formation. In terms of the limiting current shown by the amido-TEMPO grafted disk, a current density of 0.21 A m^{-2} was observed. This shows promise when using a carbon substrate with a high surface area such as the PS1000 at 1000 m^2 g^{-1}, where the recharge ability of the nitroxide catalyst is 210 A g^{-1}.

6.2 Future Directions

With the success of this work, it allows the commencement of material development to incorporate the molecular functionalities that were presented in this thesis. This includes robust methodologies to demonstrate the efficacy of the tethered urea derivatives for binding H_2O_2. In particular the electrode potential,

electrolyte composition and temperature dependence for this critical interaction.

Additionally, the present work also allows assessment of the long-term capability for tethered nitroxides to efficiently regenerate hydrogen peroxide from the electrolyte at moderate electrode potentials during charging. This will contribute significantly to the overall performance in the 'New Cathode'.

In the fabrication of the 'New Cathode', the relative proportions of binder and catalyst moieties required to achieve an effective rechargeable electrode with high H_2O_2 storage capability will need to be addressed. Additionally, incorporation of physical support for the carbon particles, such as carbon felt, will contribute to the effectiveness of the compounded macroscopic electrode material to permit the transfer of electrical charge.

1. REN21 'Renewables 2014 Global Status Report,' 2014. (Paris: REN21 Sectretariat).
2. Wang, Z.-L.; Xu, D.; Xu, J.-J.; Zhang, X.-B.: Oxygen electrocatalysts in metal-air batteries: from aqueous to nonaqueous electrolytes. *Chem. Soc. Rev.* **2014**, *43*, 7746-7786.
3. Velazco, V. A.; Buchwitz, M.; Bovensmann, H.; Reuter, M.; Schneising, O.; Heymann, J.; Krings, T.; Gerilowski, K.; Burrows, J. P.: Towards space based verification of CO_2 emmissions from strong localized sources: fossil fuel power plant emissions as seen by a CarbonSat constellation. *Atmos. Meas. Tech.* **2011**, *4*, 2809-2822.
4. European Environmental Agency. 'Late Lessons from Early Warnings: Science, precaution, innovation,' 2013, Luxembourg: Publications office of the European Union.
5. Bauer, N.; Brecha, R. J.; Luderer, G.: Economics of nuclear power and climate change mitigation policies. *Proc. Natl. Acad. Sci.* **2012**, *109*, 16805-16810.
6. Hanawa, M.; Onozaki, M.: Global utilization trends of natural gas and fossil fuels after Fukushima Dai-ichi nuclear accidents (1). Vision of fossil fuel. *Nihon Genshiryoku Gakkaishi* **2012**, *54*, 265-269.
7. 'The New Zealand Energy Data File,' Energy Information and Modelling Group, 2012, Ministry of Economic Development, Crown Copyright 2012.
8. Chen, H.; Cong, T. N.; Yang, W.; Tan, C.; Li, Y.; Ding, Y.: Progress in electrical energy storage system: A critical review. *Prog. Nat. Sci.* **2009**, *19*, 291-312.
9. Li, Y.; Dai, H.: Recent advances in zinc-air batteries. *Chem. Soc. Rev.* **2014**, *43*, 5257-5275.
10. Cheng, F.; Chen, J.: Metal-air batteries: from oxygen reduction electrochemistry to cathode catalysts. *Chem. Soc. Rev.* **2012**, *41*, 2172-2192.
11. Prabu, M.; Ramakrishnan, P.; Nara, H.; Momma, T.; Osaka, T.; Shanmugam, S.: Zinc-air battery: Understanding the structure and morphology changes of graphene-supported $CoMn_2O_4$ bifunctional catalysts under practical rechargeable conditions. *ACS Appl. Mater. Interfaces* **2014**, *6*, 16545-16555.
12. Chen, L.; Shaw, L. L.: Recent advances in lithium–sulfur batteries. *J. Power Sources* **2014**, *267*, 770-783.
13. Richman, R. H.; Tennenhouse, G. J.: Model for degradation of ceramic electrolytes in sodium-sulfur batteries. *J. Am. Ceram. Soc.* **1975**, *58*, 63-67.
14. Zhang, Q.; Lin, S.: Crack growth in β-alumina solid electrolyte under electrostress corrosion. *Wuji Cailiao Xuebao* **1989**, *4*, 71-75.
15. Yu, X.; Manthiram, A.: Room-temperature sodium-sulfur batteries with liquid-phase sodium polysulfide catholytes and binder-free multiwall

carbon nanotube fabric electrodes. *J. Phys. Chem. C* **2014**, *118*, 22952-22959.
16. Yang, Z.; Zhang, J.; Kintner-Meyer, M. C. W.; Lu, X.; Choi, D.; Lemmon, J. P.; Liu, J.: Electrochemical energy storage for green grid. *Chem. Rev.* **2011**, *111*, 3577-3613.
17. Andriamiadamanana, C.; Laberty-Robert, C.; Sougrati, M. T.; Casale, S.; Davoisne, C.; Patra, S.; Sauvage, F.: Room-temperature synthesis of iron-doped anatase TiO2 for lithium-ion batteries and photocatalysis. *Inorg. Chem.* **2014**, *53*, 10129-10139.
18. Bai, Y.; Yin, Y.; Qiu, Y.; Sun, X.; Zhang, W.: A method for modifying the surface of positive electrode active material used for lithium secondary battery. Henan University, Peop. Rep. China. 2014; pp 9.
19. Huang, G.-y.; Xu, S.-m.; Li, L.-y.; Wang, X.-j.; Lu, S.-s.: Synthesis and modification of a lamellar Co_3O_4 anode for lithium-ion batteries. *Wuli Huaxue Xuebao* **2014**, *30*, 1121-1126.
20. Julien, C. M.; Mauger, A.; Groult, H.; Zaghib, K.: Surface modification of positive electrode materials for lithium-ion batteries. *Thin Solid Films* **2014**.
21. Sun, Q.; Li, Y.; Sun, H.: A modified sulfur/carbon-doped lithium manganate positive electrode material and its preparation method. Qingdao Qianyun High-tech New Material Co., Ltd., Peop. Rep. China. 2014; pp 4.
22. 'Sealed Lead-Acid Batteries Technical Handbook 2000,' Panasonic, 2000.
23. Energizer 'Application Manual, Zinc Air (Zn/O_2),' 2004.
24. Panasonic: Safety Precautions for the Lithium Ion Battery Pack. 2007.
25. Sony: Lithium Ion Rechargeable Batteries.
26. Macdonald, F.; Lide, D. R.: CRC handbook of chemistry and physics: From paper to web. *Abstracts of Papers of the American Chemical Society* **2003**, *225*, U552-U552.
27. Goonan, T. G. 'Lithium use in batteries: U.S. Geological Survey Circular 1371,' 2012.
28. 'US Geological Survey, Mineral Commodity Summaries,' 2014.
29. Tahil, W. 'How Much Lithium does a Li Ion EV battery really need?,' Meridian International Research, 2010.
30. Gerssen-Gondelach, S. J.; Faaij, A. P. C.: Performance of batteries for electric vehicles on short and longer term. *J. Power Sources* **2012**, *212*, 111-129.
31. Moseley, P. T.: Research results from the advanced lead–acid battery consortium point the way to longer life and higher specific energy for lead/acid electric-vehicle batteries. *J. Power Sources* **1998**, *73*, 122-126.
32. Historical Nickel Prices and Price Chart. InforMine Inc.; Vol. 2014. www.infomine.com/investment/metal-prices/nickel/all

33. Toussaint, G.; Stevens, P.; Akrour, L.; Rouget, R.; Fourgeot, F.: Development of a rechargeable zinc-air battery. *ECS Transactions* **2010**, *28*, 25-34.
34. Shukla, A. K.; Venugopalan, S.; Hariprakash, B.: Nickel-based rechargeable batteries. *J. Power Sources* **2001**, *100*, 125-148.
35. Hall, S. B.; Personal Communication., 2011.
36. Zhao, Y.; Si, S.; Liao, C.: A single flow zinc-polyaniline suspension rechargeable battery. *J. Power Sources* **2013**, *241*, 449-453.
37. Guerfi, A.; Trottier, J.; Boyano, I.; De Meatza, I.; Blazquez, J. A.; Brewer, S.; Ryder, K. S.; Vijh, A.; Zaghib, K.: High cycling stability of zinc-anode/conducting polymer rechargeable battery with non-aqueous electrolyte. *J. Power Sources* **2014**, *248*, 1099-1104.
38. Novák, P.; Müller, K.; Santhanam, K. S. V.; Haas, O.: Electrochemically active polymers for rechargeable batteries. *Chem. Rev.* **1997**, *97*, 207-282.
39. Yao, M.; Senoh, H.; Yamazaki, S.-i.; Siroma, Z.; Sakai, T.; Yasuda, K.: High-capacity organic positive-electrode material based on a benzoquinone derivative for use in rechargeable lithium batteries. *J. Power Sources* **2010**, *195*, 8336-8340.
40. Oyama, N.; Pope, J. M.; Sotomura, T.: Effects of adding copper(II) salt to organosulfur cathodes for rechargeable lithium batteries. *J. Electrochem. Soc.* **1997**, *144*, L47-L51.
41. Nakahara, K.; Iwasa, S.; Satoh, M.; Morioka, Y.; Iriyama, J.; Suguro, M.; Hasegawa, E.: Rechargeable batteries with organic radical cathodes. *Chem. Phys. Lett.* **2002**, *359*, 351-354.
42. Nishide, H.; Iwasa, S.; Pu, Y.-J.; Suga, T.; Nakahara, K.; Satoh, M.: Organic radical battery: nitroxide polymers as a cathode-active material. *Electrochim. Acta* **2004**, *50*, 827-831.
43. Xu, L. H.; Yang, F.; Su, C.; Ji, L. L.; Zhang, C.: Synthesis and properties of novel TEMPO-contained polypyrrole derivatives as the cathode material of organic radical battery. *Electrochim. Acta* **2014**, *130*, 148-155.
44. Wang, S.; Yu, D.; Dai, L.: Polyelectrolyte functionalized carbon nanotubes as efficient metal-free electrocatalysts for oxygen reduction. *J. Am. Chem. Soc.* **2011**, *133*, 5182-5185.
45. Sanli, A. E.: A possible future fuel cell: the peroxide/peroxide fuel cell. *Int. J. Ener. Res.* **2013**, *37*, 1488-1497.
46. St. John, J.: Aquion Energy closes $55M VC round for grid-scale battery plans. Greentech Media, 2014; Vol. 2014.
47. Hall, S. B.: New Cathodes. Smart Ideas: Massey University, 2014. Application PROP-38127-SIP2-MAU.
48. Delamar, M.; Hitmi, R.; Pinson, J.; Saveant, J. M.: Covalent modification of carbon surfaces by grafting of functionalized aryl radicals produced from electrochemical reduction of diazonium salts. *J. Am. Chem. Soc.* **1992**, *114*, 5883-5884.

49. Way, A. 'Urea Hydrogen Peroxide (Confidential Report),' Massey University, 2013.
50. Ennis, R. J.: A study of the underlying thermodynamics of a potential new cathode for rechargeable batteries (Embargoed). Unpublished master's thesis, Massey University, 2013.
51. Fenton, H. J. H.: LXXX.-The action of phosgene on ammonia. *J. Chem. Soc., Trans.* **1879**, *35*, 793-796.
52. Carl, B., Wilhelm, Meiser: Process of manufacturing urea. BASF AG: United States, 1922.
53. Yakovkin, G. A.: Synthetic carbamide from ammonia and carbon dioxide. *Zh. Prikl. Khim. (S.-Peterburg, Russ. Fed.)* **1928**, *1*, 70-77.
54. Clark, K. G.; Gaddy, V. L.; Rist, C. E.: Equilibria in the ammonium carbamate-urea-water system. *Ind. Eng. Chem.* **1933**, *25*, 1092-1096.
55. Tsopmo, A.; Ngnokam, D.; Ngamga, D.; Ayafor, J. F.; Sterner, O.: Urea derivatives from Pentadiplandra brazzeana. *J. Nat. Prod.* **1999**, *62*, 1435-1346.
56. Wang, A.-Y.; Lu, Y.; Zhu, H.-L.; Jiao, Q.-C.: URD12: a urea derivative with marked antitumor activities. *Oncol. Lett.* **2012**, *3*, 373-376.
57. Schroeder, M. C.; Hamby, J. M.; Connolly, C. J. C.; Grohar, P. J.; Winters, R. T.; Barvian, M. R.; Moore, C. W.; Boushelle, S. L.; Crean, S. M.; Kraker, A. J.; Driscoll, D. L.; Vincent, P. W.; Elliott, W. L.; Lu, G. H.; Batley, B. L.; Dahring, T. K.; Major, T. C.; Panek, R. L.; Doherty, A. M.; Showalter, H. D. H.: Soluble 2-Substituted aminopyrido[2,3-d]pyrimidin-7-yl ureas. Structure−activity relationships against selected tyrosine kinases and exploration of *in vitro* and *in vivo* anticancer activity. *J. Med. Chem.* **2001**, *44*, 1915-1926.
58. Lidia De Luca, A. P., Giampaolo Giacomelli, Irene Murgia: Microwave-assisted synthesis of N-monosubstituted urea derivatives. *Synlett* **2010**, 2439-2442.
59. Fell, J. B.; Fischer, J. P.; Hinklin, R. J.: Preparation of piperidinyl-substituted cyclic ureas as GPR119 modulators. Array BioPharma Inc., USA . 2013; pp 86.
60. Lessene, G. L.; Baell, J.: Preparation of amino acid derivatives as α-helical mimetics. The Walter and Eliza Hall Institute of Medical Research, Australia . 2008; pp 122.
61. Funabashi, Y.; Tsubotani, S.; Koyama, K.; Katayama, N.; Harada, S.: A new anti-MRSA dipeptide, TAN-1057 A. *Tetrahedron* **1993**, *49*, 13-28.
62. Glebowska, A.; Kamienska-Trela, K.; Krowczynski, A.; Pociecha, D.; Szydlowska, J.; Szczytko, J.; Twardowski, A.; Wojcik, J.; Gorecka, E.: Mesogenic Ni(II) and Cu(II) complexes of barbituric acid derivatives-toward one-dimensional magnets. *J. Mater. Chem.* **2008**, *18*, 3419-3421.
63. Xu, X.-e.: Research on the preparation of semicarbazide hydrochloride. *Guangzhou Huagong* **2009**, *37*, 152-154.

64. Gallou, I.: Unsymmetrical ureas. Synthetic methodologies and application in drug design. *Org. Prep. Proced. Int.* **2007**, *39*, 355-383.
65. Getman, D. P.; DeCrescenzo, G. A.; Heintz, R. M.; Reed, K. L.; Talley, J. J.; Bryant, M. L.; Clare, M.; Houseman, K. A.; Marr, J. J.: Discovery of a novel class of potent HIV-1 protease inhibitors containing the (R)-(hydroxyethyl)urea isostere. *J. Med. Chem.* **1993**, *36*, 288-291.
66. Dumas, J.; Hatoum-Mokdad, H.; Sibley, R.; Riedl, B.; Scott, W. J.; Monahan, M. K.; Lowinger, T. B.; Brennan, C.; Natero, R.; Turner, T.; Johnson, J. S.; Schoenleber, R.; Bhargava, A.; Wilhelm, S. M.; Housley, T. J.; Ranges, G. E.; Shrikhande, A.: 1-Phenyl-5-pyrazolyl ureas: potent and selective p38 kinase inhibitors. *Bioorg. Med. Chem. Lett.* **2000**, *10*, 2051-2054.
67. Paugam, M.: Phosgene-triphosgene: different approach in risk management. *Chim. Oggi* **2011**, *29*, 58-60.
68. Mehlman, M. A.: Health effects and toxicity of phosgene: Scientific review. *Def. Sci. J.* **1987**, *37*, 269-279.
69. Alspach, J.; Bianchi, R. J.: Safe handling of phosgene in chemical processing. *Plant Oper. Prog.* **1984**, *3*, 40-42.
70. Staab, H. A.; Wendel, K.: 1,1'-Carbonyldiimidazole. *Org. Synth.* **1968**, *48*, 44.
71. Batey, R. A.; Santhakumar, V.; Yoshina-Ishii, C.; Taylor, S. D.: An efficient new protocol for the formation of unsymmetrical tri- and tetrasubstituted ureas. *Tetrahedron Lett.* **1998**, *39*, 6267-6270.
72. Lam, P. Y. S.; Ru, Y.; Jadhav, P. K.; Aldrich, P. E.; DeLucca, G. V.; Eyermann, C. J.; Chang, C.-H.; Emmett, G.; Holler, E. R.: Cyclic HIV protease inhibitors: Synthesis, conformational analysis, P2/P2' structure-activity relationship, and molecular recognition of cyclic ureas. *J. Med. Chem.* **1996**, *39*, 3514-3525.
73. Lebel, H.; Leogane, O.: Curtius rearrangement of aromatic carboxylic acids to access protected anilines and aromatic ureas. *Org. Lett.* **2006**, *8*, 5717-5720.
74. Scriven, E. F. V.; Turnbull, K.: Azides: their preparation and synthetic uses. *Chem. Rev.* **1988**, *88*, 297-368.
75. Yadav, D. K.; Yadav, A. K.; Srivastava, V. P.; Watal, G.; Yadav, L. D. S.: Bromodimethylsulfonium bromide (BDMS)-mediated Lossen rearrangement: synthesis of unsymmetrical ureas. *Tetrahedron Lett.* **2012**, *53*, 2890-2893.
76. Liu, P.; Wang, Z.; Hu, X.: Highly efficient synthesis of ureas and carbamates from amides by iodosylbenzene-induced Hofmann rearrangement. *Eur. J. Org. Chem.* **2012**, *10*, 1994-2000.
77. Snyder, J. K.; Stock, L. M.: Conformational preferences in alkylnitrosoureas. *J. Org. Chem.* **1980**, *45*, 886-891.

78. Lee, S.-H.; Matsushita, H.; Clapham, B.; Janda, K. D.: The direct conversion of carbamates to ureas using aluminum amides. *Tetrahedron* **2004**, *60*, 3439-3443.
79. Kotecki, B. J.; Fernando, D. P.; Haight, A. R.; Lukin, K. A.: A general method for the synthesis of unsymmetrically substituted ureas via palladium-catalyzed amidation. *Org. Lett.* **2009**, *11*, 947-950.
80. Williams, A.; Jencks, W. P.: Urea synthesis from amines and cyanic acid. Kinetic evidence for a zwitterionic intermediate. *J. Chem. Soc., Perkin Trans. 2* **1974**, 1753-1759.
81. Basavaprabhu, H.; Sureshbabu, V. V.: Iron(III) catalysed synthesis of unsymmetrical di and trisubstituted ureas - a variation of classical Ritter reaction. *Org. Biomol. Chem.* **2012**, *10*, 2528-2533.
82. Clow, A.: Resonance in urea and its derivatives.-Part I.-Diamagnetics. *Trans. Faraday Soc.* **1937**, *33*, 381-388.
83. Platts, J. A.; Maarof, H.; Harris, K. D.; Lim, G. K.; Willock, D. J.: The effect of intermolecular hydrogen bonding on the planarity of amides. *Phys. Chem. Chem. Phys.* **2012**, *14*, 11944-11952.
84. Emery, R.; Macleod, N. A.; Snoek, L. C.; Simons, J. P.: Conformational preferences in model antiviral compounds: A spectroscopic and computational study of phenylurea and 1,3-diphenylurea. *Phys. Chem. Chem. Phys.* **2004**, *6*, 2816-2820.
85. Custelcean, R.; Moyer, B. A.; Bryantsev, V. S.; Hay, B. P.: Anion coordination in metal organic frameworks functionalized with urea hydrogen-bonding groups. *Crystal Growth & Design* **2005**, *6*, 555-563.
86. Kumler, W. D.; Fohlen, G. M.: The dipole moment and structure of urea and thiourea. *J. Am. Chem. Soc.* **1942**, *64*, 1944-1948.
87. Huang, W.; Yang, Z.; Lin, H.; Lin, H.: Study on the selectivity of anion receptors based on similar (thio)urea fragments. *J. Fluoresc.* **2013**, *23*, 21-29.
88. Jose, D. A.; Kumar, D. K.; Kar, P.; Verma, S.; Ghosh, A.; Ganguly, B.; Ghosh, H. N.; Das, A.: Role of positional isomers on receptor–anion binding and evidence for resonance energy transfer. *Tetrahedron* **2007**, *63*, 12007-12014.
89. Rebarz, M.; Marcelis, L.; Menand, M.; Cornut, D.; Moucheron, C.; Jabin, I.; Kirsch-De Mesmaeker, A.: Revisited photophysics and photochemistry of a Ru-TAP complex using chloride ions and a calix[6]crypturea. *Inorg. Chem.* **2014**, *53*, 2635-2644.
90. Van Rossom, W.; Caers, J.; Robeyns, K.; Van Meervelt, L.; Maes, W.; Dehaen, W.: (Thio)ureido anion receptors based on a 1,3-alternate oxacalix[2]arene[2]pyrimidine scaffold. *J. Org. Chem.* **2012**, *77*, 2791-2797.

91. Lu, C. S.; E.W.Hughes; Giguere, P. A.: The crystal structure of the urea-hydrogen peroxide addition compound $CO(NH_2)_2.H_2O_2$. *J. Am. Chem. Soc.* **1941**, *63*, 1507-1513.
92. Dobado, J. A.; Molina, J.; Portal, D.: Theoretical study on the urea-hydrogen peroxide 1:1 complexes. *J. Phys. Chem. A* **1998**, *102*, 778-784.
93. Etter, M. C.; Urbanczyk-Lipkowska, Z.; Zia-Ebrahimi, M.; Panunto, T. W.: Hydrogen bond-directed cocrystallization and molecular recognition properties of diarylureas. *J. Am. Chem. Soc.* **1990**, *112*, 8415-8426.
94. Pavia, D.; Lampman, G.; Kriz, G.: *Introduction to Spectroscopy (3rd ed.)*; Saunders College, 2000.
95. Hilliard, C. R.; Bhuvanesh, N.; Gladysz, J. A.; Blumel, J.: Synthesis, purification, and characterization of phosphine oxides and their hydrogen peroxide adducts. *Dalton Trans.* **2012**, *41*, 1742-1754.
96. Jacobs, P. T.; Lin, S.-M.; Chen, X.: Inorganic hydrogen peroxide complexes for use in vapor sterilization of medical instruments. Advanced Sterilization Products, USA . 1997; pp 26., Cont.-in-part of U.S. Ser. No. 369,786.
97. Klemarczyk, P. T.; Birkett, D.; Farrell, D.; Wrobel, P.; McArdle, C.; Clarke, G.: Hydrogen peroxide complexes and their use in the cure system of anaerobic adhesives. Henkel Corporation, USA; Loctite R&D Limited . 2010; pp 36.
98. Wolanov, Y.; Lev, O.; Churakov, A. V.; Medvedev, A. G.; Novotortsev, V. M.; Prikhodchenko, P. V.: Preparation of pure hydrogen peroxide and anhydrous peroxide solutions from crystalline serine perhydrate. *Tetrahedron* **2010**, *66*, 5130-5133.
99. Maass, O.; Hatcher, W. H.: The properties of pure hydrogen peroxide I. *J. Am. Chem. Soc.* **1920**, *42*, 2548-2569.
100. Churakov, A. V.; Prikhodchenko, P. V.; Howard, J. A. K.; Lev, O.: Glycine and l-serine crystalline perhydrates. *Chem. Commun.* **2009**, 4224-4226.
101. Prikhodchenko, P. V.; Medvedev, A. G.; Tripol'skaya, T. A.; Churakov, A. V.; Wolanov, Y.; Howard, J. A. K.; Lev, O.: Crystal structures of natural amino acid perhydrates. *Cryst. Eng. Comm.* **2011**, *13*, 2399-2407.
102. da Silva, J. M. R.; Nascimento, M. d. G.: Chemoenzymatic epoxidation of citronellol catalyzed by lipases. *Process Biochem.* **2012**, *47*, 517-522.
103. Qiu, C.-J.; Zhang, Y.-C.; Gao, Y.; Zhao, J.-Q.: Novel Schiff-base complexes of methyltrioxorhenium(VII) and their performances in epoxidation of cyclohexene. *J. Organomet. Chem.* **2009**, *694*, 3418-3424.
104. Taylor, J. G.; Moro, A. V.; Correia, C. R. D.: Evolution and synthetic applications of the Heck-Matsuda reaction: The return of arenediazonium salts to prominence. *Eur. J. Org. Chem.* **2011**, *8*, 1403-1428.
105. Yang, Y.; Lu, S.: Substitution reaction of N,N'-diphenylurea by amines to unsymmetric phenylureas. *Org. Prep. Proced. Int.* **1999**, *31*, 559-561.

106. Crosby, D. G.; Niemann, C.: Further studies on the synthesis of substituted ureas. *J. Am. Chem. Soc.* **1954**, *76*, 4458-63.
107. Laudien, R.; Mitzner, R.: Phenylureas. Part 1. Mechanism of the basic hydrolysis of phenylureas. *J. Chem. Soc. Perk. Trans. 2* **2001**, 2226-2229.
108. Gavade, S. N.; Balaskar, R. S.; Mane, M. S.; Pabrekar, P. N.; Shingare, M. S.; Mane, D. V.: An efficient method for the N-arylation of phenylurea via copper catalyzed amidation. *Chin. Chem. Lett.* **2011**, *22*, 675-678.
109. Pihuleac, J.; Bauer, L.: Ureas from Lossen rearrangements of hydroxamic acids induced by p-toluenesulfonyl chloride or 2-chloro-1-methylpyridinium iodide in the presence of amines: a correction. *Synthesis* **1989**, 61-64.
110. Perrone, M. G.; Bleve, L.; Santandrea, E.; Vitale, P.; Niso, M.; Scilimati, A.: The tertiary amine nitrogen atom of piperazine sulfonamides as a novel determinant of potent and selective β3-adrenoceptor agonists. *Chem. Med. Chem.* **2009**, *4*, 2080-2097.
111. Azad, S.; Kumamoto, K.; Uegaki, K.; Ichikawa, Y.; Kotsuki, H.: A new practical method for the synthesis of unsymmetrical ureas via high-pressure-promoted condensation of 2,2,2-trichloroethyl carbamates (Troc-carbamates) with amines. *Tetrahedron Lett.* **2006**, *47*, 587-590.
112. Formentin, P.; Gimeno, N.; Steinke, J. H. G.; Vilar, R.: Reactivity of Grubbs' catalysts with urea- and amide-substituted olefins. Metathesis and isomerization. *J. Org. Chem.* **2005**, *70*, 8235-8238.
113. Willwacher, J.; Rakshit, S.; Glorius, F.: Investigating N-methoxy-N[prime or minute]-aryl ureas in oxidative C-H olefination reactions: an unexpected oxidation behaviour. *Org. Biomol. Chem.* **2011**, *9*, 4736-4740.
114. Jakab, G.; Tancon, C.; Zhang, Z.; Lippert, K. M.; Schreiner, P. R.: (Thio)urea organocatalyst equilibrium acidities in DMSO. *Org. Lett.* **2012**, *14*, 1724-1727.
115. Artamkina, G. A.; Sergeev, A. G.; Beletskaya, I. P.: Palladium-catalyzed arylation of ureas. *Russ. J. Org. Chem.* **2002**, *38*, 538-545.
116. Ruggli, P.; Iselin, E.: Azo compounds and their intermediates. XXVII. The hydrazo compounds from p-disazobenzene. *Helv. Chim. Acta* **1944**, *27*, 1711-18.
117. Wiley Subscription Services, Inc. (US), UBI_62362. Retrived from https://scifinder.cas.org.
118. Lin, C.-C.; Hsieh, T.-H.; Liao, P.-Y.; Liao, Z.-Y.; Chang, C.-W.; Shih, Y.-C.; Yeh, W.-H.; Chien, T.-C.: Practical synthesis of N-substituted cyanamides via Tiemann rearrangement of amidoximes. *Org. Lett.* **2014**, *16*, 892-895.
119. Khan, K. M.; Saeed, S.; Ali, M.; Gohar, M.; Zahid, J.; Khan, A.; Perveen, S.; Choudhary, M. I.: Unsymmetrically disubstituted urea derivatives: A potent class of antiglycating agents. *Bioorg. Med. Chem.* **2009**, *17*, 2447-2451.

120. Rodriguez, F.; Rozas, I.; Kaiser, M.; Brun, R.; Nguyen, B.; Wilson, W. D.; Garcia, R. N.; Dardonville, C.: New bis(2-aminoimidazoline) and bisguanidine DNA minor groove binders with potent *in vivo* antitrypanosomal and antiplasmodial activity. *J. Med. Chem.* **2008**, *51*, 909-923.
121. Meudtner, R. M.; Ostermeier, M.; Goddard, R.; Limberg, C.; Hecht, S.: Multifunctional "clickates" as versatile extended heteroaromatic building blocks: Efficient synthesis via Click chemistry, conformational preferences, and metal coordination. *Chem. Eur. J.,* **2007**, *13*, 9834-9840.
122. Iinuma, M.; Moriyama, K.; Togo, H.: Various oxidative reactions with novel ion-supported (diacetoxyiodo)benzenes. *Tetrahedron* **2013**, *69*, 2961-2970.
123. Watson, A. J. A.; Maxwell, A. C.; Williams, J. M. J.: Borrowing hydrogen methodology for amine synthesis under solvent-free microwave conditions. *J. Org. Chem.* **2011**, *76*, 2328-2331.
124. Choi, S.; Jung, K.; Ryu, J.: Efficient synthesis of 2-substituted 2,3-dihydro-4-quinolones as potential intermediates for 2-substituted 1,2,3,4-tetrahydro-4-quinolone antitumor agents. *Arch. Pharmacal Res.* **2006**, *29*, 369-374.
125. McGeary, R. P.; Bennett, A. J.; Tran, Q. B.; Prins, J.; Ross, B. P.: An 'inside-out' approach to suramin analogues. *Tetrahedron* **2009**, *65*, 3990-3997.
126. Dolomanov, O. V.; Bourhis, L. J.; Gildea, R. J.; Howard, J. A. K.; Puschmann, H.: OLEX2: a complete structure solution, refinement and analysis program. *J. Appl. Crystallogr.* **2009**, *42*, 339-341.
127. Palatinus, L.; Chapuis, G.: SUPERFLIP - a computer program for the solution of crystal structures by charge flipping in arbitrary dimensions. *J. Appl. Crystallogr.* **2007**, *40*, 786-790.
128. Palatinus, L.; van der Lee, A.: Symmetry determination following structure solution in P1. *J. Appl. Crystallogr.* **2008**, *41*, 975-984.
129. Palatinus, L.; Prathapa, S. J.; van Smaalen, S.: EDMA: a computer program for topological analysis of discrete electron densities. *J. Appl. Crystallogr.* **2012**, *45*, 575-580.
130. Sheldrick, G.: A short history of SHELX. *Acta Crystallographica Section A* **2008**, *64*, 112-122.
131. Ali, H. D. P.; Kruger, P. E.; Gunnlaugsson, T.: Colorimetric 'naked-eye' and fluorescent sensors for anions based on amidourea functionalised 1,8-naphthalimide structures: anion recognition via either deprotonation or hydrogen bonding in DMSO. *New. J. Chem.* **2008**, *32*, 1153.
132. Tsang, P. K. S.; Cofre, P.; Sawyer, D. T.: Electrochemical oxidation of hydroxide ion in acetonitrile and its facilitation by transition-metal complexes. *Inorg. Chem.* **1987**, *26*, 3604-3609.
133. Burrell, A. K.; Warner, B. P.; Mcclesky, M. T.: Electrochromic salts, solutions, and devices. US patent WO2004000800 A3, filed May 20 2003.

134. Wheeler, D. R.; Nichols, J.; Hansen, D.; Andrus, M.; Choi, S.; Watt, G. D.: Viologen catalysts for a direct carbohydrate fuel cell. *J. Electrochem. Soc.* **2009**, *156*, B1201-B1207.
135. Pedersen, J. A.: Electron spin resonance studies of oxidative processes of quinones and hydroquinones in alkaline solution; formation of primary and secondary semiquinone radicals. *J. Chem. Soc., Perk. Trans. 2* **1973**, 424-431.
136. Miyazawa, T.; Endo, T.; Shiihashi, S.; Okawara, M.: Selective oxidation of alcohols by oxoaminium salts (R_2N:O+ X-). *J. Org. Chem.* **1985**, *50*, 1332-1334.
137. Semmelhack, M. F.; Chou, C. S.; Cortes, D. A.: Nitroxyl-mediated electrooxidation of alcohols to aldehydes and ketones. *J. Am. Chem. Soc.* **1983**, *105*, 4492-4494.
138. Semmelhack, M. F.; Schmid, C. R.: Nitroxyl-mediated electro-oxidation of amines to nitriles and carbonyl compounds. *J. Am. Chem. Soc.* **1983**, *105*, 6732-6734.
139. Hunter, D. H.; Racok, J. S.; Rey, A. W.; Zea-Ponce, Y.: Oxoiminium ions for N-demethylation: 1-oxo-2,2,6,6-tetramethylpiperidinium chloride. *J. Org. Chem.* **1988**, *53*, 1278-1281.
140. Kim, J.-K.; Matic, A.; Ahn, J.-H.; Jacobsson, P.: Improving the stability of an organic battery with an ionic liquid-based polymer electrolyte. *RSC Advances* **2012**, *2*, 9795.
141. Koshika, K.; Chikushi, N.; Sano, N.; Oyaizu, K.; Nishide, H.: A TEMPO-substituted polyacrylamide as a new cathode material: an organic rechargeable device composed of polymer electrodes and aqueous electrolyte. *Green Chemistry* **2010**, *12*.
142. Kashiwagi, Y.; Nishimura, T.; Anzai, J.-i.: Voltammetric behavior of β-phosphonylated nitroxide and its application to electrocatalytic oxidation of alcohol. *Electrochim. Acta* **2002**, *47*, 1317-1320.
143. Nakahara, K.; Iwasa, S.; Iriyama, J.; Morioka, Y.; Suguro, M.; Satoh, M.; Cairns, E. J.: Electrochemical and spectroscopic measurements for stable nitroxyl radicals. *Electrochim. Acta* **2006**, *52*, 921-927.
144. Iwabuchi, Y.: Discovery and exploitation of AZADO: the highly active catalyst for alcohol oxidation. *Chem. Pharm. Bull.* **2013**, *61*, 1197-1213.
145. Bragd, P. L.; van Bekkum, H.; Besemer, A. C.: TEMPO-mediated oxidation of polysaccharides: Survey of methods and applications. *Top. Catal.* **2004**, *27*, 49-66.
146. Huber, M.: Introduction to magnetic resonance methods in photosynthesis. *Photosynth. Res.* **2009**, *102*, 305-310.
147. Keana, J. F. W.: Newer aspects of the synthesis and chemistry of nitroxide spin labels. *Chem. Rev.* **1978**, *78*, 37-64.
148. Volodarsky, L. B.; Reznikov, V. A.; Ovcharenko, V. I.: *Synthetic Chemistry of Stable Nitroxides*; CRC, 1994.

149. Miyazawa, T.; Endo, T.: Oxidation of benzyl alcohol by Fe(III) mediated by nitroxyl radical. *J. Mol. Catal.* **1985**, *31*, 217-220.
150. Rassat, A.; Rey, P.: Nitroxydes—LXIV : Decomposition thermique de radicaux libres nitroxydes isoquinuclidiniques. *Tetrahedron* **1975**, *31*, 2673-2677.
151. Henry-Riyad, H.; Tidwell, T. T.: Thermolysis of N-tetramethylpiperidinyl triphenylacetate: homolytic fragmentation of a TEMPO ester. *J. Phys. Org. Chem.* **2003**, *16*, 559-563.
152. Endo, T.; Miyazawa, T.; Shiihashi, S.; Okawara, M.: Oxidation of hydroxide ion by immonium oxide. *J. Am. Chem. Soc.* **1984**, *106*, 3877-3878.
153. Dragutan, I.; Mehlhorn, R. J.: Modulation of oxidative damage by nitroxide free radicals. *Free Radical Res.* **2007**, *41*, 303-315.
154. Bagryanskaya, E. G.; Marque, S. R. A.: Scavenging of organic C-Centered radicals by nitroxides. *Chem. Rev.* **2014**, *114*, 5011-5056.
155. Lee, T. D.; Keana, J. F. W.: *In situ* reduction of nitroxide spin labels with phenylhydrazine in deuteriochloroform solution. Convenient method for obtaining structural information on nitroxides using nuclear magnetic resonance spectroscopy. *J. Org. Chem.* **1975**, *40*, 3145-3147.
156. Misra, H. P.; Fridovich, I.: The oxidation of phenylhydrazine: superoxide and mechanism. *Biochemistry* **1976**, *15*, 681-687.
157. Smith, C. D.; Bartley, J. P.; Bottle, S. E.; Micallef, A. S.; Reid, D. A.: Electrospray ionization mass spectrometry of stable nitroxide free radicals and two isoindoline nitroxide dimers. *J. Mass Spectrom.* **2000**, *35*, 607-611.
158. Hodgson, J. L.; Namazian, M.; Bottle, S. E.; Coote, M. L.: One-electron oxidation and reduction potentials of nitroxide antioxidants: A theoretical study. *J. Phys. Chem. A* **2007**, *111*, 13595-13605.
159. Hicks, R.: *Stable Radicals: Fundamentals and Applied Aspects of Odd-Electron Compounds*; Wiley, 2011.
160. Merbouh, N.; Bobbitt, J. M.; Brückner, C.: Preparation of tetramethylpiperdine-1-oxoammonium salts and their use as oxidants in organic chemistry: A review. *Org. Prep. Proced. Int.* **2004**, *36*, 1-31.
161. Grampp, G.; Rasmussen, K.: Solvent dynamical effects on the electron self-exchange rate of the TEMPO•/TEMPO+ couple. Part I. ESR-linebroadening measurements at T = 298 K. *Phys. Chem. Chem. Phys.* **2002**, *4*, 5546-5549.
162. Shibuya, M.; Tomizawa, M.; Iwabuchi, Y.: Oxidative rearrangement of tertiary allylic alcohols employing oxoammonium salts. *J. Org. Chem.* **2008**, *73*, 4750-4752.
163. Anderson, C. D.; Shea, K. J.; Rychnovsky, S. D.: Strategies for the generation of molecularly imprinted polymeric nitroxide catalysts. *Org. Lett.* **2005**, *7*, 4879-4882.

164. Aspée, A.; Orrego, A.; Alarcón, E.; López-Alarcón, C.; Poblete, H.; González-Nilo, D.: Antioxidant reactivity toward nitroxide probes anchored into human serum albumin. A new model for studying antioxidant repairing capacity of protein radicals. *Biorg. Med. Chem. Lett.* **2009**, *19*, 6382-6385.
165. Cougnon, C.; Boisard, S.; Cador, O.; Dias, M.; Levillain, E.; Breton, T.: A facile route to steady redox-modulated nitroxide spin-labeled surfaces based on diazonium chemistry. *Chem. Commun.* **2013**, *49*, 4555-4557.
166. Fairfull-Smith, K. E.; Brackmann, F.; Bottle, S. E.: The synthesis of novel isoindoline nitroxides bearing water-solubilising functionality. *Eur. J. Org. Chem.* **2009**, 1902-1915.
167. Reid, D. A.; Bottle, S. E.: The synthesis of water soluble isoindoline nitroxides and a pronitroxide hydroxylamine hydrochloride UV–VIS probe for free radicals. *Chem. Commun.* **1998**, 1907-1908.
168. Zhang, X.; Li, H.; Li, L.; Lu, G.; Zhang, S.; Gu, L.; Xia, Y.; Huang, X.: Polyallene with pendant nitroxyl radicals. *Polymer* **2008**, *49*, 3393-3398.
169. Braslau, R.; Chaplinski, V.; Goodson, P.: Symmetrical nitroxide synthesis: meso versus d,l diastereomer formation. *J. Org. Chem.* **1998**, *63*, 9857-9864.
170. Kirilyuk, I. A.; Polienko, Y. F.; Krumkacheva, O. A.; Strizhakov, R. K.; Gatilov, Y. V.; Grigor'ev, I. A.; Bagryanskaya, E. G.: Synthesis of 2,5-bis(spirocyclohexane)-substituted nitroxides of pyrroline and pyrrolidine series, including thiol-specific spin label: an analogue of MTSSL with long relaxation time. *J. Org. Chem.* **2012**, *77*, 8016-8027.
171. Shi, H.-C.; Li, Y.: Formation of nitroxide radicals from secondary amines and peracids: A peroxyl radical oxidation pathway derived from electron spin resonance detection and density functional theory calculation. *J. Mol. Catal. A: Chem.* **2007**, *271*, 32-41.
172. Kulasekharan, R.; Jayaraj, N.; Porel, M.; Choudhury, R.; Sundaresan, A. K.; Parthasarathy, A.; Ottaviani, M. F.; Jockusch, S.; Turro, N. J.; Ramamurthy, V.: Guest rotations within a capsuleplex probed by NMR and EPR techniques. *Lang.* **2010**, *26*, 6943-6953.
173. Chalmers, B. A.; Morris, J. C.; Fairfull-Smith, K. E.; Grainger, R. S.; Bottle, S. E.: A novel protecting group methodology for syntheses using nitroxides. *Chem. Commun.* **2013**, *49*, 10382-10384.
174. Schoening, K.-U.; Fischer, W.; Hauck, S.; Dichtl, A.; Kuepfert, M.: Synthetic studies on N-alkoxyamines: A mild and broadly applicable route starting from nitroxide radicals and aldehydes. *J. Org. Chem.* **2009**, *74*, 1567-1573.
175. Eberhardt, M. K.; Colina, R.: The reaction of OH radicals with dimethyl sulfoxide. A comparative study of Fenton's reagent and the radiolysis of aqueous dimethyl sulfoxide solutions. *J. Org. Chem.* **1988**, *53*, 1071-1074.
176. Rintoul, L.; Micallef, A. S.; Bottle, S. E.: The vibrational group frequency of the N–O stretching band of nitroxide stable free radicals. *Spectrochim. Acta Part A: Mol. Biomol. Spect.* **2008**, *70*, 713-717.

177. Tansakul, C.; Lilie, E.; Walter, E. D.; Rivera, F.; Wolcott, A.; Zhang, J. Z.; Millhauser, G. L.; Braslau, R.: Distance-dependent fluorescence quenching and binding of CdSe quantum dots by functionalized nitroxide radicals. *J. Phys. Chem. C* **2010**, *114*, 7793-7805.
178. Griffiths, P. G.; Rizzardo, E.; Solomon, D. H.: Quantitative studies on free radical reactions with the scavenger 1,1,3,3-tetramethylisoindolinyl-2-oxy. *Tetrahedron Lett.* **1982**, *23*, 1309-1312.
179. Busfield, W. K.; Engelhardt, L. M.; Healy, P. C.; Jenkins, I. D.; Thang, S. H.; White, A. H.: The structures of the free-radical scavenger 1,1,3,3-tetramethylisoindolin-2-yloxyl, and of the alkoxy amine derivative 5-(1,1,3,3-tetramethylisoindolin-2-yloxy)-1-vinylpyrrolidin-2-one. *Aust. J. Chem.* **1986**, *39*, 357-365.
180. Jayawardena, V. C.; Fairfull-Smith, K. E.; Bottle, S. E.: Improving the yield of the exhaustive grignard alkylation of N-benzylphthalimide. *Aust. J. Chem.* **2013**, *66*, 619-625.
181. Blinco, J. P.; Chalmers, B. A.; Chou, A.; Fairfull-Smith, K. E.; Bottle, S. E.: Spin-coated carbon. *Chem. Sci.* **2013**, *4*, 3411.
182. Forstinger, K.; Metz, H. J.: Diazo compounds and diazo reactions. In *Ullmann's Encyclopedia of Industrial Chemistry*; Wiley-VCH Verlag GmbH & Co. KGaA, 2000.
183. Tabei, K.; Ito, C.: Infrared spectra of para-substituted benzene-diazonium cations. *Bull. Chem. Soc. Jap.* **1968**, *41*, 514-515.
184. Ding, P.; Wunnicke, D.; Steinhoff, H. J.; Seela, F.: Site-directed spin-labeling of DNA by the azide-alkyne 'click' reaction: nanometer distance measurements on 7-deaza-2'-deoxyadenosine and 2'-deoxyuridine nitroxide conjugates spatially separated or linked to a 'dA-dT' base pair. *Chem. Eur. J.* **2010**, *16*, 14385-14396.
185. Jakobsen, U.; Shelke, S. A.; Vogel, S.; Sigurdsson, S. T.: Site-directed spin-labeling of nucleic acids by Click Chemistry: Detection of abasic sites in duplex DNA by EPR spectroscopy. *J. Am. Chem. Soc.* **2010**, *132*, 10424-10428.
186. Fokin, V., V.; Wu, P: Catalytic Azide-Alkyne Cycloaddition: Reactivity and applications. *Aldrichimica Acta* **2007**, *40*, 7-17.
187. Leroux, Y. R.; Hapiot, P.: Nanostructured monolayers on carbon substrates prepared by electrografting of protected aryldiazonium salts. *Chem. Mater.* **2013**, *25*, 489-495.
188. Kavala, M.; Boča, R.; Dlháň, L.; Brezová, V.; Breza, M.; Kožíšek, J.; Fronc, M.; Herich, P.; Švorc, L.; Szolcsányi, P.: Preparation and spectroscopic, magnetic, and electrochemical studies of mono-/biradical TEMPO derivatives. *J. Org. Chem.* **2013**, *78*, 6558-6569.
189. Bushmakina, N. G.; Misharin, A. Y.: A simple synthesis of 4-amino-2,2,6,6-tetramethyl-1-piperidinyloxy radical. *Synthesis* **1986**, *11*, 966-966.

190. Leroux, Y. R.; Hui, F.; Noel, J. M.; Roux, C.; Downard, A. J.; Hapiot, P.: Design of robust binary film onto carbon surface using diazonium electrochemistry. *Lang.* **2011**, *27*, 11222-11228.
191. Leroux, Y. R.; Fei, H.; Noël, J.-M.; Roux, C.; Hapiot, P.: Efficient covalent modification of a carbon surface: Use of a silyl protecting group to form an active monolayer. *J. Am. Chem. Soc.* **2010**, *132*, 14039-14041.
192. Anderson, S.: Phenylene ethynylene pentamers for organic electroluminescence. *Chem. Eur. J.* **2001**, *7*, 4706-4714.
193. Griffiths, P. G.; Moad, G.; Rizzardo, E.: Synthesis of the radical scavenger 1,1,3,3-Tetramethylisoindolin-2-yloxyl. *Aust. J. Chem.* **1983**, *36*, 397-401.
194. Ball, M. C.; Steven, M.: The thermal decomposition of solid urea hydrogen peroxide. *Thermochim. Acta* **1995**, *261*, 95-106.
195. Schubert, J.; Wilmer, J. W.: Does hydrogen peroxide exist "free" in biological systems? *Free Radical Biol. Med.* **1991**, *11*, 545-555.
196. Serra, M. A.; Dorner, B. K.; Silver, M. E.: Structure of an adenine-hydrogen peroxide adduct. *Acta Crystallogr., Sect. C: Cryst. Struct. Commun.* **1992**, *C48*, 1957-1960.
197. Prikhodchenko, P. V.; Medvedev, A. G.; Tripol'skaya, T. A.; Churakov, A. V.; Wolanov, Y.; Howard, J. A. K.; Lev, O.: Crystal structures of natural amino acid perhydrates. *Cryst. Eng. Comm.* **2011**, *13*, 2399-2407.
198. Zhao, H.-K.; Ren, B.-Z.; Liu, G.-J.; Wang, H.-X.: Phase diagram of the system urea + hydrogen peroxide + water. *J. Chem. Eng. Data* **2003**, *48*, 548-550.
199. Campos-Martin, J. M.; Blanco-Brieva, G.; Fierro, J. L. G.: Hydrogen peroxide synthesis: An outlook beyond the anthraquinone process. *Angew. Chem. Int. Ed.* **2006**, *45*, 6962-6984.
200. Song, L.; Liu, M.; Wu, W.; Zhang, Q.; Mo, Y.: Origins of rotational barriers in hydrogen peroxide and hydrazine. *J. Chem. Theory Comput.* **2005**, *1*, 394-402.
201. Abrahams, S. C.; Collin, R. L.; Lipscomb, W. N.: The crystal structure of hydrogen peroxide. *Acta Crystallogr.* **1951**, *4*, 15-20.
202. Standard test methods for assay of organic peroxides. ASTM International, 2008; Vol. ASTM E298-08.
203. Howell, G. V.; Williams, R. L.: Triphenylarsine oxide-hydrogen peroxide adduct. *J. Chem. Soc. A* **1968**, 117-118.
204. Negita, H.; Kubo, T.; Maekawa, M.: Nitrogen-14 nuclear quadrupole resonances of the molecular complexes of urea. *Bull. Chem. Soc. Jpn.* **1977**, *50*, 2215-16.
205. Steiner, T.: Reviews: The hydrogen bond in the solid state. *Angew. Chem., Int. Ed.* **2002**, *41*, 48-76.
206. Baggi, G.; Boiocchi, M.; Fabbrizzi, L.; Mosca, L.: Moderate and advanced intramolecular proton transfer in urea-anion hydrogen-bonded complexes. *Chem. Eur. J.* **2011**, *17*, 9423-9439.

207. Dong, Z. Y.; Gao, G. H.: Recognition and sensing of anions through synergistic effects using simple benzimidazolium-urea receptors. *Chin. Sci. Bull.* **2012**, *57*, 1266-1274.
208. Pohl, L.; Eckle, M.: Sodium 3-Trimethylsilyltetradeuteriopropionate, a new water-soluble standard for ^{1}H-NMR. *Angew. Chem. Int. Ed. Engl.* **1969**, *8*, 381.
209. Coaxial Insert for 5 mm NMR Precision Sample Tube Only. Wilmad-LabGlass. www.wilmad-labglass.com/Products/WGS-5BL/.
210. Lecomte, F.; Lucas, B.; Gregoire, G.; Schermann, J. P.; Desfrancois, C.: Urea and methylurea dipole-bound anions. *Phys. Chem. Chem. Phys.* **2003**, *5*, 3120-3125.
211. Pierce, M. M.; Raman, C. S.; Nall, B. T.: Isothermal Titration Calorimetry of protein–protein interactions. *Methods* **1999**, *19*, 213-221.
212. Kim, Y. K.; Lee, Y.-H.; Lee, H.-Y.; Kim, M. K.; Cha, G. S.; Ahn, K. H.: Molecular recognition of anions through hydrogen bonding stabilization of anion-ionophore adducts: A novel trifluoroacetophenone-based binding motif. *Org. Lett.* **2003**, *5*, 4003-4006.
213. Caldwell, G.; Yan, Z.: Isothermal titration calorimetry characterization of drug-binding energetics to blood proteins. In *Optimization in Drug Discovery*; Yan, Zhengyin, Caldwell, GaryW, Eds.; Humana Press, 2004; pp 123-149.
214. Gourishankar, A.; Shukla, S.; Ganesh, K. N.; Sastry, M.: Isothermal titration calorimetry studies on the binding of DNA bases and PNA base monomers to gold nanoparticles. *J. Am. Chem. Soc.* **2004**, *126*, 13186-13187.
215. Ghai, R.; Falconer, R. J.; Collins, B. M.: Applications of isothermal titration calorimetry in pure and applied research—Survey of the literature from 2010. *J. Mol. Recog.* **2012**, *25*, 32-52.
216. Arruda, J. "MicroCal ITC200 Calcium-EDTA tutorial," Brown University, 2013.
217. Coats, A. W.; Redfern, J. P.: Thermogravimetric analysis. A review. *Analyst* **1963**, *88*, 906-924.
218. Adams, C. J.; Adams, J. M.; Pritchard, R. G.; Ramdas, V.: Hydrogen peroxide adducts of some simple guanidinium salts. *J. Inorg. Nucl. Chem.* **1979**, *41*, 937-40.
219. Piasek, Z.; Urbanski, T.: The infrared absorption spectrum and structure of urea. *Bull. Acad. Pol. Sci., Ser. Sci. Chim.* **1962**, *10*, 113-20.
220. Hermet, P.; Ghosez, P.: First-principles study of the dynamical and nonlinear optical properties of urea single crystals. *Phys. Chem. Chem. Phys.* **2010**, *12*, 835-843.
221. Penland, R. B.; Mizushima, S.; Curran, C.; Quagliano, J. V.: Infrared absorption spectra of inorganic co-ordination complexes. X. Studies of some metal-urea complexes 1a,b. *J. Am. Chem. Soc.* **1957**, *79*, 1575-1578.

222. Giguère, P. A.: The infra-red spectrum of hydrogen peroxide. *J. Chem. Phys.* **1950**, *18*, 88-92.
223. Ricciuti, C.; Coleman, J. E.; Willits, C. O.: Statistical comparison of three methods for determining organic peroxides. *Anal. Chem.* **1955**, *27*, 405-407.
224. Bassett, J.; Denney, R. C.; Jeffery, G. H.; Mendham, J.: *Vogel's Textbook of Quantitative Inorganic Analysis. 4th Ed*; Longman, 1978.
225. Goody, R. S.; Jones, A. S.; Walker, R. T.: Permanganate oxidation of cytosine derivatives. *Tetrahedron* **1971**, *27*, 65-69.
226. Pobiner, H.: Determination of hydroperoxides in hydrocarbon by conversion to hydrogen peroxide and measurement by titanium complexing. *Anal. Chem.* **1961**, *33*, 1423-1426.
227. Wolfe, W. C.: Spectrophotometric determination of hydroperoxide in diethyl ether. *Anal. Chem.* **1962**, *34*, 1328-1330.
228. Pinkernell, U.; Effkemann, S.; Karst, U.: Simultaneous HPLC determination of peroxyacetic acid and hydrogen peroxide. *Anal. Chem.* **1997**, *69*, 3623-3627.
229. Bharti, S. K.; Roy, R.: Quantitative ^{1}H NMR spectroscopy. *TrAC, Trends Anal. Chem.* **2012**, *35*, 5-26.
230. Sotirhos, N.; Herslöf, B.; Kenne, L.: Quantitative analysis of phospholipids by ^{31}P-NMR. *J. Lipid Res.* **1986**, *27*, 386-92.
231. Gordon, G.; Foundation, A. R.; Association, A. W. W.: *Disinfectant Residual Measurement Methods*; American Water Works Association, 1992.
232. Pehkonen, S.; Lundell, J.; Khriachtchev, L.; Pettersson, M.; Rasanen, M.: Matrix isolation and quantum chemical studies on the H_2O_2-SO_2 complex. *Phys. Chem. Chem. Phys.* **2004**, *6*, 4607-4613.
233. Grzechnik, K.; Mierzwicki, K.; Mielke, Z.: Matrix-isolated hydrogen-bonded and Van der Waals complexes of hydrogen peroxide with OCS and CS_2. *Chem. Phys. Chem.* **2013**, *14*, 777-787.
234. Hirose, K.: A practical guide for the determination of binding constants. *J. Incl. Phenom. Macrocycl. Chem.* **2001**, *39*, 193-209.
235. Live, D. H.; Chan, S. I.: Bulk susceptibility corrections in nuclear magnetic resonance experiments using superconducting solenoids. *Anal. Chem.* **1970**, *42*, 791-792.
236. Ernst, R. R.; Anderson, W. A.: Application of fourier transform spectroscopy to magnetic resonance. *Rev. Sci. Instrum.* **1966**, *37*, 93-102.
237. Spencer, R. G. S.; Fishbein, K. W.: Measurement of spin–lattice relaxation times and concentrations in systems with chemical exchange using the one-pulse sequence: Breakdown of the Ernst model for partial saturation in nuclear magnetic resonance spectroscopy. *J. Magn. Reson.* **2000**, *142*, 120-135.

238. Pal, S.: Study of multi-site chemical exchange in solution state by NMR: 1D experiments with multiply selective excitation. *J. Chem. Sci. (Bangalore, India)* **2010**, *122*, 471-480.
239. Amendola, V.; Fabbrizzi, L.; Mosca, L.: Anion recognition by hydrogen bonding: urea-based receptors. *Chem. Soc. Rev.* **2010**, *39*, 3889-3915.
240. Galindo, C.; Kalt, A.: UV/H_2O_2 oxidation of azodyes in aqueous media: evidence of a structure—degradability relationship. *Dyes and Pigments* **1999**, *42*, 199-207.
241. Merino, E.; Ribagorda, M.: Control over molecular motion using the cis–trans photoisomerization of the azo group. *Beilstein J. Org. Chem.* **2012**, *8*, 1071-1090.
242. Breukers, R. D.; Janssens, S.; Raymond, S. G.; Bhuiyan, M. D. H.; Kay, A. J.: Synthesis and characterization of strongly two photon absorbing and photoswitchable azo molecules. *Dyes and Pigments* **2015**, *112*, 17-23.
243. Evans, L. S.; Gale, P. A.; Light, M. E.; Quesada, R.: Anion binding vs. deprotonation in colorimetric pyrrolylamidothiourea based anion sensors. *Chem. Commun.* **2006**, 965-967.
244. Ros-Lis, J. V.; Martínez-Máñez, R.; Sancenón, F.; Soto, J.; Rurack, K.; Weibhoff, H.: Signalling mechanisms in anion-responsive push-pull chromophores: The hydrogen-bonding, deprotonation and anion-exchange chemistry of functionalized azo dyes. *Eur. J. Org. Chem.* **2007**, *15*, 2449-2458.
245. Baggi, G.; Boiocchi, M.; Ciarrocchi, C.; Fabbrizzi, L.: Enhancing the anion affinity of urea-based receptors with a $Ru(terpy)_2^{(2+)}$ chromophore. *Inorg. Chem.* **2013**, *52*, 5273-5283.
246. Esteban-Gomez, D.; Fabbrizzi, L.; Licchelli, M.: Why, on interaction of urea-based receptors with fluoride, beautiful colors develop. *J. Org. Chem.* **2005**, *70*, 5717-5720.
247. Duke, R. M.; Gunnlaugsson, T.: 3-Urea-1,8-naphthalimides are good chemosensors: A highly selective dual colorimetric and fluorescent ICT based anion sensor for fluoride. *Tetrahedron Lett.* **2011**, *52*, 1503-1505.
248. Janiszewska, A. M.; Grzeszczuk, M.: Mechanistic - kinetic scheme of oxidation/reduction of TEMPO involving hydrogen bonded dimer. RDE probe for availability of protons in reaction environment. *Electroanalysis* **2004**, *16*, 1673-1681.
249. Ma, Y.; Loyns, C.; Price, P.; Chechik, V.: Thermal decay of TEMPO in acidic media via an N-oxoammonium salt intermediate. *Org. Biomol. Chem.* **2011**, *9*, 5573-5578.
250. Tikhonov, I. V.; Sen, V. D.; Borodin, L. I.; Pliss, E. M.; Golubev, V. A.; Rusakov, A. I.: Effect of the structure of nitroxyl radicals on the kinetics of their acid-catalyzed disproportionation. *J. Phys. Org. Chem.* **2014**, *27*, 114-120.

251. Golubev, V. A.; Sen, V. D.: Mechanism of autoreduction of 2,2,6,6-tetramethyl-1,4-dioxopiperidinium cation in alkaline medium. *Russ. J. Org. Chem.* **2011**, *47*, 869-876.
252. Israeli, A.; Patt, M.; Oron, M.; Samuni, A.; Kohen, R.; Goldstein, S.: Kinetics and mechanism of the comproportionation reaction between oxoammonium cation and hydroxylamine derived from cyclic nitroxides. *Free Radical Biol. Med.* **2005**, *38*, 317-324.
253. Wardman, P.: Reduction potentials of one-electron couples involving free radicals in aqueous solution. *J. Phys. Chem. Ref. Data* **1989**, *18*, 1637-755.
254. Bailey, W. F.; Bobbitt, J. M.; Wiberg, K. B.: Mechanism of the oxidation of alcohols by oxoammonium cations. *J. Org. Chem.* **2007**, *72*, 4504-4509.
255. Limoges, B.; Degrand, C.: Electrocatalytic oxidation of hydrogen peroxide by nitroxyl radicals. *J. Electroanal. Chem.* **1997**, *422*, 7-12.
256. Wu, A.; Mader, E. A.; Datta, A.; Hrovat, D. A.; Borden, W. T.; Mayer, J. M.: Nitroxyl radical plus hydroxylamine pseudo self-exchange reactions: Tunneling in hydrogen atom transfer. *J. Am. Chem. Soc.* **2009**, *131*, 11985-11997.
257. Porel, M.; Jayaraj, N.; Raghothama, S.; Ramamurthy, V.: Chemistry in confined spaces: High-energy conformer of a piperidine derivative is favored within a water-soluble capsuleplex. *Org. Lett.* **2010**, *12*, 4544-4547.
258. Sen, V. D.; Shilov, G. V.; Golubev, V. A.: Synthesis and structure of redox derivatives of 4-(2-Amino-2-oxoethyl)-2,2,6,6-tetramethylpiperidine-1-yloxyl. *Russ. J. Org. Chem.* **2014**, *50*, 1124-1132.
259. Bobbitt, J. M.; Bartelson, A. L.; Bailey, W. F.; Hamlin, T. A.; Kelly, C. B.: Oxoammonium salt oxidations of alcohols in the presence of pyridine bases. *J. Org. Chem.* **2014**, *79*, 1055-1067.
260. Peng, J.; Shi, F.; Gu, Y.; Deng, Y.: Highly selective and green aqueous-ionic liquid biphasic hydroxylation of benzene to phenol with hydrogen peroxide. *Green Chem.* **2003**, *5*, 224-226.
261. Hirsch, A.: The era of carbon allotropes. *Nat. Mater.* **2010**, *9*, 868-871.
262. McCreery, R. L.: Advanced carbon electrode materials for molecular electrochemistry. *Chem. Rev.* **2008**, *108*, 2646-2687.
263. Jenkins, G. M.; Kawamura, K.: Structure of glassy carbon. *Nature* **1971**, *231*, 175-176.
264. Wang, J.; Hu, Z.; Xu, J.; Zhao, Y.: Therapeutic applications of low-toxicity spherical nanocarbon materials. *NPG Asia Mater* **2014**, *6*, 84.
265. Hu, I.-F.; Karweik, D. H.; Kuwana, T.: Activation and deactivation of glassy carbon electrodes. *J. Electroana.l Chem. and Interfacial Electrochem.* **1985**, *188*, 59-72.
266. Li, Z. Q.; Lu, C. J.; Xia, Z. P.; Zhou, Y.; Luo, Z.: X-ray diffraction patterns of graphite and turbostratic carbon. *Carbon* **2007**, *45*, 1686-1695.

267. Khoshroo, M.; Rostami, A.: Electrochemical and impedance spectroscopy studies of various diazonium salts on a glassy carbon electrode. *Monatshefte für Chemie / Chemical Monthly* **2010**, *141*, 841-846.
268. Hari, D. P.; Konig, B.: The photocatalyzed Meerwein arylation: classic reaction of aryl diazonium salts in a new light. *Angew. Chem. Int. Ed.* **2013**, *52*, 4734-4743.
269. Jayasundara, D. R.; Cullen, R. J.; Colavita, P. E.: *In situ* and real time characterization of spontaneous grafting of aryldiazonium salts at carbon surfaces. *Chem. Mater.* **2013**, *25*, 1144-1152.
270. Wehmeyer, K. R.; Deakin, M. R.; Wightman, R. M.: Electroanalytical properties of band electrodes of submicrometer width. *Anal. Chem.* **1985**, *57*, 1913-1916.
271. Delamar, M.; Hitmi, R.; Pinson, J.; Saveant, J. M.: Covalent modification of carbon surfaces by grafting of functionalized aryl radicals produced from electrochemical reduction of diazonium salts. *J. Am. Chem. Soc.* **1992**, *114*, 5883-5884.
272. Murphy, D. M.; Cullen, R. J.; Jayasundara, D. R.; Scanlan, E. M.; Colavita, P. E.: Study of the spontaneous attachment of polycyclic aryldiazonium salts onto amorphous carbon substrates. *RSC Advances* **2012**, *2*, 6527.
273. Cullen, R. J.; Jayasundara, D. R.; Soldi, L.; Cheng, J. J.; Dufaure, G.; Colavita, P. E.: Spontaneous grafting of nitrophenyl groups on amorphous carbon thin films: A structure–reactivity investigation. *Chem. Mater.* **2012**, *24*, 1031-1040.
274. Badawi, H. M.; Förner, W.: Analysis of the infrared and Raman spectra of the symmetrically substituted 1,3-diphenylurea and 1,3-diphenylacetone (dibenzyl ketone). *Spectrochim. Acta Part A: Mol. Biomol. Spect.* **2012**, *95*, 435-441.
275. Veres, M.; Tóth, S.; Koós, M.: New aspects of Raman scattering in carbon-based amorphous materials. *Diamond Relat. Mater.* **2008**, *17*, 1692-1696.
276. Ferrari, A. C.; Robertson, J.: Interpretation of Raman spectra of disordered and amorphous carbon. *Phys. Rev. B: Condens. Matter Mater. Phys.* **2000**, *61*, 14095-14107.
277. Deschamps, M.; Cadars, S.; Gilbert, E.; Azaïs, P.; Raymundo-Pinero, E.; Béguin, F.; Massiot, D.: A solid-state NMR study of C70: A model molecule for amorphous carbons. *Solid State Nucl. Magn. Reson.* **2012**, *42*, 81-86.
278. Coulon, E.; Pinson, J.; Bourzat, J.-D.; Commercon, A.; Pulicani, J.-P.: Surface-modified carbon felts: Possible supports for combinatorial chemistry. *J. Org. Chem.* **2002**, *67*, 8513-8518.
279. Gonzalez-Garcia, J.; Bonete, P.; Exposito, E.; Montiel, V.; Aldaz, A.; Torregrosa-Macia, R.: Characterization of a carbon felt electrode: structural and physical properties. *J. Mater. Chem.* **1999**, *9*, 419-426.

280. Kato, K.; Kano, K.; Ikeda, T.: Electrochemical characterization of carbon felt electrodes for bulk electrolysis and for biocatalyst‐Assisted electrolysis. *J. Electrochem. Soc.* **2000**, *147*, 1449-1453.
281. Liu, Z.; Guo, Q.; Shi, J.; Zhai, G.; Liu, L.: Graphite blocks with high thermal conductivity derived from natural graphite flake. *Carbon* **2008**, *46*, 414-421.
282. Setaka, T.; Morita, S.: Graphite-carbon bilayer crucible for pulling of single crystals. Tokai Carbon Co., Ltd., Japan. 2006; pp 8.
283. Ichinose, G.; Kawasaki, M.: Manufacture of electric carbons. XI. Characteristics of an ashless natural flake graphite and the effect of immersion liquids on the pycnometric density of graphite. *Tanso* **1954**, *4*, 16-18.
284. Bergognan, P.; Cornuault, P.; Bentolila, J.; Price, M. S. T.: Preparation of high-density graphite. *Proc. Conf. Carbon, 5th, Univ. Park, Pa.,* **1962**, *1*, 600-610.
285. Carta, R.; Palmas, S.; Polcaro, A. M.; Tola, G.: Behavior of a carbon felt flow by electrodes. Part I: Mass transfer characteristics. *J. Appl. Electrochem.* **1991**, *21*, 793-798.
286. Montillet, A.; Comiti, J.; Legrand, J.: Determination of structural parameters of metallic foams from permeametry measurements. *J. Mater. Sci.* **1992**, *27*, 4460-4464.
287. Olek, J.; Cohen, M. D.; Lobo, C.: Determination of surface area of portland cement and silica fume by mercury intrusion porosimetry. *ACI Mater. J.* **1990**, *87*, 473-478.
288. Gruber, P.; Faschingbauer, E.; McGoldrick, J.: An examination of corroded positive grids from a lead-acid battery. *J. Power Sources* **1986**, *17*, 369-377.
289. Bard, A. J.; Faulkner, L. R.: *Electrochemical Methods: Fundamentals and Applications*; Wiley, 1980.
290. Singh, B. P.; Jain, R. C.; Bhardwaj, I. S.: Studies on thermal stability and carbonization of oxidized PAN fiber. Allied Publ., 1994; Vol. 2; pp 917-921.
291. Yu, Z.; Jie, M.: Black carbon and its applications in environmental protection. *Adv. Mater. Res. (Durnten-Zurich, Switz.)* **2014**, *864-867*, 727-732.
292. Richard, W.; Evrard, D.; Gros, P.: New insight into 4-nitrobenzene diazonium reduction process: Evidence for a grafting step distinct from NO_2 electrochemical reactivity. *J. Electroanal. Chem.* **2012**, *685*, 109-115.
293. Blinco, J. P.; Hodgson, J. L.; Morrow, B. J.; Walker, J. R.; Will, G. D.; Coote, M. L.; Bottle, S. E.: Experimental and theoretical studies of the redox potentials of cyclic nitroxides. *J. Org. Chem.* **2008**, *73*, 6763-6771.
294. Lee, L.; Brooksby, P. A.; Leroux, Y. R.; Hapiot, P.; Downard, A. J.: Mixed monolayer organic films via sequential electrografting from

aryldiazonium ion and arylhydrazine solutions. *Lang.* **2013**, *29*, 3133-3139.

295. Amatore, C.; Saveant, J. M.; Tessier, D.: Charge transfer at partially blocked surfaces. A model for the case of microscopic active and inactive sites. *J. Electroanal. Chem. Interfacial Electrochem.* **1983**, *147*, 39-51.
296. Collman, J. P.; Devaraj, N. K.; Chidsey, C. E. D.: "Clicking" Functionality onto Electrode Surfaces. *Lang.* **2004**, *20*, 1051-1053.
297. Alévêque, O.; Blanchard, P.-Y.; Breton, T.; Dias, M.; Gautier, C.; Levillain, E.: Revisiting the determination of full steady-state coverage of redox centers on self-assembled monolayers. *Electrochem. Commun.* **2012**, *16*, 6-9.
298. Hall, S. B.; Khudaish, E. A.; Hart, A. L.: Electrochemical oxidation of hydrogen peroxide at platinum electrodes. Part 1. An adsorption-controlled mechanism. *Electrochim. Acta* **1998**, *43*, 579-588.
299. Kibena, E.; Tammeveski, K.; Matisen, L.; Hasse, U.; Scholz, F.: OH radical degradation of blocking aryl layers on glassy carbon and gold electrodes leads to film thinning on glassy carbon and pinhole films on gold. *Electrochem. Commun.* **2013**, *29*, 33-36.
300. Goldstein, S.; Merenyi, G.; Russo, A.; Samuni, A.: The role of oxoammonium cation in the SOD-mimic activity of cyclic nitroxides. *J. Am. Chem. Soc.* **2002**, *125*, 789-795.
301. Samuni, A.; Goldstein, S.; Russo, A.; Mitchell, J. B.; Krishna, M. C.; Neta, P.: Kinetics and mechanism of hydroxyl radical and OH-adduct radical reactions with nitroxides and with their hydroxylamines. *J. Am. Chem. Soc.* **2002**, *124*, 8719-8724.
302. Small, L. J.; Hibbs, M. R.; Wheeler, D. R.: Spontaneous aryldiazonium film formation on 440C stainless steel in nonaqueous environments. *Lang.* **2014**, *30*, 14212-14218.

Appendix

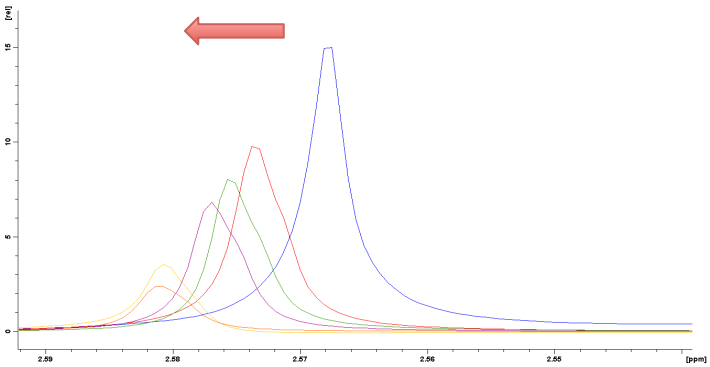

Fig A1. Stacked ^{1}H NMR spectra of 0.7 M DMU in D_2O with subsequent additions of H_2O (0 – 350 µL) showing a downfield shift in the methyl peaks. Arrow indicates increasing amounts of H_2O.

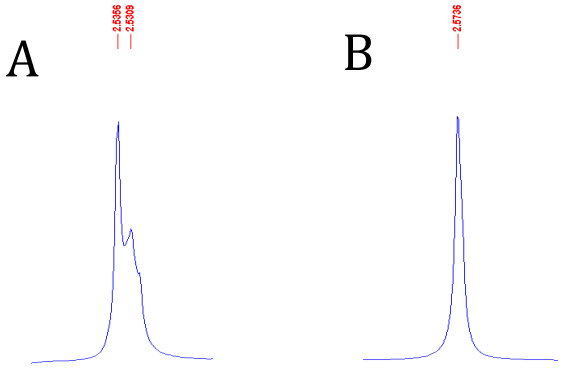

Fig. A2. ^{1}H NMR spectra of DMU in D_2O with the addition of one equivalent of H_2O_2 (A) and H_2O (B).

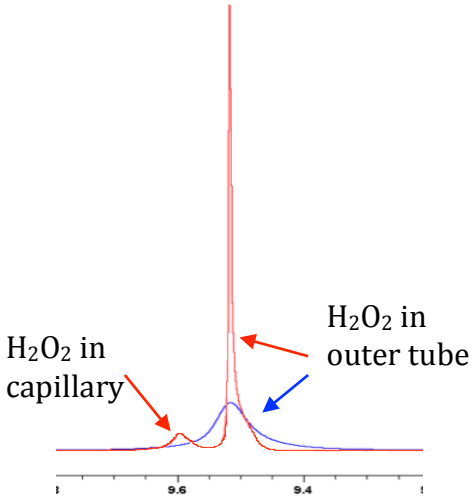

Fig. A3. ^{1}H NMR of H_2O_2 in d_8-THF with (red) and without (blue) a capillary of THF:H_2O_2.

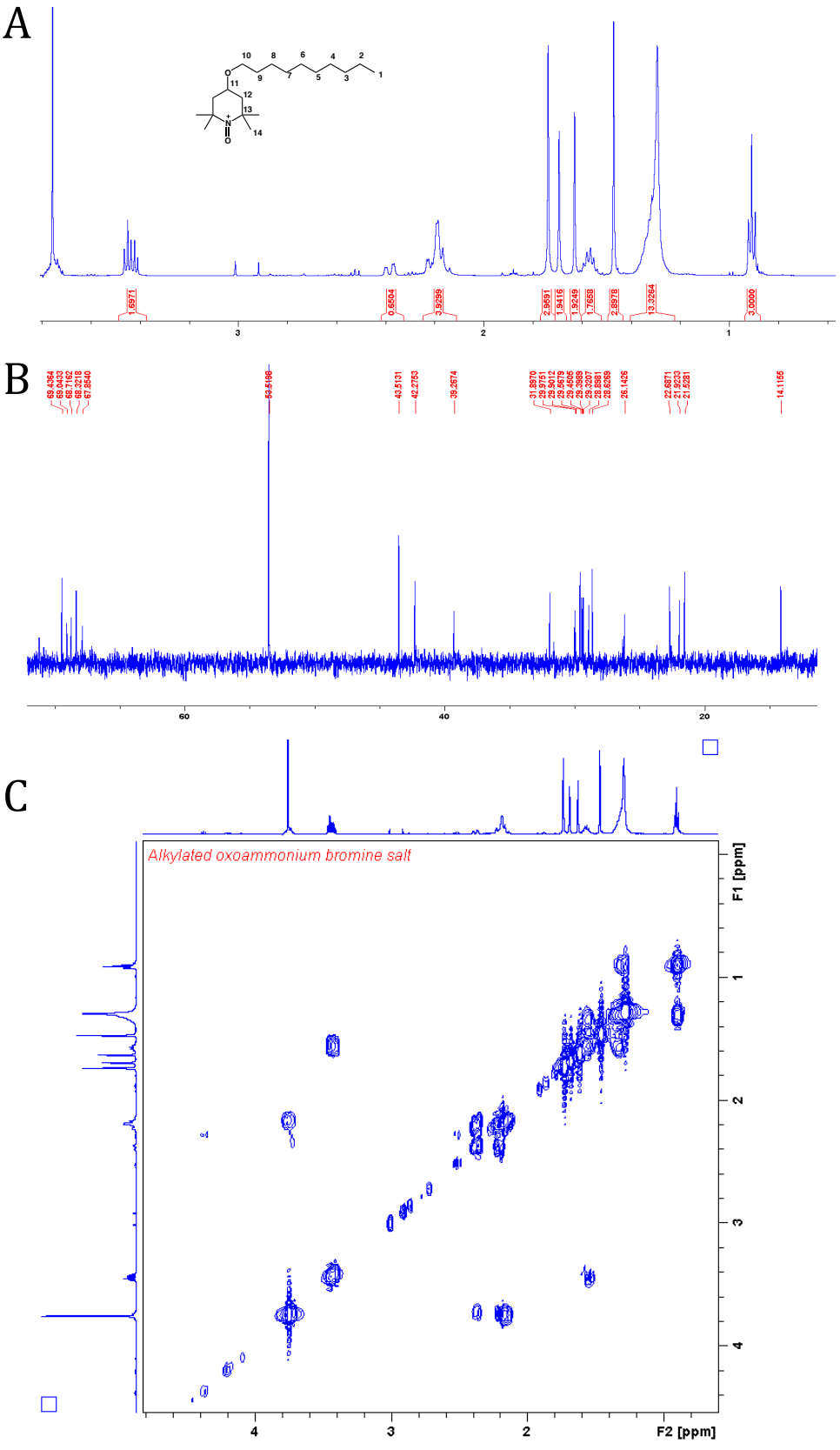

Fig. A4. A) ^{1}H NMR of alkylated oxoammonium salt (**43**) in $CDCl_3$. B) ^{13}C NMR of **43**. C) COSY spectrum of **43**.

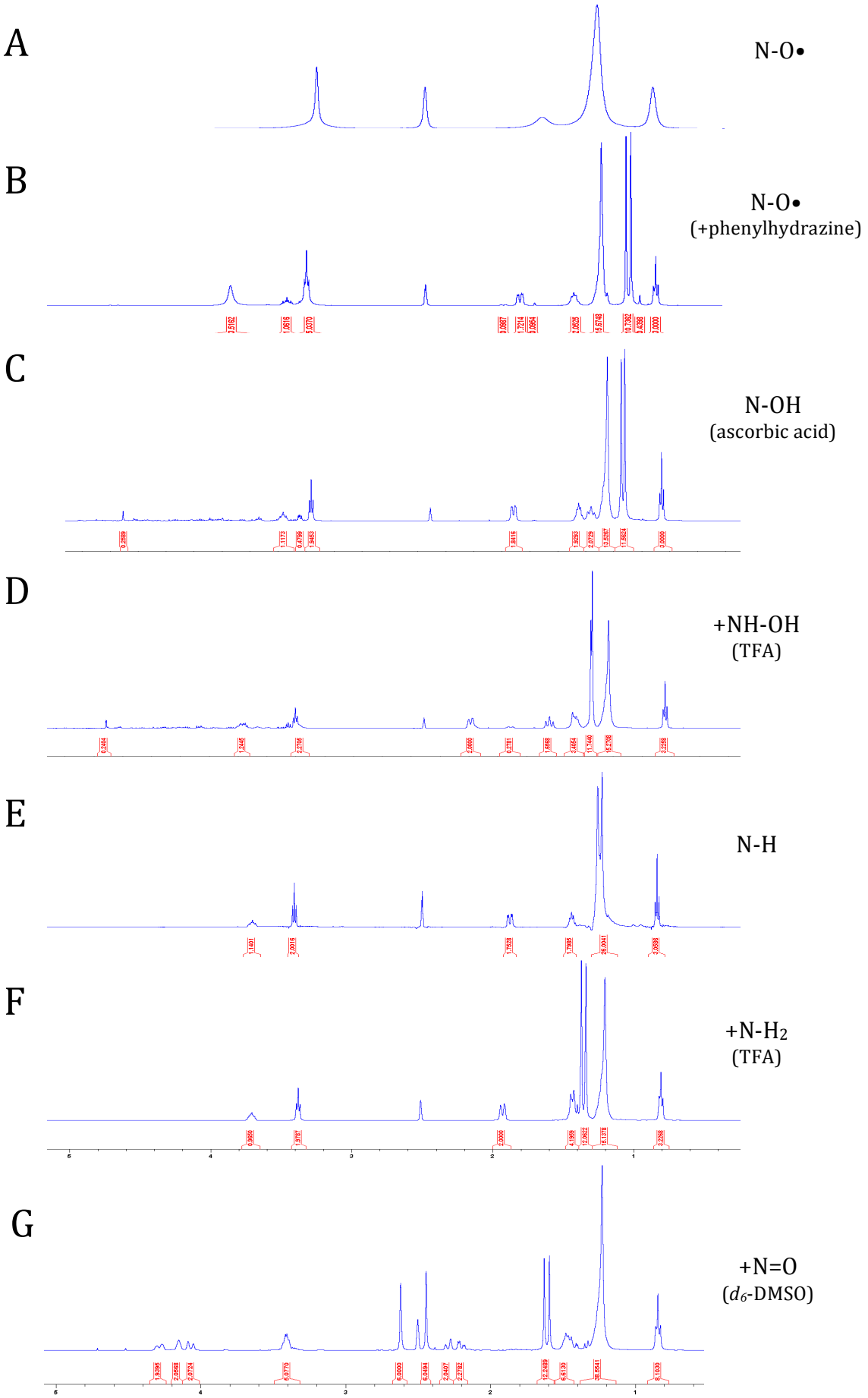

Fig. A5. A-G. Different species of the alkylated nitroxide catalyst derived from either compound **42** or **43**.

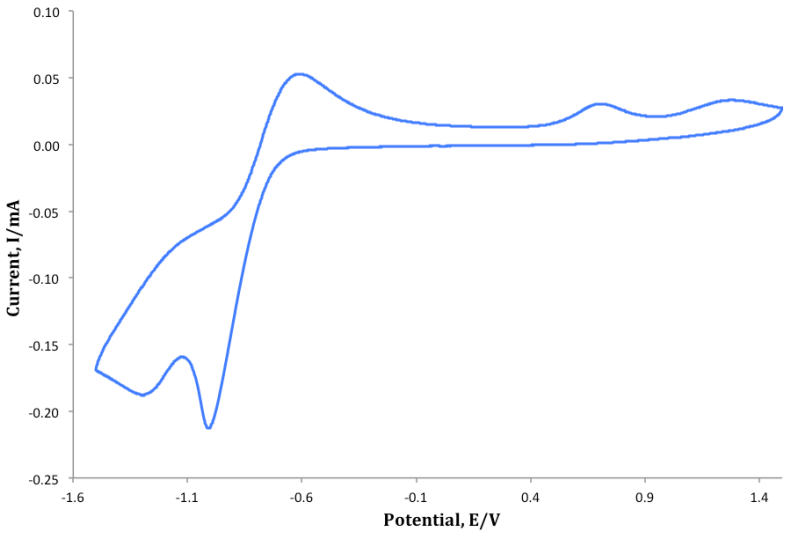

Fig. A6. CV from -1.5 to +1.5 V vs Ag/Ag^+ for grafted 4-nitrophenyl in MeCN (0.1 M NBu_4PF_6) on a GC macroelectrode (Pt CE, Ag RE). Reduction of nitro group seen at -1.27 V to give an integrated peak area of 47.75 µC.

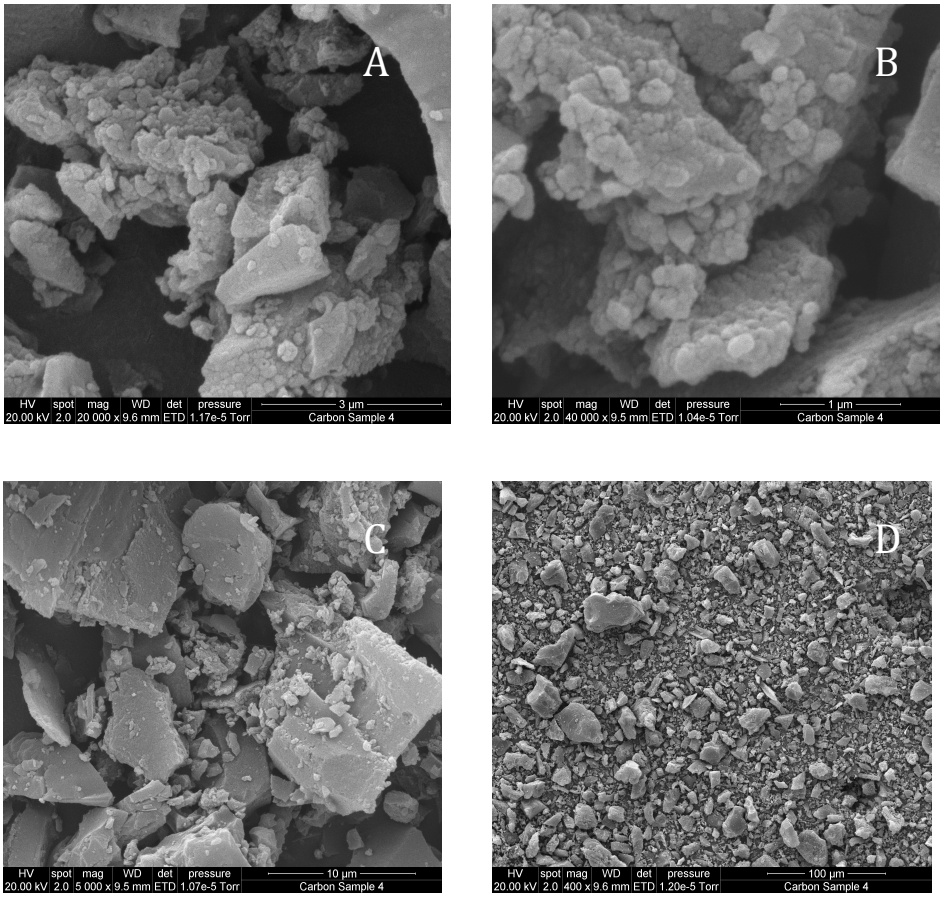

Fig. A7. PS1000 pre-treated with $H_2O_2$and HNO_3. SEM images at 20,000 (A), 40,000 (B), 5000(C) and 400 (D) magnifications.

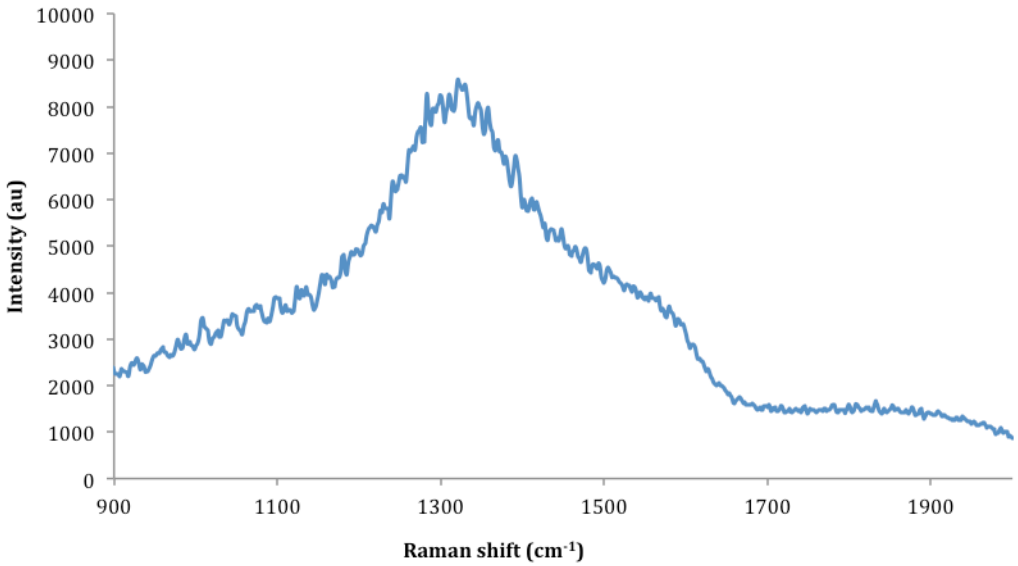

Fig. A8. Raman spectra of carbon felt.

List of Compounds

1

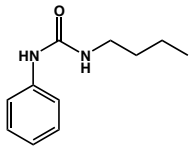

2

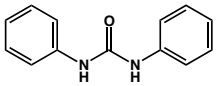

3

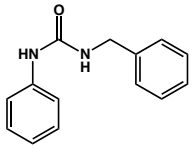

4

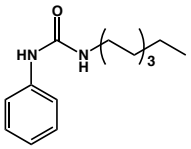

5

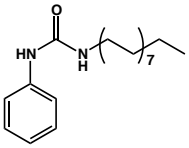

6

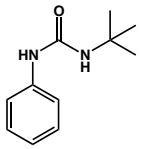

7

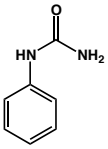

8

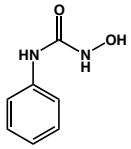

9

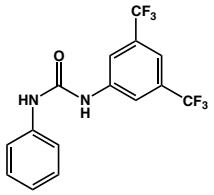

10

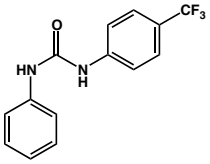

11

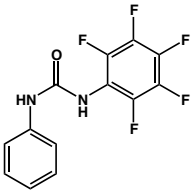

12

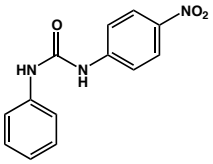

13

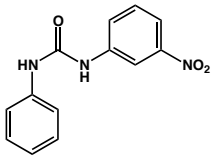

14

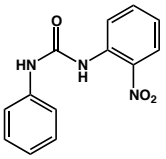

15

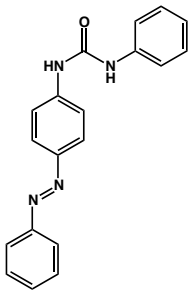

16

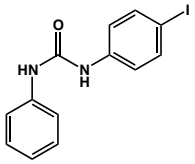

17

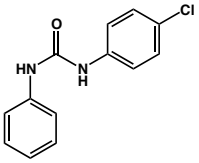

18

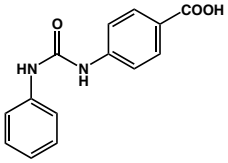

19

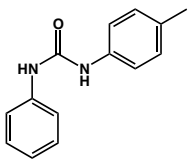

20

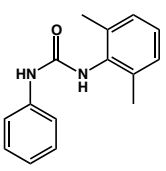

21

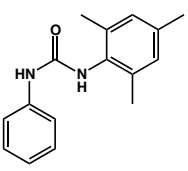

22

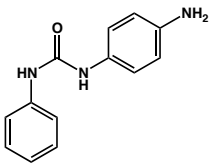

23

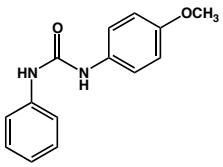

24

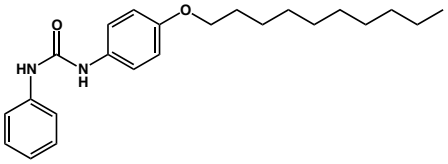

25

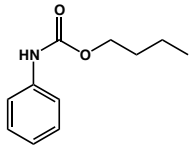

26

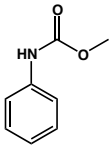

27

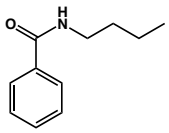

28

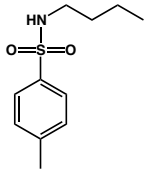

29

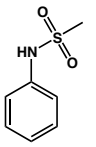

30

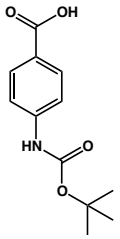

31

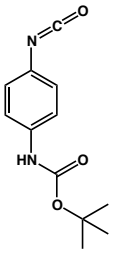

32

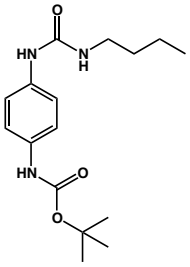

33

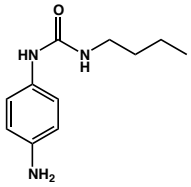

34

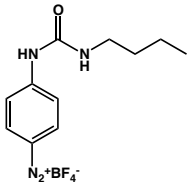

35

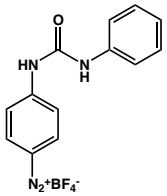

36

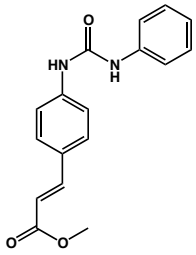

37

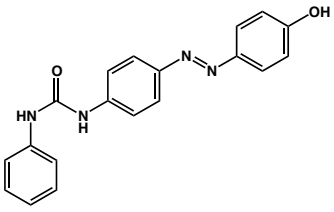

38

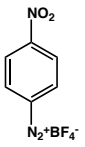

39

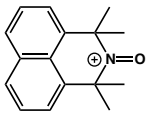

40

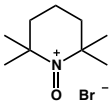

41

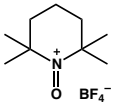

42

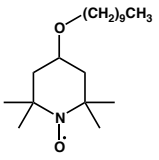

43

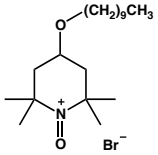

44

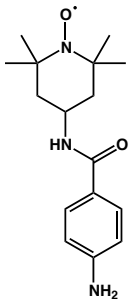

45

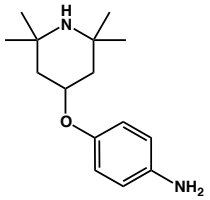

46

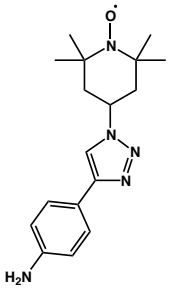

47

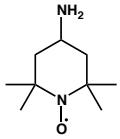

48

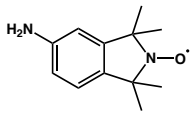

49

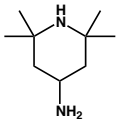

50

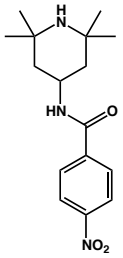

51

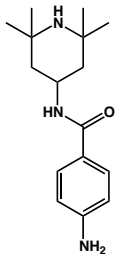

52

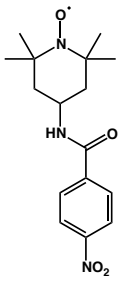

53

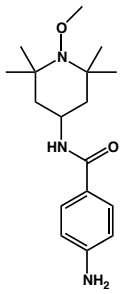

54

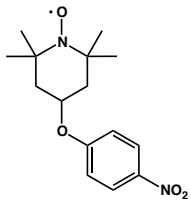

55

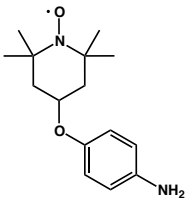

56

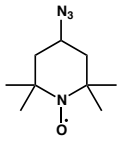

57

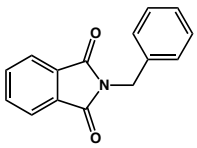

58

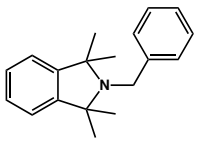

59

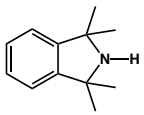

60

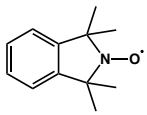

61

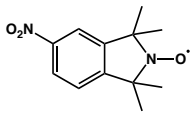

62

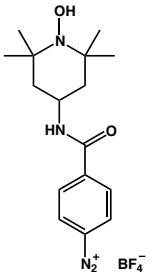

63

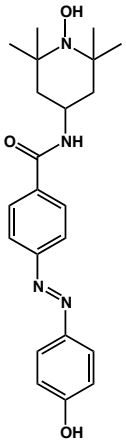

64

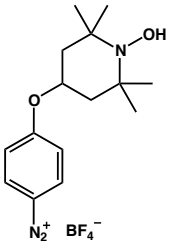

65

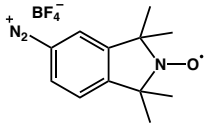

66

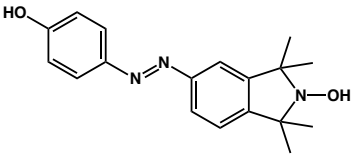

67

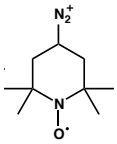

68

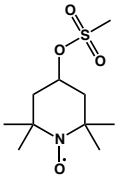

69

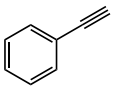

70

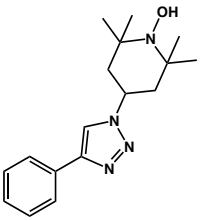

71

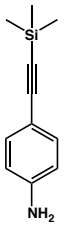

72

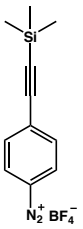

73

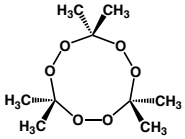

74

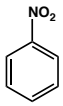

75

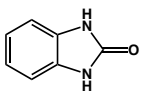

76

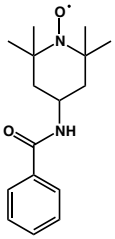

77

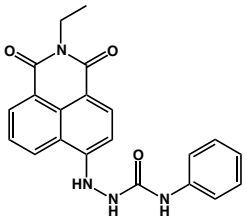

78

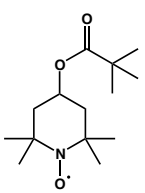

79

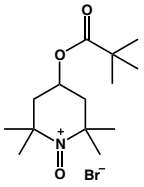

General Experimental Details

NMR Spectroscopy

Characterisation of synthesised compounds was by ^{1}H NMR, followed by ^{13}C NMR if required. Samples were prepared in $CDCl_3$, d_6-DMSO, d_8-THF, d_4-MeOD or CD_3CN and spectra were recorded on 400 or 500 MHz Bruker Avance spectrometers utilising TOPSPIN 2.1 software. Spectra were calibrated using solvent peaks or TMS. Where appropriate 2D spectra (COSY, NOESY, HMQC) were collected.

Mass Spectroscopy

Mass of the compounds synthesised were obtained in the appropriate solvent using a Micromass ZMD 400 electrospray spectrometer in either the positive or negative mode.

Microanalysis

Microanalysis was obtained for the modified carbon materials and carried out by the Campbell Microanalytical laboratory at the University of Otago.

UV-Vis Absorption Spectroscopy

When required, solution UV-Vis spectroscopy was recorded using a CARY 100 Bio UV-Vis spectrophotometer with a 1 cm pathlength quartz cell.

Infrared Spectroscopy

IR spectra were recorded on a Nicolet 5700 FT-IR from Thermo Electron Corporation using an ATR attachment.

BET Isotherm

The BET isotherm data was recorded using an Autosorb-iQ2, Quantachrome Instruments, USA.

Solvents and Reagents

Unless specified, commercial reagents and solvents (Sigma-Aldrich/Thermo Fisher) were used without purification.